National Technical University of Athens
School of Civil Engineering
Institute of Structural Analysis and Antiseismic Research

Optimum Design of Earthquake Resistant Structures implementing Computational Methods

A dissertation submitted to the School of Civil Engineering of National Technical University of Athens in partial fulfillment of the requirements for the degree of Doctor of Philosophy

by Chrysanthi Stathi

Advisor:

Professor Manolis Papadrakakis

Athens,

November 2014

Εθνικό Μετσόβιο Πολυτεχνείο
Σχολή Πολιτικών Μηχανικών
Εργαστήριο Στατικής και Αντισεισμικών Ερευνών

Βέλτιστος Αντισεισμικός Σχεδιασμός Κατασκευών με Υπολογιστικές Μεθόδους

Η παρούσα διατριβή υποβλήθηκε στη Σχολή Πολιτικών Μηχανικών του Εθνικού Μετσοβίου Πολυτεχνείου προς μερική εκπλήρωση των απαιτήσεων για την απόκτηση Διδακτορικού τίτλου σπουδών

από την Χρυσάνθη Στάθη

Επιβλέπων:

Καθηγητής Μανόλης Παπαδρακάκης

Αθήνα,

Νοέμβριος 2014

“If you dream of something worth doing and then simply go to work on and don’t think anything of personalities or emotional conflicts, or of money, or of family distractions; if you just think of, detail by detail, what you have to do next, it is a wonderful dream even though the end is a long way off, for there are about five thousands steps to be taken before we realize it; and start taking the first ten, and stay making twenty, after, it is amazing how quickly you get through those five thousand steps”

Edwin Land to Polaroid employees, 23 December 1942

PhD Examination Committee

I certify that I have read this dissertation and that in my opinion it is fully adequate, in scope and quality, as a dissertation for the degree of Doctor of Philosophy.

Manolis Papadrakakis
Professor
(Principal Advisor)
School of Civil Engineering
National Technical University of Athens

I certify that I have read this dissertation and that in my opinion it is fully adequate, in scope and quality, as a dissertation for the degree of Doctor of Philosophy.

Nikos D. Lagaros
Assistant Professor
(Member of Advisory Committee)
School of Civil Engineering
National Technical University of Athens

I certify that I have read this dissertation and that in my opinion it is fully adequate, in scope and quality, as a dissertation for the degree of Doctor of Philosophy.

Dimos Charmpis
Assistant Professor
(Member of Advisory Committee)
Department of Civil and Environmental Engineering
University of Cyprus

I certify that I have read this dissertation and that in my opinion it is fully adequate, in scope and quality, as a dissertation for the degree of Doctor of Philosophy.

Konstantinos Spiliopoulos
Professor
School of Civil Engineering
National Technical University of Athens

I certify that I have read this dissertation and that in my opinion it is fully adequate, in scope and quality, as a dissertation for the degree of Doctor of Philosophy.

Ioannis Psycharis
Professor
School of Civil Engineering
National Technical University of Athens

I certify that I have read this dissertation and that in my opinion it is fully adequate, in scope and quality, as a dissertation for the degree of Doctor of Philosophy.

Charis Gantes
Professor
School of Civil Engineering
National Technical University of Athens

I certify that I have read this dissertation and that in my opinion it is fully adequate, in scope and quality, as a dissertation for the degree of Doctor of Philosophy.

Michalis Fragiadakis
Lecturer
School of Civil Engineering
National Technical University of Athens

Περίληψη

Οι οικονομικές απώλειες από τις βλάβες που παρουσιάστηκαν σε κτήρια μετά από καταστρεπτικούς σεισμούς στις ΗΠΑ και την Ιαπωνία ήταν περισσότερες του αναμενομένου. Επιπλέον εκτεταμένες βλάβες σε κατασκευές μετά από σπάνια σεισμικά γεγονότα (2/50 επίπεδο επιτελεστικότητας) αποδίδονται στην άνιση κατανομή των εσωτερικών δράσεων, ειδικότερα των τεμνουσών δυνάμεων από τα κατακόρυφα δομικά στοιχεία, η οποία οφείλεται στην χωροθέτηση των δομικών στοιχείων. Η στρεπτική ροπή, η οποία αναπτύσσεται στην κατασκευή, μεγεθύνεται λόγω της μη κανονικότητας του κτηρίου σε κάτοψη και παραλαμβάνεται ως ζεύγος δυνάμεων, με αποτέλεσμα οι πρόσθετες τέμνουσες δυνάμεις λόγω στρέψης να δρουν σε σύζευξη με τις μεταφορικές τέμνουσες δυνάμεις προκαλώντας επιβάρυνση της εντατικής κατάστασης των δομικών στοιχείων. Δεδομένου ότι ο κύριος στόχος των σύγχρονων αντισεισμικών κανονισμών είναι η προστασία της ανθρώπινης ζωής, είναι φανερό ότι θα πρέπει να ληφθούν υπόψη επιπλέον κριτήρια σχετικά με την επίδοση της κατασκευής, τα οποία να περιορίζουν τις οικονομικές απώλειες καθώς και δείκτες βλάβης ώστε να ποσοτικοποιηθεί η τρωτότητα των κατασκευών σε ενδεχόμενο σεισμικό γεγονός. Έτσι άρχισε να υιοθετείται μία νέα θεώρηση σχεδιασμού με κριτήρια επιτελεστικότητας (performance-based design). Οι αντισεισμικοί σχεδιασμοί με βάση την επιτελεστικότητα στοχεύουν στην απόκριση της κατασκευής με ελεγχόμενες βλάβες-ζημιές σε διάφορα επίπεδα σεισμικής επικινδυνότητας. Προκειμένου να υλοποιηθεί αυτή η αντίληψη σχεδιασμού απαιτείται η ποσοτικοποίηση της βλάβης με δείκτες βλάβης, των οποίων οι τιμές μπορούν να συσχετισθούν με συγκεκριμένη κατάσταση βλάβης του κτηρίου.

Στην παρούσα διατριβή παρουσιάζεται ένας νέος δείκτης αποτίμησης της απόκρισης της κατασκευής υπό την επιρροή του στρεπτικού φαινομένου, ο λόγος στρέψης, ο οποίος ποσοτικοποιεί τις πρόσθετες τέμνουσες δυνάμεις που αναπτύσσονται στα κατακόρυφα δομικά στοιχεία λόγω του φαινομένου της στρέψης και την επιρροή τους στην απόκριση της κατασκευής. Στόχος είναι η ποσοτικοποίηση της επίδρασης του στρεπτικού φαινομένου (torsional effect) στη

σεισμική απόκριση των κατασκευών. Ο λόγος στρέψης εκτός από κριτήριο αποτίμησης επεκτείνεται και σε κριτήριο σχεδιασμού, μέσω της διαδικασίας βελτιστοποίησης ελαχιστοποιώντας τη συνιστώσα των πρόσθετων τεμνουσών δυνάμεων λόγω στρέψης (torsion-induced forces).

Στη συνέχεια αναζητώνται οι βέλτιστοι σχεδιασμοί των κατασκευών που θα προκύψουν μέσω μη-γραμμικής δυναμικής ανάλυσης. Με τον όρο 'βέλτιστος δομοστατικός σχεδιασμός' εννοούμε την εύρεση του καλύτερου δυνατού σχεδιασμού που μπορεί να εξευρεθεί στο πλαίσιο ενός πολύπλοκου πολύ-παραμετρικού προβλήματος βελτιστοποίησης, και όχι τον "μαθηματικά" βέλτιστο σχεδιασμό ο οποίος είναι δύσκολο εώς αδύνατο να εξευρεθεί. Οι Στρατηγικές Εξέλιξης είναι Δαρβίνειες μέθοδοι βελτιστοποιήσης οι οποίες μέσα από διαδοχικές βελτιώσεις του σχεδιασμού οδηγούν την αντικειμενική συνάρτηση στο "καθολικό" της βέλτιστο. Η διαδικασία βελτιστοποίησης στοχεύει στην ταυτόχρονη εξεύρεση ενός ικανοποιητικού ελαχίστου της αντικειμενικής συνάρτησης και στην ικανοποίηση όλων των περιορισμών του αντισεισμικού κανονισμού καθώς και των αρχιτεκτονικών περιορισμών για διάφορα επίπεδα σεισμικής επικινδυνότητας. Εκτός από τον προτεινόμενο δείκτη και το κόστος κατασκευής ως αντικειμενικές συναρτήσεις χρησιμοποιήθηκαν η εκκεντρότητα ως προς την ακαμψία και ως προς την αντοχή προκειμένου να μελετηθεί η επιρροή του φαινομένου της στρέψης στην απόκριση της κατασκευής για όλα τα επίπεδα σεισμικής επικινδυνότητας. Η αποτίμηση των βέλτιστων σχεδιασμών που προέκυψαν με ελαχιστοποίηση των ανωτέρω αντικειμενικών συναρτήσεων πραγματοποιείται με υποβολή των τελικών σχεδιασμών σε μη γραμμικες δυναμικές αναλύσεις για όλα τα επίπεδα σεισμικής επικινδυνότητας. Ακολουθεί η υπέρθεση των περιβαλλουσών χρονοιστοριών τέμνουσας βάσης-στρέψης βάσης για την εύρεση του σχεδιασμού με την ελάχιστη επιρροή του στρεπτικού φαινομένου.

Η παρούσα διδακτορική διατριβή αποτελείται από επτά κεφάλαια. Μετά από την εισαγωγή στο 1^{ο} Κεφάλαιο, στο 2^{ο} Κεφάλαιο παρουσιάζεται η διατύπωση του ραβδωτού στοιχείου δυνάμεων δοκού με τη μέθοδο των ινών καθώς και οι καταστατικές σχέσεις που χρησιμοποιήθηκαν για την αναλυτική προσομοίωση των κατασκευών από οπλισμένο σκυρόδεμα στα επόμενα κεφάλαια. Στο 3^{ο} Κεφάλαιο περιγράφονται οι βασικές αρχές των περιγραφικών διαδικασιών σχεδιασμού καθώς

και η έννοια του σχεδιασμού με βάση την επιτελεστικότητα. Επιπλέον στο κεφάλαιο αυτό περιλαμβάνονται τα βασικά χαρακτηριστικά αποτίμησης της επιρροής του στρεπτικού φαινομένου στην αντισεισμική συμπεριφορά των κατασκευών τόσο σε ελαστική όσο και σε ανελαστική απόκριση. Στο 4^{ο} Κεφάλαιο παρουσιάζεται ο προτεινόμενος δείκτης για την αποτίμηση του στρεπτικού φαινομένου στην απόκριση μη συμμετρικών κατασκευών καθώς και αριθμητικές εφαρμογές. Οι εφαρμογές του κεφαλαίου αυτού χωρίζονται σε δύο ενότητες, εκείνες που αφορούν μονώροφα και εκείνες που αφορούν πολυώροφα συστήματα. Και στις δύο περιπτώσεις εξετάζονται τόσο κτήρια κανονικά σε κάτοψη όσο και μη κανονικά. Το 5^{ο} Κεφάλαιο αναφέρεται στο πρόβλημα βέλτιστου σχεδιασμού και περιγράφει τον αλγόριθμο των στρατηγικών εξέλιξης που χρησιμοποιήθηκε στην παρούσα εργασία. Στο 6^{ο} Κεφάλαιο διατυπώνεται το πρόβλημα βέλτιστου σχεδιασμού των κατασκευών και ο προτεινόμενος δείκτης αποτίμησης στρέψης επεκτείνεται σε δείκτη σχεδιασμού μέσω της διαδικασίας βελτιστοποίησης. Παρουσιάζονται επιπλέον δύο μονώροφες εφαρμογές. Η πρώτη εφαρμογή είναι κανονική ενώ η δεύτερη είναι μη κανονική σε κάτοψη. Τέλος, στο 7^{ο} Κεφάλαιο περιέχονται τα συμπεράσματα της διατριβής, η πρωτότυπη συμβολή της και θέματα που θα μπορούσαν να αποτελέσουν τα επόμενα ερευνητικά βήματα μέσα από την κατεύθυνση που έχει ήδη δοθεί στην διατριβή.

Εκτεταμένη Περίληψη Διατριβής

Εκτεταμένες βλάβες σε κατασκευές μετά από σπάνια σεισμικά γεγονότα (2/50 επίπεδο επιτελεστικότητας) αποδίδονται στην άνιση κατανομή των εσωτερικών δράσεων, ειδικότερα των τεμνουσών δυνάμεων που αναπτύσσονται στα κατακόρυφα δομικά στοιχεία, η οποία οφείλεται στην χωροθέτηση των δομικών στοιχείων. Η στρεπτική ροπή, η οποία αναπτύσσεται στην κατασκευή, μεγεθύνεται λόγω της μη κανονικότητας του κτηρίου σε κάτοψη και παραλαμβάνεται ως ζεύγος δυνάμεων, με αποτέλεσμα οι πρόσθετες τέμνουσες δυνάμεις λόγω της επιρροής στρεπτικού φαινομένου να δρουν σε σύζευξη με τις μεταφορικές τέμνουσες δυνάμεις προκαλώντας επιβάρυνση της εντατικής κατάστασης των δομικών στοιχείων.

Οι κύριοι παράμετροι που σχετίζονται με την ελαστική απόκριση της κατασκευής στην επιρροή του στρεπτικού φαινομένου είναι η στατική εκκεντρότητα e_{CR} και ο λόγος μη συζευγμένης στρεπτικής προς μη συζευγμένη μεταφορική συχνότητα Ω. Ανάλογα με την τιμή του λόγου Ω τα κτήρια κατατάσσονται σε εύστρεπτα και δύστρεπτα. Για τιμές του λόγου μεγαλύτερες της μονάδας τα κτήρια χαρακτηρίζονται δύστρεπτα, ενώ για τιμές μικρότερης της μονάδας χαρακτηρίζονται εύστρεπτα. Για τα δύστρεπτα κτήρια κυρίαρχη ιδιομορφή είναι η μεταφορική ενώ για τα εύστρεπτα η στρεπτική. Οι πλευρές τους χαρακτηρίζονται ως δύσκαμπτες ή εύκαμπτες ανάλογα με την απόστασή τους από το κέντρο ελαστικής στροφής και το κέντρο μάζας. Ειδικότερα, όταν η απόσταση μια πλευράς από το κέντρο μάζας είναι μικρότερη από εκείνη από το κέντρο ελαστικής στροφής η πλευρά χαρακτηρίζεται εύκαμπτη, ενώ σε αντίθετη περίπτωση χαρακτηρίζεται δύσκαμπτη. Ένα κτήριο μπορεί να είναι εύκαμπτο ως προς τη μία διεύθυνση και δύσκαμπτο ως προς την άλλη. Στα δύστρεπτα κτήρια έχουν παρατηρηθεί αυξημένες μετατοπίσεις στην εύκαμπτη πλευρά και μειωμένες στην δύσκαμπτη σε σύγκριση με το συμμετρικό τους αντίστοιχο. Ενώ στα εύστρεπτα κτήρια, μια μερίδα ερευνητών έχει παρατηρήσει συμπεριφορά όμοια με εκείνη των δύστρεπτων κτηρίων [1], κάποιοι άλλοι επισημαίνουν αύξηση των μετατοπίσεων τόσο στην εύκαμπτη όσο και στην δύσκαμπτη πλευρά σε σύγκριση με το συμμετρικό τους αντίστοιχο[2].

Στους περισσότερους αντισεισμικούς κανονισμούς το φαινόμενο αυτό αντιμετωπίζεται με τη χρήση στατικών και τυχηματικών εκκεντροτήτων για τον ορισμό του σημείου εφαρμογής των στατικών δυνάμεων. Η τυχηματική εκκεντρότητα ορίζεται ως ένα ποσοστό (για παράδειγμα 5%) της διάστασης του κτηρίου στην κάθετη διεύθυνση από εκείνη της εφαρμογής του φορτίου. Ενώ η στατική εκκεντρότητα ορίζεται ως η απόσταση του κέντρου ελαστικής στροφής από το κέντρο μάζας. Ειδικότερα στα πολυώροφα κτήρια δεν είναι πάντα εφικτό να οριστεί το κέντρο ελαστικής στροφής [3]. Ο Μακάριος [4], [5] όρισε τον πλασματικό ελαστικό άξονα και τις ακτίνες δυστρεψίας, ώστε μέσω του πλασματικού ελαστικού κέντρου να είναι πάντα εφικτός ο υπολογισμός των στατικών εκκεντροτήτων πολυώροφων ασύμμετρων κτηρίων. Ως πλασματικός ελαστικός άξονας ή ελαστικός άξονας βέλτιστης στρέψης ορίζεται εκείνος ο άξονας στον οποίο όταν τοποθετείται οριζόντια στατική φόρτιση τότε η στρέψη ολόκληρου του κτηρίου ελαχιστοποιείται ενώ μηδενίζεται στην οριακή περίπτωση που ο υπόψη άξονας αποτελεί τον πραγματικό ελαστικό άξονα του κτηρίου. Στην κατάσταση βέλτιστης στρέψης του κτηρίου οι στροφές που αναπτύσσονται σε κάθε όροφο είναι μικρότερες από εκείνες που προκύπτουν για διαφορετική θέση του φορτιστικού επιπέδου του κτηρίου. Έτσι, μπορεί να θεωρηθεί προσεγγιστικά ότι το κτήριο εκτελεί μεταφορική κίνηση και μεταφέρεται παράλληλα με τον εαυτό του με αμελητέα στροφή. Ο κατακόρυφος άξονας μπορεί να υπολογισθεί για όλα τα κτήρια που διαθέτουν κανονικότητα καθ’ ύψος σύμφωνα με τους κανονισμούς. Ενώ η ακτίνα δυστρεψίας αντιστοιχεί στο μοχλοβραχίονα των ελαστικών δυνάμεων επαναφοράς για στρεπτική φόρτιση του κτηρίου. Πλήθος ερευνητών ασχολήθηκε με την επιρροή του στρεπτικού φαινομένου στη σεισμική απόκριση των κατασκευών. Ο Paulay [6] πρότεινε το εκκεντρότητα αντοχής ως καταλληλότερη ιδιότητα αποτίμησης του στρεπτικού φαινομένου στην ανελαστική περιόχη απόκρισης σε σύγκριση με τη στατική εκκεντρότητα, εφόσον τα στοιχεία έχουν διαρρεύσει και οι τιμές της στιβαρότητας τους έχουν διαφοροποιηθεί από τις αρχικές. Η εκκεντρότητα αντοχής ορίζεται ως η απόσταση του κέντρου αντοχής από το κέντρο μάζας. Ως κέντρο αντοχής ορίζεται το σημείο εκείνο του διαφράγματος από το οποίο περνά η συνισταμένη των μεταφορικών δυνάμεων, ώστε όταν ο όροφος γίνει μηχανισμός δεν αναπτύσσεται σε αυτόν στροφή. Επιπλέον ο Paulay [7] διαχώρισε τα κτήρια σε

στρεπτικά δεσμευμένα και μη δεσμευμένα ανάλογα με την ικανότητά τους να περιορίζουν την ανελαστική στροφή. Σύμφωνα με αυτό το διαχωρισμό τα κτήρια διατηρούν κάποια υπολλειματική στρεπτική στιβαρότητα ίση με:

$$K_{tr} = \lambda_t K_t \tag{1}$$

Όπου K_t η στρεπτική στιβαρότητα του κτηρίου η οποία δίνεται από τη σχέση:

$$K_t = \sum x_i^2 k_{iy} + \sum y_i^2 k_{ix} \tag{2}$$

όπου x_i και y_i οι αποστάσεις των στοιχείων από το κέντρο μάζας, k_{ix} και k_{iy} οι μεταφορικές στιβαρότητες στις αντίστοιχες διευθύνσεις. Η παράμετρος λ_t ποσοτικόποιεί το βαθμό στρεπτικής δέσμευσης και μπορεί να υπολογιστεί από τις παρακάτω σχέσεις:

$$\lambda_{tx} = \sum \left(x_i^2 k_{iy} \right) / K_t \tag{3}$$

$$\lambda_{ty} = \sum \left(y_i^2 k_{ix} \right) / K_t \tag{4}$$

Για τιμές $\lambda_t = 0$ το σύστημα χαρακτηρίζεται στρεπτικά μη δεσμευμένο, ενώ για τιμές $\lambda_t > 0.15$ το σύστημα χαρακτηρίζεται στρεπτικά δεσμευμένο.

Οι De La Llera και Chopra [8] πρότειναν τις καμπύλες τέμνουσας βάσης – στρέψης βάσης (base shear and torque – BST ultimate surface), οι οποίες αποτελούνται από όλους τους συνδυασμούς τέμνουσας βάσης – στρέψης βάσης οι οποίοι όταν εφαρμοστούν στατικά οδηγούν την κατασκευή σε κατάρρευση (Εικόνα 1). Όλοι οι συνδυασμοί τέμνουσας βάσης – στρέψης βάσης οι οποίοι βρίσκονται πάνω στην καμπύλη αφορούν τους μηχανισμούς κατάρρευσης ενώ οι συνδυασμοί εκτός της καμπύλης είναι ανέφικτοι.

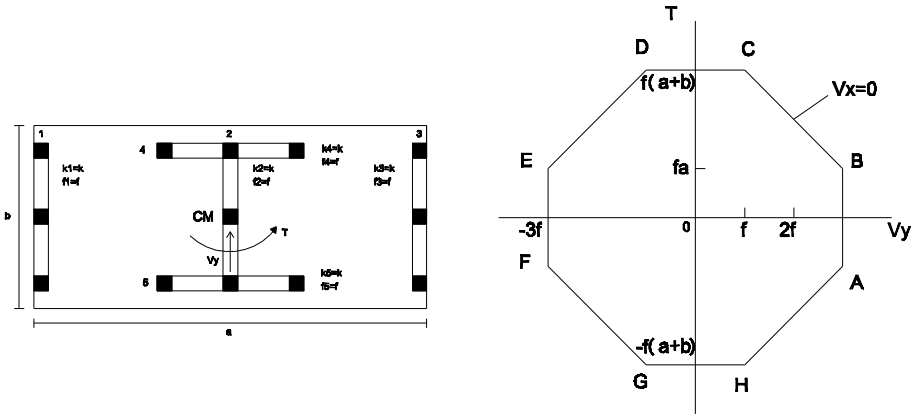

Εικόνα 1. Παράδειγμα καπύλης τέμνουσας βάσης – στρέψης βάσης [8].

Οι De La Llera και Chopra [9] επίσης επέκτειναν την ιδέα αυτή και σε πολυώροφα συστήματα, την καμπύλη τέμνουσας ορόφου – στρέψης ορόφου (story shear and torque - SST ultimate surface) (Εικόνα 2). Η καμπύλη αυτή κατασκευάζεται για κάθε όροφο και απεικονίζει όλους τους συνδυασμούς τεμνουσών δυνάμεων ορόφου και στρέψης ορόφου οι οποίοι εφαρμοζόμενοι στατικά οδηγούν τον όροφο σε κατάρρευση. Η κατασκευή της καμπύλης βασίζεται σε ένα υπερστοιχείο (super element – SE) ανά όροφο ικανό να αντιπροσωπεύσει τις ελαστικές και ανελαστικές ιδιότητες του ορόφου. Το στοιχείο αυτό έχει τρεις βαθμούς ελευθερίας σε κάθε κόμβο, δύο οριζόντιους μεταφορικούς και ένα στροφικό που αποτιμά τη στροφή μεταξύ των ορόφων που συνδέονται με το στοιχείο (Εικόνα 3)

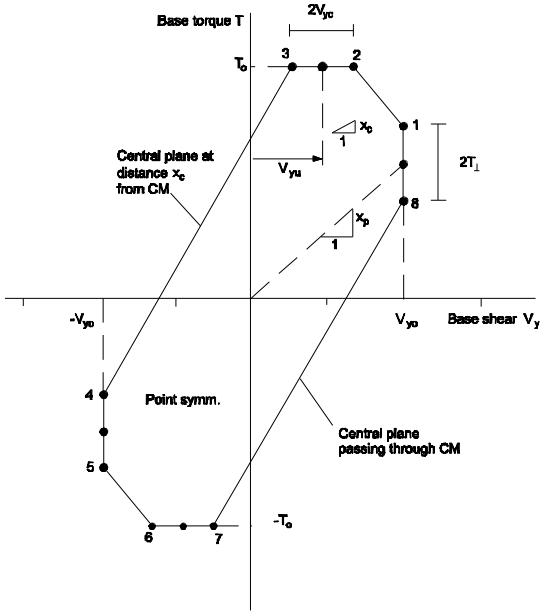

Εικόνα 2. Παράδειγμα καμπύλης τέμνουσας ορόφου – στρέψης ορόφου [9].

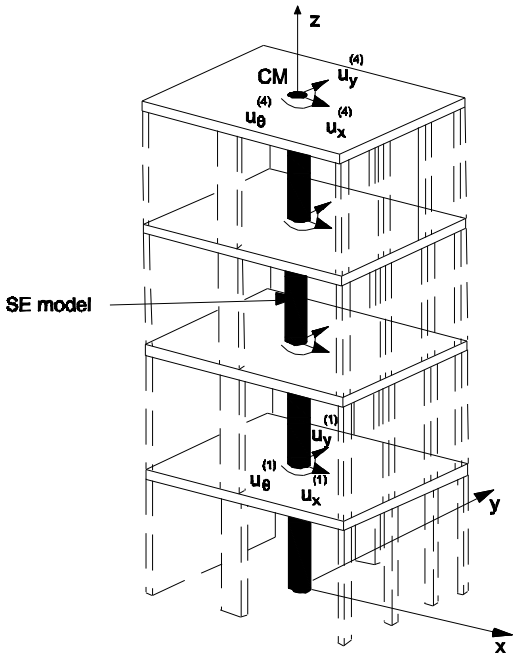

Εικόνα 3. Μοντέλο υπερστοιχείου για πολυώροφο κτήριο [9].

Ενώ οι Κύρκος και Αναγνωστόπουλος [2] πρότειναν μια διαδικασία τροποποίησης για τον αντισεισμικό σχεδιασμό κατασκευών από χάλυβα. Το πρώτο βήμα στη διαδικασία αυτή είναι ο υπολογισμός των μετατοπίσεων του ανώτερου ορόφου στις εύκαμπτες και δύσκαμπτες πλευρές του κτηρίου και στις δύο οριζόντιες διευθύνσεις λόγω του σεισμικού φορτίου και ο υπολογισμός των παρακάτω συντελεστων σε κάθε διεύθυνση:

$$f_{i,\,flex} = 2\frac{u_{i,\,flex}}{\left(u_{i,\,flex} + u_{i,stiff}\right)} \tag{5}$$

$$f_{i,\,flex} = 2\frac{u_{i,stiff}}{\left(u_{i,\,flex} + u_{i,stiff}\right)} \tag{6}$$

όπου $u_{i,\,flex}$ η μετατόπιση του ανώτερου ορόφου στην εύκαμπτη πλευρά για την i^{th} διεύθυνση και $u_{i,stiff}$ στην δύσκαμπτη πλευρά. Στη συνέχεια τα εμβαδά της διατομής των διαγωνίων συνδέσμων και στις δύο πλευρές πολλαπλασιάζονται με τους αντίστοιχους συντελεστές για κάθε διεύθυνση. Η ίδια διαδικασία ακολουθείται για τα υποστηλώματα και τις δοκούς τόσο στην εύκαμπτη όσο και στη δύσκαμπτη πλευρά. Αξίζει να σημειωθεί ότι στην έυκαμπτη πλευρά αυξάνεται η στιβαρότητα καθώς και η αντοχή των στοιχείων. Οι διατομές στην δύσκαμπτη πλευρά δεν μειώνονται καθώς η αντοχή τους καθορίζεται κυρίως από τα μόνιμα φορτία. Οι

τιμές των συντελεστών διαφέρουν από 1.25-1.50 για την εύκαμπτη πλευρά και από 0.85-1.00 για την άκαμπτη πλευρά.

Στην παρούσα διατριβή παρουσιάζεται ένας νέος δείκτης αποτίμησης της επιρροής του στρεπτικού φαινομένου στην απόκριση της κατασκευής, ο λόγος στρέψης, ο οποίος ποσοτικοποιεί τις πρόσθετες τέμνουσες δυνάμεις που αναπτύσσονται στα κατακόρυφα δομικά στοιχεία λόγω του φαινομένου της στρέψης. Στόχος είναι η ποσοτικοποίηση της επίδρασης του στρεπτικού φαινομένου (torsional effect) στη σεισμική απόκριση των κατασκευών.

Ο προτεινόμενος δείκτης βασίζεται στην παρατήρηση ότι το άθροισμα των απολύτων τιμών των τεμνουσών δυνάμεων που αναπτύσσονται στα κατακόρυφα δομικά στοιχεία είναι διαφορετικός από το αλγεβρικό τους άθροισμα για μη συμμετρικά συστήματα. Η διαφορά αυτή οφείλεται στις επιπλέον τέμνουσες δυνάμεις που αναπτύσσονται στα κατακόρυφα δομικά στοιχεία λόγω του φαινομένου της στρέψης, η οποία παραλαμβάνεται από την κατασκευή ως ζεύγος δυνάμεων. Επομένως ενώ για συμμετρικά συστήματα ισχύει η σχέση:

$$\sum_{k=1}^{n}\left|V_{kij}\right| = \sum_{k=1}^{n} V_{kij} \tag{7}$$

Για μη συμμετρικά συστήματα:

$$\sum_{k=1}^{n}\left|V_{kij}\right| \neq \sum_{k=1}^{n} V_{kij} \tag{8}$$

όπου n ο αριθμός των στοιχείων, i η διεύθυνση της τέμνουσας δύναμης που αναπτύσσεται στο στοιχείο k και j η διεύθυνση της επιβαλλόμενης σεισμικής διέγερσης.

Για ένα απλό τυχαίο έκκεντρο σύστημα (Εικόνα 4), στο οποίο επιβάλλουμε σεισμική διέγερση κατά την y διεύθυνση V_{Ey}, ισχύουν οι παρακάτω σχέσεις:

$$\sum_{k=1}^{n}\left|V_{kxy}\right| \neq \sum_{k=1}^{n} V_{kxy} = 0 \tag{9}$$

$$\sum_{k=1}^{n}\left|V_{kyy}\right| \neq \sum_{k=1}^{n} V_{kyy} = V_{Ey} \tag{10}$$

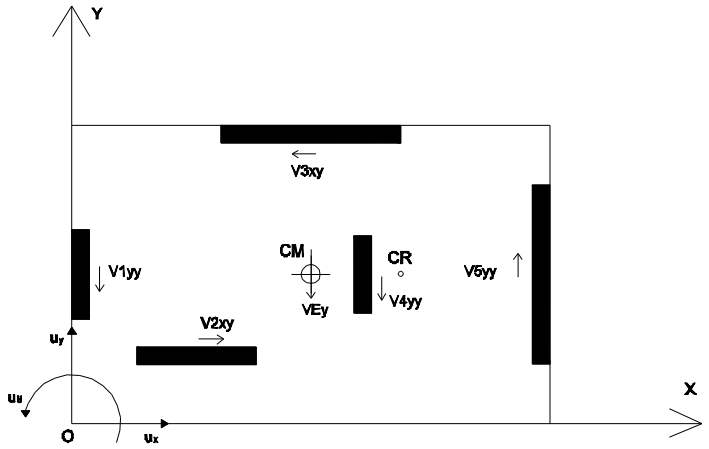

Εικόνα 4. Έκκεντρο σύστημα υποβαλλόμενο σε σεισμική διέγερση κατά την y διεύθυνση.

Ειδικότερα, θεωρούμε το μονώροφο σύστημα με κάτοψη όπως στην Εικόνα 5. Το σύστημα είναι μονοσυμμετρικό με άξονα συμμετρίας κατά τη x διεύθυνση και υποβάλλεται σε σεισμική διέγερση κατά την y διεύθυνση (V_{Ey}). Η θέση των κέντρων μάζας και ακαμψίας φαίνεται στην εικόνα 5. Η στροφή η οποία αναπτύσσεται στο σύστημα είναι αποτέλεσμα της στρέψης M_t που προκάλειται από την τέμνουσα βάσης V_{Ey} όταν ασκείται με εκκεντρότητα e_{CRX} .

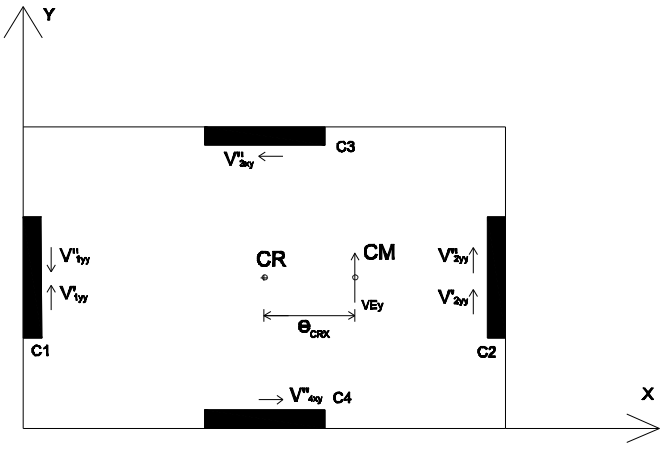

Εικόνα 5. Έκκεντρο σύστημα υποβαλλόμενο σε σεισμική διέγερση κατά την y διεύθυνση.

Η στρέψη παραλαμβάνεται ως ζεύγος δυνάμεων επιδρώντας στις τέμνουσες δυνάμεις που αναπτύσσονται στα στοιχεία. Η μεταφορική συνιστώσα (translational component) τέμνουσας δύναμης που αναπτύσσεται στα στοιχεία υπολογίζεται από τη σχέση:

$$V_{kiy}^{'} = \frac{k_{iy}}{\sum_{i=1}^{n} k_{iy}} V_{Ey} \tag{11}$$

όπου V_{Ey} η τέμνουσα βάσης σχεδιασμού, k_{iy} η μεταφορική στιβαρότητα του στοιχείου κατά την y διεύθυνση και n ο αριθμός των στοιχείων. Η στρεπτική συνιστώσα (torsional component) δίνεται από τη σχέση:

$$V_{kiy}^{"} = x_i k_{iy} \frac{M_t}{K_t} \tag{12}$$

όπου x_i η απόσταση του στοιχείου από το κέντρο μάζας, M_t η στρέψη που παράγεται από την τέμνουσα βάσης, ενώ K_t η στρεπτική στιβαρότητα του συστήματος, η οποία υπολογίζεται από τη σχέση:

$$K_t = \sum y_i^2 k_{ix} + \sum x_i^2 k_{iy} \tag{13}$$

Η συνολική τέμνουσα δύναμη που αναπτύσσεται σε ένα στοιχείο δίνεται από τη σχέση:

$$V_{kiy} = V_{kiy}^{'} + V_{kiy}^{"} \tag{14}$$

Ανάλογες σχέσεις ισχύουν για τις τέμνουσες δυνάμεις που αναπτύσσονται κατά τη x διεύθυνση. Ο προτεινόμενος δείκτης, λόγος στρέψης (Ratio Of Torsion) υπολογίζεται από την παρακάτω σχέση:

$$ROT = \frac{\sum_{k=1}^{n} \sum_{i=x,\, j=y}^{y,x} \left|V_{kij}\right| - \left|V_{Ex}\right| - \left|V_{Ey}\right|}{\left|V_{Ex}\right| + \left|V_{Ey}\right|} \tag{15}$$

όπου *n* ο συνολικός αριθμός των στοιχείων, k ο αριθμός του στοιχείου, i η διεύθυνση της τέμνουσας δύναμης που αναπτύσσεται στο στοιχείο και j η διεύθυνση στης σεισμικής διέγερσης, V_{Ex} και V_{Ey} η ένταση που επιβάλλει η

σεισμική διέγερση στην κατασκευή κατά τις διευθύνσεις x και y, η οποία αντιστοιχεί στην τέμνουσα βάσης στις αντίστοιχες διευθύνσεις.

Λαμβάνοντας όμως υπόψη ότι η τέμνουσα βάσης ισούται με το αλγεβρικό άθροισμα των τεμνουσών δυνάμεων που αναπτύσσονται στα στοιχεία ανά κατεύθυνση ισχύει:

$$V_{Ex} = \sum_{k=1}^{n} \sum_{j=y}^{x} V_{kxj} \tag{16}$$

$$V_{Ey} = \sum_{k=1}^{n} \sum_{j=y}^{x} V_{kyj} \tag{17}$$

Επομένως για το σύστημα της Εικόνας 5 ο λόγος στρέψης ισούται με:

$$ROT = \frac{\left|V_{1yy}^{'} - V_{1yy}^{"}\right| + \left|V_{2yy}^{'} + V_{2yy}^{"}\right| + \left|V_{3xy}^{"}\right| + \left|V_{4xy}^{"}\right| - \left|V_{Ey}\right|}{\left|V_{Ey}\right|} \tag{18}$$

Λαμβάνοντας υπόψη ότι:

$$\left|V_{Ey}\right| = \left|V_{1yy}^{'} - V_{1yy}^{"}\right| + \left|V_{2yy}^{'} + V_{2yy}^{"}\right| \tag{19}$$

το ROT μπορεί να γραφεί:

$$ROT = \frac{\left|V_{1yy}^{'} - V_{1yy}^{"}\right| + \left|V_{2yy}^{'} + V_{2yy}^{"}\right| + \left|V_{3xy}^{"}\right| + \left|V_{4xy}^{"}\right| - \left|V_{1yy}^{'} - V_{1yy}^{"}\right| - \left|V_{2yy}^{'} + V_{2yy}^{"}\right|}{\left|V_{1yy}^{'} - V_{1yy}^{"}\right| + \left|V_{2yy}^{'} + V_{2yy}^{"}\right|} \tag{20}$$

η οποία καταλήγει στην παρακάτω σχέση, της οποίας ο αριθμητής ισούται με τις στρεπτικές συνιστώσες των τεμνουσών δυνάμεων ενώ ο παρονομαστής με τη συνολική ένταση που παραλαμβάνει η κατασκευή κατά τη σεισμική διέγερση.

$$ROT = \frac{\left|V_{3xy}^{"}\right| + \left|V_{4xy}^{"}\right|}{\left|V_{Ey}\right|} \tag{21}$$

Ο λόγος στρέψης για πολυώροφα κτήρια υπολογίζεται από τη σχέση:

$$ROT = \sum_{m=1}^{l} ROT_m \tag{22}$$

όπου l ο αριθμός των ορόφων του κτηρίου.

Προκειμένου να αξιολογηθεί ο προτεινόμενος δείκτης χρησιμοποιήθηκαν τόσο μονώροφα όσο και πολυώροφα κτήρια. Στο πλαίσιο της παρούσας εργασίας τα κτήρια που υιοθετήθηκαν είναι δύστρεπτα και έκκεντρα ως προς τη μάζα. Ο

σχεδιασμός του συμμετρικού αναλόγου βασίστηκε στον Ευρωκώδικα (EC8) [10]. Στη συνέχεια δημιουργήθηκαν τρεις αντίστοιχοι σχεδιασμοί της ίδια κάτοψης με εκκεντρότητα 5%, 10% και 20% ως προς τη μάζα. Η στρέψη βάσεως του συστήματος, η στροφή οροφής και ο λόγος στρέψης συγκρίθηκαν για διαφορετικές τιμές εκκεντρότητας ως προς τη μάζα. Επιπλέον καταγράφηκαν οι τιμές τεμνουσών δυνάμεων, μετατοπίσεων και παραμορφώσεων για τα κατακόρυφα στοιχεία για τις διαφορετικές τιμές της εκκεντρότητας. Τα μέλη του συστήματος προσομοιώθηκαν με το ραβδωτό στοιχείο δυνάμεων δοκού-στύλου βασισμένο στη μέθοδο των ινών (fiber approach). Η μέθοδος αυτή παρουσιάζει κάποιες ιδιαιτερότητες. Σύμφωνα με τη διατύπωση αυτή οι εσωτερικές δράσεις διορθώνονται ώστε να υπάρχει συμβατότητα με τις μετατοπίσεις στους κόμβους του στοιχείου. Η διαδικασία διόρθωσής τους ονομάζεται διαδικασία καθορισμού κατάστασης στοιχείου (element state determination). Επιπλέον σύμφωνα με τη διατύπωση αυτή απαιτείται ο καθορισμός του μητρώου ενδοσιμότητας για τις εσωτερικές διατομές του στοιχείου (section flexibility matrix) από όπου υπολογίζεται το μητρώο στιβαρότητας του στοιχείου και οι εσωτερικές δράσεις κάθε διατομής. Η βασική υπόθεση στο στοιχείο ενδοσιμότητας είναι η χρήση συναρτήσεων παρεμβολής προκειμένου από τα επικόμβια φορτία να προκύψουν τα φυσικά εντατικά εντατικά μεγέθη σε διάφορες διατομές στο εσωτερικό του στοιχείου[11]. Σύμφωνα με αυτή τη διατύπωση ένα στοιχείο δοκού – στύλου είναι αρκετό για να προσομοιώσει τη συμπεριφορά ενός μέλους. Σε αντίθεση με το στοιχείο δυνάμεων, για την προσομοίωση μελών με το στοιχείο μετατοπίσεων ειδικότερα στην ανελαστική περιοχή είναι απαραίτητο κάθε μέλος να διακριτοποιηθεί με περισσότερα από ένα στοιχεία δοκού-στύλου. Ένω αναμένεται πύκνωση του δικτύου στις περιοχές όπου αναπτύσσονται μεγάλες ανελαστικές παραμορφώσεις. Η συμπεριφορά του σκυροδέματος σε θλίψη προσομοιώθηκε με το μοντέλο των Kent και Park (1973) [12] όπως τροποποιήθηκε από τους Scott *et al.* (1982) [13]. Ενώ η συμπεριφορά του χάλυβα περιγράφεται από διγραμμικό μοντέλο.

Για τις αναλύσεις χρησιμοποιήθηκε το λογισμικό OPENSEES. Το αρχικό σύστημα είναι συμμετρικό (symmetric: *sym*) ενώ συγκρίνεται με τα αντίστοιχα που παρουσιάζουν εκκεντρότητες ως προς τη μάζα κατά 5% (mass eccentric: *ecc_0.05*), 10% (mass eccentric: *ecc_0.10*) και 20% (mass eccentric: *ecc_0.02*). Όλοι οι

σχεδιασμοί υποβλήθηκαν σε μη γραμμικές δυναμικές αναλύσεις για τα τρία επίπεδα σεισμικής επικινδυνότητας. Η στρέψη βάσης του συστήματος, η στροφή οροφής και ο λόγος στρέψης συγκρίθηκαν για διαφορετικές τιμές της εκκεντρότητας ως προς τη μάζα για τα διαφορετικά επίπεδα σεισμικής επικινδυνότητας. Επιπλέον καταγράφηκαν οι τιμές τεμνουσών δυνάμεων μετατοπίσεων και παραμορφώσεων για τα κατακόρυφα στοιχεία και συγκρίθηκαν για τις διαφορετικές τιμές της εκκεντρότητας.

Αριθμητική Εφαρμογή 1

Στην πρώτη αριθμητική εφαρμογή εξετάζεται ένα μονώροφο, κανονικό σε κάτοψη, διαξονικά έκκεντρο κτήριο ρεαλιστικών διαστάσεων υποβαλλόμενο σε σεισμική διέγερση κατά τις δύο διευθύνσεις x και y (Εικόνα 6). Τόσο το συμμετρικό όσο και τα έκκεντρα ως προς τη μάζα αντίστοιχά του όπως φαίνεται από τον πίνακα 1 κατατάσσονται στην κατηγορία των δύστρεπτων κτηρίων, εφόσον ο λόγος της μη συζευγμένης στρεπτικής προς τη μη συζευγμένη μεταφορική συχνότητα είναι μεγαλύτερος της μονάδας. Στην εικόνα 7 απεικονίζονται οι τέμνουσες δυνάμεις επιλεγμένων υποστηλωμάτων κατά την y διεύθυνση όπου παρατηρείται η αναμενόμενη συμπεριφορά για στρεπτικά μη ευαίσθητα συστήματα (torsionally stiff systems) κατά την ελαστική απόκριση του συστήματος. Ειδικότερα, σημειώνεται αύξηση των τεμνουσών δυνάμεων μονοτονικά με την εκκεντρότητα στην εύκαμπτη πλευρά (η απόσταση από το κέντρο μάζας είναι μικρότερη από την απόστασή της από το κέντρο ακαμψίας _columns 11, 16) και μείωση τους στη δύσκαμπτη πλευρά (η απόσταση από το κέντρο ακαμψίας είναι μικρότερη από αυτή από το κέντρο μάζας _ columns 1, 6). Όταν κάποιο από τα στοιχεία διαρρεύσει μεταβάλλεται η στιβαρότηά του και κατά συνέπεια η εκκεντρότητα του συστήματος. Το σύστημα εισέρχεται στην ανελαστική περιοχή της απόκρισης όπου η στιβαρότητα των στοιχείων μεταβάλλετα, όμοια και η εκκεντρότητα. Η ανακατανομή των δυνάμεων ειδικά για δυναμική φόρτιση δεν είναι δυνατό να προβλεφθεί. Το ίδιο συμβαίνει και με τη θέση του κέντρου ελαστικής στροφής. Επομένως δε μπορεί με ασφάλεια να προβλεφθεί ποια πλευρά είναι εύκαμπτη ή δύσκαμπτη. Η ίδια τάση παρατηρήθηκε για τις μετατοπίσεις και τις παραμορφώσεις (Εικόνα 8).

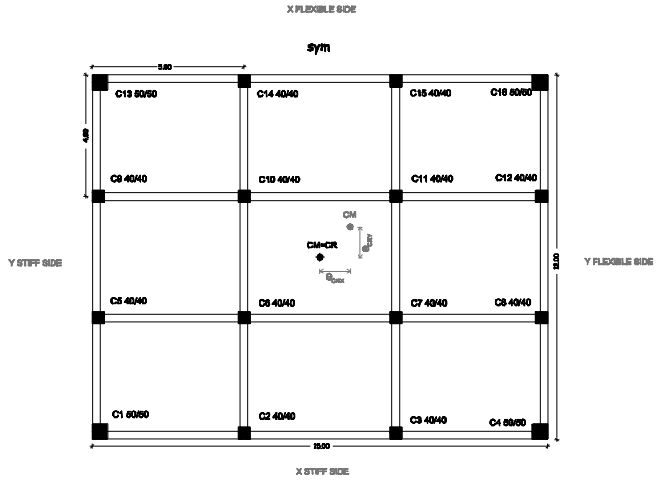

Εικόνα 6. Αριθμητική Εφαρμογή 1 - Έκκεντρο διαξονικά κανονικό σύστημα υποβαλλόμενο σε σεισμική διέγερση κατά τις δύο διευθύνσεις x και y.

Πίνακας 1. Αριθμητική Εφαρμογή 1 - Ιδιοπερίοδος και λόγος μη συζευγμένης στρεπτικής προς μη συζευγμένη μεταφορική ιδιοσυχνότητα.

	T_1	T_2	T_3	$\Omega_x = \frac{\omega_t}{\omega_x}$	$\Omega_y = \frac{\omega_t}{\omega_y}$
sym	0.3593 ^{x}	0.3484 ^{y}	0.2526 ^{t}	1.4224	1.3793
ecc0.05	0.3620 ^{x}	0.3512 ^{y}	0.2524 ^{t}	1.4342	1.3914
ecc0.10	0.3753 ^{x}	0.3539 ^{y}	0.2519 ^{t}	1.4898	1.4049
ecc0.20	0.4320 ^{x}	0.3549 ^{y}	0.2509 ^{t}	1.7218	1.4145

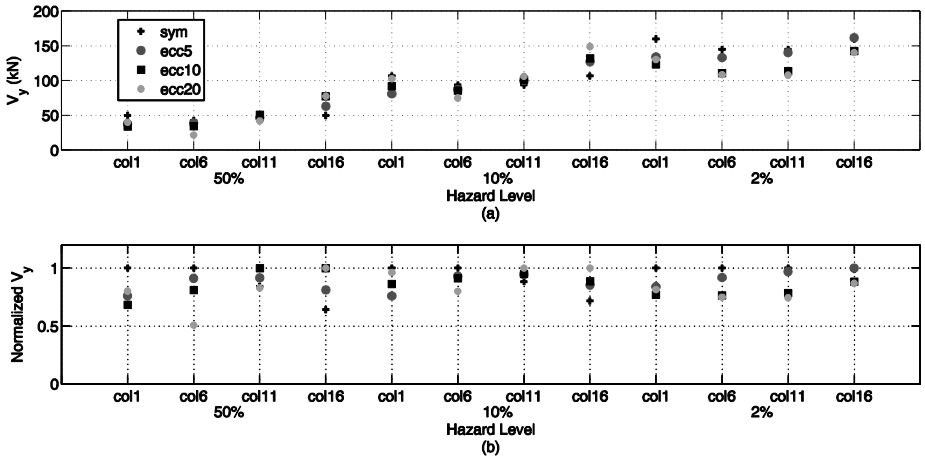

Εικόνα 7. Αριθμητική εφαρμογή 1 – Τέμνουσες δυνάμεις υποστηλωμάτων κατά την y διεύθυνση για κάθε επίπεδο σεισμικής επικινδυνότητας και κάθε σχεδιασμό – (a) απόλυτη μέγιστη τιμή τεμνουσών δυνάμεων και (b) κανονικοποιημένες τέμνουσες δυνάμεις ως προς τη μέγιστη τιμή.

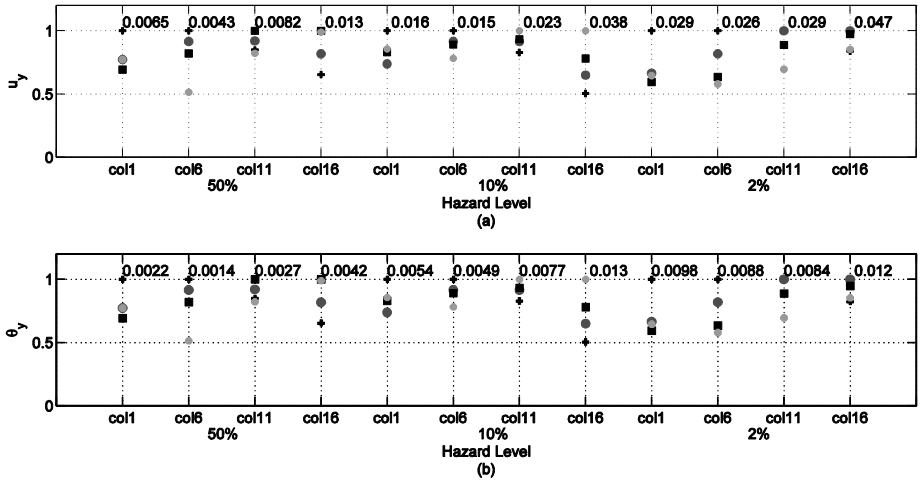

Εικόνα 8. Αριθμητική εφαρμογή 1 – Κανονικοποιημένες ως προς τη μέγιστη τιμή κατά την y διεύθυνση για κάθε επίπεδο σεισμικής επικινδυνότητας και κάθε σχεδιασμό – (a) μετατοπίσεις υποστηλωμάτων και (b) παραμορφώσεις υποστηλωμάτων.

Όσον αφορά τα μεγέθη που σχετίζονται με την επιρροή του στρεπτικού φαινομένου - στρέψη βάσης, στροφή οροφής και λόγος στρέψης - παρατηρούμε ότι αυξάνονται μονοτονικά με την εκκεντρότητα για όλα τα επίπεδα σεισμικής επικινδυνότητας (Εικόνα 9). Για τα συμμετρικά συστήματα παρατηρείται ότι ο λόγος στρέψης είναι μηδενικός για την ελαστική περιοχή απόκρισης. ΄Οπως αναφέρθηκε παραπάνω στην ανελαστική περιοχή η στιβαρότητα των στοιχείων επηρεάζεται μεταβάλλοντας την εκκεντρότητα. Για το λόγο αυτό παρατηρούνται τιμές διαφορετικές του μηδενός για το συμμετρικό αντιστοιχο στην ανελαστική περιοχή απόκρισης. Έκτος από το λόγο στρέψης, η στρέψη βάσης καθώς και η στροφή οροφής αυξάνουν τις τιμές τους για το συμμετρικό αντίστοιχο στην ανελαστική περιοχή σε σύγκριση με εκείνες στην ελαστική. Επειδή η τάξη μεγέθους τους είναι πολύ μικρή και η αύξηση του δεν είναι ορατή στην εικόνα 9, παρατίθεται ο πίνακας 2.

Πίνακας 2. Συμμετρικό αντίστοιχο – Στρέψη βάσης, στροφή οροφής και λόγος στρέψης για όλα τα επίπεδα σεισμικής επικινδυνότητας.

Symmetric design	**Hazard Levels**		
	50/50	10/50	2/50
ROT	8.78E-03	1.66E-01	3.99E-01
Base Torque	5.66E-08	1.16E-02	5.60E-02
Diaphragm Rotation	5.76E-12	1.62E-07	8.40E-07

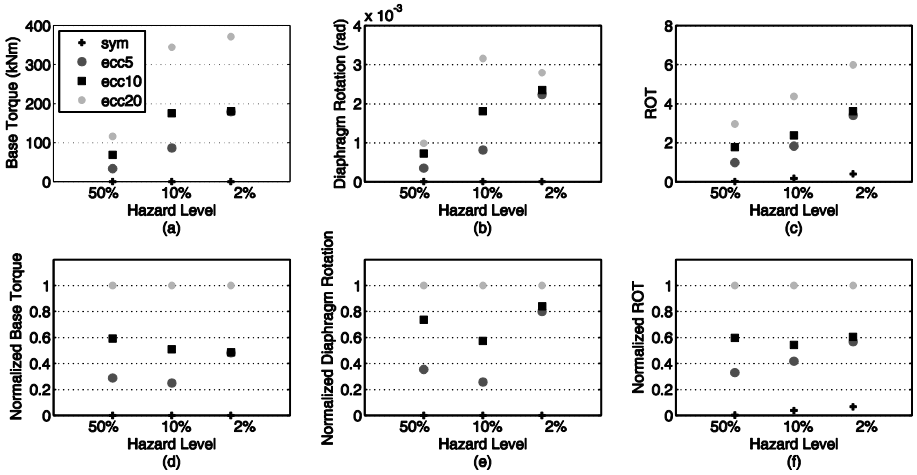

Εικόνα 9. Αριθμητική εφαρμογή 1 – (a) μέγιστη απόλυτη τιμή στρέψης βάσης, (b) μέγιστη απόλυτη τιμή στροφής διαφράγματος, (c) μέγιστη απόλυτη τιμή λόγου στρέψης (ROT), (d) κανονικοποιημένη ως προς τη μέγιστη τιμή στρέψη βάσης, (e) κανονικοποιημένη ως προς τη μέγιστη τιμή στροφή οροφής και (f) κανονικοποιημένος ως προς τη μέγιστη τιμή λόγος στρέψης (ROT) για όλα τα επίπεδα σεισμικής επικινδυνότητας και όλους τους σχεδιασμούς.

Όπως παρατηρείται στην εικόνα 9 (a), (b), (c) η μεταβολή της στροφής οροφής δεν ακολουθεί πάντα αυτή της στρέψης βάσης. Για το μη συμμετρικό αντίστοιχο με 20% εκκεντρότητα ως προς τη μάζα παρατηρούμε ότι ενώ η τιμή της μέγιστη στρέψης βάσης αυξάνεται από το επίπεδο με πιθανότητα υπέρβασης 2% στα πενήντα χρόνια σε σύγκριση με εκείνο με πιθανότητα υπέρβασης 10% στα πενήντα χρόνια, η τιμή της στροφής οροφής μειώνεται. Ο λόγος στρέψης μεταβάλλεται σύμφωνα με τη στρέψη βάσης. Αξίζει να σημειωθεί ότι όμοια συμπεράσματα έχουν επαληθευθεί για πιο απλά μοντέλα καθώς και για πιο πολύπλοκα μη κανονικά σε

κάτοψη κτήρια υποβαλλόμενα τόσο σε μονοαξονική όσο και σε διαξονική σεισμική διέγερση, τα οποία δεν παραβάλλονται εδώ για λόγους οικονομίας χώρου.

Αριθμητική Εφαρμογή 2

Η δεύτερη αριθμητική εφαρμογή αφορά ένα τετραώροφο μη κανονικό σε κάτοψη διαξονικά έκκεντρο κτήριο (Εικόνα 10) υποβαλλόμενο σε σεισμική διέγερση κατά τις δύο διευθύνσεις. Λόγω της μη κανονικότητας του κτηρίου σε κάτοψη ήταν ανέφικτο να οριστεί συμμετρικός σχεδιασμός, επομένως ορίστηκε σχεδιασμός με τη μικρότερη δυνατή εκκεντρότητα ίση με 0.4 % και συμβολίζεται ως *ecc* το αντίστοιχό του στα γραφήματα. Τα υπόλοιπα έκκεντρα αντίστοιχα αφορούν εκκεντρότητες 5%, 10% και 20% όπως και στην προηγούμενη εφαρμογή και συμβολίζονται με *ecc0.05*, *ecc0.10* και *ecc0.20* αντίστοιχα. Πρόκειται και σε αυτή την περίπτωση για δύστρεπτο σύστημα όπως φαίνεται στον πίνακα 3 από τις τιμές του λόγου μη συζευγμένης στρεπτικής προς μη συζευγμένη μεταφορική συχνότητα, ο οποίος ξεπερνά τη μονάδα για όλους τους σχεδιασμούς.

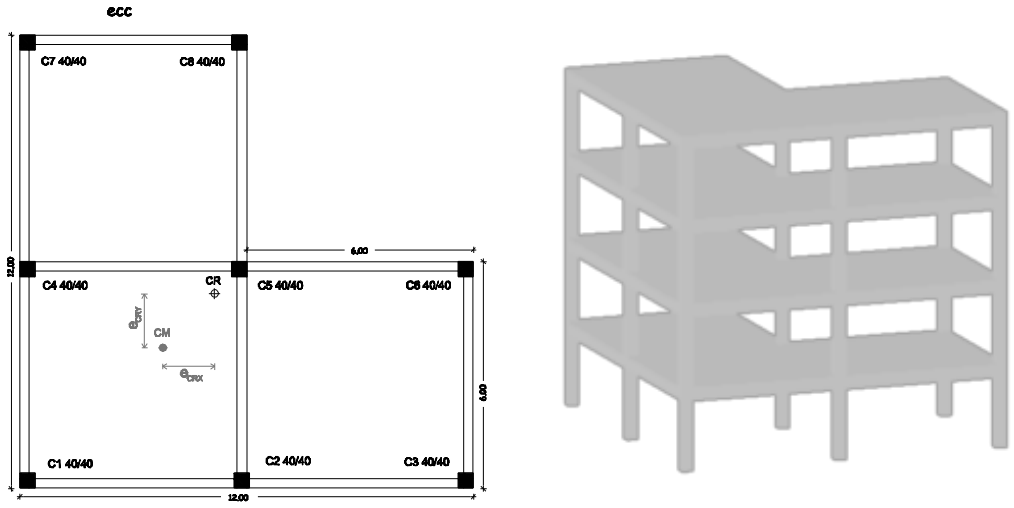

Εικόνα 10. Αριθμητική Εφαρμογή 2 - Έκκεντρο διαξονικά μη κανονικό τετραώροφο σύστημα υποβαλλόμενο σε σεισμική διέγερση κατά τις δύο διευθύνσεις x και y.

Όπως φαίνεται στην εικόνα 11 και στην εικόνα 12 τα εντατικά μεγέθη (τέμνουσες δυνάμεις, μετατοπίσεις και παραμορφώσεις) αυξάνονται για τα υποστηλώματα που βρίσκονται στην εύκαμπτη πλευρά (columns 1, 7) και μειώνονται για εκείνα στην δύσκαμπτη (columns 3, 6). Τα εντατικά μεγέθη των

εικόνων 11 και 12 αφορούν τα στοιχεία του ανώτερου διαφράμγατος. Έτσι, η ήδη παρατηρημένη κι από αλλους ερευνητές τάση μεταβολής εντατικών μεγεθών δύστρεπτων κανονικών κτηρίων, επαληθεύεται και για μη κανονικά σε κάτοψη κτήρια.

Πίνακας 3. Αριθμητική Εφαρμογή 2 - Ιδιοπερίοδος και λόγος μη συζευγμένης στρεπτικής προς μη συζευγμένη μεταφορική ιδιοσυχνότητα.

	T_1	T_2	T_3	$\Omega_x = \frac{\omega_t}{\omega_x}$	$\Omega_y = \frac{\omega_t}{\omega_y}$
ecc	1.0074^{x}	1.0059^{y}	0.6988^{t}	1.4416	1.4395
ecc0.05	1.0218^{x}	1.0074^{y}	0.7006^{t}	1.4585	1.4379
ecc0.10	1.0633^{x}	1.0074^{y}	0.6851^{t}	1.5520	1.4704
ecc0.20	1.1933^{x}	1.0074^{y}	0.6313^{t}	1.8902	1.5958

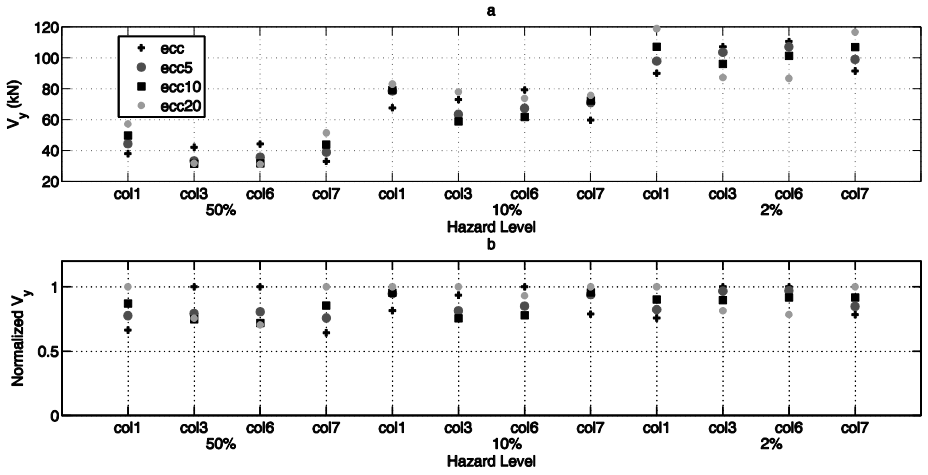

Εικόνα 11. Αριθμητική εφαρμογή 2 – Τέμνουσες δυνάμεις υποστηλωμάτων κατά την y διεύθυνση για κάθε επίπεδο σεισμικής επικινδυνότητας και κάθε σχεδιασμό – (a) μέγιστη απόλυτη τιμή τεμνουσών δυνάμεων και (b) κανονικοποιημένες τέμνουσες δυνάμεις ως προς τη μέγιστη τιμή.

Για τον έκκεντρο σχεδιασμό με 0.4% εκκεντρότητα *ecc* η στρέψη βάσης, η στροφή οροφής και ο λόγος στρέψης έχουν σχεδόν μηδενική τιμή στην ελαστική περιοχή απόκρισης (με πιθανότητα υπέρβασης 50% στα πενήντα χρόνια). Για τους υπόλοιπους σχεδιασμούς οι τιμές των αντίστοιχων μεγεθών αυξάνονται μονοτονικά με την εκκεντρότητα. Η ίδια τάση παρατηρείται και για τα άλλα δύο επίπεδα σεισμικής επικινδυνότητας (με πιθανότητα υπέρβασης 2% και 10% στα πενήντα

χρόνια), επαληθεύοντας την αξιοπιστία του λόγου στρέψης και στην ανελαστική περιοχή απόκρισης. Όμοια συμπεράσματα έχουν παρατηρηθεί και για κανονικά σε κάτοψη τετραώροφα κτήρια, τόσο σε απλά μοντέλα όσο και σε κτήρια ρεαλιστικών διαστάσεων υποβαλλόμενα σε μονοαξονική ή/και διαξονική σεισμική διέγερση, τα οποία δεν παρατίθενται εδώ για λόγους οικονομίας χώρου.

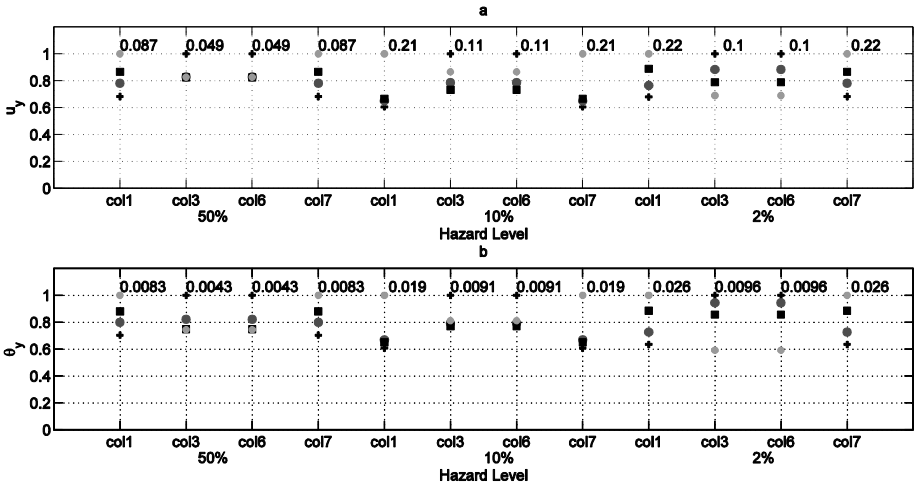

Εικόνα 12. Αριθμητική εφαρμογή 2 – Κανονικοποιημένες ως προς τη μέγιστη τιμή κατά την y διεύθυνση για κάθε επίπεδο σεισμικής επικινδυνότητας και κάθε σχεδιασμό – (a) μετατοπίσεις υποστηλωμάτων και (b) παραμορφώσεις υποστηλωμάτων.

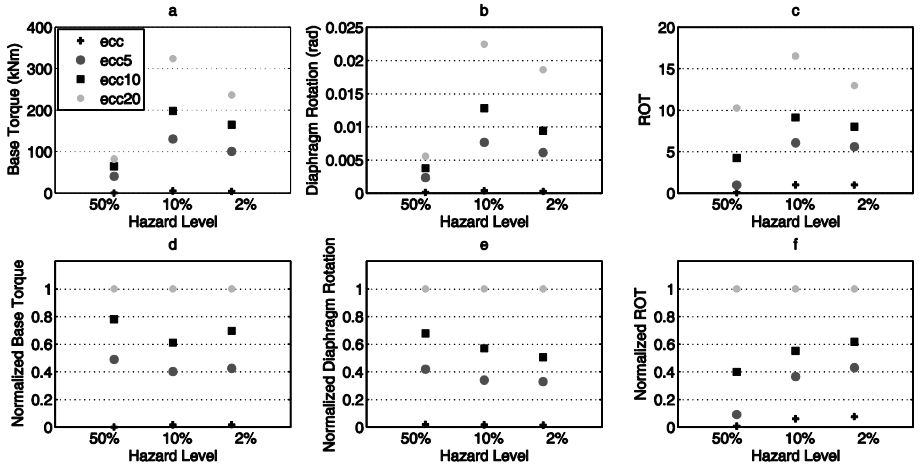

Εικόνα 13. Αριθμητική εφαρμογή 2 – (a) μέγιστη απόλυτη τιμή στρέψης βάσης, (b) μέγιστη απόλυτη τιμή στροφής οροφής διαφράγματος, (c) μέγιστη απόλυτη τιμή λόγου στρέψης (ROT), (d) κανονικοποιημένη ως προς τη μέγιστη τιμή στρέψη βάσης, (e) κανονικοποιημένη ως προς τη μέγιστη τιμή στροφή οροφής και (f) κανονικοποιημένος ως προς τη μέγιστη τιμή λόγος στρέψης (ROT) για όλα τα επίπεδα σεισμικής επικινδυνότητας και όλους τους σχεδιασμούς.

Ο λόγος στρέψης εκτός από δείκτης αποτίμησης επεκτείνεται και σε δείκτη σχεδιασμού, μέσω της διαδικασίας βελτιστοποίησης ελαχιστοποιώντας το ποσοστό των πρόσθετων τεμνουσών δυνάμεων λόγω στρέψης (torsion-induced forces).

Δεδομένου ότι ο κύριος στόχος των σύγχρονων αντισεισμικών κανονισμών είναι η προστασία της ανθρώπινης ζωής, είναι φανερό ότι θα πρέπει να ληφθούν υπόψη επιπλέον κριτήρια σχετικά με την επίδοση της κατασκευής, τα οποία να περιορίζουν τις οικονομικές απώλειες καθώς και δείκτες βλάβης ώστε να ποσοτικοποιηθεί η τρωτότητα των κατασκευών σε ενδεχόμενο σεισμικό γεγονός. Έτσι άρχισε να υιοθετείται μία νέα θεώρηση σχεδιασμού με κριτήρια επιτελεστικότητας (performance-based design). Συμφωνά με το σχεδιασμό με βάση την επιτελεστικότητα η κατασκευή ελέγχεται για διάφορα επίπεδα σεισμικής έντασης. Σε αντίθεση με τον Ευρωκώδικα όπου μόνο δύο επίπεδα επιτελεστικότητας λαμβάνονται υπόψη, η οριακή κατάσταση λειτουργικότητας και η οριακή κατάσταση αστοχίας. Για παράδειγμα η FEMA-356 προτείνει τέσσερα επίπεδα επιτελεστικότητας: το επίπεδο λειτουργικότητας, το επίπεδο άμεσης χρήσης, το επίπεδο προστασίας ζωής και το επίπεδο αποφυγής κατάρρευσης. Αξίζει να σημειωθεί ότι η σεισμική ένταση ορίζεται ως συνάρτηση της πιθανότητας υπέρβασης του σεισμού σχεδιασμού κατά τη διάρκεια του χρόνου ζωής της κατασκευής ο οποίος συνήθως λαμβάνεται ίσως με 50 χρόνια. Η σπουδαιότητα μιας κατασκευής λαμβάνεται υπόψη χρησιμοποιώντας για κάθε επίπεδο επιτελεστικότητας σεισμό με κατάλληλη περίοδο επαναφοράς.

Στο πλαίσιο του αντισεισμικού σχεδιασμού με βάση την επιτελεστικότητα γίνεται διαχωρισμός μεταξύ ικανότητας και απαίτησης. Με τον όρο απαίτηση εννοούνται οι επιβαλλόμενες μετατοπίσεις (ή εναλλακτικά, παραμορφώσεις, καμπυλότητες, στροφές και γωνίες σχετικής μετακίνησης δύο ορόφων) λόγω της σεισμικής φόρτισης, ενώ με τον όρο ικανότητα εννοείται η μέγιστη μετατόπιση (ή εναλλακτικά, παραμόρφωση, καμπυλότητα, στροφή και γωνία σχετικής μετακίνησης) που μπορεί να αναπτύξει μια κατασκευή, ένα μέλος της ή μια διατομή της [11].

Οι αντισεισμικοί σχεδιασμοί με βάση την επιτελεστικότητα στοχεύουν στην απόκριση της κατασκευής με ελεγχόμενες βλάβες-ζημιές για τα διάφορα επίπεδα σεισμικής επικινδυνότητας. Προκειμένου να υλοποιηθεί αυτή η αντίληψη

σχεδιασμού απαιτείται η ποσοτικοποίηση της βλάβης με δείκτες βλάβης, των οποίων οι τιμές μπορούν να συσχετισθούν με συγκεκριμένη κατάσταση βλάβης του κτηρίου.

Στη συνέχεια της διατριβής αναζητώνται οι βέλτιστοι σχεδιασμοί των κατασκευών που θα προκύψουν μέσω μη-γραμμικής δυναμικής ανάλυσης. Με τον όρο ‘βέλτιστος δομοστατικός σχεδιασμός’ εννοούμε την εύρεση του καλύτερου δυνατού σχεδιασμού που μπορεί να εξευρεθεί στο πλαίσιο ενός πολύπλοκου πολύ-παραμετρικού προβλήματος βελτιστοποίησης, και όχι τον “μαθηματικά” βέλτιστο σχεδιασμό ο οποίος είναι δύσκολο εώς αδύνατο να εξευρεθεί. Οι Στρατηγικές Εξέλιξης είναι Δαρβίνειες μέθοδοι βελτιστοποιήσης οι οποίες μέσα από διαδοχικές βελτιώσεις του σχεδιασμού οδηγούν την αντικειμενική συνάρτηση στο ”καθολικό” της βέλτιστο.

Για τον υπολογισμό του βέλτιστου σχεδιασμού αρχικά είναι απαραίτητη η μαθηματική διατύπωση του προβλήματος και στη συνέχεια η επίλυση του με τη βοήθεια ενός αλγόριθμου βελτιστοποίησης. Αρχικά πρέπει να ορισθούν οι παράμετροι σχεδιασμού και η μεταξύ τους σχέση. Στη συνέχεια να καθοριστεί η προς βελτιστοποίηση συνάρτηση και οι περιορισμοί του προβλήματος. Η διαδικασία ολοκληρώνεται με την επιλογή του κατάλληλου αλγόριθμου βελτιστοποίησης και την εφαρμογή του για την τελική επίλυση του προβλήματος. Οι περιορισμοί του προβλήματος συνήθως αναφέρονται στο εύρος στο οποίο κινούνται οι παράμετροι σχεδιασμού και επιβάλλονται μέσω των συναρτήσεων περιορισμού καθορίζοντας το χώρο αποδεκτών λύσεων του προβλήματος. Ακολούθως παρουσιάζεται ο αλγόριθμος στρατηγικών εξέλιξης που χρησιμοποιήθηκε στη διατριβή.

Ένα συνεχές πρόβλημα βέλτιστου σχεδιασμού μπορεί να διατυπωθεί ως εξής:

$$\begin{aligned} &\min F(\boldsymbol{s}) \\ &\boldsymbol{s} = \{s_1, s_2, ..., s_n\}^T \\ &l_i \le s_i \le u_i, i = 1, 2, ..., n \\ &g_j(\boldsymbol{s}) \ge 0,\ j = 1, 2, ..., m \\ &h_j(\boldsymbol{s}) = 0,\ j = m+1, m+2, ..., t \end{aligned} \tag{23}$$

όπου $\boldsymbol{s}$ είναι το διάνυσμα των μεταβλητών σχεδιασμού, l_i, u_i είναι το κάτω και το άνω όριο της μεταβλητής σχεδιασμού s_i, $F(\boldsymbol{s})$ είναι η αντικειμενική συνάρτηση ενώ $g_j(\boldsymbol{s}), h_j(\boldsymbol{s})$ είναι οι συναρτήσεις περιορισμού ανισοτήτων και ισοτήτων αντίστοιχα.

Εκτός από τα συνεχή προβλήματα βέλτιστου σχεδιασμού, υπάρχουν τα διακριτά και τα μεικτού τύπου προβλήματα. Διακριτά ονομάζονται τα προβλήματα εκείνα στα οποία οι μεταβλητές σχεδιασμού παίρνουν διακριτές τιμές. Ενώ μεικτού τύπου ονομάζονται τα προβλήματα εκείνα στα οποία οι μεταβλητές σχεδιασμού παίρνουν τόσο συνεχείς όσο και διακριτές τιμές.

Ένα διακριτό πρόβλημα βέλτιστου σχεδιασμού διατυπώνεται ως εξής:

$$\begin{aligned} &\min F(\boldsymbol{s}) \\ &\boldsymbol{s} = \{s_1, s_2, ..., s_n\}^T \\ &l_i \le s_i \le u_i, i = 1, 2, ..., n \\ &\boldsymbol{s}_i \in R^d, i = 1, 2, ..., n \\ &g_j(\boldsymbol{s}) \ge 0,\ j = 1, 2, ..., m \\ &h_j(\boldsymbol{s}) = 0,\ j = m+1, m+2, ..., t \end{aligned} \tag{24}$$

όπου R^d είναι το πεδίο τιμών των διακριτών μεταβλητών σχεδιασμού $\boldsymbol{s}$.

Ως μεταβλητές σχεδιασμού ορίζονται εκείνες οι παράμετροι, οι οποίες όταν λάβουν συγκεκριμένη τιμή καθορίζουν πλήρως ένα σχεδιασμό. Όταν κάποιοι περιορισμοί παραβιάζονται από ένα συνδυασμό μεταβλητών τότε ο σχεδιασμός καλείται ανέφικτος, στην αντίθετη περίπτωση ονομάζεται εφικτός. Ένας εφικτός σχεδιασμός δεν είναι πάντα βέλτιστος αλλά είναι πάντα εφαρμόσιμος. Η κατάλληλη προσομοίωση βασίζεται στην σωστή επιλογή των μεταβλητών σχεδιασμού. Απαραίτητη προϋπόθεση είναι οι μεταβλητές να είναι ανεξάρτητες μεταξύ τους. Καθώς σε περίπτωση που κάποια μεταβλητή είναι εξαρτημένη από κάποια άλλη τότε παύει πλέον να είναι μεταβλητή, αλλά μία παράμετρος η οποία λαμβάνει τιμές σύμφωνα με την μεταβλητή από την οποία εξαρτάται. Επιπλέον η αντικειμενική συνάρτηση οφείλει να είναι επαρκώς εξαρτώμενη από όλες τις παραμέτρους σχεδιασμού. Για τον λόγο αυτό πριν την τελική επιλογή του μαθηματικού μοντέλου βελτιστοποίησης συνίσταται η διενέργεια μιας ανάλυσης ευαισθησίας ώστε να

ελεγχθεί το μέγεθος ευαισθησίας της αντικειμενικής συνάρτησης σε σχέση με όλες τις παραμέτρους σχεδιασμού. Ως αντικειμενική συνάρτηση ορίζεται το κριτήριο εκείνο βάσει του οποίου επιλέγεται ο βέλτιστος σχεδιασμός από ένα σύνολο εφικτών σχεδιασμών. Ένα πρόβλημα μπορεί να συνίσταται από περισσότερες από μία αντικειμενικές συναρτήσεις. Τα προβλήματα αυτού του τύπου ονομάζονται προβλήματα βελτιστοποίησης με πολλαπλές αντικειμενικές συναρτήσεις ή αλλιώς προβλήματα Pareto. Κάθε απαίτηση του σχεδιασμού εισάγεται στο μαθηματικό πρόβλημα βελτιστοποίησης με τη μορφή ανισοτήτων και ισοτήτων, οι οποίες αντιπροσωπεύουν τους περιορισμούς του προβλήματος. Κάθε περιορισμός πρέπει να εξαρτάται από τουλάχιστον μία μεταβλητη σχεδιασμού ώστε να έχει φυσικό νόημα. Μία συνάρτηση περιορισμού ονομάζεται ανενεργός όταν ικανοποιείται αυστηρώς η ανισότητα $g_j(\boldsymbol{s}^*) < 0$. Η ανισοτική συνάρτηση περιορισμού θεωρείται ότι παραβιάζεται για τον σχεδιασμό $\boldsymbol{s}^*$ στην περίπτωση που λαμβάνει θετική τιμή $g_j(\boldsymbol{s}^*) > 0$. Αντίστοιχα, μία ισοτική συνάρτηση περιορισμού $h_j(\boldsymbol{s}) = 0$ θεωρείται ότι παραβιάζεται στο σημείο $\boldsymbol{s}^*$ αν δεν ισχύει η ισότητα $h_j(\boldsymbol{s}^*) \neq 0$. Συνεπώς κάθε εφικτός σχεδιασμός ορίζεται από ενεργές ή ανενεργές ανισοτικές συναρτήσεις περιορισμού καθώς και από ενεργές ισοτικές συναρτήσεις περιορισμού. Προκειμένου να εντοπιστούν οι ενεργές συναρτήσεις περιορισμού πρέπει πρώτα οι συναρτήσεις τους να κανονικοποιηθούν ώστε να είναι εφικτή η σύγκρισή τους .

Όπως προαναφέρθηκε στην παρούσα εργασία χρησιμοποιήθηκε η μέθοδος Στρατηγικών Εξέλιξης. Η μέθοδος των Στρατηγικών Εξέλιξης [14], [15], [16] κατατάσσεται στην κατηγορία των Δαρβίνειων μεθόδων ή αλλιώς εξελικτικών αλγορίθμων. Το όνομα τους αποδίδεται στο γεγονός ότι μιμούνται τη διαδικασία εξέλιξης των ειδών στη φύση, όπως παρουσιάστηκε από το Δαρβίνο και ανήκουν στις τυχηματικές μεθόδους βελτιστοποίησης. Άλλες μέθοδοι Εξελικτικών Αλγορίθμων είναι η μέθοδος των Γενετικών Αλγορίθμων [17], η μέθοδος του Εξελικτικού Προγραμματισμού [18] και η μέθοδος του Γενετικού Προγραμματισμού [19]. Σε αυτή την κατηγορία ανήκει και η διαφορετικής τεχνικής μέθοδος της Προσομοίωσης Ανόπτησης [20].

Σύμφωνα με τη μέθοδο των Στρατηγικών Εξέλιξης ένας πληθυσμός ανεξάρτητων σχεδιασμών χρησιμοποιείται σε κάθε βήμα της διαδικασίας. Αρχικά

επιλέγεται με τυχαίο τρόπο ο αρχικός πληθυσμός. Στη συνέχεια με τη χρήση των τελεστών ανασυνδυασμού, μετάλλαξης και επιλογής, ο αρχικός πληθυσμός εξελίσσεται. Με κριτήριο την επιβίωση του ισχυροτέρου (survival of the fittest) οδηγούμαστε στη βέλτιστη λύση. Η μέθοδος των Στρατηγικών Εξέλιξης έχει εφαρμοστεί στον χώρο του βέλτιστου σχεδιασμού κατασκευών [21], [22]. Το βασικό της πλεονέκτημα είναι ότι λόγω της τυχηματικότητας του τρόπου της έρευνας του χώρου σχεδιασμού έχει περισσότερες πιθανότητες για την έυρεση του απόλυτα βέλτιστου σχεδιασμού σε σχέση με τις μαθηματικές μεθόδους. Ειδικότερα, σε δύσκολα προβλήματα βελτιστοποίησης με πολλά τοπικά ελάχιστα ή για προβλήματα με πολλαπλές αντικειμενικές συναρτήσεις [11].

Στην παρούσα εργασία χρησιμοποιήθηκε η μέθοδος των Στρατηγικών Εξέλιξης πολλών μελών. Σύμφωνα με αυτή τη μέθοδο η επιλογή των μελών της επόμενης γενιάς γίνεται από τα ικανότερα μέλη μεταξύ των μ γονέων και των λ απογόνων και ονομάζονται ($\mu+\lambda$)ESs. Με βάση αυτό το μοντέλο ένας γονέας με ανώτερη ικανότητα επιβίωσης των υπολοίπων μελών του πληθυσμού συμμετέχει στη διαδικασία αναπαραγωγής για περισσότερες γενιές. Η ικανότητα επιβίωσης κάθε μέλους του πληθυσμού καθορίζεται από την τιμή της αντικειμενικής συνάρτησης. Το δεύτερο μοντέλο επιλογής είναι το (μ,λ)ESs όπου κάθε γονέας έχει χρόνο ζωής ίσο με μία γενιά. Οι γονείς της επόμενης γενιάς επιλέγονται από τους απογόνους μόνο της προηγούμενης.

Η διαδικασία βελτιστοποίησης στοχεύει στην ταυτόχρονη εξεύρεση ενός ικανοποιητικού ελαχίστου της αντικειμενικής συνάρτησης και στην ικανοποίηση όλων των περιορισμών του αντισεισμικού κανονισμού καθώς και των αρχιτεκτονικών περιορισμών για διάφορα επίπεδα σεισμικής επικινδυνότητας. Εκτός από τον προτεινόμενο δείκτη και το κόστος κατασκευής ως αντικειμενικές συναρτήσεις στην παρούσα διατριβή χρησιμοποιήθηκαν επίσης η εκκεντρότητα ως προς την ακαμψία και ως προς την αντοχή προκειμένου να μελετηθεί η επιρροή του φαινομένου της στρέψης στην απόκριση της κατασκευής για όλα τα επίπεδα σεισμικής επικινδυνότητας.

Η αποτίμηση των βέλτιστων σχεδιασμών που προέκυψαν με ελαχιστοποίηση των ανωτέρω αντικειμενικών συναρτήσεων πραγματοποιείται με υποβολή των

τελικών σχεδιασμών σε μη γραμμικες δυναμικές αναλύσεις για όλα τα επίπεδα σεισμικής επικινδυνότητας. Ακολουθεί η υπέρθεση των περιβαλλουσών των χρονοιστοριών τέμνουσας βάσης-στρέψης βάσης για την εύρεση του σχεδιασμού με την ελάχιστη επιρροή του στρεπτικού φαινομένου.

Αριθμητική Εφαρμογή 3

Στην τρίτη αριθμητική εφαρμογή αποτιμώνται οι βέλτιστοι αντισεισμικοί σχεδιασμοί που προέκυψαν για το κανονικό σε κάτοψη απλό μοντέλο της Εικόνας 14. Στην εικόνα 14 φαίνονται επίσης και οι βέλτιστοι σχεδιασμοί που προέκυψαν χρησιμοποιώντας το κόστος, τη στατική εκκεντρότητα, την εκκεντρότητα αντοχής και το λόγο στρέψης ως αντικειμενικές συναρτήσεις, ενώ ταυτόχρονα ικανοποιούνται οι περιορισμοί που επιβάλλονται από τον Ευρωκώδικα 8 για τις περιπτώσεις CASE A, CASE B, CASE C και CASE D αντίστοιχα. Για τις ίδιες αντικειμενικές συναρτήσεις αλλά υπό τους περιορισμούς σχεδιασμού με βάση την επιτελεστικότητα απεικονίζονται οι βέλτιστες κατόψεις επίσης στην Εικόνα 14 ως CASE E, CASE F, CASE G και CASE H αντίστοιχα. Οι βέλτιστοι σχεδιασμοί που προέκυψαν υποβλήθηκαν σε 2 σεισμικές διεγέρσεις για κάθε επίπεδο σεισμικής επικινδυνότητας προκειμένου να αποτιμηθεί η αντισεισμική τους συμπεριφορά. Οι χρονοϊστορίες τέμνουσας βάσης - στρέψης βάσης καταγράφηκαν και οι περιβάλλουσες τους συγκρίθηκαν ώστε να αξιολογηθεί η επιρροή του στρεπτικού φαινομένου στην απόκριση των βέλτιστων σχεδιασμών. Στην εικόνα 15 απεικονίζονται οι χρονοϊστορίες τέμνουσας βάσης – στρέψης βάσης του βέλτιστου σχεδιασμού που προέκυψε με αντικειμενική συνάρτηση το κόστος υποβαλλόμενο στου περιορισμούς του Ευρωκώδικα 8 για συνήθη σεισμικά φαινόμενα (πιθανότητα υπέρβασης 50% στα πενήντα χρόνια). Στις επόμενες εικόνες γίνεται υπέρθεση των περιβαλλουσών χρονοιστοριών τέμνουσας βάσης – στρέψης βάσης για όλους τους σχεδιασμούς και όλα τα επίπεδα σεισμικής επικινδυνότητας.

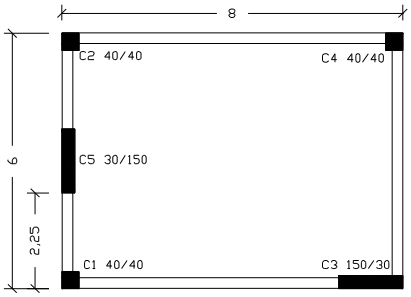

Initial Layout

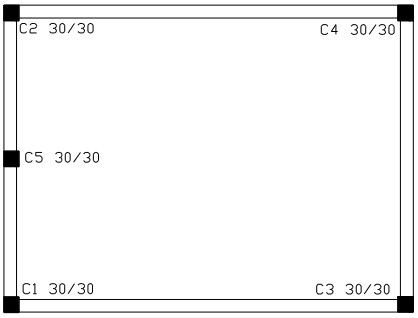

Cases A,B

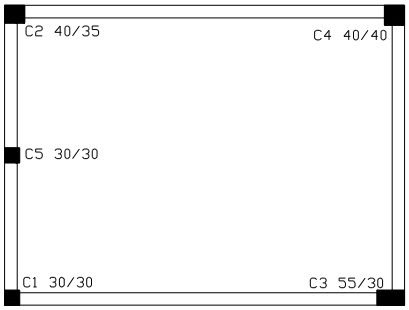

Case C

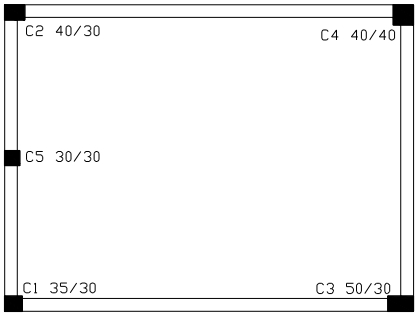

Case D

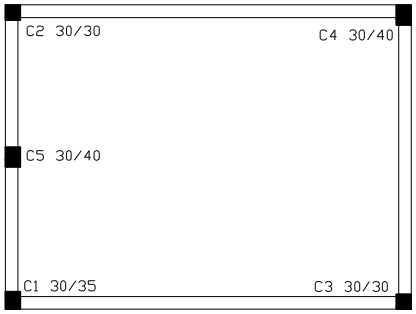

Case E

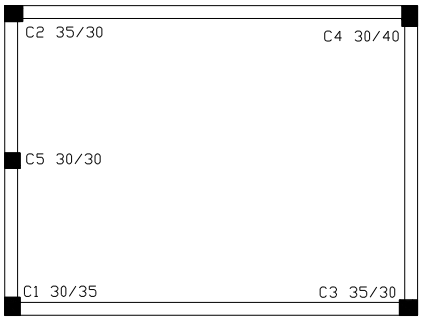

Case F

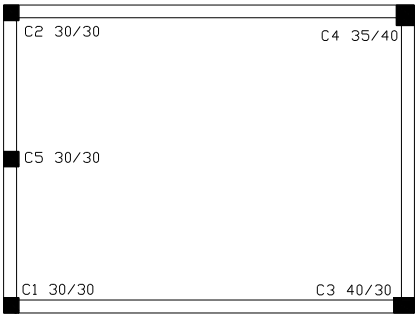

Case G

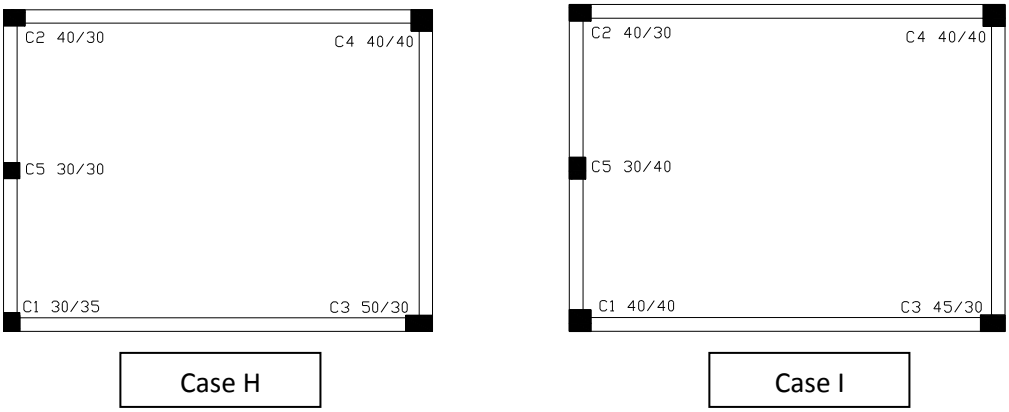

Εικόνα 14. Αριθμητική εφαρμογή 3 – Αρχικός και βελτιστοποιημένοι σχεδιασμοί για όλες τις αντικειμενικές συναρτήσεις.

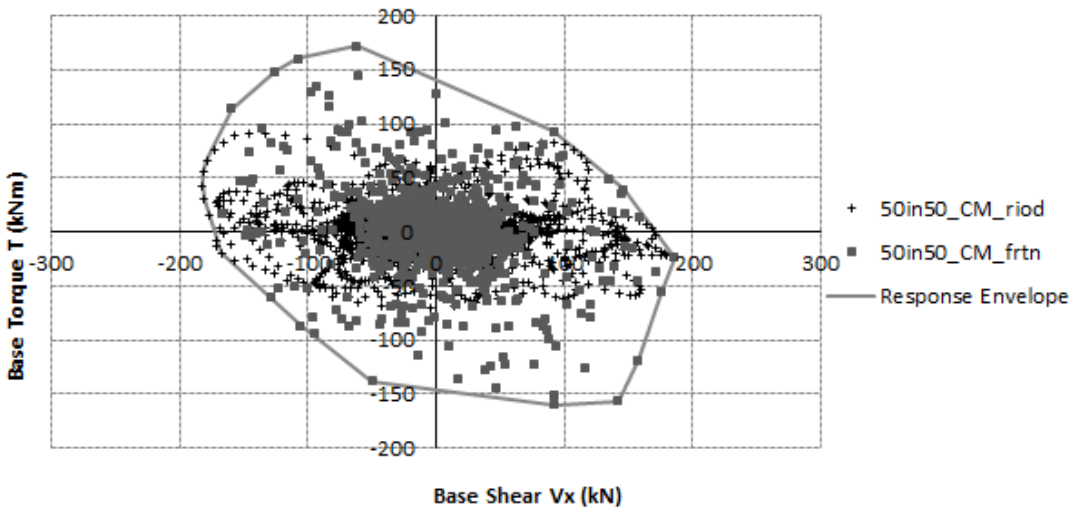

Εικόνα 15. Αριθμητική εφαρμογή 3 – Χρονοιστορίες τέμνουσας βάσης – στρέψης βάσης και η περιβάλλουσα για το σχεδιασμό της CASE A για συνήθη σεισμικά φαινόμενα.

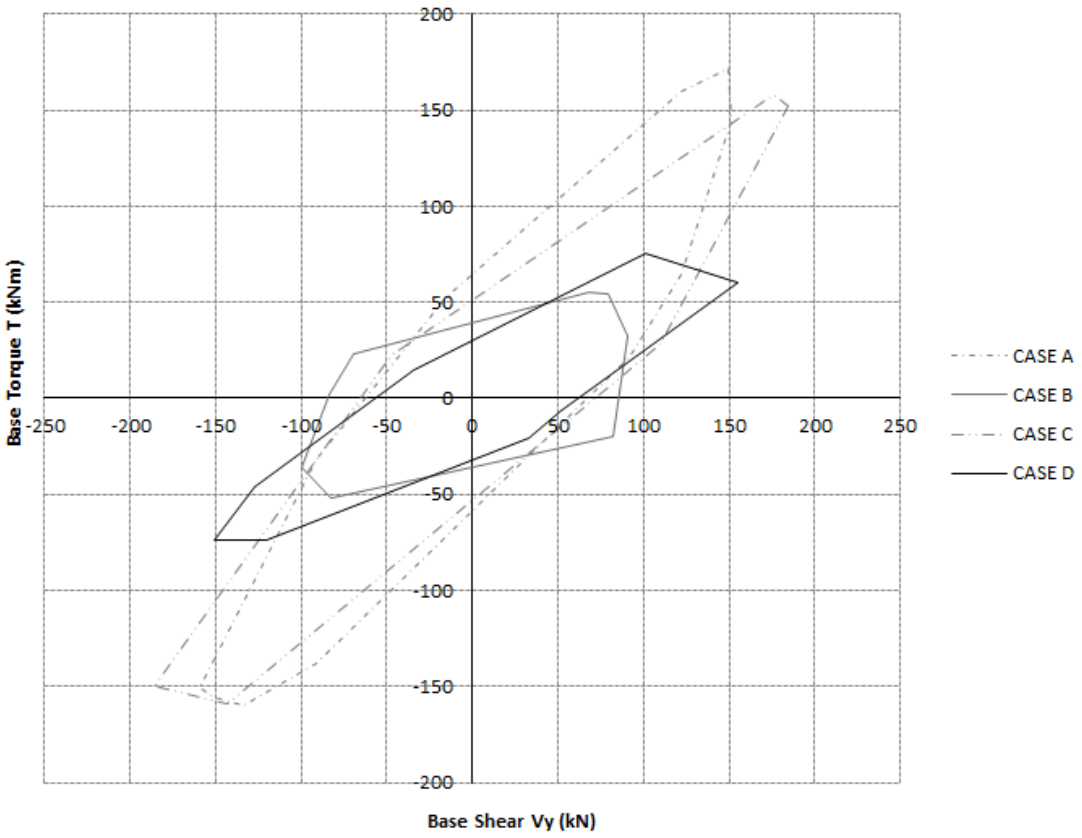

Εικόνα 16. Αριθμητική εφαρμογή 3 – Περιβάλλουσες χρονοϊστοριών τέμνουσας βάσης – στρέψης βάσης κατά την *y* διεύθυνση για συχνά σεισμικά φαινόμενα (50in50) για όλα τα κριτήρια υπό τους περιορισμούς που επιβάλλονται από τον Ευρωκώδικα 8.

Όπως φαίνεται από την εικόνα 16, οι σχεδιασμοί οι οποίοι βελτιστοποιήθηκαν με αντικειμενική συνάρτηση το λόγο στρέψης και την εκκεντρότητα ακαμψίας ανέπτυξαν μικρότερη στρέψη βάσης σε σύγκριση με εκείνους που βελτιστοποιήθηκαν βάσει του κόστους και της εκκεντρότητας αντοχής υποβαλλόμενοι στους περιορισμούς του Ευρωκώδικα 8 για συχνά σεισμικά φαινόμενα. Όμοια συμπεράσματα προκύπτουν και για περιστασιακά και σπάνια σεισμικά γεγονότα (Εικόνες 18, 20).

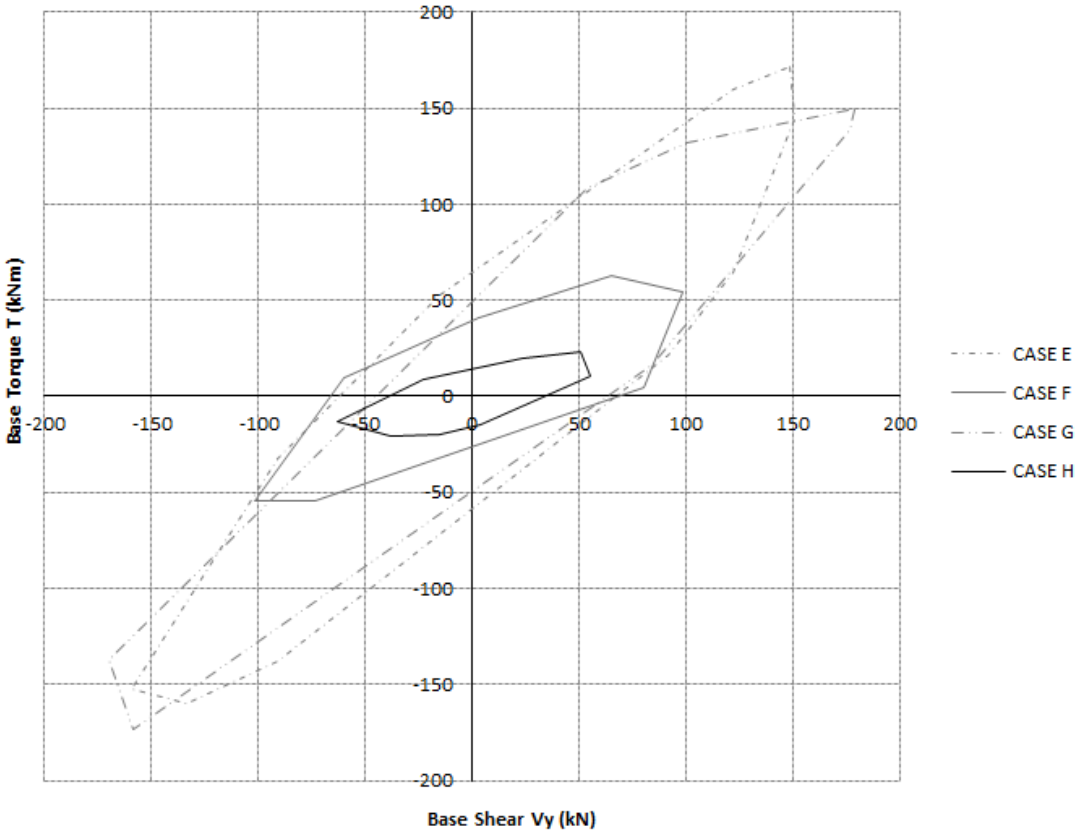

Εικόνα 17. Αριθμητική εφαρμογή 3 – Περιβάλλουσες χρονοϊστοριών τέμνουσας βάσης – στρέψης βάσης κατά την *y* διεύθυνση για συχνά σεισμικά φαινόμενα (50in50) για όλα τα κριτήρια υπό τους περιορισμούς που επιβάλλονται από τον σχεδιασμό με βάση την επιτελεστικότητα.

Στην εικόνα 17 παρουσιάζονται οι περιβάλλουσες χρονοϊστοριών τέμνουσας βάσης – στρέψης βάσης για όλους τους σχεδιασμούς υποβαλλόμενους σε περιορισμούς βάσει της επιτελεστικότητας για συχνά σεισμικά φαινόμενα. Οι σχεδιασμοί με αντικειμενικό κριτήριο το λόγο στρέψης και την εκκεντρότητα ακαμψίας και σε αυτή την περίπτωση έχουν την καλύτερη επίδοση καθώς αναπτύσσουν την μικρότερη στρέψη βάσης. Τα ίδια συμπεράσματα εξάγονται για περιστασιακά και σπάνια σεισμικά φαινόμενα (Εικόνες 19,21).

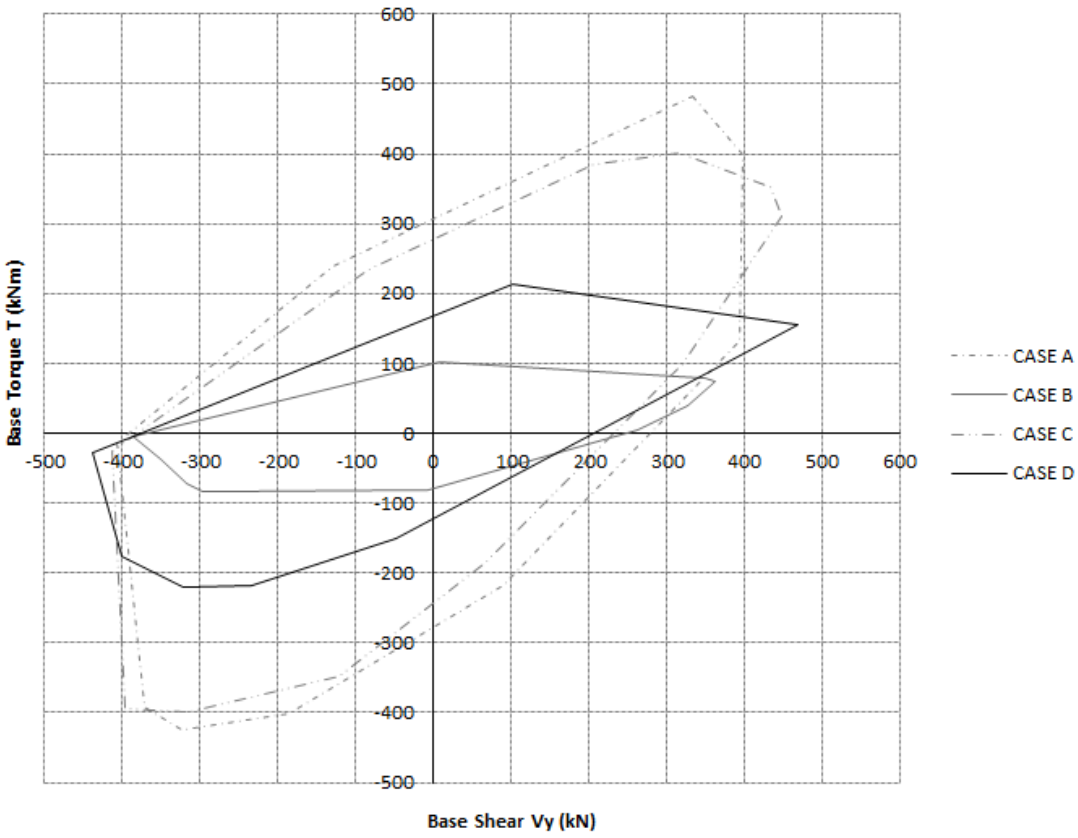

Εικόνα 18. Αριθμητική εφαρμογή 3 – Περιβάλλουσες χρονοϊστοριών τέμνουσας βάσης – στρέψης βάσης κατά την y διεύθυνση για περιστασιακά σεισμικά φαινόμενα (10in50) για όλα τα κριτήρια υπό τους περιορισμούς που επιβάλλονται από τον Ευρωκώδικα 8.

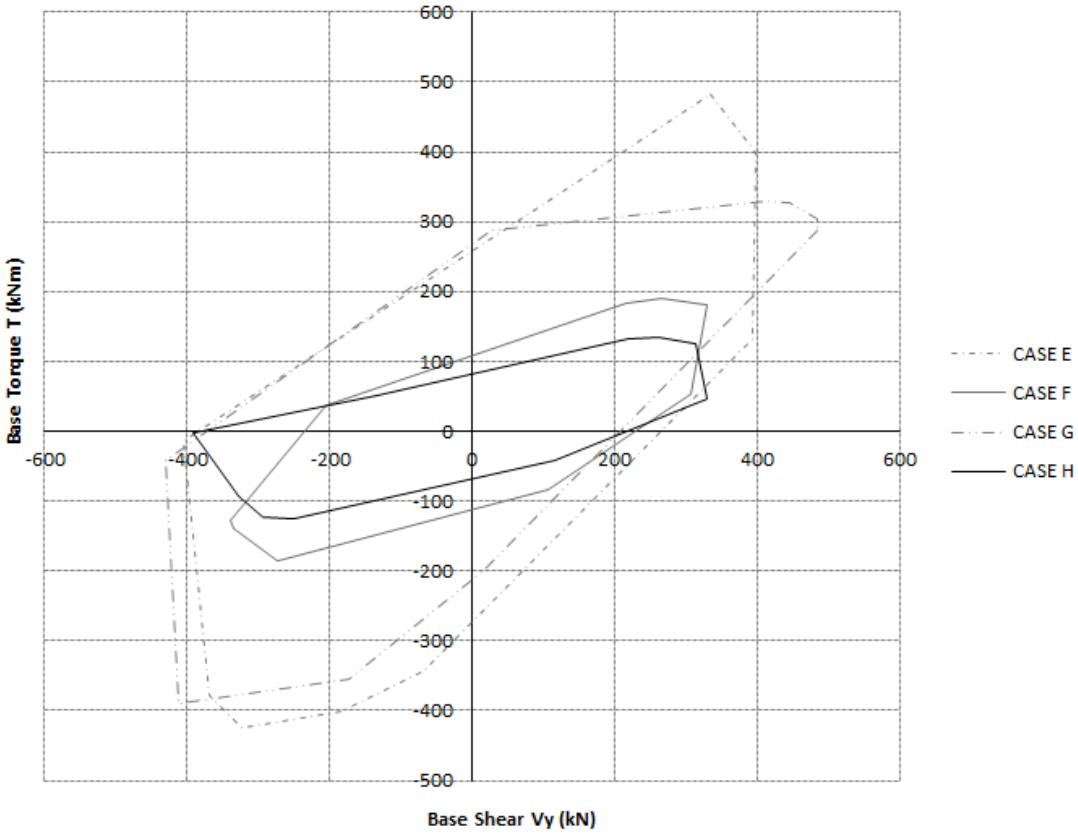

Εικόνα 19. Αριθμητική εφαρμογή 3 – Περιβάλλουσες χρονοϊστοριών τέμνουσας βάσης – στρέψης βάσης κατά την y διεύθυνση για περιστασιακά σεισμικά φαινόμενα (10in50) για όλα τα κριτήρια υπό τους περιορισμούς που επιβάλλονται από τον σχεδιασμό με βάση την επιτελεστικότητα.

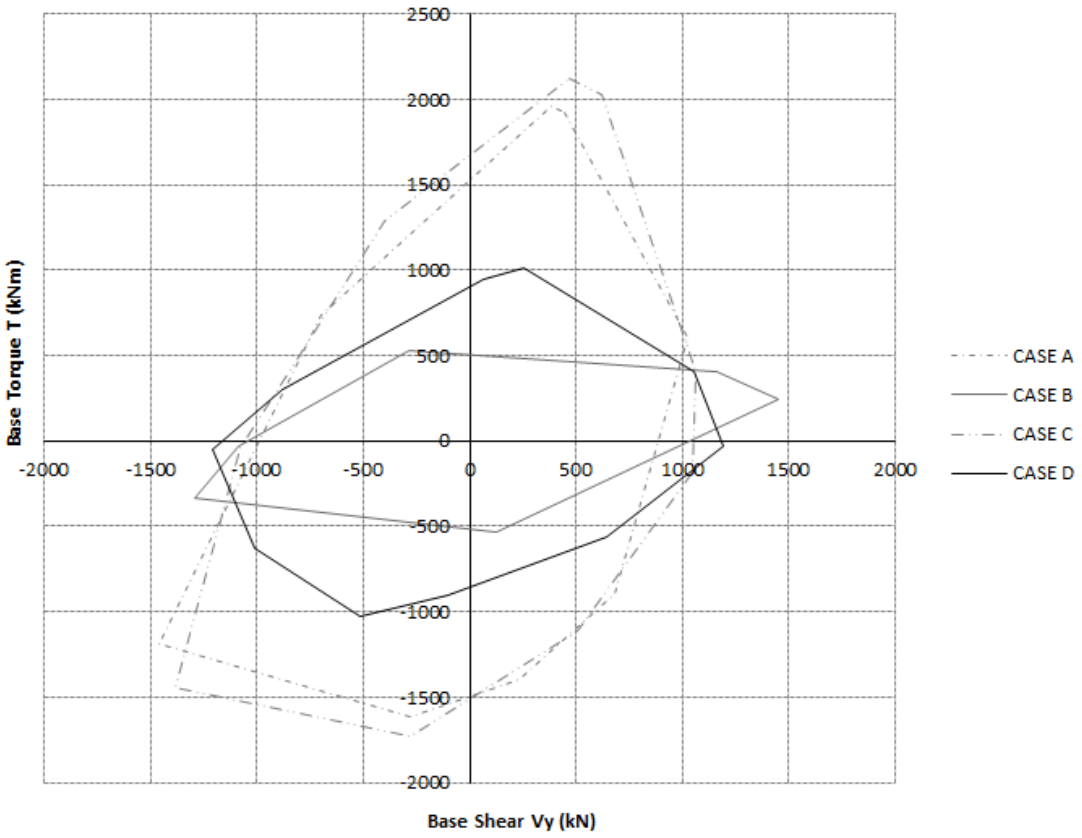

Εικόνα 20. Αριθμητική εφαρμογή 3 – Περιβάλλουσες χρονοϊστοριών τέμνουσας βάσης – στρέψης βάσης κατά την y διεύθυνση για σπάνια σεισμικά φαινόμενα (2in50) για όλα τα κριτήρια υπό τους περιορισμούς που επιβάλλονται από τον Ευρωκώδικα 8.

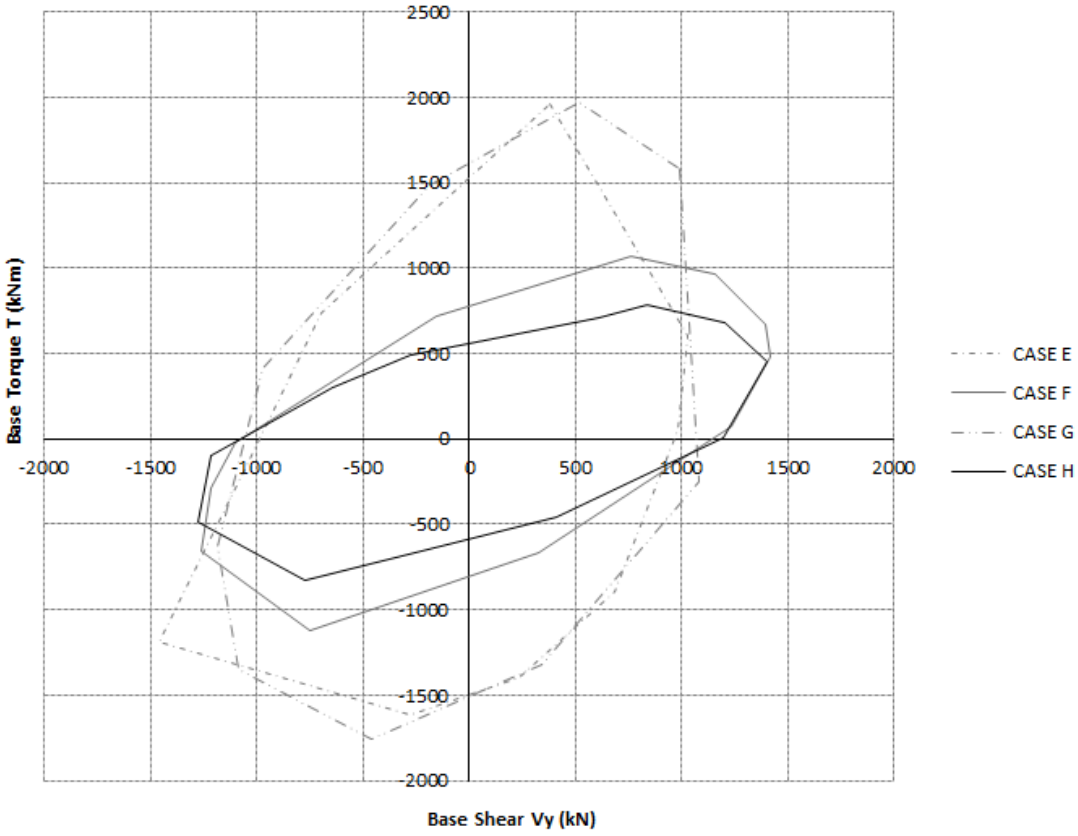

Εικόνα 21. Αριθμητική εφαρμογή 3 – Περιβάλλουσες χρονοϊστοριών τέμνουσας βάσης – στρέψης βάσης κατά την y διεύθυνση για σπάνια σεισμικά φαινόμενα (2in50) για όλα τα κριτήρια υπό τους περιορισμούς που επιβάλλονται από τον σχεδιασμό με βάση την επιτελεστικότητα.

Πρέπει να σημειωθεί ότι όμοια συμπεράσματα έχουν εξαχθεί και για μη κανονικό σε κάτοψη κτήριο, δεν παρατίθεται εδώ για λόγους οικονομίας χώρου. Η απόδοση των σχεδιασμών που βελτιστοποιήθηκαν βάσει του προτεινόμενου κριτηρίου σημειώθηκε για όλες τις περιπτώσεις και όλα τα σεισμικά επίπεδα επικινδυνότητας ανάμεσα στις δύο καλύτερες τόσο σε κανονικά σε κάτοψη κτήρια όσο και σε μη κανονικά. Σε αντίθεση με τα υπόλοιπα κριτήρια των οποίων η συμπεριφορά για κάποια επίπεδα σεισμικής επικινδυνότητας ήταν ικανοποιητική ενώ για κάποια άλλα όχι.

Συνοψίζοντας, στην παρούσα διατριβή παρατηρήθηκε ότι:

- Για απλά μοντέλα, τα εντατικά μεγέθη που σχετίζονται με τη στρεπτική απόκριση της κατασκευής – στρέψη βάσης, στροφή οροφής και λόγος στρέψης – αυξάνονται μονοτονικά με την εκκεντρότητα για όλα τα επίπεδα σεισμικής επικινδυνότητας. Ενώ για μοντέλα ρεαλιστικών

διαστάσεων η στρέψη βάσης και η στροφή οροφής δεν ακολουθούν πάντα την ίδια τάση μεταβολής. Ο λόγος στρέψης ακολουθεί πάντα την τάση μεταβολής της στρέψης βάσης.

- Προτείνεται νέος δείκτης αποτίμησης στρεπτικού φαινομένου στην απόκριση των κατασκευών, ο λόγος στρέψης. Ο προτεινόμενος δείκτης ποσοτικοποιεί το φαινόμενο σε όρους τεμνουσών δυνάμεων και εκφράζει το ποσοστό μεγέθυνσης αυτών λόγω στρεπτικού φαινομένου. Η τιμή του δείκτη για συμμετρικά κτήρια είναι μηδενική. Συνεπώς, σε αντίθεση με όλα τα άλλα εντατικά μεγέθη που σχετίζονται με τη στρέψη, δεν χρειάζεται ανάλυση του συμμετρικού αντιστοίχου της κατασκευής.
- Η ήδη παρατηρημένη τάση μεταβολής των εντατικών μεγεθών (τέμνουσες δυνάμεις, μετατοπίσεις, παραμορφώσεις) για κανονικά σε κάτοψη δύστρεπτα κτήρια – αύξηση τους στην εύκαμπτη πλευρά και μείωση στη δύσκαμπτη – επιβεβαιώθηκε και για μη κανονικά σε κάτοψη κτήρια.
- Το κριτήριο αποτίμησης επίδρασης στρεπτικού φαινομένου μέσω της διαδικασίας βελτιστοποίησης επεκτείνεται σε κριτήριο σχεδιασμού. Η απόδοση των σχεδιασμών που προέκυψαν χρησιμοποιώντας ως αντικειμενική συνάρτηση το λόγο στρέψης είναι πάντα άναμεσα στις δύο καλύτερες σε σύγκριση με τα υπόλοιπα κριτήρια. Τα αποτελέσματα επιβεβαιώθηκαν και για μη κανονικά σε κάτοψη κτήρια. Αξίζει να σημειωθεί ότι η απόδοση του ήταν σταθερή για όλα τα επίπεδα σεισμικής επικινδυνότητας.
- Τέλος, ο προτεινόμενος δείκτης, λόγος στρέψης, μπορεί να αποτελέσει ένα χρήσιμο εργαλείο για τους μηχανικούς για την ποσοτικοποίηση της επίδρασης του στρεπτικού φαινομένου στην απόκριση της κατασκευής. Επιπλέον, λαμβάνοντας υπόψη ότι προκύπτει από την τιμή των τεμνουσών δυνάμεων, οι οποίες μπορούν να υπολογιστούν από οποιοδήποτε λογισμικό, είναι εύκολα εφαρμόσιμο σε κτήριο οποιασδήποτε γεωμετρίας.

ΑΝΑΦΟΡΕΣ:

[1] Marušić, D., Fajfar, P. (2005), On the inelastic seismic response of asymmetric buildings under bi-axial excitation, *Earthquake Engineering and Structural Dynamics*, **34**, 943-963.

[2] Kyrkos, T.M., Anagnostopoulos, A.S. (2013), Improved earthquake resistant design of eccentric steel buildings, *Soil Dynamics and Earthquake Engineering*, **47**, 144-156.

[3] Reem, H., Chopra, A.K., Earthquake Response of Torsionally-Coupled Buildings, Earthquake Engineering Research Center, College of Engineering, University of California at Berkeley, 1987.

[4] Makarios, T., Anastassiadis, A. (1998), Real and fictitious elastic axes of multi-storey buildings: theory, *The Structural Design of Tall and Special Buildings*, **7**(1), 33-55.

[5] Makarios, T., Anastassiadis, A. (1998), Real and fictitious elastic axes of multi-storey buildings: applications, *The Structural Design of Tall and Special Buildings*, **7**(1), 57-71.

[6] Paulay, T., Torsional mechanisms in ductile building systems, *Earthquake Engineering and Structural Dynamics* 1998; **27**:1101-1121.

[7] Paulay, T. (1998), Torsional mechanisms in ductile building systems, *Earthquake Engineering and Structural Dynamics*, **27**, 1101-1121.

[8] De La Llera, J.C., Chopra, A.K. (1995), Understanding the inelastic seismic behaviour of asymmetric plan buildings, *Earthquake Engineering and Structural Dynamics*, **24**, 549-572.

[9] De La Llera, J.C., Chopra, A.K. (1995), A simplified model for analysis and design of asymmetric plan buildings, *Earthquake Engineering and Structural Dynamics*, **24**, 573-594.

[10] EC8-Eurocode 8. (2004) Design provisions for earthquake resistance of structures. European StandardEN1998-1.

[11] Fragiadakis, M. (2006), 'Optimum Seismic Design of Structures using Nonlinear Analysis Methods', PhD Thesis, National Technical University of Athens, Greece.

[12] Kent, D.C., Park, R. (1971), Flexural members with confined concrete, *Journal of Structural Division*, **97**(7), 1969 – 1990.

[13] Scott, B.D., Park R., Priestley, M.J.N. (1982), Stress – Strain behavior of concrete confined by overlapping hoops at low and high strain rates, *ACI Journal*, **79**, 13 – 27.

[14] Rechenberg, I. (1973), 'Evolutionsstrategie: Optimierung technischer Systeme nach Principien der biologischen Evolution', Frommann-Holzboog, Stuttgart.

[15] Schwefel, H.P. (1977), 'Nuerische Optimierung von Computer-Modellen mittels der Evolutionsstrategie', Vol. 26 of Interdisciplinary Systems Research, Birkauser, Basel.

[16] Schwefel, H.P. (1981), 'Numerical optimization of computer models', Wiley & Sons, Chichester, UK.

[17] Holland, J.H. (1975), 'Adaptation in natural and artificial systems', University of Michigan Press, Ann Arbor.

[18] Fogel, L.J., Owens, A.J., Walsh, M.J. (1966), 'Artificial intelligence through simulated evolution', John Wiley, New York.

[19] Koza, J.R. (1992), 'Genetic Programming / On the programming of computers by means of natural selection', The MIT Press.

[20] Kirkpatric, S., Gelatt, C.D., Vecchi, M.P. (1983), Optimization by simulation annealing, *Science*, **220**, 671-680.

[21] Thierauf, G., Cai, J. (1994), Evolution Strategies, its parallelization and application to discrete optimization problems, NATO Advanced Research Workshop: Emergent Computing Methods in Engineering Design, Nafplio, Greece, August 25-27.

[22] Papadrakakis, M., Lagaros, N.D., Tsompanakis, Y. (1997), Structural optimization using evolution strategies and neural networks, *Fourth U.S. National Congress on Computational Mechanics*, San Francisco, USA, August 6-8.

Acknowledgements

I am deeply grateful to my advisor, Professor **Manolis Papadrakakis**, for his excellent guidance, his invaluable and discretionary support, his discreet presence and his confidence in me throughout all these years of my PhD research. His highly appreciated qualities such as his devotion to science, his great scientific inspiration, his kindness, his continuous availability, his enthusiastic encouragement towards students are beyond inspirational. I enjoyed the most working with him and his research team.

I would also like to thank the other two members of the PhD advisory committee: Associate Professor **Nikos D. Lagaros** of the School of Civil Engineering (NTUA), for his support, assistance, advice, encouragement and availability during the preparation of the current work and Associate Professor **Dimos Charmpis** of the Department of Civil and Environmental Engineering, University of Cyprus, for his availability whenever necessary. I also thank them for their time for the careful reading of the manuscript and their valuable comments and suggestions which contributed to improving the quality of the dissertation.

I would also like to thank all the research team of Professor Manolis Papadrakakis for their excellent collaboration and advice during my PhD research.

Finally, I am grateful to my family and my friends for their patience and support during my research activity.

Athens, Novemeber 2014
Chrysanthi Stathi

This dissertation has been co-financed by the European Union (European Social Fund – ESF) and Greek national funds through the Operational Program "Education and Lifelong Learning" of the National Strategic Reference Framework (NSRF) - Research Funding Program: Heracleitus II. Investing in knowledge society through the European Social Fund.

Η παρούσα έρευνα έχει συγχρηματοδοτηθεί από την Ευρωπαϊκή Ένωση (Ευρωπαϊκό Κοινωνικό Ταμείο - ΕΚΤ) και από εθνικούς πόρους μέσω του Επιχειρησιακού Προγράμματος <<Εκπαίδευση και Δια Βίου Μάθηση>> του Εθνικού Στρατηγικού Πλαισίου Αναφοράς (ΕΣΠΑ) – Ερευνητικό Χρηματοδοτούμενο Έργο: Ηράκλειτος ||. Επένδυση στην κοινωνία της γνώσης μέσω του Ευρωπαϊκού Κοινωνικού Ταμείου.

Table of Contents

List of Figures

List of Tables

1 INTRODUCTION

1.1 Introduction

Buildings subjected to ground shaking undergo simultaneously lateral as well as torsional motions if their structural plan views do not possess two axes of mass and stiffness symmetry. Coupled lateral-torsional motions can also occur in nominally symmetric buildings if ground shaking includes a torsional component or due to unforeseen conditions such as unbalanced load distributions or differences between actual and assumed mass and stiffness distributions. Lateral-torsional coupling causes the building to experience torsional moments and rotational deformations around vertical axes. Due to the rotational deformation, non-uniform distribution demand in lateral force resisting elements appear, which leads to increased damages in an eccentric building. The experience of past earthquakes such as Mexico City 1986 [1, 2] confirms the existence of this torsional effect. The vulnerability of asymmetric buildings has been addressed by building seismic design codes in the form of special torsional provisions. In most structural design codes, the effect of torsion is treated by implementing “accidental” and “static eccentricities” together with specific provisions for addressing the design of irregular buildings. Accidental eccentricity is defined as a percentile (e.g. 5%) of the plan view dimension that is perpendicular to the direction of the lateral forces applied. On the other hand the

implementation of the static eccentricity is more complicated, since it is defined with reference to the location of the rigidity center whose position, for the case of multistory buildings, is not unique and is load-dependent. It is for this reason that the efficiency of torsional codified provisions has been studied by many researchers.

Usually the investigations of asymmetric buildings are carried out using single-story structures generally asymmetric along one axis only. Lumped mass models with unidirectional resisting elements are adopted. Most of the studies use structural elements with ideal elasto-plastic behavior; more complicated constitutive models have also been used; examples of such models are bilinear models with post-yielding stiffness and hysteretic models (e.g. Clough model [3]) that account for element stiffness degradation under cyclic loading conditions.

The research effort on single-story models have been focusing on the inelastic behavior of structural elements, the effects of bi-directional excitation and the influence of the ground motion intensity. In particular, inelastic behavior is of great interest, since the ability of structures to withstand strong earthquakes depends upon their ductility and capacity for energy dissipation. Investigations have also been conducted with reference to double eccentric models, besides to the monosymmetric used so far. In spite of extensive research efforts, the complexity of inelastic seismic response and the large number of parameters influencing the behavior of irregular buildings, as compared to their elastic counterparts, has lead to a lack of general and universally accepted conclusions. Hence, drawing some definitive conclusions on this problem remains an open issue within the structural engineering community.

Although single-story models represent the most extreme idealization of plan irregular buildings, they have been widely used in the past due to their simplicity in clarifying the influence of the governing parameters and deriving effective design criteria. However, in recent years multistory building models have been used increasingly for the following two reasons: (i) The shortcomings of single-story models in predicting torsional behavior of real structures, as was evidenced by several authors, who critically discussed the effectiveness of such models. (ii) The

development of powerful computational tools which made feasible extensive and refined numerical analyses of three-dimensional multistory building structures.

A number of studies adopting more realistic multistory models have demonstrated [4] the shortcomings of simplified single-story models, especially in predicting qualitative features of inelastic response, such as the location of the most stressed resisting elements. Furthermore, it was realized that code-designed plan irregular structures have also shown that specifications subscribed by current major seismic codes are in need of re-examination in order to properly deal with nonlinear behavior. More recently, extensive research efforts have been devoted to developing pushover procedures for plan irregular systems, in order to reach effective conclusions [5, 6].

As an alternative to traditional design solutions, fresh ideas are coming from studies on the use of passive control systems by means of various innovative technologies aimed at mitigating the effects of building torsional response. In particular, in addition to base isolation, various types of devices, viscous and frictional, have been considered through ever more refined modelling, and different optimization techniques have proved effective in identifying the amount and location of such devices needed to achieve significant reductions in torsional response [7,8].

Limited research has been devoted to vertically irregular building structures compared to the plan-asymmetric ones. Nevertheless, in recent years, research interest in the field of building structures with vertical irregularity has grown, partly as a result of ever greater availability of efficient nonlinear computer codes that enable dynamic analysis of large multistory buildings [9, 10].

Recent activities on vertically irregular structures have clarified that discontinuities of mass, stiffness or strength along the height, considered by current seismic codes as irregularities in elevation, do not necessarily result in actual increases in plastic demands and, more generally, in poor seismic behavior. In this context some researchers have proposed modifications to the nonlinear pushover procedures for vertically irregular buildings, achieving good correlation of results with those from nonlinear dynamic analysis [11]. Thus, criteria in major international

codes aimed at identifying vertical irregularities seem to penalize such discontinuities excessively and codes are in need of improvement in order to define indicators that actually predict structural behavior for such cases. On the other hand, despite some exceptions, design rules specified by major seismic codes for vertically irregular buildings have resulted in satisfactory seismic performances.

In conclusion, research activity on seismic response of irregular buildings, both in plan or in elevation, is still very lively, as revealed by the number of papers published, and full clarification of the main issues, both behavioral and design oriented, is on the way.

1.2 Objectives and scope

As mentioned above many issues arise as far as the estimation of the torsional effect on the seismic response of asymmetric in plan buildings is concerned. The main cause is attributed to the fact that there is not unequivocal definition for the static eccentricity considering realistic multistory buildings. Moreover, it does not remain the same for all states of response. Once the elements start yielding entering the elastoplastic state of response, their stiffness is affected. Consequently, the value of static eccentricity changes. Taking into consideration that eccentricity is the main indicator according to which codified torsional provisions treat torsion, further investigation of the effect of the lateral torsional coupling on the structural behavior of multistory buildings is necessary. Many researchers noticed that as a result of coupled lateral torsional motions, the lateral forces experienced by vertical structural resisting elements would differ by those experienced by the same elements if the building had symmetric plan and hence responded without torsional induced vibrations. Based on this observation, an index for assessing the amplification of shear forces due to torsional effect, called “ratio of torsion” (*ROT*), is proposed in the current investigation. Ratio of torsion expresses the percentage of torsion-induced shear forces normalized to the imposed base shear by the seismic excitation.

In order to evaluate the reliability of the proposed index, a group of single-story systems is implemented first with monosymmetric as well as double eccentric features, subjected to one- and two-component earthquake excitation. Subsequently, more realistic plan view single-story systems are used exhibiting also unidirectional and bidirectional eccentricity. Finally, horizontally irregular single-story systems are examined. Nonlinear dynamic analyses are performed using natural records for three hazard levels. In addition to the proposed index, previously proposed indices, base torque, diaphragm rotation, interstory drifts, displacements and shear forces, are chosen as response quantities for assessing the structural behavior of the buildings studied.

At the second part of this investigation, the proposed index is evaluated for multistory buildings. In particular, four-story buildings exhibiting unidirectional as well as bidirectional eccentricity are chosen subjected to one - and/or two - component earthquake excitations. Simple mathematical models, buildings with realistic plan views and horizontally irregular buildings are chosen in this case too. The same response quantities as in the case of single-story systems are considered.

At the last part of the investigation, the assessment index *ROT*, proposed in this study is extended to a design tool in the framework of evolutionary-based structural design optimization. *ROT* is implemented in order to achieve improved designs by solving a combined topology-sizing optimization problem. In addition to *ROT*, cost, static and strength eccentricity are also adopted as objective functions. The location and cross-sectional size of vertical structural elements are chosen as design variables. The restrictions imposed by Eurocodes and performance-based design procedure constitute the behavioral constraints. The optimum designs obtained by the implementation of various problem formulations were assessed for nonlinear dynamic excitations and the envelopes of their earthquake response are superimposed for all hazard levels.

1.3 Organization and outline

The thesis consists of seven chapters, while its structure is organized as follows:

Chapter 1 includes the introduction of the dissertation which provides a general description of the motivation and the goals pursued.

Chapter 2 presents the formulation of the flexibility-based beam-column element implemented for the modelling of structural elements. A step-by-step outline of the state determination process is also provided. Afterwards, the concrete and steel material constitutive laws used for the simulation of the models are described. Finally, a summary of the nonlinear solution algorithm implemented is given.

Chapter 3 contains the basic principles of the conventional prescriptive and the Performance-based design procedures. Furthermore, the basic features are presented associated with the parameters that characterize the torsional effect on structural behavior subjected to earthquake excitation in elastic as well as inelastic range of response.

Chapter 4 presents the proposed index for assessing the torsional effect on the structural behavior of eccentric plan buildings. The numerical applications are also included and are divided into two groups. The first group contains mass eccentric, torsionally stiff, horizontally regular as well as irregular single-story systems, while the second one consists of multistory buildings.

Chapter 5 describes the adopted algorithm for the solution of the optimization problem. Basic definitions as well as the concept of structural design and the formulation of the deterministic problem are described. More specifically, the evolution strategies method is explained in detail.

Chapter 6 presents the results of the extension of the proposed assessment index as a design tool, by implementing the formerly described optimization procedure and the numerical applications examined in two single-story, horizontally regular and irregular buildings.

Finally, in Chapter 7 the conclusions of the research work are presented, as well as the natural extension of this work and ideas for future work.

REFERENCES:

[1] Rosenbleuth, E., Meli, R., The 1985 earthquake: causes and effects in Mexico City, *Concrete Int.* 1986; **8**(5), 23-34.

[2] Chandler, A.M., Duan, X.N. and Rutenberg, A., Seismic torsional response: Assumptions, controversies and research progress, *Eur. Earthquake Eng.* 1996; **1**, 37-51.

[3] Clough, R.W., Effect on stiffness degradation on earthquake ductility requirements, Structural and Materials Research, Str. Eng. Lab, Univ. of California, Berkeley, Report 66-16, 1966.

[4] Anagnostopoulos, S.A., Alexopoulou, C. and Stathopoulos, G., An answer to an important controversy and the need for caution when using simple models to predict inelastic earthquake response of buildings with torsion, *Earthquake Engineering and Structural Dynamics.* 2010; **39**, 521-540.

[5] Penelis, Gr.G., Kappos, A.J., Inelastic torsion effects in 3D pushover analysis of buildings, *Proceedings of the 4th European workshop on the seismic behavior of irregular and complex structures,* Thessaloniki, August 2005.

[6] Fajfar, P., Marušić, D., Peruš, I., The extension of the N2 method to asymmetric buildings, *Proceedings of the 4th European workshop on the seismic behavior of irregular and complex structures,* Thessaloniki, August 2005.

[7] Goel, R.K., Seismic behaviour of asymmetric buildings with supplemental damping, *Earthquake Engineering and Structural Dynamics* 2000; **29**, 461-480.

[8] Lin, W.H., Chopra, A.K., Understanding and predicting effects of supplemental viscous damping on seismic response of asymmetric one-storey systems, *Earthquake Engineering and Structural Dynamics* 2000; **30**, 1475-1494.

[9] Das, S., Nau, M., Seismic design aspects of vertically irregular reinforced concrete buildings, *Earthquake Spectra* 2003; **19**, 455-477.

[10] Chintanapakdee, C., Chopra, A.K., Evaluation of modal pushover analysis using vertically irregular frames, *Proceedings of 13th World conference on earthquake*

engineering, Vancouver, August 2004.

[11] Tremblay, R., Poncet, L., Seismic performance of concentrically braced steel frames in multistory buildings with mass irregularity, *Journal of Structural Engineering* 2005; **131**, 1363-1375.

2 NUMERICAL AND MATERIAL MODELLING

2.1 Introduction

This chapter presents the general formulation of a beam-column finite element based on the flexibility method which is implemented in the current dissertation for modelling the structural members as well as the constitutive material laws used for the simulation of concrete and steel.

The formulation of flexibility-type elements is based on interpolation functions for the internal forces. For geometrically linear structures it is straightforward to select polynomials that satisfy the element equilibrium in a strict sense, such as constant axial force and linearly varying bending moments in the absence of element loads [1, 2]. These interpolation functions represent the exact solution to the governing equations, irrespective of the geometry and constitutive law of the beam element. A discretization error, as generally encountered in stiffness-based formulations, does not occur.

The main obstacle in the widespread use of flexibility-based beam finite elements was the difficulty of integrating the nonlinear state determination in an analysis program that is based on direct stiffness method. This obstacle was overcome by a state determination procedure that iteratively determines the element resisting forces and stiffness matrix while strictly satisfying element

equilibrium and compatibility at each iteration. This procedure is considerably more involved than for stiffness-based elements [3-5].

2.2 Force-based beam-column element

The implemented beam-column element is based on the assumption that deformations are small and that plane sections remain plane during the loading history. The formulation of the element is based on the mixed method: the description of the force distribution within the element by interpolation functions that satisfy equilibrium is the starting point of the formulation. Based on the concepts of the mixed method it is shown that the selection of flexibility dependent shape functions for the deformation field of the element results in a considerable simplification of the final equations. With this particular selection of deformation shape functions the general mixed method reduces to the special case of the flexibility method. The mixed method formalism is, nonetheless, very useful in understanding the procedure for the element state determination.

The implemented formulation offers several advantages over previous models:

- Equilibrium and compatibility are always satisfied along the element: equilibrium is satisfied by the selection of force interpolation functions and compatibility is satisfied by integrating the section deformations to obtain the corresponding element deformations and end displacements. An iterative procedure is then used to satisfy the nonlinear section force-deformation relation within the specified tolerance.
- The softening response of reinforced concrete members, which are either poorly reinforced or are subjected to high axial forces, can be described without computational difficulties.

2.2.1 Definition of generalized forces and deformations

The beam-column finite element is schematically shown in Fig. 2.1. The reference frame for the element is the local coordinate system x, y, z, while X, Y, Z denotes the global reference system. The longitudinal axis x is the union of geometric centroids of each section.

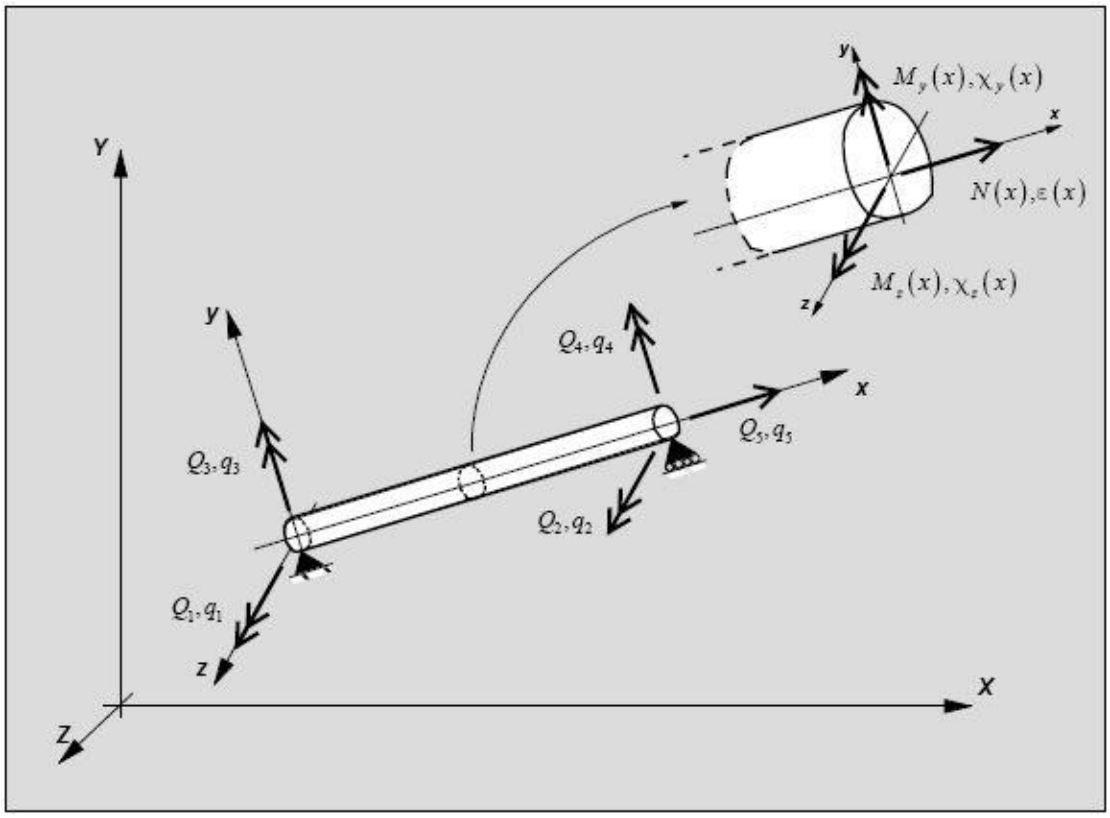

Figure 2.1. Generalized forces and deformations at the element and section level [10].

The following convention is followed for the notation of forces, displacements and deformations: forces are represented by uppercase letters and corresponding deformations or displacements are denoted by the same letter in lowercase. Normal letters denote scalar quantities, while boldface letters denote vectors and matrices.

Fig. 2.1 shows the element forces with the corresponding deformations. Rigid body modes are not included in Fig. 2.1. Since the present formulation is based on linear geometry, rigid body modes can be incorporated with a simple geometric transformation. The element has 5 degrees of freedom: one axial extension, q_5, and two rotations relative to the chord at each end node, (q_1, q_3) and (q_2, q_4), respectively. For the sake of clarity these are called element generalized

deformations or simply element deformations in the following discussion. Q_1 through Q_5 indicate the corresponding generalized forces: one axial force, Q_5, and two bending moments at each end node Q_1 , Q_3 and Q_2, Q_4 , respectively. The end rotations and corresponding moments refer to two arbitrary, orthogonal axes y and z . The element generalized forces and deformations are grouped in the following vectors:

Element force vector:
$$\boldsymbol{Q} = \begin{Bmatrix} Q_1 \\ Q_2 \\ Q_3 \\ Q_4 \\ Q_5 \end{Bmatrix} \tag{2.1}$$

Element deformation vector:
$$\boldsymbol{q} = \begin{Bmatrix} q_1 \\ q_2 \\ q_3 \\ q_4 \\ q_5 \end{Bmatrix} \tag{2.2}$$

Fig. 2.1 also shows the generalized forces and deformations at a section of the element. Section deformations are represented by three strain resultants: the axial strain $\varepsilon(x)$ along the longitudinal axis and two curvatures $x_z(x)$ and $x_y(x)$ about two arbitrary, orthogonal axes z and y , respectively. The corresponding force resultants are the axial force $N(x)$ and two bending moments $M_z(x)$ and $M_y(x)$. The section generalized forces and deformations are grouped in the following vectors:

Section force vector:
$$\boldsymbol{D}(x) = \begin{Bmatrix} M_z(x) \\ M_y(x) \\ N(x) \end{Bmatrix} = \begin{Bmatrix} D_1(x) \\ D_2(x) \\ D_3(x) \end{Bmatrix} \tag{2.3}$$

Section deformation vector:
$$\boldsymbol{d}(x) = \begin{Bmatrix} x_z(x) \\ x_y(x) \\ \varepsilon(x) \end{Bmatrix} = \begin{Bmatrix} d_1(x) \\ d_2(x) \\ d_3(x) \end{Bmatrix} \tag{2.4}$$

The element formulation can be readily extended to include the torsional degrees of freedom, as long as these are uncoupled from the present degrees of

freedom and are governed by linear elastic behavior. The focus of the present study is the element in Fig. 2.1., which describes the nonlinear behavior of frame members under arbitrary cyclic load histories of biaxial bending and axial load.

2.2.2 Beam-column element formulation

In the following the mixed finite element method is used to formulate the beam-column element. At this stage no reference is made to specific interpolation functions. It is shown, however, that, if flexibility dependent deformation shape functions are selected, then the mixed method simplifies to the flexibility method. The nonlinear section force-deformation relation is also kept general.

The derivation follows the two-field mixed method which uses the integral form of equilibrium and section force-deformation relations to derive the matrix relation between element's generalized forces and corresponding deformations. In order to arrive at a linear relation, the section force-deformation relation is linearized about the present state. An iterative algorithm is then used to satisfy the nonlinear section force-deformation relation within the required tolerance.

In the two-field mixed method [6] independent shape functions are used for approximating the force and deformation fields along the element. Denoting with Δ increments of the corresponding quantities, the two fields are written

$$\Delta \boldsymbol{d}^i(x) = a(x)\Delta \boldsymbol{q}^i(x) \tag{2.5}$$

$$\boldsymbol{D}^i(x) = b(x)\boldsymbol{Q}^i(x) \text{ and } \Delta \boldsymbol{D}^i(x) = b(x)\Delta \boldsymbol{Q}^i(x) \tag{2.6}$$

where matrices $\boldsymbol{a}(x)$ and $\boldsymbol{b}(x)$ are the deformation and force interpolation matrices, respectively. Superscript i indicates the i^{th} iteration of the Newton-Raphson (N-R) iteration loop, which is performed at the structure degrees of freedom until equilibrium between applied loads and internal resisting forces is satisfied [6]. The use of the superscript in the element formulation becomes necessary because of the special form of the deformation interpolation functions, which are flexibility dependent.

In the mixed method formulation the integral forms of equilibrium and section force deformation relations are expressed first. These are then combined to obtain the relation between element force and deformation increments.

The weighted integral form of the linearized section force-deformation relation is

$$\int_0^L \delta \boldsymbol{D}^T(x) \cdot \left[\Delta \boldsymbol{d}^i(x) - \boldsymbol{f}^{i-1}(x) \cdot \Delta \boldsymbol{D}^i(x) \right] dx = 0 \tag{2.7}$$

The section force-deformation relation appears in the flexibility form

$$\Delta \boldsymbol{d}^i(x) = \boldsymbol{f}^{i-1}(x) \cdot \Delta \boldsymbol{D}^i(x) \tag{2.8}$$

so that the resulting element flexibility matrix is symmetric, as discussed in [6]. The superscript $i-1$ indicates that at the i^{th} Newton-Raphson iteration the section flexibility at the end of the previous iteration is used. Substituting Eqs. (2.5) and (2.6) in Eq. (2.7) results in

$$\delta \boldsymbol{Q}^T \int_0^L \boldsymbol{b}^T(x) \cdot \left[\boldsymbol{a}(x) \Delta \boldsymbol{q}^i(x) - \boldsymbol{f}^{i-1}(x) \cdot \boldsymbol{b}(x) \Delta \boldsymbol{Q}^i \right] dx = 0 \tag{2.9}$$

Since Eq. (2.9) must hold for any $\delta \boldsymbol{Q}^T$, it follows that

$$\left[\int_0^L \boldsymbol{b}^T(x) \cdot \boldsymbol{a}(x) \cdot dx \right] \Delta \boldsymbol{q}^i - \left[\int_0^L \boldsymbol{b}^T(x) \cdot \boldsymbol{f}^{i-1}(x) \cdot \boldsymbol{b}(x) \cdot dx \right] \cdot \Delta \boldsymbol{Q}^i = 0 \tag{2.10}$$

The expressions in square brackets represent the following matrices:

$$\boldsymbol{F}^{i-1} = \left[\int_0^L \boldsymbol{b}^T(x) \cdot \boldsymbol{f}^{i-1}(x) \cdot \boldsymbol{b}(x) \cdot dx \right] \tag{2.11}$$

$$\boldsymbol{T} = \left[\int_0^L \boldsymbol{b}^T(x) \cdot \boldsymbol{a}(x) \cdot dx \right] \tag{2.12}$$

where $\boldsymbol{F}$ is the element flexibility matrix and $\boldsymbol{T}$ is a matrix that only depends on the interpolation function matrices. Using Eqs. (2.11) and (2.12), Eq. (2.10) can be written in the form

$$\boldsymbol{T} \Delta \boldsymbol{q}^i - \boldsymbol{F}^{i-1} \cdot \Delta \boldsymbol{Q}^i = 0 \tag{2.13}$$

or equivalently

$$\boldsymbol{T} \Delta \boldsymbol{q}^i = \boldsymbol{F}^{i-1} \cdot \Delta \boldsymbol{Q}^i \tag{2.14}$$

This is the matrix expression of the integral form of the linearized section force-deformation relation.

In the next step the equilibrium of the beam element is satisfied. In the classical two-field mixed method the integral form of the equilibrium equation is derived from the virtual displacement principle

$$\int_0^L \delta \boldsymbol{d}^T(x) \cdot \left[\boldsymbol{D}^{i-1}(x) + \Delta \boldsymbol{D}^i(x) \right] dx = \delta \boldsymbol{q}^{\mathrm{T}} \cdot \boldsymbol{P}^i \tag{2.15}$$

where $\boldsymbol{P}^i$ is the vector of applied loads that are in equilibrium with the internal forces $\boldsymbol{D}^{i-1}(x) + \Delta \boldsymbol{D}^i(x)$. Eqs. (2.5) and (2.6) are substituted in Eq. (2.15) to yield

$$\delta \boldsymbol{q}^T \int_0^L \boldsymbol{a}^T(x) \cdot \left[\boldsymbol{b}(x) \boldsymbol{Q}^{i-1} + \boldsymbol{b}(x) \Delta \boldsymbol{Q}^i \right] dx = \delta \boldsymbol{q}^T \cdot \boldsymbol{P}^i \tag{2.16}$$

Observing that Eq. (2.16) must hold for arbitrary $\delta \boldsymbol{q}^T$, it follows that

$$\left[\int_0^L \boldsymbol{b}^T(x) \cdot \boldsymbol{a}(x) \cdot dx \right] \cdot \boldsymbol{Q}^{i-1} + \left[\int_0^L \boldsymbol{b}^T(x) \cdot \boldsymbol{a}(x) \cdot dx \right] \cdot \Delta \boldsymbol{Q}^i = \boldsymbol{P}^i \tag{2.17}$$

If the notation introduced in Eq. (2.12) is used, Eq. (2.17) can be written in matrix form

$$\boldsymbol{T}^T \cdot \boldsymbol{Q}^{i-1} + \boldsymbol{T}^T \cdot \Delta \boldsymbol{Q}^i = \boldsymbol{P}^i \tag{2.18}$$

This is the matrix expression of the integral form of the element equilibrium equations. The rearrangement and combination of Eqs. (2.13) and (2.18) results in

$$\begin{bmatrix} -\boldsymbol{F}^{i-1} & \boldsymbol{T} \\ \boldsymbol{T}^T & \boldsymbol{0} \end{bmatrix} \cdot \begin{Bmatrix} \Delta \boldsymbol{Q}^i \\ \Delta \boldsymbol{q}^i \end{Bmatrix} = \begin{Bmatrix} \boldsymbol{0} \\ \boldsymbol{P}^i - \boldsymbol{T}^T \cdot \boldsymbol{Q}^{i-1} \end{Bmatrix} \tag{2.19}$$

If the first equation in Eq. (2.19) is solved for $\Delta \boldsymbol{Q}^i$ and the result is substituted in the second equation, the following expression results

$$\boldsymbol{T}^T \cdot \left[\boldsymbol{F}^{i-1} \right]^{-1} \cdot \boldsymbol{T} \cdot \Delta \boldsymbol{q}^i = \boldsymbol{P}^i - \boldsymbol{T}^T \cdot \boldsymbol{Q}^{i-1} \tag{2.20}$$

So far, the specific selection of force and deformation interpolation functions $\boldsymbol{b}(x)$ and $\boldsymbol{a}(x)$, respectively, has not been addressed. Even though in a mixed finite element method the deformation interpolation functions $\boldsymbol{a}(x)$, are completely

independent of $\boldsymbol{b}(x)$, Eq. (2.12) reveals that a special choice of the deformation shape functions $\boldsymbol{a}(x)$, results in considerable simplification. With this simplification in mind $\boldsymbol{a}(x)$, are selected as flexibility dependent shape functions according to the following expression

$$\boldsymbol{a}(x) = \boldsymbol{f}^{i-1}(x) \cdot \boldsymbol{b}(x) \cdot \left[\boldsymbol{F}^{i-1}\right]^{-1} \tag{2.21}$$

These interpolation functions, thus, relate the section deformations with the corresponding element deformations according to

$$\Delta \boldsymbol{d}^{i}(x) = \boldsymbol{f}^{i-1}(x) \cdot \boldsymbol{b}(x) \cdot \left[\boldsymbol{F}^{i-1}\right]^{-1} \cdot \Delta \boldsymbol{q}^{i} \tag{2.22}$$

$\boldsymbol{F}^{i-1}$ is the tangent element flexibility matrix at the end of the previous Newton-Raphson iteration. This special selection of the deformation shape functions reduces matrix $\boldsymbol{T}$ in Eq. (2.12) to a 3x3 identity matrix $\boldsymbol{I}$**.** This can be readily proven by substituting Eq. (2.21) in Eq. (2.12):

$$\boldsymbol{T} = \left[\int_0^L \boldsymbol{b}^T(x) \cdot \boldsymbol{a}(x) \cdot dx\right] = \left[\int_0^L \boldsymbol{b}^T(x) \cdot \boldsymbol{f}^{i-1}(x) \cdot \boldsymbol{b}(x) \cdot dx\right] \cdot \left[\boldsymbol{F}^{i-1}\right]^{-1} = \boldsymbol{I} \tag{2.23}$$

With this choice of the deformation shape functions $\boldsymbol{a}(x)$ Eq. (2.20) becomes

$$\left[\boldsymbol{F}^{i-1}\right]^{-1} \cdot \Delta \boldsymbol{q}^{i} = \boldsymbol{P} - \boldsymbol{Q}^{i-1} \tag{2.24}$$

At the same time this choice of functions $\boldsymbol{a}(x)$ reduces the general mixed method to the flexibility method. The final matrix equation, Eq. (2.24), expresses the linearized relation between the applied unbalanced forces $\boldsymbol{P} - \boldsymbol{Q}^{i-1}$ and the corresponding deformation increments $\Delta \boldsymbol{q}^{i}$ at the element level. The element stiffness matrix is written in the form $\left[\boldsymbol{F}\right]^{-1}$ to indicate that it is obtained by inverting the element flexibility matrix. The linear equation system in Eq. (2.24) is different from that obtained by the classical stiffness method in two respects: (a) the element stiffness matrix is obtained by inverting the element flexibility matrix, as in the flexibility method, and, (b) the state determination phase of the nonlinear analysis is different, as will be described in detail in the following section.

Even though the classical flexibility method yields the same system of linearized equations in Eq. (2.24), the above derivation was based on the two-field mixed method for the following reasons: (a) The mixed method formulation yields directly the expression for the flexibility dependent deformation shape functions $\boldsymbol{a}(x)$ in Eq. (2.21). (b) It reveals the consistent implementation of the state determination process. (c) It is more general in scope allowing alternative deformation shape functions to be explored in future studies.

Since $\boldsymbol{a}(x)$ is not independent of $\boldsymbol{b}(x)$ and changes during the iterative solution process, as is apparent from Eq. (2.21), the current method corresponds to the classical flexibility method. Moreover, this procedure reduces to the stiffness method for the case that the section constitutive relation is perfectly linear. In other words, the independence between the two fields is not intrinsic in the definition of the shape functions, but derives from the material nonlinearity of the section force-deformation relation.

2.2.3 State determination

Most studies to date concerned with the analysis of reinforced concrete frame structures are based on finite element models that are derived with the stiffness method. Recent studies have focused on the advantages of flexibility based models [1], but have failed to give a clear and consistent method of calculating the resisting forces from the given element deformations. This problem arises when the formulation of a finite element is based on the application of the virtual force principle. While the element is flexibility-dependent, the computer program into which it is incorporated is based on the direct stiffness method of analysis. In this case the solution of the global equilibrium equations yields the displacements of the structural degrees of freedom. During the phase of state determination the resisting forces of all elements in the structure need to be determined. Since in a flexibility based element there are no deformation shape functions to relate the deformation field inside the element to the end displacements (or element deformations) this process is not straightforward and is not well developed in flexibility based models proposed to date. This fact has led to some confusion in the numerical

implementation of previous models. The description of the consistent state determination process in this study benefits from the derivation of the governing equations by the two-field mixed method.

In a nonlinear structural analysis program each load step corresponds to the application of an external load increment to the structure. The corresponding structural displacement increments are determined and the element deformations are extracted for each element. The process of finding the resisting forces that correspond to the given element deformations is known as state determination. The state determination process is made up of two nested phases: a) *The element state determination*, when the element resisting forces are determined for the given end deformations. b) *The structure state determination*, when the element resisting forces are assembled to the structure resisting force vector. The resisting forces are then compared with the total applied loads and the difference, if any, yields the unbalanced forces which are then applied to the structure in an iterative solution process until external loads and internal resisting forces agree within a specified tolerance.

In the present study the nonlinear algorithm consists of three distinct nested processes, which are illustrated in Fig. 2.2. The two outermost processes denoted by indices k and i involve structural degrees of freedom and correspond to classical nonlinear analysis procedures. The innermost process denoted by index j is applied within each element and corresponds to the element state determination. Fig. 2.2. shows the evolution of the structure, element and section states during one load increment $\Delta \boldsymbol{P}_E^k$ that requires several Newton - Raphson iterations i.

In summary, *k:* denotes the applied load step. The external load is imposed in a sequence of load increments $\boldsymbol{P}_E^k$. At load step *k* the total external load is equal to $\boldsymbol{P}_E^k = \boldsymbol{P}_E^{k-1} + \Delta \boldsymbol{P}_E^k$ with $k = 1, ..., nstep$ and $\boldsymbol{P}_E^0 = \boldsymbol{0}$; *i :* denotes the Newton - Raphson iteration scheme at the structure level, i.e. the structure state determination process. This iteration loop yields the structural displacements $\boldsymbol{p}^k$ that correspond to applied loads $\boldsymbol{P}_E^k$; *j :* denotes the iteration scheme at the element level, i.e. the element state determination process. This iteration loop is

necessary for the determination of the element resisting forces that correspond to element deformations $\boldsymbol{q}^i$ during the i^{th} Newton-Raphson iteration.

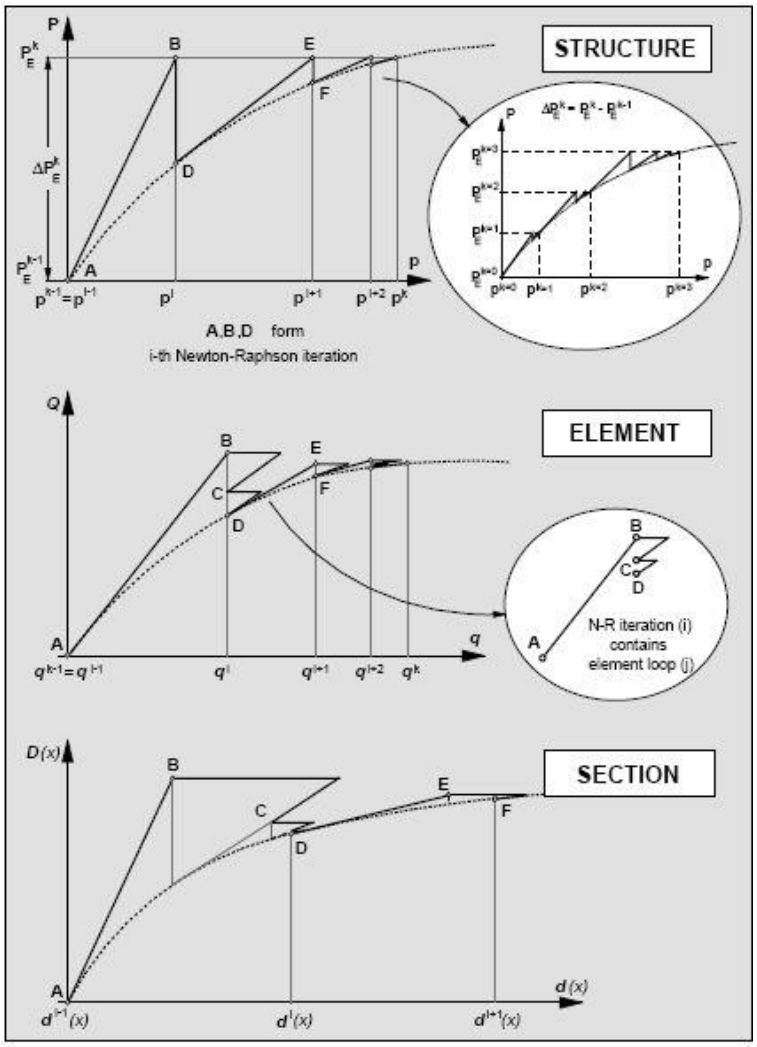

Figure 2.2. Schematic illustration of state determination at the structure, element and section level: k denotes the load step, i the structure Newton-Raphson iteration and j the iteration for the element state determination [10].

The processes denoted by indices k and i are common in nonlinear analysis programs and will not be discussed further. The iteration process denoted by the index j, on the other hand, is special to the beam-column element formulation implemented in this study and will be described in detail. It should be pointed out that any suitable nonlinear solution algorithm can be used for the iteration process denoted by index i. In this study the Newton-Raphson method is used. The selection of this method for iteration loop i does not affect the strategy for iteration loop j,

which has as its goal the determination of the element resisting forces for the given element deformations.

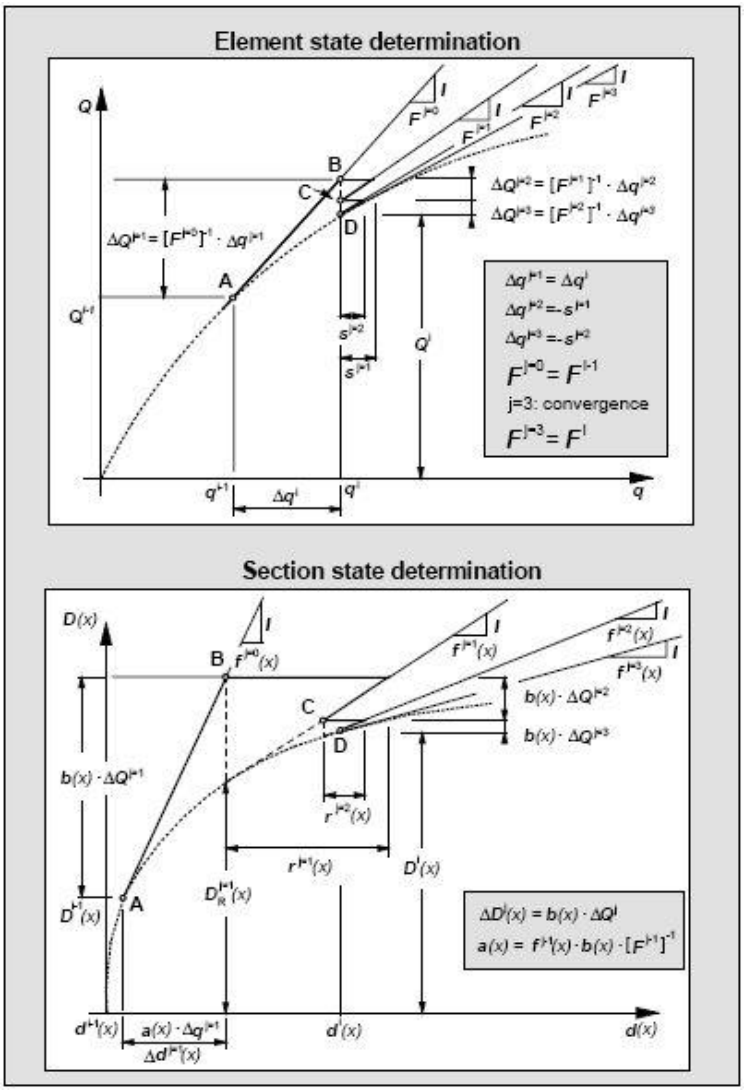

Figure 2.3. Element and section state determination for flexibility-based element: computation of element resisting forces Q^i corresponding to the element deformations q^i [10].

In a finite element that is based on the stiffness method of analysis the section deformations are obtained directly from the element end deformations by deformation interpolation functions. The corresponding section resisting forces are determined subsequently from the section force-deformation relation. The weighted integral of the *section resisting forces* over the element length yields the *element resisting forces* and completes the process of element state determination.

In a flexibility-based finite element the first step is the determination of the element forces from the current element deformations using the stiffness matrix at the end of the last iteration. The force interpolation functions yield the forces along the element. The first problem is, then, the determination of the section deformations from the given section forces, since the nonlinear section force-deformation relation is commonly expressed as an explicit function of section deformations. The second problem arises from the fact that changes in the section stiffness produce a new element stiffness matrix which, in turn, changes the element forces for the given deformations.

These problems are solved by a special nonlinear solution method. In this method residual element deformations are determined at each iteration. Deformation compatibility at the structural level requires that these residual deformations be corrected. This is accomplished at the element level by applying corrective element forces based on the current stiffness matrix. The corresponding section forces are determined from the force interpolation functions so that equilibrium is always satisfied along the element. These section forces cannot change during the section state determination in order to maintain equilibrium along the element. Consequently, the linear approximation of the section force-deformation relation about the present state results in residual section deformations. These are then integrated along the element to obtain new residual element deformations and the whole process is repeated until convergence occurs. It is important to stress that *compatibility of element deformations and equilibrium along the element are always satisfied in this process.*

The nonlinear solution procedure for the element state determination is schematically illustrated in Fig. 2.3 for one Newton-Raphson iteration *i*; while for loop *j* convergence is reached in three iterations. The consistent notation between Figs. 2.2. and 2.3. highlights the relation between the corresponding states of the structure, the element and the section, which are denoted by uppercase Roman letters.

At the i^{th} Newton-Raphson iteration it is necessary to determine the element resisting forces for the current element deformations

$$\boldsymbol{q}^{i} = \boldsymbol{q}^{i-1} + \Delta\boldsymbol{q}^{i} \tag{2.25}$$

To this end an iterative process denoted by index j is introduced inside the i^{th} Newton-Raphson iteration. The first iteration corresponds to $j=1$. The initial state of the element, represented by point **A** and $j=0$ in Fig. 2.3., corresponds to the state at the end of the last iteration of loop j for the $(i-1)$ Newton-Raphson iteration. With the initial element tangent stiffness matrix

$$\left[\boldsymbol{F}^{\,j=0}\right]^{-1} = \left[\boldsymbol{F}^{\,i-1}\right]^{-1} \tag{2.26}$$

and the given element deformation increments

$$\Delta\boldsymbol{q}^{\,j=1} = \Delta\boldsymbol{q}^{i} \tag{2.27}$$

the corresponding element force increments are:

$$\Delta\boldsymbol{Q}^{\,j=1} = \left[\boldsymbol{F}^{\,j=0}\right]^{-1} \cdot \Delta\boldsymbol{q}^{\,j=1} \tag{2.28}$$

The section force increments can now be determined from the force interpolation functions:

$$\Delta\boldsymbol{D}^{j=1}(x) = \boldsymbol{b}(x) \cdot \Delta\boldsymbol{Q}^{\,j=1} \tag{2.29}$$

With the section flexibility matrix at the end of the previous Newton-Raphson iteration

$$\boldsymbol{f}^{\,j=0}(x) = \boldsymbol{f}^{\,i-1}(x) \tag{2.30}$$

the linearization of the section force-deformation relation yields the section deformation increments $\Delta\boldsymbol{d}^{\,j=1}(x)$:

$$\Delta\boldsymbol{d}^{\,j=1}(x) = \boldsymbol{f}^{\,j=0}(x) \cdot \Delta\boldsymbol{D}^{j=1}(x) \tag{2.31}$$

The section deformations are updated to the state that corresponds to point **B** in Fig. 2.3.:

$$\boldsymbol{d}^{\,j=1}(x) = \boldsymbol{d}^{\,j=0}(x) + \Delta\boldsymbol{d}^{\,j=1}(x) \tag{2.32}$$

According to the section force-deformation relation, which is here assumed to be explicitly known for simplicity's sake, section deformations $\boldsymbol{d}^{\,j=1}(x)$ correspond to

resisting forces $\boldsymbol{D}_R^{j=1}(x)$ and a new tangent flexibility matrix $\boldsymbol{f}^{j=1}(x)$ (Fig. 2.3.). In a finite element based on the stiffness method the section resisting forces $\boldsymbol{D}_R^{j=1}(x)$ would be directly transformed to element resisting forces $\boldsymbol{Q}^{j=1}$ thus violating the equilibrium along the element in a strict sense. Since this is undesirable, in this approach the section unbalanced forces are first determined

$$\boldsymbol{D}_U^{j=1}(x) = \Delta\boldsymbol{D}^{j=1}(x) - \boldsymbol{D}_R^{j=1}(x) \tag{2.33}$$

and are then transformed to residual section deformations $\boldsymbol{r}^{j=1}(x)$

$$\boldsymbol{r}^{j=1}(x) = \boldsymbol{f}^{j=1}(x) \cdot \boldsymbol{D}_U^{j=1}(x) \tag{2.34}$$

The residual section deformations are thus the linear approximation to the deformation error made in the linearization of the section force-deformation relation (Fig. 2.3.). While any suitable flexibility matrix can be used in calculating the residual deformations, the tangent flexibility matrix used in this study offers the fastest convergence rate.

The residual section deformations are integrated along the element based on the virtual force principle to obtain the residual element deformations:

$$\boldsymbol{s}^{j=1} = \int_0^L \boldsymbol{b}^T(x) \cdot \boldsymbol{r}^{j=1}(x) \cdot dx \tag{2.35}$$

At this point the first iteration $j=1$ of the corresponding iteration loop is complete. The final element and section states for $j=1$ correspond to point **B** in Fig. 2.3. The residual section deformations $\boldsymbol{r}^{j=1}(x)$ and the residual element deformations $\boldsymbol{s}^{j=1}$ are determined in the first iteration, but the corresponding deformation vectors are not updated. Instead, they are the starting point of the remaining steps within iteration loop j. The presence of residual element deformations $\boldsymbol{s}^{j=1}$ violates compatibility, since elements sharing a common node would now have different end displacements. In order to restore the inter-element compatibility corrective forces equal to $-\left[\boldsymbol{F}^{j=1}\right]^{-1} \cdot \boldsymbol{s}^{j=1}$ must be applied at the ends of the element, where $\boldsymbol{F}^{j=1}$ is the updated element tangent flexibility matrix determined by integration of the section flexibility matrices according to Eq. (2.11). A

corresponding force increment $-\boldsymbol{b}(x)\left[\boldsymbol{F}^{j=1}\right]^{-1}\cdot\boldsymbol{s}^{j=1}$ is applied at all control sections inducing a deformation increment $-\boldsymbol{f}^{j=1}(x)\cdot\boldsymbol{b}(x)\cdot\left[\boldsymbol{F}^{j=1}\right]^{-1}\cdot\boldsymbol{s}^{j=1}$. Thus, in the second iteration *j*=2 the state of the element and of the sections within the element change as follows: the element forces are updated to the value

$$\boldsymbol{Q}^{j=2}=\boldsymbol{Q}^{j=1}+\Delta\boldsymbol{Q}^{j=2} \tag{2.36}$$

where $\Delta\boldsymbol{Q}^{j=2}=-\left[\boldsymbol{F}^{j=1}\right]^{-1}\cdot\boldsymbol{s}^{j=1}$ and the section forces and deformations are updated to the values

$$\boldsymbol{D}^{j=2}(x)=\boldsymbol{D}^{j=1}(x)+\Delta\boldsymbol{D}^{j=2}(x) \tag{2.37}$$

And

$$\boldsymbol{d}^{j=2}(x)=\boldsymbol{d}^{j=1}(x)+\Delta\boldsymbol{d}^{j=2}(x) \tag{2.38}$$

where $\Delta\boldsymbol{D}^{j=2}(x)=-\boldsymbol{b}(x)\cdot\left[\boldsymbol{F}^{j=1}\right]^{-1}\cdot\boldsymbol{s}^{j=1}$

$$\Delta\boldsymbol{d}^{j=2}(x)=\boldsymbol{r}^{j=1}(x)-\boldsymbol{f}^{j=1}(x)\cdot\boldsymbol{b}(x)\cdot\left[\boldsymbol{F}^{j=1}\right]^{-1}\cdot\boldsymbol{s}^{j=1}$$

The state of the element and the sections within the element at the end of the second iteration $j=2$ corresponds to point **C** in Fig. 2.3. The new tangent flexibility matrices $\boldsymbol{f}^{j=2}(x)$ and the new residual section deformations

$$\boldsymbol{r}^{j=2}(x)=\boldsymbol{f}^{j=2}(x)\cdot\boldsymbol{D}_U^{j=2}(x) \tag{2.39}$$

are computed for all sections. The residual section deformations are then integrated to obtain the residual element deformations $\boldsymbol{s}^{j=2}$ and the new element tangent flexibility matrix $\boldsymbol{F}^{j=2}$ is determined by integration of the section flexibility matrices $\boldsymbol{f}^{j=2}(x)$ according to Eq. (2.24). This completes the second iteration within loop j.

The third and subsequent iterations follow exactly the same scheme. Convergence is achieved when the selected convergence criterion is satisfied. With the conclusion of iteration loop j the element resisting forces for the given deformations $\boldsymbol{q}^i$ are established, as represented by point **D** in Figs. 2.2. and 2.3. The Newton-Raphson iteration process can now proceed with step $i+1$.

It is important to point out that during iteration loop *j* the element deformations $\boldsymbol{q}^i$ do not change except in the first iteration $j=1$, when increments $\Delta\boldsymbol{q}^{j=1}=\Delta\boldsymbol{q}^i$ are added to the element deformations $\boldsymbol{q}^{i-1}$ at the end of the previous Newton-Raphson iteration. These deformation increments result from the application of corrective loads $\Delta\boldsymbol{P}_E^i$ at the structural degrees of freedom during the Newton-Raphson iteration process. For $j>1$ only the element forces change until the nonlinear solution procedure converges to the element resisting forces $\boldsymbol{Q}^i$ which correspond to element deformations $\boldsymbol{q}^i$. This is illustrated at the top of Fig. 2.3. where points **B**, **C** and **D,** which represent the state of the element at the end of subsequent iterations in loop j, lie on the same vertical line, while the corresponding points at the control sections of the element do not, as shown in the bottom of Fig. 2.3. This feature of the nonlinear solution procedure ensures displacement compatibility at the element ends.

The described nonlinear analysis method offers several advantages. Equilibrium along the element is always strictly satisfied, since section forces are derived from element forces by the force interpolation functions according to Eq. (2.6). Compatibility is also satisfied, not only at the element ends, but also along the element. In fact, in the expression for the section deformation corrections

$$\Delta\boldsymbol{d}^j(x)=\boldsymbol{r}^{j-1}(x)-\boldsymbol{f}^{j-1}(x)\cdot\boldsymbol{b}(x)\cdot\left[\boldsymbol{F}^{j-1}\right]^{-1}\cdot\boldsymbol{s}^{j-1} \tag{2.40}$$

the second term satisfies Eqs. (2.21) and (2.22), which express the relation between section and element deformations by means of shape functions $\boldsymbol{a}(x)$. The residual section deformations $\boldsymbol{r}^{j-1}(x)$, however, do not strictly satisfy this compatibility condition. It is possible to satisfy this requirement by integrating the residual deformations $\boldsymbol{r}^{j-1}(x)$ to obtain $\boldsymbol{s}^{j-1}(x)$ and then using the deformation shape functions $\boldsymbol{a}(x)$ to calculate the section deformation increments as $\boldsymbol{a}(x)\cdot\boldsymbol{s}^{j-1}(x)$. Since this is, however, rather inefficient from a computational standpoint, the small compatibility error in the calculation of residual section deformations $\boldsymbol{r}^{j-1}(x)$ is neglected.

While equilibrium and compatibility are satisfied along the element during each iteration of loop j, the section force-deformation relation and, consequently, the element force-deformation relation is only satisfied within a specified tolerance when convergence is achieved at point **D** in Fig. 2.3. In other words, during subsequent iterations the element forces approach the value that corresponds to the imposed element deformations, while maintaining equilibrium and compatibility along the element at all times. This approximation of the force-deformation relation in the implemented nonlinear analysis method is preferable to the approximation of either the equilibrium or the compatibility conditions of the element, particularly when considering the uncertainty in the definition of constitutive relations for reinforced concrete structures.

2.3 Material modelling

2.3.1 Concrete stress-strain relation

In order to compute the concrete stress in each layer, a material law describing the concrete stress-strain relation under arbitrary cyclic strain histories is needed. There is some uncertainty as to the influence of the concrete model on the overall behavior of RC members subjected to bending and small values of axial force. Some investigators have concluded that a crude concrete model suffices to accurately predict experimental results. This might be true in the case of monotonic loading and cyclic loading that is restricted to small excitations. It is not true, however, in the case of severe cyclic loading. The strength deterioration of RC members under large cyclic excitations depends largely on the capacity of confined concrete to sustain stresses in the strain range beyond the maximum strength. This requires the use of a refined concrete model.

The model implemented in this study is summarized below:

The monotonic envelope curve of concrete in compression follows the model of Kent and Park (1971) [17] that was later extended by Scott et al. (1982) [18]. Even though more accurate and complete models have been published since, the so-

called modified Kent and Park model offers a good balance between simplicity and accuracy.

In the modified Kent and Park model the monotonic concrete stress-strain relation incompression is described by three regions:

$$\varepsilon_c \le \varepsilon_0 \qquad \sigma_c = Kf_c^{'}\left[2\left(\frac{\varepsilon_c}{\varepsilon_0}\right)-\left(\frac{\varepsilon_c}{\varepsilon_0}\right)^2\right] \tag{2.41}$$

$$\varepsilon_0 \le \varepsilon_c \le \varepsilon_u \qquad \sigma_c = Kf_c^{'}\left[1-Z\left(\varepsilon_c-\varepsilon_0\right)\right] \ge 0.2Kf_c^{'} \tag{2.42}$$

where

$$\varepsilon_0 = 0.002K \tag{2.43}$$

$$K = 1+\frac{\rho_s f_{yh}}{f_c^{'}} \tag{2.44}$$

$$Z = \frac{0.5}{\dfrac{3+0.29f_c^{'}}{145f_c^{'}-1000}+0.75\rho_s\sqrt{\dfrac{h^{'}}{s_h}}-0.002K} \tag{2.45}$$

ε_0 is the concrete strain at maximum stress, K is a factor which accounts for the strength increase due to confinement, Z is the strain softening slope, $f_c^{'}$ is the concrete compressive cylinder strength in MPa ($1\,MPa$ =145 psi), f_{yh} is the yield strength of stirrups in MPa, ρ_s is the ratio of the volume of hoop reinforcement to the volume of concrete core measured to outside of stirrups, $h^{'}$ is the width of concrete core measured to outside of stirrups, and s_h is the center to center spacing of stirrups or hoop sets.

In the case of *concrete confined by stirrup-ties*, Scott et al. suggest that ε_u be determined conservatively from the following equation:

$$\varepsilon_u = 0.004+0.9\rho_s\left(\frac{f_{yh}}{300}\right) \tag{2.46}$$

To account for crushing of *concrete cover* the strength in a cover layer is reduced to $0.2f_c^{'}$ once the compressive strain exceeds the value of ε_u, which in this study is set equal to 0.005. The tensile strength of concrete is neglected in the model, since

it only influences the response of a RC section during cycles prior to yielding.

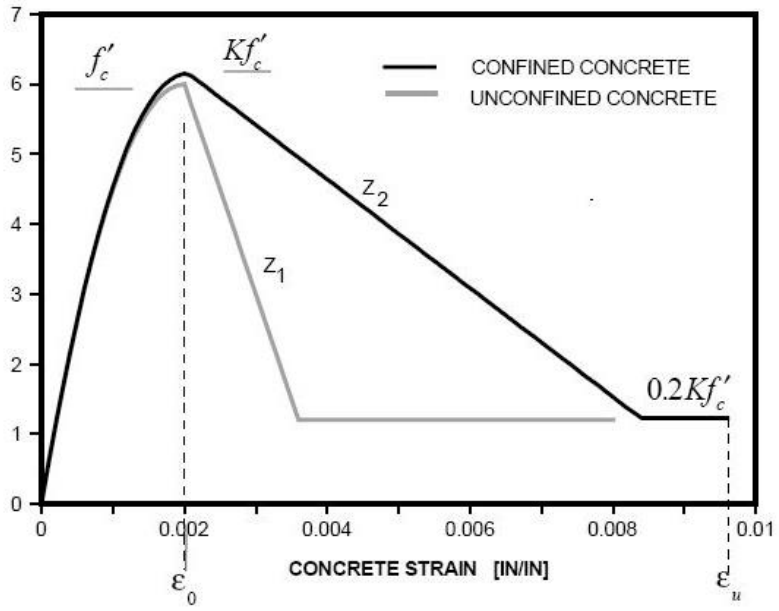

Figure 2.4. Stress-Strain relation for confined and unconfined concrete.

The following rules govern the hysteretic behavior of the concrete stress-strain relation (Fig. 2.5):

1. Unloading from a point on the envelope curve takes place along a straight line connecting the point ε_r at which unloading starts to a point *p* ε on the strain axis given by the equations

$$\frac{\varepsilon_p}{\varepsilon_0} = 0.145\left(\frac{\varepsilon_r}{\varepsilon_0}\right)^2 + 0.13\left(\frac{\varepsilon_r}{\varepsilon_0}\right) \quad \text{for} \quad \left(\frac{\varepsilon_r}{\varepsilon_0}\right) < 2 \tag{2.47}$$

$$\frac{\varepsilon_p}{\varepsilon_0} = 0.707\left(\frac{\varepsilon_r}{\varepsilon_0} - 2\right) + 0.834 \quad \text{for} \quad \left(\frac{\varepsilon_r}{\varepsilon_0}\right) \geq 2 \tag{2.48}$$

where ε_0 is the strain level corresponding to the maximum stress in compression.

Eq. (2.47) was proposed by Karsan and Jirsa (1969) [19] and relates the normalized strain on the envelope with the strains at the completion of unloading through a quadratic formula. Since Eq. (2.47) exhibits unreasonable behavior under high compressive strain conditions, Eq. (2.48) is added to the model so that the unloading modulus of elasticity remains positive under high compressive strains.

2. The concrete stress is equal to zero for strains smaller than the strain at complete unloading (open crack) since the tensile resistance is neglected in this study.

3. On reloading in compression the stress is zero as long as the strain is smaller than the strain at complete unloading (open crack). Once the concrete strain becomes larger than that value, reloading continues along the previous unloading path (Fig. 2.5). In reality unloading and reloading follow nonlinear paths which together form a hysteresis loop. This was neglected here for reasons of simplicity, since it has a minor influence on the hysteretic response of the member. The proposed hysteretic behavior of concrete in compression does not account for the cyclic damage of concrete. The importance of this effect on the hysteretic behavior of RC members merits further study, but is beyond the scope of the present report.

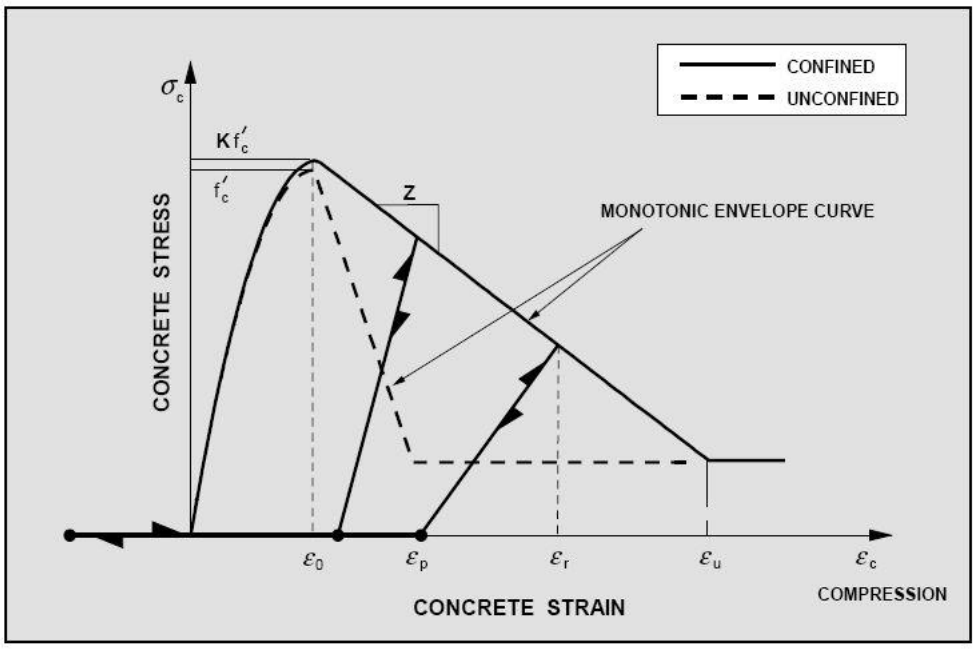

Figure 2.5. Modified Kent-Park model during loading and unloading.

2.3.2 Reinforcement steel stress-strain relation – Bilinear material model

For a bilinear model (Fig. 2.6) the elastic behavior is defined by Hooke law, having initial modulus of elasticity E and the yielding point is defined by yielding stress σ_y. Post yield behavior is defined by a second slope having inclination equal to tangent modulus of elasticity E_T, which is related to the initial modulus of elasticity by the hardening ratio b:

$$E_T = bE \tag{2.49}$$

For a perfectly plastic material the hardening ratio is equal to zero. Instead of the hardening ratio b, sometimes the hardening parameter H is used that relates stress σ and plastic strain ε_{pl}:

$$\sigma = H\varepsilon_{pl} \tag{2.50}$$

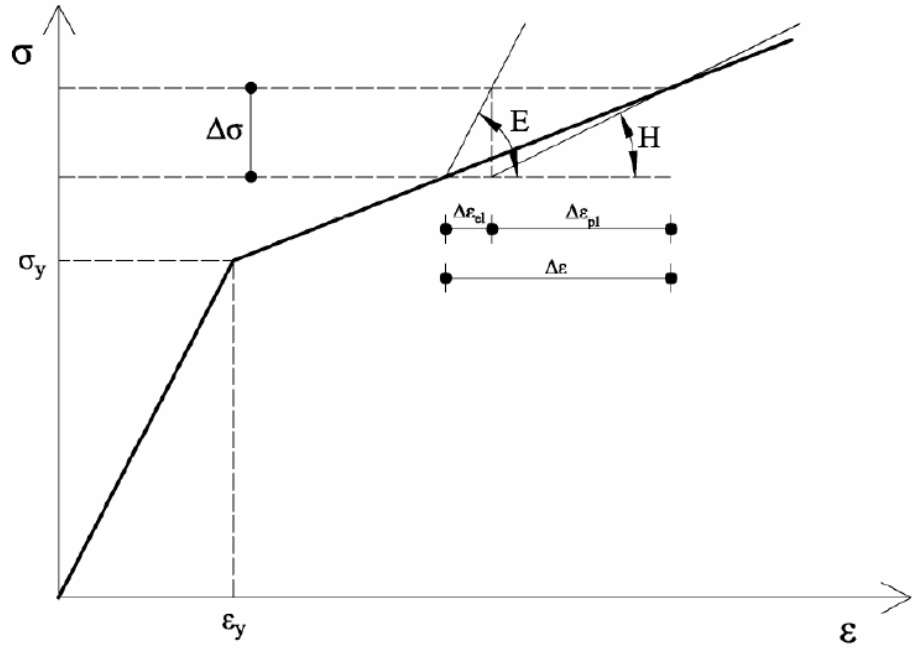

Figure 2.6. Bi-linear steel material law.

The hardening parameter H, tangent modulus of elasticity E_T and hardening ratio b are given by:

$$H = \frac{E_T}{1-b} \tag{2.51}$$

$$E_T = E\left(1 - \frac{E}{E-H}\right) \tag{2.52}$$

For steel members, when the yield stress has been exceeded in tension followed by compression, then yield strength will be different for the next loading cycle. This is known as Bauschinger effect. The Bauschinger effect refers to a property of materials where the material's stress/strain characteristics change as a result of the microscopic stress distribution of the material. For example, an increase in tensile yield strength occurs at the expense of compressive yield strength. Bauschinger effect can be simulated using kinematic of isotropic hardening.

For the isotropic hardening the yield surface is assumed to expand isotropically in size, keeping its center by this hypothesis. This means that plastic strain does not affect the shape of yield surface. If the initial yield point is denoted by Y on the stress-strain curve in Fig. 2.7, unloaded stress AB from point A is the same as the compressive yield stress BC and is larger than the initial yield stress. The concept of this hypothesis is too simple to express the generalized Bauschinger effect, but nevertheless it is widely used for many kinds of analyses when the direction of loading changes slightly.

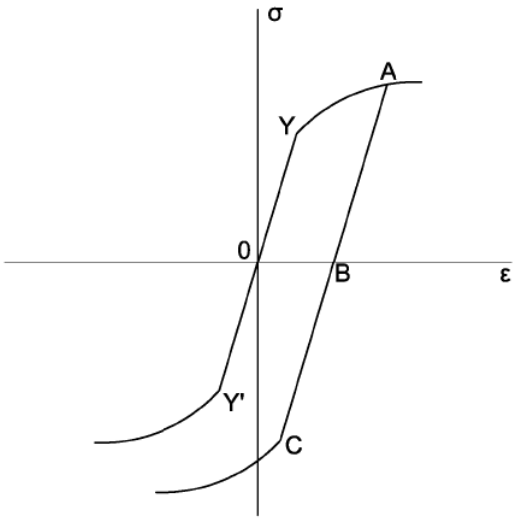

Figure 2.7. Isotropic hardening.

For kinematic hardening the model assumes that the yield surface with unchanging shape moves in stress space due to plastic deformation as illustrated in Fig. 2.8 and stress-strain diagram is given under the condition $YY' = AC$. This results to a movement of the center of hysteretic loops in a stress-strain curve.

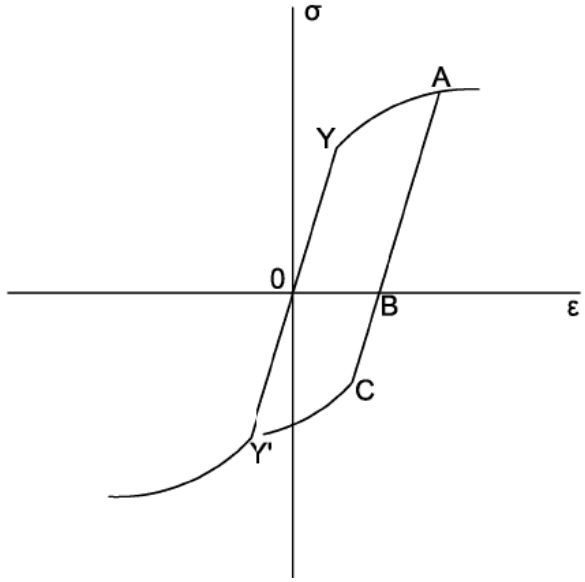

Figure 2.8. Kinematic hardening.

2.4 Summary of nonlinear solution algorithm

After the description of the element state determination process in one of the previous sections a step-by-step summary of the computations is presented below. The summary focuses on a single iteration i at the structural degrees of freedom. The rest of the nonlinear solution algorithm follows well established methods, such as the Newton-Raphson method selected in this study. Alternative solution strategies can be implemented without additional effort, since these are independent of the element state determination. The relation of the Newton-Raphson iteration to the nonlinear solution of the entire structure is illustrated at the top of Fig. 2.2, which also shows the relation between the overall solution strategy and the element state determination process with corresponding states denoted by uppercase Roman letters. Fig. 2.3 shows in detail the evolution of the state determination process for an element and corresponds to steps **(4)** through **(13)** in

the following summary. The flow chart of computations for the entire solution algorithm is shown in Fig. 2.9, while the flow chart of computations for the element state determination is shown in Fig. 2.10.

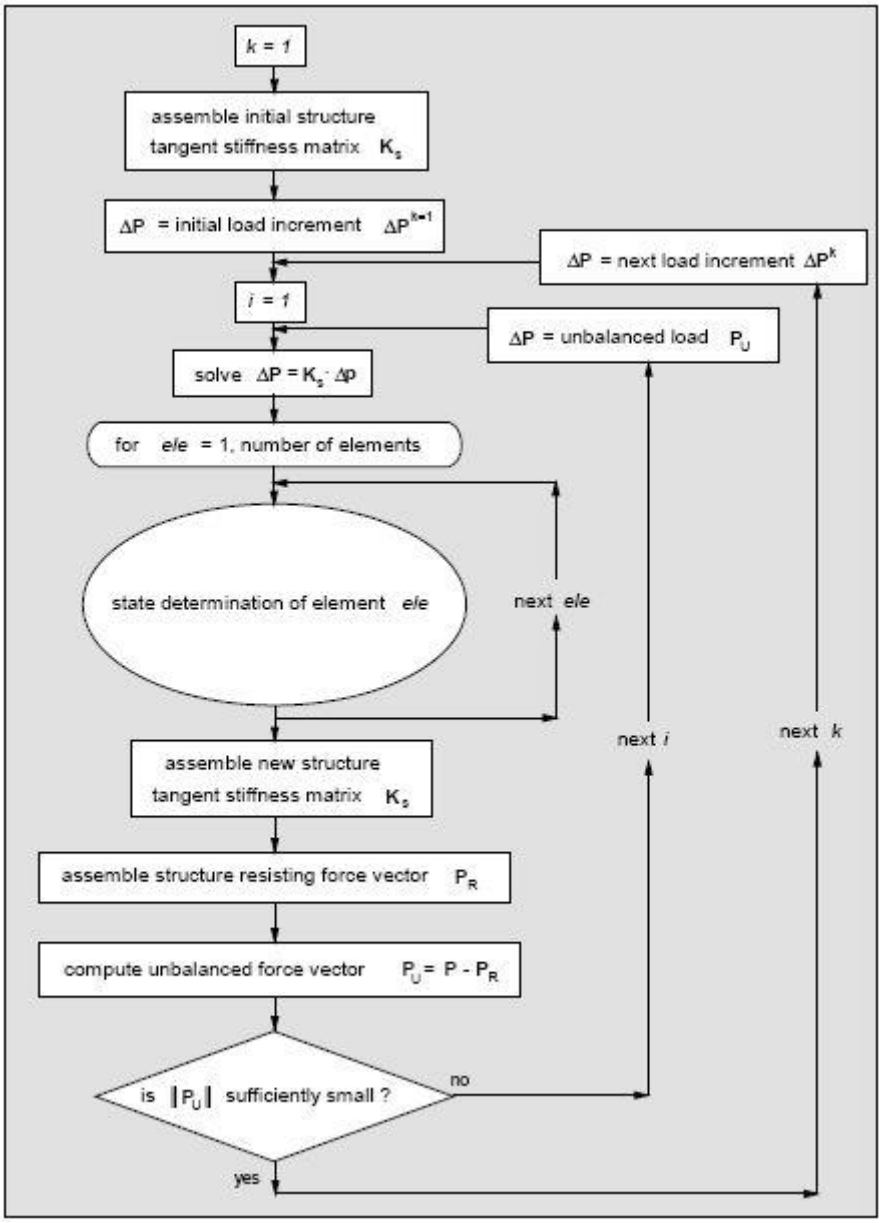

Figure 2.9. Flow chart of structure state determination.

The *i*-th Newton-Raphson iteration is organized as follows:

(1) *Solve the global system of equations and update the structural displacements.*

At the i^{th} Newton-Raphson iteration the structure stiffness matrix $\boldsymbol{K}_s^{i-1}$ at the end of the previous iteration $i-1$ is used to compute the displacement

increments $\Delta \boldsymbol{p}^i$ for the given load increments $\Delta \boldsymbol{P}_E^i$ which represent the unbalanced forces from the previous iteration.

$$\boldsymbol{K}_s^{i-1} \cdot \Delta \boldsymbol{p}^i = \Delta \boldsymbol{P}_E^i \tag{2.53}$$

$$\boldsymbol{p}^i = \boldsymbol{p}^{i-1} + \Delta \boldsymbol{p}^i \tag{2.54}$$

(2) *Calculate the element deformation increments and update the element deformations.* Using matrix $\boldsymbol{L}_{ele}$, which relates structural displacements with element deformations, the element deformation increments $\Delta \boldsymbol{q}^i$ are determined:

$$\Delta \boldsymbol{q}^i = \boldsymbol{L}_{ele} \cdot \Delta \boldsymbol{p}^i \tag{2.55}$$

$$\boldsymbol{q}^i = \boldsymbol{q}^{i-1} + \Delta \boldsymbol{q}^i \tag{2.56}$$

Note that matrix $\boldsymbol{L}_{ele}$ is the combination of two transformations: in the first transformation the element displacements in the global reference system **p** are transformed to the displacements $\bar{\boldsymbol{q}}$ in the element local reference system. In the second transformation the element displacements $\bar{\boldsymbol{q}}$ are transformed to element deformations $\boldsymbol{q}$ by elimination of the rigid-body modes.

As discussed in Section 2.2.3, the new element deformations $\boldsymbol{q}^i$ do not change until the following $(i+1)$ Newton-Raphson iteration. The remaining operations of the nonlinear solution algorithm make up the element state determination process which establishes the element resisting forces for the given element deformations $\boldsymbol{q}^i$.

(3) *Start the element state determination. Loop over all elements in the structure.* The state determination of each element is performed in loop *j*. The index of the first iteration is $j = 1$.

(4) *Determine the element force increments.* The element force increments $\Delta \boldsymbol{Q}^j$ are determined with the element stiffness matrix $\boldsymbol{K}^{j-1}$ at the end of the previous iteration in loop j

$$\Delta \boldsymbol{Q}^j = \boldsymbol{K}^{j-1} \cdot \Delta \boldsymbol{q}^j \tag{2.57}$$

When $j=1$, $\boldsymbol{K}^0 = \boldsymbol{K}^{i-1}$ and $\Delta \boldsymbol{q}^1 = \Delta \boldsymbol{q}^i$ where $i-1$ corresponds to the state of the element at the end of the last Newton-Raphson iteration. When $j>1$ $\Delta \boldsymbol{q}^j$ is equal to the residual element deformations of the previous iteration, as determined in Step **(13)**.

(5) *Update the element forces.*

$$\boldsymbol{Q}^j = \boldsymbol{Q}^{j-1} + \Delta \boldsymbol{Q}^j \tag{2.58}$$

When $j=1, \boldsymbol{Q}^0 = \boldsymbol{Q}^{i-1}$ where $i-1$ corresponds to the state at the end of the last Newton-Raphson iteration.

(6) *Determine the section force increments*. *Steps* **(6)** *through* **(11)** *are performed for all control sections (integration points) of the element.* The section force increments $\Delta \boldsymbol{D}^j(x)$ are determined from the force interpolation functions $\boldsymbol{b}(x)$. Subsequently, the section forces $\boldsymbol{D}(x)$ are updated.

$$\Delta \boldsymbol{D}^j(x) = \boldsymbol{b}(x) \cdot \Delta \boldsymbol{Q}^j \tag{2.59}$$

$$\boldsymbol{D}^j(x) = \boldsymbol{D}^{j-1}(x) + \Delta \boldsymbol{D}^j(x) \tag{2.60}$$

(7) *Determine the section deformation increments.* The section deformation increments $\Delta \boldsymbol{d}^i(x)$ are determined by adding the residual section deformations from the previous iteration $\boldsymbol{r}^{j-1}(x)$ to the deformation increments caused by the section force increments $\Delta \boldsymbol{D}^j(x)$. The latter are determined with the section flexibility matrix $\boldsymbol{f}^{j-1}(x)$ at the end of the previous iteration in loop j.

$$\Delta \boldsymbol{d}^j(x) = \boldsymbol{r}^{j-1}(x) + \boldsymbol{f}^{j-1}(x) \Delta \boldsymbol{D}^j(x) \tag{2.61}$$

$$\boldsymbol{d}^j(x) = \boldsymbol{d}^{j-1}(x) + \Delta \boldsymbol{d}^j(x) \tag{2.62}$$

when $j=1$, $\boldsymbol{r}^0(x) = 0$

(8) *Determine the tangent stiffness and flexibility matrices of the section*. Assuming for simplicity that the section force-deformation relation is known

explicitly, the tangent stiffness matrix $\boldsymbol{k}^j(x)$ is updated for the new section deformations $\boldsymbol{d}^j(x)$. Stiffness matrix $\boldsymbol{k}^j(x)$ is then inverted to obtain the new tangent flexibility matrix $\boldsymbol{f}^j(x)$ of the section.

$$\boldsymbol{f}^j(x) = \left[\boldsymbol{k}^j(x)\right]^{-1} \tag{2.63}$$

(9) *Determine the section resisting forces.* The resisting forces $\boldsymbol{D}_R^j(x)$ are determined for the current deformations $\boldsymbol{d}^j(x)$ from the section force-deformation relation.

(10) *Determine the unbalanced forces at the section.* The section unbalanced forces $\boldsymbol{D}_U^j(x)$ are the difference between the applied forces $\boldsymbol{D}^j(x)$ and the resisting forces $\boldsymbol{D}_R^j(x)$.

$$\boldsymbol{D}_U^j(x) = \boldsymbol{D}^j(x) - \boldsymbol{D}_R^j(x) \tag{2.64}$$

(11) *Determine the residual section deformations.* The section unbalanced forces and the new section flexibility yield the residual section deformations $\boldsymbol{r}^j(x)$

$$\boldsymbol{r}^j(x) = \boldsymbol{f}^j(x)\boldsymbol{D}_U^j(x) \tag{2.65}$$

(12) *Determine the element flexibility and stiffness matrices*. The element flexibility matrix $\boldsymbol{F}^j$ is formed by integration of the section flexibility matrices $\boldsymbol{f}^j(x)$. This matrix is then inverted to obtain the element tangent stiffness matrix $\boldsymbol{K}^j$.

$$\boldsymbol{F}^j = \left[\int_0^L \boldsymbol{b}^T(x)\cdot \boldsymbol{f}^j(x)\cdot \boldsymbol{b}(x)\cdot dx\right] \tag{2.66}$$

$$\boldsymbol{K}^j = \left[\boldsymbol{F}^j\right]^{-1} \tag{2.67}$$

(13) *Check for element convergence.* a) If the unbalanced forces at all element sections are sufficiently small, the element is considered to have converged. After setting $\boldsymbol{Q}^i = \boldsymbol{Q}^j$ and $\boldsymbol{K}^i = \boldsymbol{K}^j$ the process continues with step **(14)**. b) If some sections have not converged, the residual element deformations $\boldsymbol{s}^j$ are determined by integration of the residual section deformations $\boldsymbol{r}^j(x)$.

$$\boldsymbol{s}^j = \left[\int_0^L \boldsymbol{b}^T(x) \cdot \boldsymbol{r}^j(x) \cdot dx \right] \tag{2.68}$$

At this point j is incremented to $j+1$ and a new iteration begins in loop j. In this case $\Delta \boldsymbol{q}^j$ in Eq. (2.57) is replaced with $\Delta \boldsymbol{q}^{j+1}$ which is set equal to $-\boldsymbol{s}^j$

$$\Delta \boldsymbol{q}^{j+1} = -\boldsymbol{s}^j \tag{2.69}$$

and steps **(4)** through **(13)** are repeated until convergence is achieved at all sections of the element.

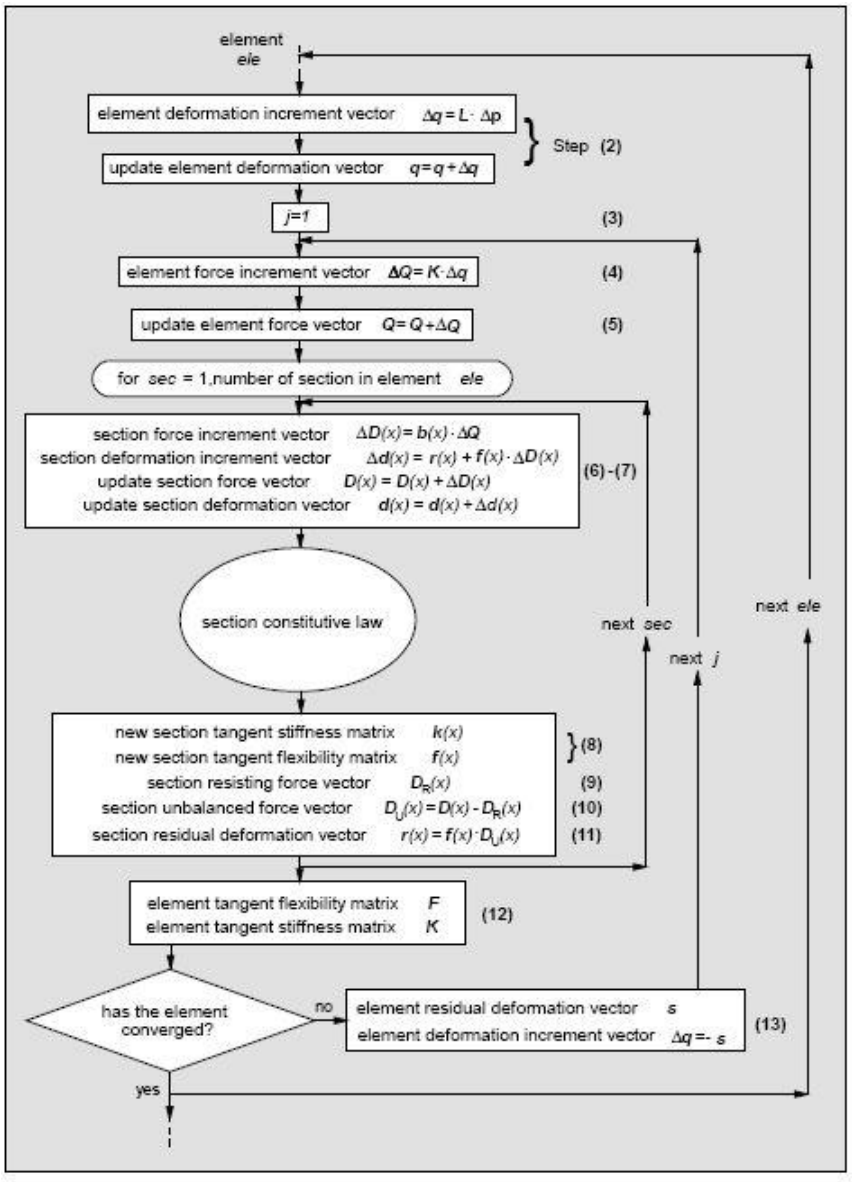

Figure 2.10. Flow chart of structure state determination: the section.

(14) *Determine the resisting forces and the new stiffness matrix of the entire structure.* When all elements have converged, the i^{th} step of the Newton-Raphson iteration is complete. The element force vectors are assembled to form the updated structure resisting forces

$$\boldsymbol{P}_R^i = \sum_{ele=1}^{n} \boldsymbol{L}_{ele}{}^T \cdot \left(\boldsymbol{Q}^i\right)_{ele} \tag{2.70}$$

where n is the total number of beam-column elements in the structure and the subscript *ele* is added as a summation index. The new structure stiffness matrix is formed by assembling the current element stiffness matrices

$$\boldsymbol{K}_s^i = \sum_{ele=1}^{n} \boldsymbol{L}_{ele}{}^T \cdot \left(\boldsymbol{K}^i\right)_{ele} \cdot \boldsymbol{L}_{ele} \tag{2.71}$$

At this point the structure resisting forces $\boldsymbol{P}_R^i$ are compared with the total applied loads. If the difference $\boldsymbol{P}_U^i$, which is the structure unbalanced force vector, is not within the specified tolerance, i is incremented to $i+1$ and the next Newton-Raphson iteration begins. Steps **(1)** through **(14)** are repeated after replacing $\Delta\boldsymbol{P}_E^i$ with $\Delta\boldsymbol{P}_E^{i+1} = \Delta\boldsymbol{P}_U^i$ until convergence takes place at the structure degrees of freedom.

A graphical overview of the entire nonlinear analysis procedure is presented in Figs. 2.9 and 2.10. Fig. 2.9 provides an overview of the entire process with the nesting of the individual iteration loops, while Fig. 10 presents the features of the element state determination algorithm. Since all integrations along the element in Eqs. (2.66) and (2.68) need to be performed numerically, an additional iteration loop over all control sections of the element is introduced in this diagram.

REFERENCES:

[1] Zeris, C., Mahin, S.A., Analysis of reinforced concrete beam-columns under uniaxial excitation, *Journal of Structural Engineering*, ASCE 1988; **114**(4), 804-820.

[2] Zeris, C., Mahin, S.A., Behavior of reinforced concrete structures subjected to biaxial excitation, *Journal of Structural Engineering*, ASCE 1991; **117**(9), 2657-2673.

[3] Ciampi, V., Carlasimo, L., Anonlinear beam element for seismic analysis of structures, *Proceedings 8th European Conference on Earthquake Engineering.* 1986; Laboratorio National de Engenharia Civil, Lisbon, Portugal.

[4] Taucer, F.F., Spacone, E., Filippou, F.C., A fiber beam-column element for seismic response analysis of reinforced concrete structures, Report No. UCB/EERC-91/17, Earthquake Engineering Research Center, College of Engineering, University of California, Berkeley.

[5] Weiler, G., Nonlinear finite element analysis of reinforced and prestressed concrete frame structures, PhD dissertation, Rheinisch-Westfalische Technische Hochschule, Aachen, Germany.

[6] Zienkiewicz, O.C., Taylor, R.L., *The Finite Element Method Vol.1*, McGraw-Hill: New York.

[7] Neuenhofer, A., Filippou, F.C., On the solution of multi-point constraints – Application to FE analysis of reinforced concrete structures, *Journal of Structural Engineering* 1998; **124**(6), 704-711.

[8] Neuenhofer, A., Filippou, F.C., Evaluation of Nonlinear Frame Finite-Element Models, *Journal of Structural Engineering* 1997; **123**(7), 958-966.

[9] Spacone, E., Ciapi, V., Filippou, F.C., A Beam Element for Seismic Damage Analysis, Report No. UCB/EERC-92/07, Earthquake Engineering Research Center, College of Engineering, University of California, Berkeley, August 1992.

[10] Spacone, E., Filippou, F.C., Taucer, F.F., Fiber beam-column model for non-linear analysis of RC frames: part I. Formulation, *Earthquake Engineering and Structural Dynamics* 1996; **25**, 711-725.

[11] Spacone, E., Filippou, F.C., Taucer, F.F., Fiber beam-column model for non-linear analysis of RC frames: part II. Applications, *Earthquake Engineering and Structural Dynamics* 1996; **25**, 727-742.

[12] Argyris, J.H., Recent advances in matrix methods of structural analysis, *Progress in aeronautical sciences* 1963; **4**, Pergamon Press.

[13] Papaioannou, I., Fragiadakis, M., Papadrakakis, M., Inelastic analysis of framed structures using the fiber approach, *Proceedings of the 5th International Congress on Computational Mechanics (GRACM 05)*, Limassol, Cyprus, 29 June – 1 July.

[14] Παπαδρακάκης, Μ., *Ανάλυση φορέων με τη μέθοδο των πεπερασμένων στοιχείων*, Εκδόσεις Παπασωτηρίου, Αθήνα 1996.

[15] Monti, G., Spacone, E., Filippou, F.C., A Beam Element for Seismic Damage Analysis, Report No. UCB/EERC-93/08, Earthquake Engineering Research Center, College of Engineering, University of California, Berkeley, December 1993.

[16] Kaba, S.A., Mahin, S.A., Refined modeling of reinforced concrete columns for seismic analysis, Report No. UCB/EERC-84/03, Earthquake Engineering Research Center, College of Engineering, University of California, Berkeley, 1984.

[17] Kent, D.C., Park, R., Flexural members with confined concrete, *Journal of Structural Division, ASCE* 1971; **97**, 1964-1990.

[18] Scott, B.D., Park, R., Priestley, M.J.N., Stress-strain behavior of concrete confined by overlapping hoops at low and high strain rates, *ACI Journal*, **79**, 13-27.

[19] Karsan, I.D., Jirsa, J.O., Behavior of concrete under compressive loadings, *Journal of the Structural Division, ASCE* 1969; **95**, 2543-2563.

3 DESIGN AND ASSESSMENT PROCEDURES AGAINSTS THE SEISMIC LOADING

3.1 Introduction

The majority of the seismic design codes belong to the category of the prescriptive building design codes, which include: site selection and development of conceptual, preliminary and final design stages. According to a prescriptive design code, the strength of the structure is evaluated at one limit state between life-safety and near collapse using a response spectrum corresponding to one design earthquake [1]. In addition, serviceability limit state is usually checked in order to ensure that the structure will not deflect or vibrate excessively during its functioning. Apart from the minimum level of protection in order to safeguard adequately against partial collapse that endangers human lives, society has responsibilities including continuing operation of critical facilities, protection against the discharge of hazardous materials, and protection against excessive damage that may have far-reaching consequences for society on a local, regional, national, or international level. Performance-based design is a different approach for the seismic design which includes, apart from the site selection and the definition of the design stages, the construction and maintenance of the building in order to ensure reliable and

predictable seismic performance over its life and to achieve targeted performance objectives [2]. A performance objective pairs a single hazard level with a single performance level. Its advantage compared to other seismic design provisions is its capability to specify the performance for a range of hazard levels [3].

3.2 Prescriptive design procedures

According to the EC8 [4] a number of checks must be performed in order to ensure that the structure will meet the design requirements and also to ensure the followings, in the event of earthquakes :

- human lives are protected
- damage is limited and
- structures important for civil protection remain operational.

Each candidate design is assessed using these constraints. All EC2 [5] checks must be satisfied for the gravity loads using the following load combination:

$$S_d = 1.35\sum_j G_{kj} "+" 1.50\sum_i Q_{ki} \tag{3.1}$$

where "+" implies "to be combined with", the summation symbol "Σ" implies "the combined effect of", G_{kj} denotes the characteristic value "k" of the permanent action j and Q_{ki} refers to the characteristic value "k" of the variable action i. If the above constraints are satisfied, multi-modal response spectrum analysis is performed, according to EC8 [4] and earthquake loading is considered using the following load combination (3.2):

$$S_d = \sum_j G_{kj} "+" E_d "+" \sum_i \psi_{2i} Q_{ki} \tag{3.2}$$

where E_d is the design value of the seismic action for the two components (longitudinal and transverse) respectively and ψ_{2i} is the combination coefficient for the quasi-permanent action i, here taken equal to 0.30.

The combination coefficient ψ_{2i} is computed from the following expression (3.3) :

$$\psi_{Ei} = \varphi \cdot \psi_{2i} \tag{3.3}$$

Table 3.1: Value of φ for calculating ψ_{Ei}

Type of variable action	Storey	ϕ
Categories A-C*	Roof	1.00
	Storeys with correlated occupancies	0.8
	Independently occupied storeys	0.5
Categories D-F* and Archives		1.00

* Categories as defined in EN 1991-1-1:2002 [6].

The following table 2 shows the values of ψ_{2i} for the earlier mentioned categories:

Table 3.2: Recommended values of ψ_{2i} factor for buildings (EC0 [7])

Action	ψ_{2i}
Imposed loads in buildings, category (see EN 1991-1-1)	
Category A : domestic, residential areas	0.3
Category B : office areas	0.3
Category C : congregation areas	0.6
Category D : shopping areas	0.6
Category E : storage areas	0.8
Category F : traffic area	0.6

Furthermore, for spatial problems, E_d seismic actions is considered in the Multi-modal Response Spectrum (MmRS) analysis method for the current case, or for nonlinear static (pushover) analysis and nonlinear time history analysis in general, using the following load combinations:

$$E_d = E_{dx} + 0.3E_{dy} \tag{3.4}$$

$$E_d = 0.3E_{dx} + E_{dy} \tag{3.5}$$

where E_{dx} and E_{dy} represent earthquake loading in two directions that are perpendicular to each other.

The main principle EC8 [4] is to design structural systems based on energy dissipation and on ductility in order to control the inelastic seismic response. Designing a multistory RC building for energy dissipation comprises the following features:

(i) Fulfillment of the strong column/weak beam rule,

(ii) Member verification in terms of forces and resistances for the ultimate strength limit state under the design earthquake (with return period of 475 years, probability of exceedance 10% in 50 years), with the elastic spectrum reduced by the q-factor equal to 3.0 times,

(iii) Damage limitation for the serviceability limit state and

(iv) Capacity design of beams and columns against shear failure.

3.3 Performance-based design procedure

Performance-based seismic design has the following distinctive features with respect to the prescriptive design codes: (i) Allows the owner, architect, and structural engineer to choose both the appropriate level of seismic hazard and the corresponding performance level of the structure. (ii) The structure is designed to meet a series of combinations of hazard levels in conjunction with corresponding performance levels. Figure 3.1 illustrates a global framework, which identifies processes, concepts and major issues that need to be addressed. The issues encompass seismological, geotechnical, structural, architectural and socio-economic considerations.

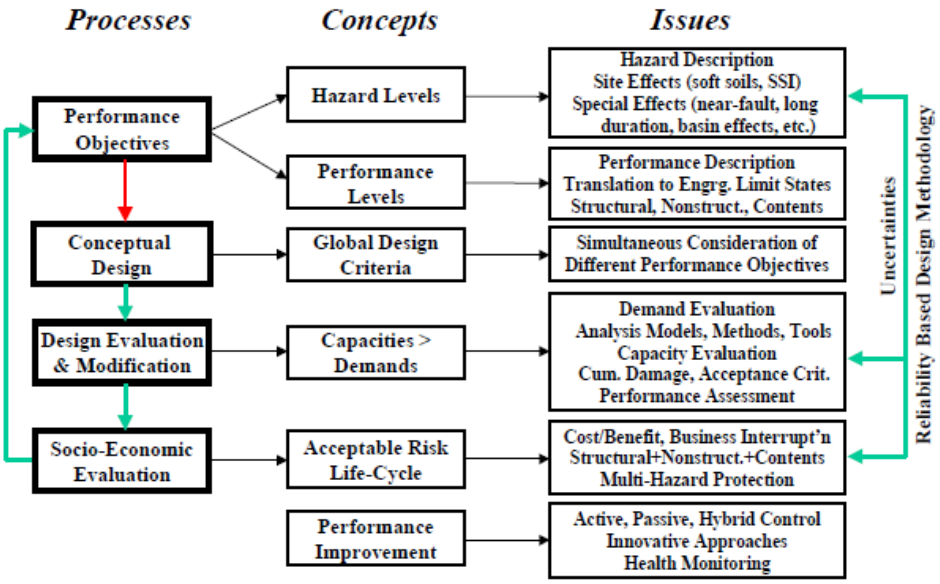

Figure 3.1. A global framework for Performance-Based Engineering [8].

The PBD process is a displacement-based design procedure where the design criteria and the capacity demand comparisons are expressed in terms of displacements rather than forces [9-11]. In order to assess the capacity of deformation-controlled actions an appropriate Earthquake Demand Parameter (EDP) should be implemented. Interstory drifts, inelastic deformations, section curvatures, floor accelerations and velocities are some of the most widespread EDPs [12, 13]. The main part in a performance-based seismic design procedure is the definition of the performance objectives that will be used. The proposed PBD process can be described with the following two steps:

(1) **Conceptual Design**: Proportioning of the longitudinal and transverse reinforcement of all members on the basis of the serviceability limit state. In this phase, a structural system capable of fulfilling diverse requirements at various performance levels needs to be configured. This design phase is critical since most of the important design decisions are being made in it. Later design phases serve primarily to evaluate, fine tune, and detail an already existing system. Engineers are used to design for strength and elastic stiffness, with an implicit understanding of the importance of ductility, and with a single-level design in mind. Performance-based design will impose diverse multi-level requirements whose relationship between ground motion and engineering parameters need to be established and quantified in

order to provide targets for strength, stiffness and ductility design. Different performance levels may control different aspects of the design, and simultaneous consideration of different performance objectives will become a fundamental aspect of conceptual design.

(2) **Design Evaluation and Modification**: Use of non-linear dynamic analysis in order to estimate the structural capacities of the design in the different intensity levels employed. Revise the reinforcement and the dimension of the members so that the capacities exceed the seismic demands [10]. This process is at the core of performance-based design and encompasses all aspects of demand and capacity predictions needed to carry out design evaluation through assessment of performance at different levels (or estimation of total costs) and to modify design decisions of the stated performance objectives are not met (or the costs are unacceptable). From an engineering perspective, satisfactory performance implies that the demands imposed by earthquakes do not exceed the capacities the structural, non-structural and contents components-systems are capable to provide. Demands and capacities are general terms that take on a specific meaning for different parameters that may control component and system performance at various performance levels.

The completion of the *Step 1* is necessary for *Step 2* as the structural capacity depends both on the reinforcement and the dimensions of the members. The constraints considered for *Step 2* of the PBD procedure are related to the maximum interstory drift limits Δ, which are the largest values of the height-wise peak interstory drift ratios for each hazard level. This is a commonly used measure of both structural and non-structural damage because of its close relationship to plastic rotation demands on individual beam–column connection assemblies. In this study, three performance objectives are considered that correspond to 50, 10 and 2% probabilities of exceedance in 50 years hazard levels. The drift limits Δ, for the three performance objectives considered, are 0.5%, 1.0% and 3.0% for the three hazard levels 50in50, 10in50 and 2in50 respectively.

Performance assessment must be based on a probabilistic hazard representation and a prediction of seismic demands and capacities for all important components soil-foundation-structure system and of non-structural and content systems. At this time neither capacities nor demands can be predicted with good accuracy, because of insufficient knowledge, lack of tools, and randomness and modelling uncertainties. We must try to improve description of the randomness and reduce the modelling uncertainties, but we must acknowledge that we will not be able to eliminate either. Appropriate analysis methods need to be developed to provide adequate yet simple means of demand prediction. Nonlinear inelastic time history analysis is desirable but likely not necessary in many cases. Research on the most effective demand prediction methods needs to be performed, with emphasis on the following aspects:

- Assessment of the quality of demand prediction that can be achieved by various analysis methods (elastic-static, elastic-dynamic, inelastic-static and inelastic-dynamic).
- Three-dimensional analysis procedures for soil-foundation-structure systems.
- Sufficiently realistic modelling of strength, stiffness and mass irregularities in plan and elevation.
- Sufficiently realistic modelling of component behavior under cyclic loading.
- Modelling of non-structural components and systems.
- Validation of modelling and analysis procedures through the utilization of laboratory and field experimentation, earthquake damage data, and vibration measurements from instrumented structures.

3.3.1 Performance Levels

One performance objective is defined as the combination of a performance level for a specific hazard level. In this work three performance objectives have been considered corresponding to the ‘Enhanced Objectives’ of FEMA 356 [14]. The first step in the definition of the performance objectives is the selection of the

performance levels. The performance levels that have been considered are the following:

(i) Operational (OPER): the overall damage level is characterized as very light. No permanent drift is encountered, while the structure essentially retains original strength and stiffness.

To attain the operational building performance level, the structural components of the building shall meet the requirements the immediate occupancy (IO) structural performance level and the nonstructural components shall meet the requirements for the operational nonstructural performance level. The immediate occupancy structural performance level shall be defined as the post-earthquake damage state that remains safe to occupy, essentially retains the pre-earthquake design strength and stiffness of the structure.

Also the immediate occupancy structural performance level, means the post-earthquake damage state in which only very limited structural damage has occurred. The basic vertical- and lateral-force-resisting systems of the building retain nearly all of their pre-earthquake strength and stiffness. The risk of life threatening injury as a result of structural damage is very low, and although some minor structural repairs may be appropriate, these would generally not be required prior to reoccupancy. And the operational nonstructural performance level shall be defined as the post-earthquake damage state in which the nonstructural components are able to support the pre-earthquake functions present in the building.

At this level, most nonstructural systems required for normal use of the building—including lighting, plumbing, HVAC, and computer systems—are functional, although minor cleanup and repair of some items may be required. This nonstructural performance level requires considerations beyond those that are normally within the sole province of the structural engineer. In addition to assuring that nonstructural components are properly mounted and braced within the structure, it is often necessary to provide emergency standby utilities. It also may be necessary to perform rigorous qualification testing of the ability of key electrical and mechanical equipment items to function during or after strong shaking. Users wishing to design for this nonstructural performance level will need to refer to

appropriate criteria from other sources (such as equipment manufacturers' data) to ensure the performance of mechanical and electrical systems.

Therefore, buildings meeting this target Building Performance Level are expected to sustain minimal or no damage to their structural and nonstructural components. The building is suitable for its normal occupancy and use, although possibly in a slightly impaired mode, with power, water, and other required utilities provided from emergency sources, and possibly with some nonessential systems not functioning. Buildings meeting this target Building Performance Level pose an extremely low risk to life safety.

Under very low levels of earthquake ground motion, most buildings should be able to meet or exceed this target building performance level. Typically, however, it will not be economically practical to design for this target building performance level for severe ground shaking, except for buildings that house essential services.

(ii) Life safety (LS): the overall damage level is characterized as moderate. Permanent drift is encountered while strength and stiffness has left in all stories. Gravity-load bearing elements continue to function while there is no out-of plane failure of the walls. The overall risk of life-threatening injury as a result of structural damage is expected to be low. It should be possible to repair the structure; however, for economic reasons this may not be practical.

To attain the life safety building performance level, the structural components of the building shall meet the requirements for the Life Safety Structural Performance Level and the nonstructural components shall meet the requirement for the Life Safety Nonstructural Performance Level.

The structural performance level shall be defined as the post-earthquake damage state that includes damage to structural components but retains a margin against onset of partial or total collapse.

Also the structural performance level means the post-earthquake damage state in which significant damage to the structure has occurred, but some margin against either partial or total structural collapse remains. Some structural elements and components are severely damaged, but this has not resulted in large falling debris hazards, either within or outside the building. Injuries may occur during the

earthquake; however, the overall risk of life-threatening injury as a result of structural damage is expected to be low. It should be possible to repair the structure; however, for economic reasons this may not be practical. While the damaged structure is not an imminent collapse risk, it would be prudent to implement structural repairs or install temporary bracing prior to reoccupancy. And the life safety nonstructural performance level shall be defined as the post-earthquake damage state that includes damage to nonstructural components but the damage is non-life threatening.

Also the life safety nonstructural performance level is the post-earthquake damage state in which potentially significant and costly damage has occurred to nonstructural components but they have not become dislodged and fallen, threatening life safety either inside or outside the building. Egress routes within the building are not extensively blocked, but may be impaired by lightweight debris. HVAC, plumbing, and fire suppression systems may have been damaged, resulting in local flooding as well as loss of function. While injuries may occur during the earthquake from the failure of nonstructural components, overall, the risk of life-threatening injury is very low. Restoration of the nonstructural components may take extensive effort.

So, buildings meeting this level may experience extensive damage to structural and nonstructural components. Repairs may be required before reoccupancy of the building occurs, and repair may be deemed economically impractical. The risk to life safety in buildings meeting this target Building Performance Level is low.

This target Building Performance Level entails somewhat more damage than anticipated for new buildings that have been properly designed and constructed for seismic resistance when subjected to their design earthquakes. Many building owners will desire to meet this target Building Performance Level for severe ground shaking.

(iii) Collapse prevention: the overall damage level is characterized as severe. Substantial damage has occurred to the structure, including significant degradation in the stiffness and strength of the lateral-force resisting system. Large permanent lateral deformation of the structure and degradation in vertical-load bearing capacity

is encountered. However, all significant components of the gravity load-resisting system continue to carry their gravity load demands. The structure may not be technically practical to repair and is not safe for reoccupancy, since aftershock activity could induce collapse.

To attain the Collapse Prevention Building Performance Level, the structural components of the building shall meet the requirements for the Collapse Prevention Structural Performance Level. Nonstructural components are not considered.

The structural performance level shall be defined as the post-earthquake damage state that includes damage to structural components such that the structure continues to support gravity loads but retains no margin against collapse.

However, the structural performance level means the post-earthquake damage state in which the building is on the verge of partial or total collapse. Substantial damage to the structure has occurred, potentially including significant degradation in the stiffness and strength of the lateral-force-resisting system, large permanent lateral deformation of the structure, and—to a more limited extent— degradation in vertical-load-carrying capacity. However, all significant components of the gravity load- resisting system must continue to carry their gravity load demands. Significant risk of injury due to falling hazards from structural debris may exist. The structure may not be technically practical to repair and is not safe for reoccupancy, as aftershock activity could induce collapse. And as nonstructural performance is not considered shall be classified a building rehabilitation that does not address nonstructural components.

Additionally, in some cases, the decision to rehabilitate the structure may be made without addressing the vulnerabilities of nonstructural components. It may be desirable to do this when rehabilitation must be performed without interruption of building operation. In some cases, it is possible to perform all or most of the structural rehabilitation from outside occupied building areas. Extensive disruption of normal operation may be required to perform nonstructural rehabilitation. Also, since many of the most severe hazards to life safety occur as a result of structural vulnerabilities, some municipalities may wish to adopt rehabilitation ordinances that require structural rehabilitation only.

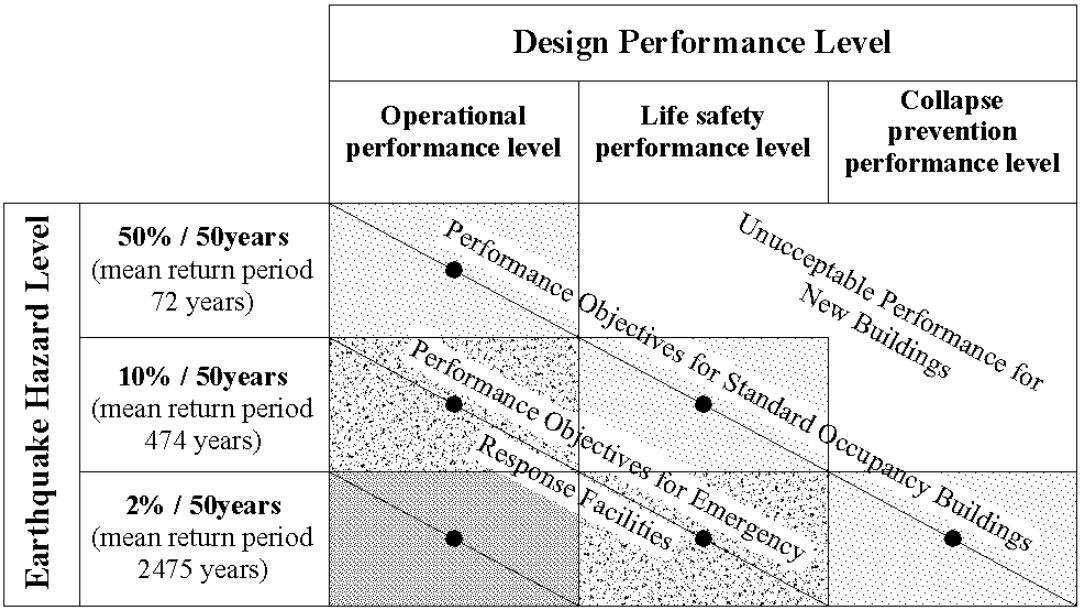

Figure 3.2. The Design Performances.

3.3.2 Hazard levels

The second step in the definition of the performance objectives is to determine the earthquake hazard levels. Earthquake hazards include direct ground fault rupture, ground shaking, liquefaction, lateral spreading and land sliding FEMA-350 [15]. Ground shaking is the only earthquake hazard that the structural design provisions of the building codes directly address. Ground shaking hazards are typically characterized by a hazard curve, which indicates the probability that a given value of a ground motion parameter, for example peak ground acceleration, will be exceeded over a certain period of time. The ground shaking hazard levels that have been considered are the following:

(i) Occasional earthquake hazard level: with probability of exceedance 50% in 50 years with interval of recurrence 72 years.

(ii) Rare earthquake hazard level: with probability of exceedance 10% in 50 years with interval of recurrence 475 years.

(iii) Maximum considered event earthquake hazard level: with probability of exceedance 2% in 50 years with interval of recurrence 2475 years.

Performance-based design by itself will not accomplish improved or more predictable structural performance. Design provides only a set of drawings and instructions to the builder. The quality of the build product will depend on the clarity of the documentation and its communication, and the capability and willingness of the builder to implement the instructions. Thus performance-based design must be followed by performance-based construction, in which construction engineering services and quality control play key roles. A rigorous implementation of Performance-Based Earthquake Engineering may well necessitate radical changes in engineering and construction practices. Architects, engineers and contractors will have to work together rather than take on adversary positions, and academic researchers will have to interact much more than in the past.

3.4 Design Procedures

Depending on the design procedure adopted, as it was described in the previous section of this chapter, the structural system is assessed using linear or nonlinear analysis procedures in order to calculate force and displacement response quantities. In this thesis I focus on the study of the torsional effect on building structures' response.

3.4.1 General Overview of EC8

In order to ensure that the structure will satisfy the requirements properties of the EC8 [4], after the calculation of the solution of the structural optimization problem, which was considered for this comparative study, were employed checks. The checks that were applied are: For the case of columns, these elements should be assessed for (i) bending (biaxial bending: simultaneous bending about two principal axes, primary tension, centroidal compression (pure buckling : failure due to instability of a member or structure under perfectly axial compression and without transverse load), (ii) combination of bending moment and compression force (compression, yielding of shear reinforcement, yielding of the total longitudinal reinforcement, yielding of compression reinforcement, yielding of compression

reinforcement and compression of the total reinforcement, interaction criterion) and (iii) shear (check inclined compression, check reinforcement bars with seismic action in shear force, check confined concrete). For the case of beams these elements should be assessed for (i) bending (uniaxial bending without seismic action, checking for reinforcement bars in tension and in compression, shear and compression reinforcement in failure, shear reinforcement in failure and compression reinforcement in elastic region) and (ii) shear (check stem region, check inclined compression, check reinforcement bars with seismic action in shear force).

3.4.2 Treatment of torsional effect

A main problem for engineers that has great impact on the dynamic response of buildings is the lateral-torsional coupling. Coupled lateral-torsional motions occur in buildings subjected to ground shaking if their plan layouts do not possess two axes of mass and stiffness symmetry or ground shaking includes a torsional component. They can also appear due to unbalanced load distributions or differences between actual and assumed mass and stiffness distributions.

In most structural design codes, the effect of torsion is treated by implementing accidental and static eccentricities together with specific provisions for addressing the design of irregular buildings. Accidental eccentricity is defined, with reference to the location of the mass center, as a percentile (e.g. 5%) of the plan view dimension that is perpendicular to the direction of the lateral forces applied. On the other hand, the implementation of the static eccentricity is more complicated, since it is defined with reference to the location of the rigidity center whose position, for the case of multistory buildings, is not unique and is load-dependent. It is for this reason that many researchers studied the efficiency of torsional codified provisions [16, 17]. Inconsistent observations have been attributed to the varying model assumptions implemented, while a detailed overview has been presented by Rutenberg [18]. Cheung and Tso [19] proposed the generalized center of rigidity and twist under linear response, while Tso [20] compared two approaches in an effort to measure the story torsional moments for multistory buildings. In particular, the torsional moment is calculated using the floor eccentricity in the first approach, while in the

second one using the story eccentricity. Smith and Vezina [21] defined the story rigidity center of multistory buildings as the point on the story diaphragm where no torsional action is developed from the application of external horizontal load. Riddell and Vaquez [22] concluded that the centers of rigidity exist only for a special class of multistory buildings. Lagaros *et al.* [23] proposed a combined topology-sizing optimum design formulation for RC buildings aiming at minimizing the material cost as well as the static and strength eccentricities taking into account both design code and architectural restrictions.

Research interest extended also to the inelastic response of single-story structures [24-26]. De la Llera and Chopra [27] proposed the base shear and torque surfaces (BST), which represent all combinations of base shear and torque that would lead to structural collapse when applied statically. Paulay [28, 29] proposed the center of resistance and identified the elastoplastic mechanism, aiming at estimating the torsional effects on the seismic response of ductile buildings, classifying them either as torsionally unrestrained or as torsionally restrained. Dutta and Das [30, 31] investigated the effects of strength degradation on the bidirectional response of code-designed systems. The two simple hysteretic models proposed by the authors accounting for stiffness and strength deterioration characteristics of RC structural elements indicated that local peak demands, at both stiff and flexible edge, are more significant when strength degradation is taken into consideration. Contrary to these conclusions, Tso and Myslimaj [32] observed that results obtained by a degrading hysteretic model do not differ significantly from those obtained by an elasto-plastic model. Moreover, Myslimaj and Tso [33, 34] proved that the torsional effect can be reduced for asymmetric wall-type systems by locating the center of strength and the center of rigidity on the opposite sides of the center of mass. Overestimation of torsional response was noticed by De Stefano and Pintucchi [35] when the inelastic interaction between axial force and bidirectional horizontal forces in resisting elements is ignored. Aziminejad and Moghadam [36] studied the nonlinear behavior of irregular code designed single-story structures in order to optimize configuration of mass, stiffness and strength centers with respect to different levels of plastic excursions in the framework of performance-based seismic

design. They concluded that the best configuration varies not only with the assumed performance level, but also with the selected response parameter or damage indices.

Trombetti and Conte [37] developed a simplified procedure, the ALPHA method, for estimating the maximum rotational response under free and forced vibrations of single-story linear elastic systems. An alternative pushover procedure was introduced by Moghadam and Tso [38]. The two steps of analysis are: (i) A three-dimensional elastic response spectrum analysis, in order to compute the roof displacements and the distribution of lateral forces. (ii) By implementing the target displacement and the lateral force distribution obtained at the previous step conduct a planar pushover analysis for each resisting element. With the aim to study the inelastic torsional response of buildings in nonlinear static (pushover) analysis, Penelis and Kappos [39] proposed a method consisted of a three-dimensional pushover analysis, applying spectral load vectors defined from dynamic elastic spectral analysis. They implemented a generalized equivalent SDOF, taking into account translational and torsional modes, to record response quantities. Code recommendations for torsionally unbalanced multistory buildings were assessed by De-la-Colina [40]. Tena-Colunga [41] studied the response of two irregular 14-story reinforced concrete buildings. The first one has one bay in slender direction, while the other two. The results indicate that codified provisions should penalize buildings with one bay.

3.4.3 Elastic torsional response

For the case of single-story systems there is a position on the diaphragm with the following properties: (i) Does not rotate when a lateral load is applied to it (rigidity center); (ii) does not rotate when the resultant of the shear forces is applied to it (shear center); (iii) remains constant when the structure is subjected to torque loading (center of twist). For the case of single-story systems only these centers coincide and they are load-independent. However, for the case of multistory buildings these centers do not coincide and their effect has been the subject of extensive research by many researchers in the past.

The most popular parameters characterizing the torsional effect on a building for elastic structural behavior are the static eccentricity (e_{CR}) perpendicular to the direction of ground motion and the ratio of the uncoupled torsional to lateral frequency ratio (Ω). The static eccentricity e_{CR} of single-story structures is defined as the distance between the center of mass (CM) and the rigidity center (CR). The rigidity center (CR) is defined as the point on the diaphragm through which a static horizontal force causes only translation on the diaphragm, irrespective of the force direction, while mass center (CM) is defined as the point on the diaphragm where the resultant of the inertia forces is applied to. The buildings are classified as torsionally-stiff for Ω values greater than unity or as torsionally-flexible for Ω values lower than unity. For torsionally-stiff structures the predominant mode is translational while for torsionally-flexible systems the predominant mode is torsional. Furthermore, the edges of the structures are denoted as stiff or flexible, with reference to the position of the mass and rigidity centers. In particular, when the distance of the edge from CM is smaller than that from CR, the edge is characterized as flexible otherwise the edge is characterized as stiff. It is worth noting that a building can be torsionally stiff in one direction and flexible in the other. Torsionally stiff buildings display increased displacements at the flexible edge and decreased at the stiff one, compared to the symmetric design, while torsionally flexible buildings do not follow any specific pattern [32, 33].

3.4.3.1 Location of the center of rigidity for single-story systems

The undamped equations of motion for single-story system, assuming linear behavior, subjected to earthquake ground motion accelerations $a_{gx}(t)$, $a_{gy}(t)$ along x and y axes are:

$$\begin{bmatrix} m & 0 & -my_{CM} \\ 0 & m & mx_{CM} \\ -my_{CM} & mx_{CM} & J_0 \end{bmatrix} \begin{Bmatrix} \ddot{u}_X \\ \ddot{u}_Y \\ \ddot{u}_\theta \end{Bmatrix} + \begin{bmatrix} K_X & K_{XY} & K_{X\theta} \\ K_{YX} & K_Y & K_{Y\theta} \\ K_{\theta X} & K_{\theta Y} & K_\theta \end{bmatrix} \begin{Bmatrix} u_X \\ u_Y \\ u_\theta \end{Bmatrix} = -m \begin{Bmatrix} a_{gx}(t) \\ a_{gy}(t) \\ -y_M a_{gx}(t) + x_M a_{gy}(t) \end{Bmatrix} \quad (3.6)$$

where m is the mass moment of the deck, x_{CM} and y_{CM} are the coordinates of the center of mass, $K_X, K_Y, K_{XY}, K_{X\theta}$ and $K_{Y\theta}$ are the terms of the stiffness matrix corresponding to translational (x and y) and rotational (θ) degrees of freedom of the one-story structure, and J_0 is the polar moment of inertia of the deck about vertical axis passing through reference point O, given by:

$$J_0 = m\left(r^2 + x_{CM}^2 + y_{CM}^2\right) \tag{3.7}$$

where r is the radius of gyration of the deck about a vertical axis passing through the center of mass of the deck.

The building stiffness matrix $\boldsymbol{K}$ for degrees of freedom $\boldsymbol{u}^T = \langle u_X u_Y u_\theta \rangle$, defined at O, is given by superposition of the element stiffness matrices resulting in:

$$\boldsymbol{K} = \begin{bmatrix} K_X & K_{XY} & K_{X\theta} \\ K_{YX} & K_Y & K_{Y\theta} \\ K_{\theta X} & K_{\theta Y} & K_\theta \end{bmatrix} \tag{3.8}$$

with,

$$K_X = \sum_i K_{Xi}\ ,\ K_Y = \sum_i K_{Yi}\ ,\ K_\theta = \sum_i K_{\theta i}$$

$$K_{X\theta} = K_{\theta X} = \sum_i K_{X\theta i}\ ,\ K_{Y\theta} = K_{\theta Y} = \sum_i K_{Y\theta i}$$

$$K_{XY} = K_{YX} = \sum_i K_{XYi}$$

While if the equations of motion are written for degrees of freedom $\tilde{\boldsymbol{u}}$, where $\tilde{\boldsymbol{u}}^T = \langle \tilde{u}_X \tilde{u}_Y u_\theta \rangle$ with $\tilde{u}_X$ and $\tilde{u}_Y$ the lateral displacements at the center of rigidity along the x and y axes, the building stiffness matrix assumes the form:

$$\tilde{\boldsymbol{K}} = \begin{bmatrix} \tilde{K}_X & \tilde{K}_{XY} & 0 \\ \tilde{K}_{YX} & \tilde{K}_Y & 0 \\ 0 & 0 & \tilde{K}_\theta \end{bmatrix} \tag{3.9}$$

Since any horizontal static force applied through the center of rigidity causes only lateral displacements and no rotation of the deck.

The equations of motion written with respect to $\tilde{\boldsymbol{u}}$ are then given by:

$$\begin{bmatrix} m & 0 & -me_{CRy} \\ 0 & m & me_{CRx} \\ -me_{CRy} & me_{CRx} & J_R \end{bmatrix} \begin{Bmatrix} \ddot{\tilde{u}}_X \\ \ddot{\tilde{u}}_Y \\ \ddot{\tilde{u}}_\theta \end{Bmatrix} + \begin{bmatrix} \tilde{K}_X & \tilde{K}_{XY} & 0 \\ \tilde{K}_{YX} & \tilde{K}_Y & 0 \\ 0 & 0 & \tilde{K}_\theta \end{bmatrix} \begin{Bmatrix} \tilde{u}_X \\ \tilde{u}_Y \\ u_\theta \end{Bmatrix} = -m \begin{Bmatrix} a_{gx}(t) \\ a_{gy}(t) \\ -e_{CRy} a_{gx}(t) + e_{CRx} a_{gy}(t) \end{Bmatrix} \quad (3.10)$$

where e_{CRx} and e_{CRy}, the x and y components of static eccentricity e_{CR} are:

$$e_{CRx} = x_{CM} - x_{CR} \quad (3.11)$$

$$e_{CRy} = y_{CM} - y_{CR} \quad (3.12)$$

in which x_{CR} and y_{CR} are the coordinates of the center of rigidity and J_R is the polar moment of inertia about a vertical axis passing through the center of rigidity, given by:

$$J_R = m\left(e_{CR}^2 + r^2\right) \quad (3.13)$$

From the building stiffness matrix $\boldsymbol{K}$ defined with respect to the degrees of freedom $\boldsymbol{u}$ at reference point O, where $\boldsymbol{u}^T = \langle u_X u_Y u_\theta \rangle$, the building stiffness matrix at any other point can be determined by simple transformation of $\boldsymbol{K}$. In particular, the building stiffness matrix $\tilde{\boldsymbol{K}}$ with respect to degrees of freedom $\tilde{\boldsymbol{u}}$, where $\tilde{\boldsymbol{u}}^T = \langle \tilde{u}_X \tilde{u}_Y \tilde{u}_\theta \rangle$ is defined at the center of rigidity of the system, is related to the building stiffness matrix $\boldsymbol{K}$ by:

$$\tilde{\boldsymbol{K}} = \tilde{\boldsymbol{a}}^T \boldsymbol{K}\, \tilde{\boldsymbol{a}} \quad (3.14)$$

in which $\tilde{\boldsymbol{a}}$ is a transformation matrix relating $\boldsymbol{u}$ to $\tilde{\boldsymbol{u}}$:

$$\boldsymbol{u} = \begin{Bmatrix} u_X \\ u_Y \\ u_\theta \end{Bmatrix} = \begin{bmatrix} 1 & 0 & y_{CR} \\ 0 & 1 & x_{CR} \\ 0 & 0 & 1 \end{bmatrix} \begin{Bmatrix} \tilde{u}_X \\ \tilde{u}_Y \\ u_\theta \end{Bmatrix} = \tilde{\boldsymbol{a}} \tilde{\boldsymbol{u}} \quad (3.15)$$

Substituting equations (3.15) and (3.8) into (3.14), leads to:

$$\tilde{\boldsymbol{K}} = \begin{bmatrix} K_X & K_{XY} & K_X y_{CR} - K_{XY} x_R + K_{X\theta} \\ K_{YX} & K_Y & K_{YX} y_{CR} - K_Y x_R + K_{Y\theta} \\ K_{\theta X} + y_{CR} K_X - x_{CR} K_{YX} & K_{\theta Y} + y_{CR} K_{XY} - x_{CR} K_Y & \tilde{K}_\theta \end{bmatrix} \quad (3.16)$$

in which $\tilde{K}_\theta = K_\theta + 2K_{\theta X} y_{CR} - 2K_{\theta Y} x_{CR} + K_X y_{CR}^2 - 2K_{XY} x_{CR} y_{CR} + K_Y x_{CR}^2$

Comparison of equations (3.16) and (3.9) leads to the following conditions:

$$K_X y_{CR} - K_{XY} x_R + K_{X\theta} = 0 \quad (3.17)$$

$$K_{\theta Y} + y_{CR} K_{XY} - x_{CR} K_Y = 0 \quad (3.18)$$

$$\tilde{K}_X = K_X, \tilde{K}_Y = K_Y \text{ and } \tilde{K}_{XY} = \tilde{K}_{YX} = K_{XY} \quad (3.19)$$

and

$$\tilde{K}_\theta = K_\theta + 2K_{\theta X} y_{CR} - 2K_{\theta Y} x_{CR} + K_X y_{CR}^2 - 2K_{XY} x_{CR} y_{CR} + K_Y x_{CR}^2 \quad (3.20)$$

Solution of equations (3.17) and (3.18) yields the coordinates of the center of rigidity:

$$x_{CR} = \frac{K_X K_{Y\theta} - K_{XY} K_{X\theta}}{K_X K_Y - K_{XY}^2} \quad (3.21)$$

$$y_{CR} = \frac{K_Y K_{X\theta} - K_{XY} K_{Y\theta}}{K_X K_Y - K_{XY}^2} \quad (3.22)$$

Equations (3.21) and (3.22) are further simplified on two special cases:

1. The building has one axis of symmetry, which coincides with one of the principal axes of the system and the other is perpendicular to it. For instance, if x axis is chosen in the direction of the symmetry axis, the terms K_{XYi} and $K_{X\theta i}$ occur in pairs that are equal in absolute values but are of opposite algebraic signs. It follows that:

$$K_{XY} = K_{YX} = 0 \quad (3.23)$$

and

$$K_{X\theta} = K_{\theta X} \tag{3.24}$$

from which equations (3.21) and (3.22) are simplified to become:

$$x_{CR} = \frac{K_{Y\theta}}{K_Y} \tag{3.25}$$

$$y_{CR} = -\frac{K_{X\theta}}{K_X} = 0 \tag{3.26}$$

2. The resisting elements of the building are arranged such that their principal axes form an orthogonal grid in plan. The principal axes of the system are also in the directions of the elemental principal axes. The coordinates of the center of rigidity are simplified to:

$$x_{CR} = \frac{K_{Y\theta}}{K_Y} = \frac{\sum_i K_{Yi} x_i}{\sum_i K_{Yi}} \tag{3.27}$$

$$y_{CR} = -\frac{K_{X\theta}}{K_X} = \frac{\sum_i K_{Xi} y_i}{\sum_i K_{Xi}} \tag{3.28}$$

3.4.3.2 Location of the shear center for single-story systems

The shear center is the point in the plane of the diaphragm through which the resultant of the shear forces of the resisting elements passes when the diaphragm is subjected to a system of horizontal lateral forces causing no twist ($u_\theta = 0$) of the diaphragm. Substituting $u_\theta = 0$ and utilizing the equilibrium of moments of all shearing forces acting in the plane of the diaphragm about a vertical axis passing through O, gives an equation which leads to the same expression as the center of rigidity. It should be noted that center of twist, rigidity and shear centers for one-story structures coincide [44]; thus, the coordinates of the shear center and the center of twist are also obtained from Eqs. (3.21), (3.22).

3.4.3.3 Location of the center of twist for single-story systems

Since the center of twist is the point in the plane of diaphragm that does not undergo any translational displacement when the diaphragm is subjected to a static horizontal torsional moment, the building stiffness matrix is identical to (3.8) considering that the degrees of freedom of the diaphragm are defined at its center of twist. The same procedure as the one followed for the center of rigidity leads to the same expressions (eqns. (3.21) and (3.22)) for the coordinates of the center of twist.

3.4.3.4 Location of the center of rigidity for multistory systems

The rigidity centers of the stories for the case of multistory buildings cannot be defined in a strict manner and many definitions have been proposed so far [19, 21, 45, 46]. Indicatively, Humar [42] defined the location of story rigidity center as the point where the resultant lateral forces of the story when applied to that point does not cause rotation of the specific story. The other stories may or may not have rotations. Smith and Vezina [21] defined the location of story rigidity center of multistory buildings for given distribution of the lateral loads, as the point on the story where if the external lateral load is applied no torque is observed.

The undamped equations of motion for multistory building, assuming linear behavior, subjected to earthquake ground motion accelerations $a_{gx}(t)$ and $a_{gy}(t)$ along x and y axes are:

$$\begin{bmatrix} m & 0 & -my_M \\ 0 & m & mx_M \\ -my_M & mx_M & J_0 \end{bmatrix} \begin{Bmatrix} \ddot{u}_X \\ \ddot{u}_Y \\ \ddot{u}_\theta \end{Bmatrix} + \begin{bmatrix} K_X & K_{XY} & K_{X\theta} \\ K_{YX} & K_Y & K_{Y\theta} \\ K_{\theta X} & K_{\theta Y} & K_\theta \end{bmatrix} \begin{Bmatrix} u_X \\ u_Y \\ u_\theta \end{Bmatrix} = - \begin{Bmatrix} m l a_{gx}(t) \\ m l a_{gy}(t) \\ -y_M m l a_{gx}(t) + x_M m l a_{gy}(t) \end{Bmatrix} \quad (3.29)$$

where $\mathbf{I}$ denotes a vector of ones of dimension N, the number of stories of the building, $\mathbf{m}$ is a diagonal matrix of dimension N with diagonal entry m_j equal to the mass of the j^{th} floor, $\boldsymbol{x}_{CM}$ and $\boldsymbol{y}_{CM}$ are diagonal matrices of dimension N with

diagonal entries equal to x_{CMj} and y_{CMj}, the coordinates of the center of mass of the j^{th} floor relative to reference axes X_j and Y_j, $\boldsymbol{J}_0$ is a diagonal matrix of dimension N with diagonal entries J_{oj} the polar moment of inertia of the j^{th} floor diaphragm about Z, the reference vertical axis passing through reference points O_j, given by:

$$J_{Oj} = m_j \left(r_j^2 + x_{CMj}^2 + y_{CMj}^2 \right) \tag{3.30}$$

where r_j is the radius of gyration of the j^{th} deck about a vertical axis passing through its center of mass.

The building stiffness matrix $\boldsymbol{K}$ for degrees of freedom $\boldsymbol{u}^T = \left\langle \boldsymbol{u}_X^T \boldsymbol{u}_Y^T \boldsymbol{u}_\theta^T \right\rangle$, defined at reference points O_j, is given by the superposition of the element stiffness matrices resulting in:

$$\boldsymbol{K} = \begin{bmatrix} \boldsymbol{K}_X & \boldsymbol{K}_{XY} & \boldsymbol{K}_{X\theta} \\ \boldsymbol{K}_{YX} & \boldsymbol{K}_Y & \boldsymbol{K}_{Y\theta} \\ \boldsymbol{K}_{\theta X} & \boldsymbol{K}_{\theta Y} & \boldsymbol{K}_\theta \end{bmatrix} \tag{3.31}$$

Provided that centers of rigidity exist for a building, the equations of motion with respect to rigidity centers can be written as:

$$\begin{bmatrix} \boldsymbol{m} & 0 & -\boldsymbol{m}\boldsymbol{e}_{CRy} \\ 0 & \boldsymbol{m} & \boldsymbol{m}\boldsymbol{e}_{CRx} \\ -\boldsymbol{m}\boldsymbol{e}_{CRy} & \boldsymbol{m}\boldsymbol{e}_{CRx} & \boldsymbol{J}_R \end{bmatrix} \begin{Bmatrix} \ddot{\tilde{\boldsymbol{u}}}_X \\ \ddot{\tilde{\boldsymbol{u}}}_Y \\ \ddot{\boldsymbol{u}}_\theta \end{Bmatrix} + \begin{bmatrix} \tilde{\boldsymbol{K}}_X & \tilde{\boldsymbol{K}}_{XY} & \boldsymbol{0} \\ \tilde{\boldsymbol{K}}_{YX} & \tilde{\boldsymbol{K}}_Y & \boldsymbol{0} \\ \boldsymbol{0} & \boldsymbol{0} & \tilde{\boldsymbol{K}}_\theta \end{bmatrix} \begin{Bmatrix} \tilde{\boldsymbol{u}}_X \\ \tilde{\boldsymbol{u}}_Y \\ \boldsymbol{u}_\theta \end{Bmatrix} = - \begin{Bmatrix} \boldsymbol{m}\boldsymbol{I}a_{gx}(t) \\ \boldsymbol{m}\boldsymbol{I}a_{gy}(t) \\ -\boldsymbol{e}_{CRy}\boldsymbol{m}\boldsymbol{I}a_{gx}(t) + \boldsymbol{e}_{CRx}\boldsymbol{m}\boldsymbol{I}a_{gy}(t) \end{Bmatrix} \tag{3.32}$$

where $\boldsymbol{e}_{CRx}$ and $\boldsymbol{e}_{CRy}$ are diagonal matrices of dimension N diagonal entries e_{CRxj} and e_{CRyj}, the x and y components of the static eccentricity e_{CRj} of the j^{th} floor, given by:

$$e_{CRxj} = x_{CMj} - x_{CRj} \tag{3.33}$$

$$e_{CRyj} = y_{CMj} - y_{CRj} \tag{3.34}$$

in which x_{CRj} and y_{CRj} are the x and y components of the center of rigidity of the j^{th} floor relative to its reference axes x_j and y_j, $\boldsymbol{J}_R$ is a diagonal matrix of

dimension N with diagonal entries J_{Rj} equal to the polar moment of inertia of the j^{th} deck about a vertical axis passing through its center of rigidity, given by:

$$J_{Rj} = m_j \left(e_{CRj}^2 + r_j^2 \right) \tag{3.35}$$

The form of the building stiffness matrix $\tilde{\boldsymbol{K}}$ given in equation below follows from the definition given for centers of rigidity as the points on floor levels at which static horizontal forces cause no twist in any of the floors.

$$\tilde{\boldsymbol{K}} = \begin{bmatrix} \tilde{\boldsymbol{K}}_X & \tilde{\boldsymbol{K}}_{XY} & 0 \\ \tilde{\boldsymbol{K}}_{YX} & \tilde{\boldsymbol{K}}_Y & 0 \\ 0 & 0 & \tilde{\boldsymbol{K}}_\theta \end{bmatrix} \tag{3.36}$$

If the rigidity centers are not unique, it would not be possible to determine a building stiffness matrix in the form of $\tilde{\boldsymbol{K}}$ given by equation (3.36).

The building stiffness matrix $\tilde{\boldsymbol{K}}$ written with respect to the degrees of freedom $\tilde{\boldsymbol{u}}^T = \left\langle \tilde{\boldsymbol{u}}_X^T \tilde{\boldsymbol{u}}_Y^T \tilde{\boldsymbol{u}}_\theta^T \right\rangle$ defined at the centers of rigidity is related to the building stiffness matrix $\boldsymbol{K}$ written with respect to degrees of freedom $\boldsymbol{u}$ at reference point O_j, where $\boldsymbol{u}^T = \left\langle \boldsymbol{u}_X^T \boldsymbol{u}_Y^T \boldsymbol{u}_\theta^T \right\rangle$, by:

$$\tilde{\boldsymbol{K}} = \tilde{\boldsymbol{a}}^T \boldsymbol{K}\, \tilde{\boldsymbol{a}} \tag{3.37}$$

in which $\tilde{\boldsymbol{a}}$ is a transformation matrix relating $\boldsymbol{u}$ to $\tilde{\boldsymbol{u}}$:

$$\boldsymbol{u} = \begin{Bmatrix} \boldsymbol{u}_X \\ \boldsymbol{u}_Y \\ \boldsymbol{u}_\theta \end{Bmatrix} = \begin{bmatrix} \boldsymbol{I} & \boldsymbol{0} & \boldsymbol{y}_{CR} \\ \boldsymbol{0} & \boldsymbol{I} & \boldsymbol{x}_{CR} \\ \boldsymbol{0} & \boldsymbol{0} & \boldsymbol{I} \end{bmatrix} \begin{Bmatrix} \tilde{\boldsymbol{u}}_X \\ \tilde{\boldsymbol{u}}_Y \\ \boldsymbol{u}_\theta \end{Bmatrix} = \tilde{\boldsymbol{a}} \tilde{\boldsymbol{u}} \tag{3.38}$$

Substituting equations (3.37) and (3.35) into (3.36), leads to:

$$\tilde{\boldsymbol{K}} = \begin{bmatrix} \boldsymbol{K}_X & \boldsymbol{K}_{XY} & \boldsymbol{K}_X \boldsymbol{y}_{CR} - \boldsymbol{K}_{XY} \boldsymbol{x}_R + \boldsymbol{K}_{X\theta} \\ \boldsymbol{K}_{YX} & \boldsymbol{K}_Y & \boldsymbol{K}_{YX} \boldsymbol{y}_{CR} - \boldsymbol{K}_Y \boldsymbol{x}_R + \boldsymbol{K}_{Y\theta} \\ \boldsymbol{K}_{\theta X} + \boldsymbol{y}_{CR} \boldsymbol{K}_X - \boldsymbol{x}_{CR} \boldsymbol{K}_{YX} & \boldsymbol{K}_{\theta Y} + \boldsymbol{y}_{CR} \boldsymbol{K}_{XY} - \boldsymbol{x}_{CR} \boldsymbol{K}_Y & \tilde{\boldsymbol{K}}_\theta \end{bmatrix} \tag{3.39}$$

in which $\tilde{\boldsymbol{K}}_\theta = \boldsymbol{K}_\theta + 2\boldsymbol{K}_{\theta X} \boldsymbol{y}_{CR} - 2\boldsymbol{K}_{\theta Y} \boldsymbol{x}_{CR} + \boldsymbol{K}_X \boldsymbol{y}_{CR}^2 - 2\boldsymbol{K}_{XY} \boldsymbol{x}_{CR} \boldsymbol{y}_{CR} + \boldsymbol{K}_Y \boldsymbol{x}_{CR}^2$

Comparison of equations (3.36) and (3.39) yields the coordinates of the centers of rigidity:

$$\mathbf{x}_{CR} = \frac{\boldsymbol{K}_{Y\theta} - \boldsymbol{K}_{YX}\boldsymbol{K}_X^{-1}\boldsymbol{K}_{X\theta}}{\boldsymbol{K}_Y - \boldsymbol{K}_{YX}\boldsymbol{K}_X^{-1}\boldsymbol{K}_{XY}} \tag{3.40}$$

$$\mathbf{y}_{CR} = -\frac{\boldsymbol{K}_{X\theta} - \boldsymbol{K}_{XY}\boldsymbol{K}_Y^{-1}\boldsymbol{K}_{Y\theta}}{\boldsymbol{K}_X - \boldsymbol{K}_{XY}\boldsymbol{K}_Y^{-1}\boldsymbol{K}_{YX}} \tag{3.41}$$

where $\boldsymbol{K}_X$, $\boldsymbol{K}_Y$, $\boldsymbol{K}_{XY}$, $\boldsymbol{K}_{X\theta}$ and $\boldsymbol{K}_{Y\theta}$ are submatrices of the building global stiffness matrix corresponding to translational (x and y) and rotational (θ) degrees of freedom of the system. Eqs. (3.40), (3.41) do not lead to a unique definition of the story rigidity centers. This is due to the fact that the product of the operations of the second part of Eqs. (3.40), (3.41) in general do not yield diagonal matrices. This deficiency is addressed if static lateral loads are introduced as follows:

$$\mathbf{x}_{CR} = \left\{\tilde{\mathbf{P}}_Y\right\}^{-1} \frac{\boldsymbol{K}_{Y\theta} - \boldsymbol{K}_{YX}\boldsymbol{K}_X^{-1}\boldsymbol{K}_{X\theta}}{\boldsymbol{K}_Y - \boldsymbol{K}_{YX}\boldsymbol{K}_X^{-1}\boldsymbol{K}_{XY}} \tilde{\mathbf{P}}_Y \tag{3.42}$$

$$\mathbf{y}_{CR} = -\left\{\tilde{\mathbf{P}}_X\right\}^{-1} \frac{\boldsymbol{K}_{X\theta} - \boldsymbol{K}_{XY}\boldsymbol{K}_Y^{-1}\boldsymbol{K}_{Y\theta}}{\boldsymbol{K}_X - \boldsymbol{K}_{XY}\boldsymbol{K}_Y^{-1}\boldsymbol{K}_{YX}} \tilde{\mathbf{P}}_X \tag{3.43}$$

where $\boldsymbol{P}_X$ and $\boldsymbol{P}_Y$ are the vectors of the static lateral loads. Thus, the definition of the coordinates of Eqs. (3.42), (3.43) are load-dependent [44]. However, there is a special class of buildings, called proportional framing buildings, for which the rigidity center, shear center and center of twist can be defined and coincide, they are load independent and lie on a vertical line [22, 44].

3.4.3.5 Location of the shear center for multistory systems

The location of the shear center of a floor is determined by finding the centroid of the shear forces experienced by individual resisting elements due to a static loading that causes no twist ($u_\theta = 0$) at any of the stories. The solution of equilibrium of moments about reference axis Z of all shear forces acting at each floor level, leads to the coordinates of shear centers $\boldsymbol{x}_S$ and $\boldsymbol{y}_S$:

$$\boldsymbol{x}_S = \left[\boldsymbol{P}_y^{'}\right]^{-1} \boldsymbol{S}\left(\boldsymbol{K}_{\theta Y} - \boldsymbol{K}_{\theta X}\boldsymbol{K}_X^{-1}\boldsymbol{K}_{XY}\right)\left(\boldsymbol{K}_Y - \boldsymbol{K}_{YX}\boldsymbol{K}_X^{-1}\boldsymbol{K}_{XY}\right)\tilde{\boldsymbol{P}}_Y \tag{3.44}$$

$$\boldsymbol{y}_S = \left[\boldsymbol{P}_X^{'}\right]^{-1} \boldsymbol{S}\left(\boldsymbol{K}_{\theta X} - \boldsymbol{K}_{\theta Y}\boldsymbol{K}_Y^{-1}\boldsymbol{K}_{YX}\right)\left(\boldsymbol{K}_X - \boldsymbol{K}_{XY}\boldsymbol{K}_Y^{-1}\boldsymbol{K}_{YX}\right)\tilde{\boldsymbol{P}}_X \tag{3.45}$$

where $\boldsymbol{S}$ is a summation matrix which is upper triangular, of dimension N and of the form:

$$\boldsymbol{S} = \begin{bmatrix} 1 & 1 & \dots & 1 & 1 \\ & 1 & \dots & 1 & 1 \\ & & \dots & & \\ & & & 1 & 1 \\ & & & & 1 \end{bmatrix} \tag{3.46}$$

And $\left[\boldsymbol{P}_X^{'}\right]$, $\left[\boldsymbol{P}_Y^{'}\right]$ denote the diagonal matrix forms of vectors $\boldsymbol{S}\tilde{\boldsymbol{P}}_X$ and $\boldsymbol{S}\tilde{\boldsymbol{P}}_Y$.

When equations (3.44) and (3.45) lead to diagonal matrix with equal diagonal entries, simplify to (3.40) and (3.41) and are load-independent.

3.4.3.6 Location of the center of twist for multistory systems

The center of twist is defined as the point on the diaphragm that is not subjected to translation but only to twist about it, when torsional moment is statically applied on the diaphragm. The building stiffness matrix written with respect to degrees of freedom defined at center of twist would be of the form of equation (3.36). Following the same procedure as for the center of rigidity leads to the same expressions for the coordinates of the center of twist as the center of rigidity (3.40) and (3.41). If these expressions yield diagonal matrices, centers of twist and centers of rigidity are coincident.

If the equations do not lead to diagonal matrices, the locations of the center of twist depend on the applied set of static torsional moments. The coordinates of the center of twist, $\boldsymbol{x}_T$ and $\boldsymbol{y}_T$, can be determined through the procedure below:

$$\tilde{\boldsymbol{P}} = \tilde{\boldsymbol{K}}\tilde{\boldsymbol{u}} \tag{3.47}$$

$$\begin{Bmatrix} \tilde{\boldsymbol{P}}_X \\ \tilde{\boldsymbol{P}}_Y \\ \tilde{\boldsymbol{P}}_\theta \end{Bmatrix} = \begin{bmatrix} \boldsymbol{K}_X & \boldsymbol{K}_{XY} & \boldsymbol{K}_X \boldsymbol{y}_T - \boldsymbol{K}_{XY} \boldsymbol{x}_T + \boldsymbol{K}_{X\theta} \\ \boldsymbol{K}_{YX} & \boldsymbol{K}_Y & \boldsymbol{K}_{YX} \boldsymbol{y}_T - \boldsymbol{K}_Y \boldsymbol{x}_T + \boldsymbol{K}_{Y\theta} \\ \boldsymbol{K}_{\theta X} + \boldsymbol{y}_T \boldsymbol{K}_X - \boldsymbol{x}_T \boldsymbol{K}_{YX} & \boldsymbol{K}_{\theta Y} + \boldsymbol{y}_T \boldsymbol{K}_{XY} - \boldsymbol{x}_T \boldsymbol{K}_Y & \tilde{\boldsymbol{K}}_\theta \end{bmatrix} \begin{Bmatrix} \tilde{\boldsymbol{u}}_X \\ \tilde{\boldsymbol{u}}_Y \\ \boldsymbol{u}_\theta \end{Bmatrix} \quad (3.48)$$

For a particular set of forces $\tilde{\boldsymbol{P}}$ with $\tilde{\boldsymbol{P}}_X = \tilde{\boldsymbol{P}}_Y = \boldsymbol{0}$ and $\tilde{\boldsymbol{T}}_\theta \neq \boldsymbol{0}$, it is possible to determine $\boldsymbol{x}_T$ and $\boldsymbol{y}_T$, the coordinates locating the centers of twist, where according to definition $\tilde{\boldsymbol{u}}_X = \tilde{\boldsymbol{u}}_Y = \boldsymbol{0}$ but $\tilde{\boldsymbol{u}}_\theta \neq 0$:

$$\{\boldsymbol{x}_T\} = [\boldsymbol{u}_\theta]^{-1} \left(\boldsymbol{K}_Y - \boldsymbol{K}_{YX} \boldsymbol{K}_X^{-1} \boldsymbol{K}_{XY} \right)^{-1} \left(\boldsymbol{K}_{Y\theta} - \boldsymbol{K}_{YX} \boldsymbol{K}_X^{-1} \boldsymbol{K}_{X\theta} \right) \boldsymbol{u}_\theta \quad (3.49)$$

$$\{\boldsymbol{y}_T\} = [\boldsymbol{u}_\theta]^{-1} \left(\boldsymbol{K}_X - \boldsymbol{K}_{YX} \boldsymbol{K}_Y^{-1} \boldsymbol{K}_{YX} \right)^{-1} \left(\boldsymbol{K}_{X\theta} - \boldsymbol{K}_{XY} \boldsymbol{K}_Y^{-1} \boldsymbol{K}_{Y\theta} \right) \boldsymbol{u}_\theta \quad (3.50)$$

where $[\boldsymbol{u}_\theta]$ represents the diagonal matrix form of vector $\boldsymbol{u}_\theta$, $\{\boldsymbol{x}_T\}$ and $\{\boldsymbol{y}_T\}$ the vector forms of diagonal matrices $\boldsymbol{x}_T$ and $\boldsymbol{y}_T$.

3.4.3.7 Torsional moment estimation through static eccentricity concept

Tso [20] compared two approaches in order to estimate the torsional moment of multistory buildings. According to the first one, the floor torques at different floors are determined as the product of the lateral load and the floor eccentricity at that floor. The story torsional moment is then obtained by summing the floor torques of the above stories. A two-bay, four-story building consisting of frames A, B, C spanning the y direction connected with rigid floor diaphragms is implemented (Fig. 3.3). Static load distribution P_i is acting at CM of each story. The load is decomposed in a translational and a rotational component (Fig. 3.3).

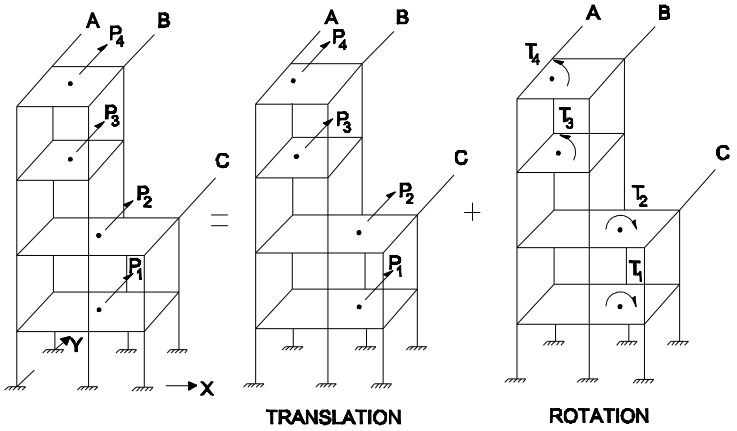

Figure 3.3. Eccentricity concept for multistory building [20].

The translational component causes only translation but no rotation of the floors. In this way, the load is relocated horizontally to act at center of rigidity of the floor. Considering that the locus of the centers of rigidity of building are determined, the floor torques T_i can be obtained by the expression:

$$T_i = P_i e_{CRi} \tag{3.51}$$

where e_{CRi} is the floor eccentricity defined as the distance between the center of mass and the center of rigidity at that floor.

$$e_{CRi} = x_{CMi} - x_{CRi} \tag{3.52}$$

The torsional moment at a story k is calculated by the relationship:

$$\left(M_t\right)_k = \sum_{i=k}^{4} T_i \tag{3.53}$$

In the second approach, the story eccentricity is employed to obtain the torsional moment via story shear [20]. The torsional moment at any story k is obtained directly from the story shear by:

$$\left(M_t\right)_k = V_k e_k \tag{3.54}$$

where V_k is the story shear and e_k is the story eccentricity at story k considering a cut at story k and lateral and torsional equilibrium of the free body diagram above

the cut (Fig. 3.4), defined as the horizontal distance between the shear center at the story and the resultant of all lateral forces above the story being considered.

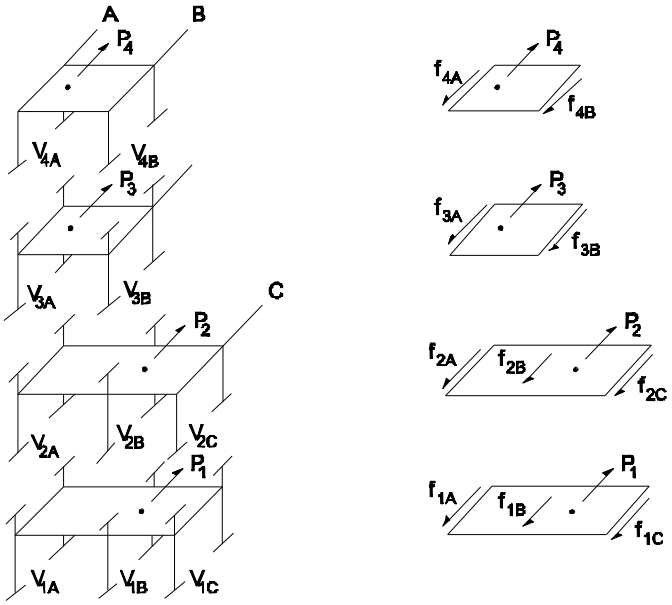

Figure 3.4. Free body diagrams of each floor [20].

The two approaches proved to be equivalent resulting to the same story torsional moments provided that proper definitions of eccentricity are implemented. Moreover, it has been also proved that the story eccentricity is less sensitive to load distribution than the floor eccentricity. Therefore, the second approach is supposed to be more appropriate for structural asymmetry assessment [20].

3.4.3.8 Optimum torsion axis and torsional radii of gyration for multistory buildings

Makarios *et al.* [47-49] proposed the optimum torsion axis for multistory buildings. The optimum torsion axis of the system is an axis upon which when the level of lateral static seismic forces is placed then the twist of the whole system is minimalized. In the boundary case that the relevant axis is a real elastic axis of the system, the twist is marked with zero [50].

In order to define the location of the optimum torsion axis a multistory spatial frame-wall system is divided into two spatial subsystems, the bending one and the shear one. Each one of them contain the elastic centers K and S, respectively, and

its principal elasticity axes I , II , provided that they maintain their elastic and geometric characteristics unchangeable in elevation. The frame-wall multistory systems have been proved [51] to possess three vertical torsion axis, Ω_1, Ω_2, Ω_3, which are not upon the same line. The final response of the system, due to the lateral static loading $F(z)$ continuous distribution in elevation, arises from the superposition of the three enforced rotations of the system around the relevant axes (Figure 3.5a). It has been proved [47] that when there is a vertical real elastic axis in the system is identified with Ω_3 while the Ω_1, Ω_2 axes move to infinity (Figure 3.6a).

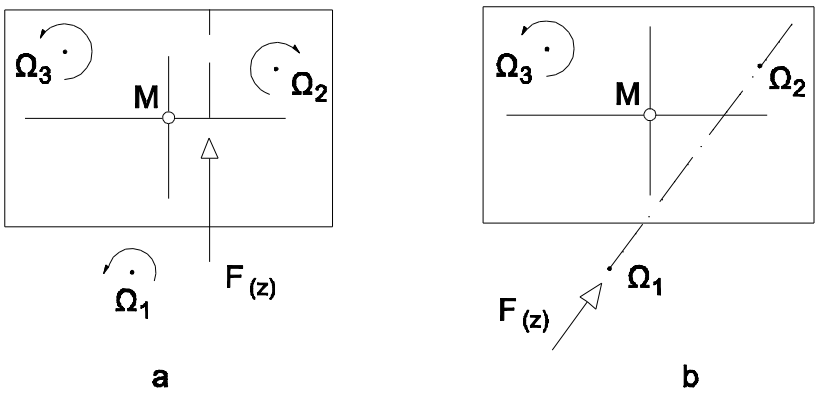

Figure 3.5. Axes of enforced torsion in a frame-wall multistory system [50].

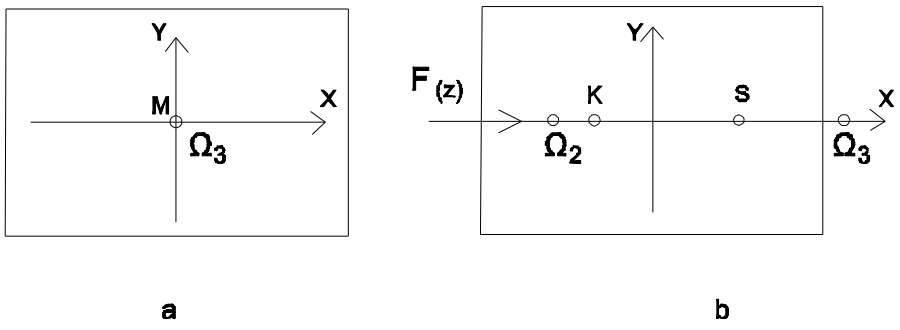

Figure 3.6. Axes of enforced torsion in symmetrical system [50].

On the special occasion that the multistory frame-wall system is monosymmetric, symmetrical axis x, the axis Ω_1 moves to the y -infinity while the

other two axes Ω_2, Ω_3 are upon x. The elastic centers K and S of the bending and the shear subsystem correspondingly are also upon x. The axes Ω_2, Ω_3 are always outside of the (KS) space [50]. When the lateral static loading $F(z)$ has a direction perpendicular to the symmetric axis of the system and is inside the ($\Omega_2\Omega_3$) space the two rotations have opposite direction (Figure 3.7b). When the following expression is satisfied

$$\min \theta^2 = \left(\theta_1^2 + \theta_2^2 + ... + \theta_{\mathrm{N}}^2\right) / \mathrm{N} \tag{3.55}$$

the effects of torsion on the system are minimized.

in which θ_i is the rotation angle of the i^{th} floor.

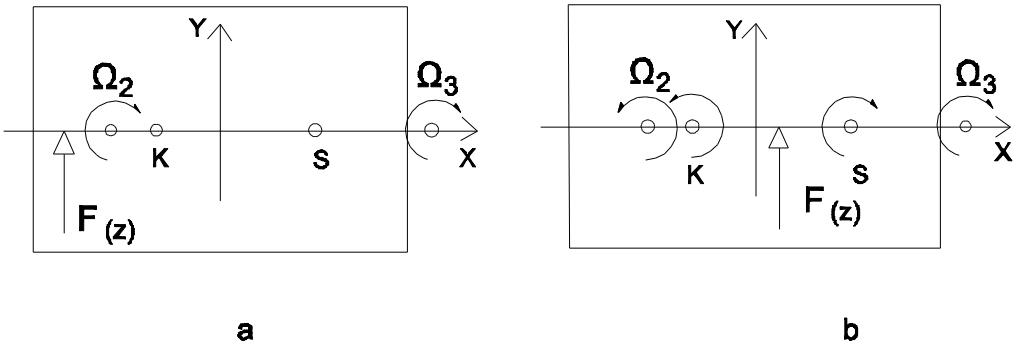

Figure 3.7. Superposition of two rotation about Ω_1, Ω_2 [50].

The relation (3.55) is satisfied when the rotation angle of the floor is equal to zero at level $z = 0.8H$ (figure 3.8) [37], [48], [49]. Solving the equation that stems from this condition, the location of the optimum torsion axis is defined, point P_0.

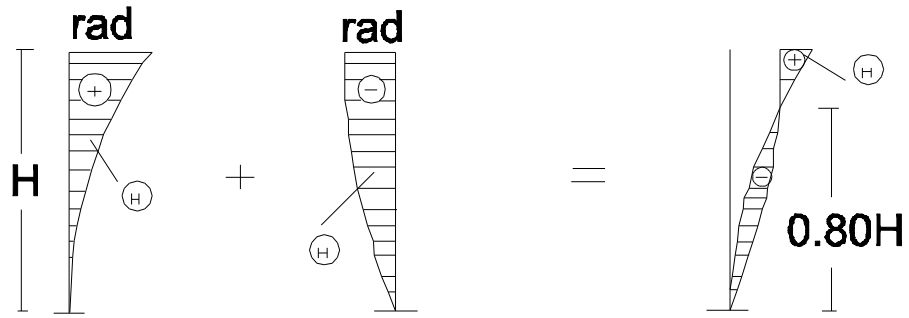

Figure 3.8. State Optimum Torsion in multistory frame-wall building [50].

The optimum torsion axis satisfies the following boundary conditions [49]:

a) Its position in the plan coincides with point K, called the elastic/stiffness center, in the boundary case where the multistory system reduces to the single-story system.
b) Its position in the plan coincides with point K when the system transforms into a purely bending one.
c) Finally its position in the plan coincides with point S when the building transforms into purely shear one.

According to a study on a five-story asymmetric building, the optimum torsion axis is characterized by the following attributes:

I. The sum of squares of the deck rotations and the sum of squares of the deck displacements along the fictitious principal II - axis is minimum, when the vertical plane of the lateral static seismic forces passes through the fictitious elastic center P_0 and is parallel to the fictitious principal I - axis. The results are similar for lateral seismic forces along the II - axis.
II. The translational and rotational components are weakly coupled when the vertical mass axis coincides with the fictitious elastic axis.
III. The earthquake ground motion along the fictitious principal I - axis or II - axis causes nearly translational vibration along the same axis when the vertical mass axis coincides with the fictitious elastic axis. The maximum deck rotations are very small.
IV. The translational and the rotational components of motion are strongly coupled when the mass axis does not coincide with the fictitious elastic axis [42].

The torsional radius of gyration ρ_I represents the lever arm, according to K, of the elastic forces of restoration during the torsional loading of the single-story/monosymmetric system [50].

It can be calculated in two different ways, which result in the same value:

I. It can be calculated directly from the relation:

$$\rho_I = \sqrt{\frac{k_{III}}{k_{II}}} \tag{3.56}$$

where k_{III} the torsional stiffness of the single-story system about the axis III and k_{II} the translational stiffness of the single-story system according to principal axis II.

II. It can also be calculated according to the ratio of special displacement:

$$\rho_I = \sqrt{\frac{k_{III}}{k_{II}}} = \sqrt{\frac{(1 \cdot F_{II}) / \theta_Z}{F_{II} / u_{II}}} \tag{3.57}$$

where $u_{II} = F_{II} / k_{II}$ is the displacement for static load force F_{II} at the point K, $\theta_Z = F_{II} / k_{III}$ is the twist angle about K for torsional loading $M = 1 \cdot F_{II}$ of the system.

The torsional radius of gyration ρ_I of the frame-wall monosymmetric systems has not the same value for every level ξ, but the one in diagrams of Figs 3.9a and 3.9b. It is suggested that the torsional radius of gyration of level $z = 0.8H$ is approximately equal to the torsional radius of gyration of the whole system, since the optimum torsional axis is defined at this level. According to the relation between the torsional radius of gyration ρ_I at the center of mass and the radius of gyration of the diaphragm r the torsional flexibility of the system for dynamic translational excitation is defined. Actually if $\rho_{mx} \le r$ the system is torsionally flexible.

$$\rho_{mx} = \sqrt{\rho_1^{\,2} + e_{0x}^2} \tag{3.58}$$

where e_{0x} is the static eccentricity along x axis.

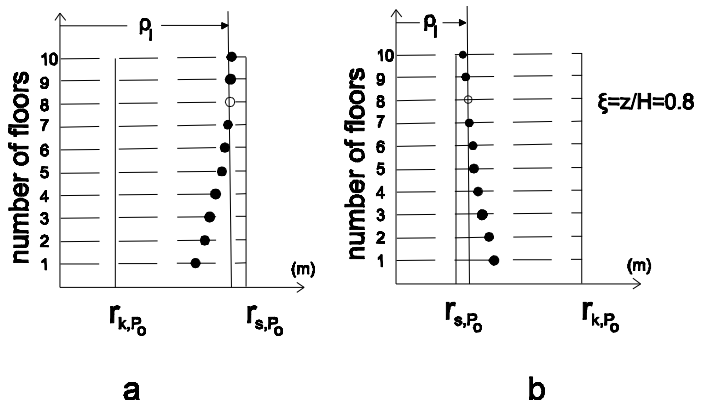

Figure 3.9. Distribution of torsional radius of the floors [47].

Another criterion for the torsional flexibility of a building is the coordinates of the center of vibration O_i of the floors. A system is characterized as torsionally flexible when the vibration centers, calculated for the first and the second modal shape, occur into the circle of the radius of inertia of the diaphragm, which means that the torsional vibrations of the diaphragm dominate the translational one for pure translational excitation. The coordinates of the center of vibration $O_i\left(e_{xi}, e_{yi}\right)$ are given by the expressions below:

$$e_{yi} = \frac{\varphi_{xi}}{\varphi_{zi}} \tag{3.59}$$

$$e_{xi} = -\frac{\varphi_{yi}}{\varphi_{zi}} \tag{3.60}$$

The equivalent static eccentricities e_f , e_r are used in order to define the location of the point of application of the lateral static seismic forces and are given by the expressions (3.59) and (3.60), respectively. The accidental eccentricity $e_{\tau i}$ is also taken into consideration.

$$e_f = \frac{\rho_I^2}{r} \cdot R_f \tag{3.61}$$

$$e_r = \frac{\rho_I^2}{r} \cdot \frac{1 - D_r}{l_r - \varepsilon_0} \tag{3.62}$$

where

$$R_f = \frac{\sin 2\theta}{2} \cdot \left(\frac{1}{A_1^{2n}} + \frac{1}{A_2^{2n}} - 2\varepsilon_{12} \cdot \frac{1}{A_1^n \cdot A_2^n} \right)^{1/2} \tag{3.63}$$

$$D_r = \frac{\sin 2\theta}{2} \cdot \left(\frac{\delta_{r1}^2}{A_1^{2n}} + \frac{\delta_{r2}^2}{A_2^{2n}} + 2\varepsilon_{12} \cdot \frac{\delta_{r1} \cdot \delta_{r2}}{A_1^n \cdot A_2^n} \right)^{1/2} \tag{3.64}$$

$$\tan \alpha_0 = \frac{2\varepsilon_0}{\varepsilon_0^2 + \mu^2 - 1} \tag{3.65}$$

If $\tan \alpha_0 \geq 0$, then $\theta = \alpha_0 / 2$

else $\theta = 90 - |a_0| / 2$

$\varepsilon_0 = \frac{e_0}{r}$, $\rho_I = \sqrt{\frac{k_{III}}{k_{II}}} = \sqrt{\frac{u_{,F}}{\theta_{,M}}}$, $\mu = \frac{\rho_1}{r}$

$A_1 = 1 - \varepsilon_0 \cdot \tan\theta$, $A_2 = 1 + \varepsilon_0 \cdot \cot\theta$

$\delta_{r1} = \cot\theta - l_r$, $\delta_{r2} = \tan\theta + l_r$, $l_r = \frac{L_r}{r}$

$\varepsilon_{12}(\zeta = 5\%), r_{12} = \sqrt{\frac{A_2}{A_1}}$

$$\varepsilon_{12} = \frac{8\zeta^2 \cdot (1 + r_{12}) \cdot r_{12}^{3/2}}{\left(1 - r_{12}^2\right)^2 + 4\zeta^2 \cdot r_{12} \cdot (1 + r_{12})^2}$$

3.4.3.9 Modification procedure for design of earthquake resistant steel structures

Anagnostopoulos *et al.* [46] proposed a modification procedure in order to improve the design of asymmetric eccentric steel structures. A structural design can be characterized as satisfactory when the limiting values of the controlling response parameters do not have wide variations within the groups of structural members to which they apply. In the opposite case, suboptimal use of material may be present as well as a potentially higher risk of failure in cases of unexpected overloads. Observed

differences in ductility demands between the opposite edges point to the need for a design modification that would eliminate or reduce these differences. The proposed modification procedure aims at increasing the strength of the structural members (columns, beams, braces) at the flexible edges and reducing the strength of the braces at the stiff edges without affecting the strength of the other structural elements (columns, beams).

The first step for application of this modification is to obtain the top story displacements at the flexible and stiff edges of the buildings in both horizontal directions due to earthquake loading considered and then compute the following factors in each horizontal direction:

$$f_{i,\,flex} = 2\frac{u_{i,\,flex}}{\left(u_{i,\,flex} + u_{i,stiff}\right)} \tag{3.66}$$

$$f_{i,stiff} = 2\frac{u_{i,stiff}}{\left(u_{i,\,flex} + u_{i,stiff}\right)} \tag{3.67}$$

where $u_{i,\,flex}$ is the top story displacement of the flexible edge in the i^{th} direction and $u_{i,stiff}$ the top story displacement of the stiff edge also in the i^{th} direction. According to the design modification, the axial areas of the bracing members in both the stiff and flexible edges are multiplied by the corresponding factors in each direction and to do the same for the beam and column sections but only in the flexible edges to increase both stiffness and strength of the corresponding frames. The cross sections of columns and beams of the stiff edges are not reduced, as their strength is controlled mainly by gravity loads. These factors vary from 1.25 - 1.50 for the flexible edges and from 0.85 - 1.00 for the stiff edges.

3.4.4 Inelastic Torsional Response

Once a structural element reaches yield, its stiffness changes affecting the period as well as the static eccentricity of the structure. The location of the rigidity center changes as well as the eccentricity of the structure. Based on this observation Paulay [28] stated that the strength eccentricity is a reliable measure for the

elastoplastic range. The strength eccentricity is the distance between the CM and the strength center CV. The strength center is defined as the point through which the resultant of the lateral forces passes, while if the story becomes a mechanism no rotation of the diaphragm is developed and its components along the x and y directions are given by:

$$e_{CVX} = \frac{\sum_{i=1}^{n_{col}} x_i V_{nyi}}{\sum_{i=1}^{n_{col}} V_{nyi}} \tag{3.68}$$

$$e_{CVY} = \frac{\sum_{i=1}^{n_{col}} y_i V_{nxi}}{\sum_{i=1}^{n_{col}} V_{nxi}} \tag{3.69}$$

where V_{nxi} and V_{nyi} are the nominal strength of the i^{th} resisting element along x and y directions. It is worth noting that the strength eccentricity is given by Eqs. (3.68), (3.69) on condition that the resisting elements achieve their nominal strength. In case that some of them did not reach their nominal strength, the shear forces computed of those elements are used instead in Eqs. (3.68), (3.69).

The wise assignment of the nominal strength of translatory elements would lead the system to the optimum response, provided that $\sum V_{ni} \geq V_E$. The location of CV is of crucial importance, since during a damaging earthquake some of the lateral force resisting elements yield and stiffness eccentricity is inappropriate to represent the asymmetry of structure. In this case, the structure is subjected for portions of time in the elastic state and for others in the plastic state. It has been proved that the produced rotations in the different states cancel one another when stiffness and strength eccentricity have opposite signs, which means that the location of the center of rigidity and the center of strength are on the opposite sides of the center of mass.

3.4.4.1 The BST surface

Moreover, in order to understand the inelastic behavior of one-story buildings De La Llera and Chopra [27] proposed the base shear and torque surface (BST) Fig. 3.10 which consists of all combinations of base shear and torque that applied statically would lead to collapse of the structure. In Fig. 3.10(b) is shown the BST surface of the one-story system depicted in Fig. 3.10(a).

The surface is convex, composed of linear branches and point symmetric with reference to the origin for identical yield displacements considering load reversals. The slope of the tangent suggests the position of the element in the building plan that remains elastic during the mechanism considered. Moreover, the ultimate surface has as many branches with finite slope as twice the number of resisting planes in the direction of excitation.

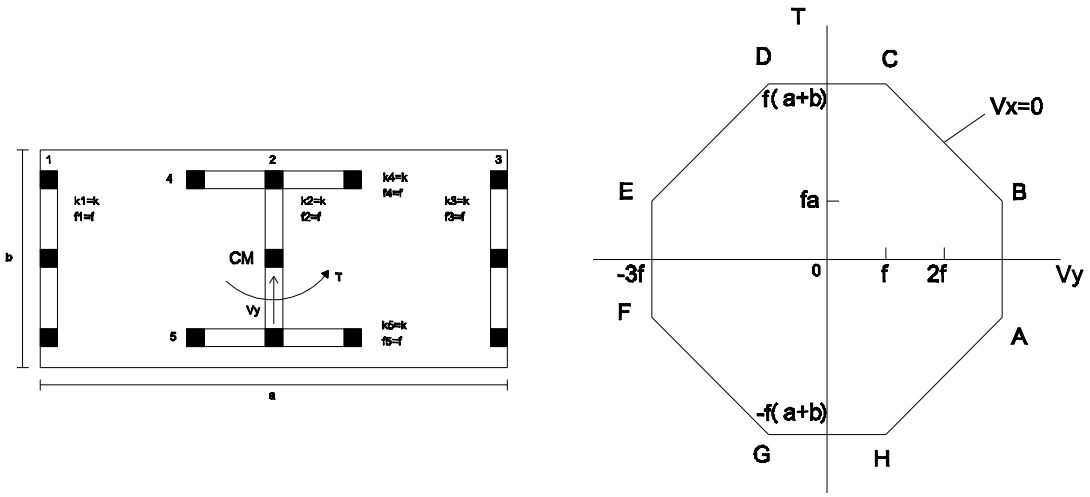

Figure 3.10. Example of construction of a BST ultimate surface [27].

Subsequently the five parameters that control the shape of the BST surface are discussed: (i) strength of resisting planes, doubling the strength of resisting planes results in surface expansion by factor two (Fig. 3.11(b)), (ii) strength of resisting planes in the orthogonal direction, an increase in strength of resisting planes in orthogonal direction causes stretching of the BST surface along the base torque axis in the positive and negative directions (Fig. 3.11(c)), (iii) asymmetry in strength,

strength distribution among elements affects the skewness and stretching of the BST surface (Fig. 3.11(d)),

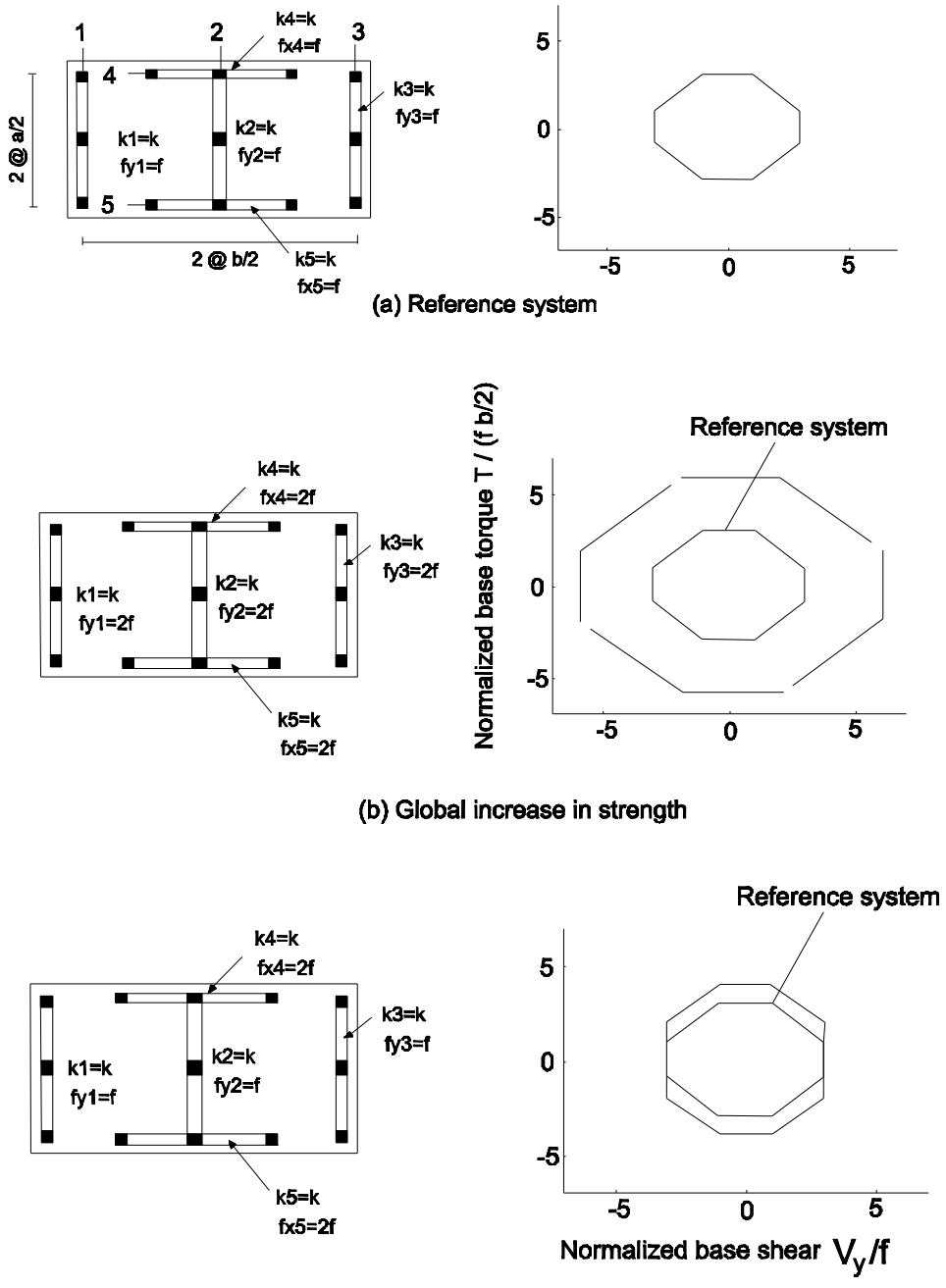

Figure 3.11. Effect of different parameters on the shape of the BST surface [27].

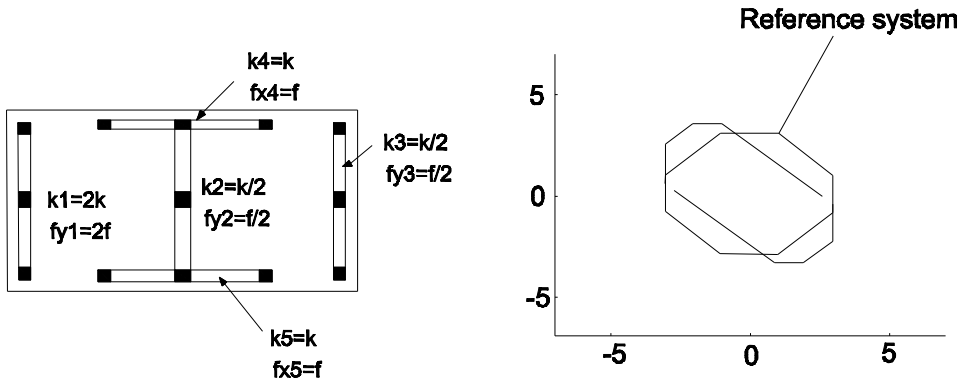

(d) Strength asymmetry

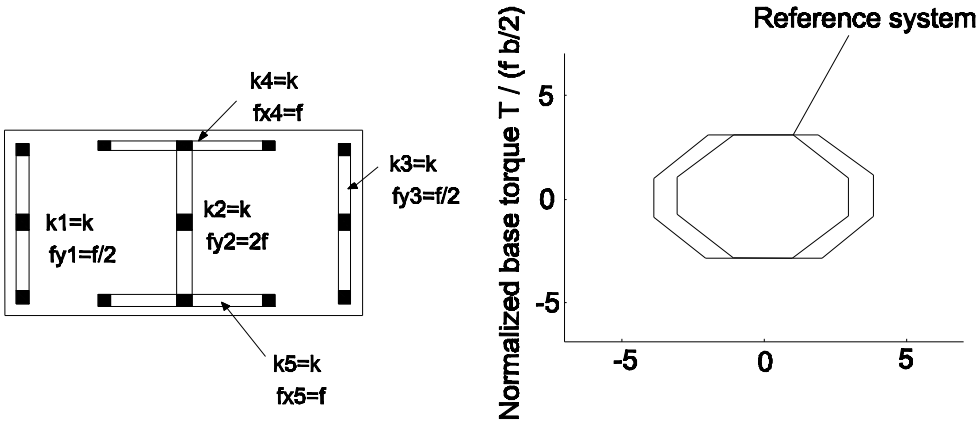

(e) Planwise distribution of strength

Figure 3.11. Effect of different parameters on the shape of the BST surface [27].

(iv) planwise distribution of strength, increasing strength in resisting plane two passing through CM, for instance (like buildings with strong central cores), relative to two other planes, the torsional capacity of the system is reduced and the length of the constant base-torque branches of the BST surface associated with purely torsional mechanisms is increased (Fig. 3.11(e)), (v) number of resisting planes, increasing the number of resisting planes the BST surface becomes rounder (Fig. 3.11(f)). It is worth noting that stiffness distribution does not cause any change to the shape of surface since it is an important parameter considering the elastic behavior of the structure.

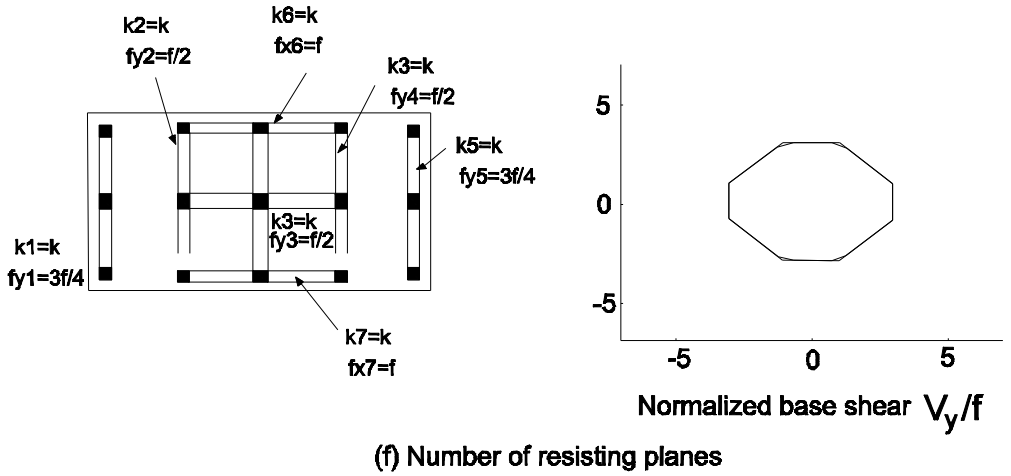

Figure 3.11. Effect of different parameters on the shape of the BST surface [27].

3.4.4.2 The SST ultimate surface

De La Llera and Chopra [53] extended the same idea to multistory buildings, the so-called story shear and torque (SST) ultimate surface. The surface is constructed for each story and depicts all combinations of story shears $V_x^{(j)}$, $V_y^{(j)}$, and torque $T^{(j)}$ that applied statically would lead the story to collapse. The construction of the surface is based on the implementation of a single super- element (SE) per building story, which represents its elastic and inelastic properties. The SE element of building consists of a single fictitious structural element per story capable of representing the elastic and inelastic properties of the story and possesses three degrees of freedom per node (Fig. 3.12) – two horizontal translations and the rotation of the floors connected by the element.

The elastic and inelastic properties of the SE model are matched to those of the story with multiple resisting planes. The surface is parametrized in terms of seven important parameters controlling the seismic response of asymmetric structures.

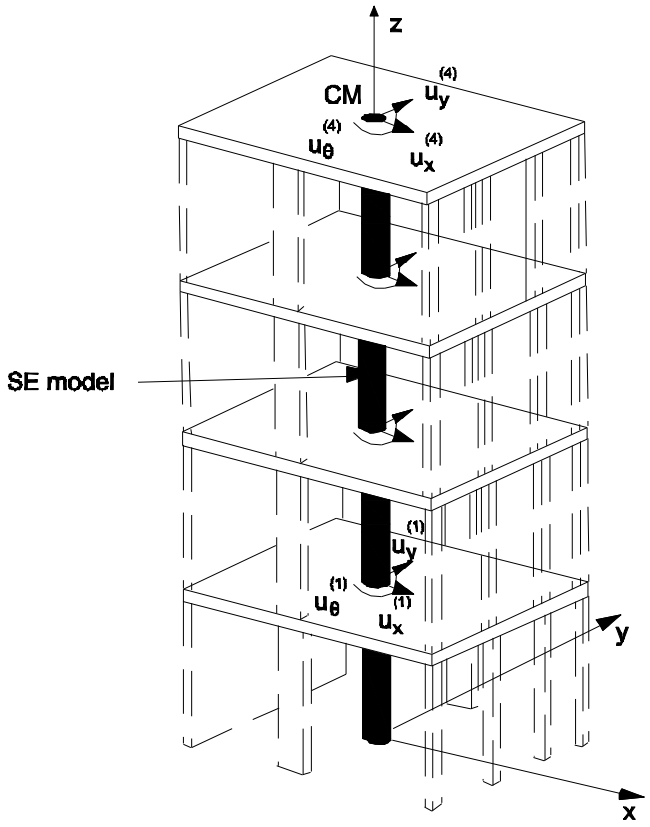

Figure 3.12. SE model of a building [43].

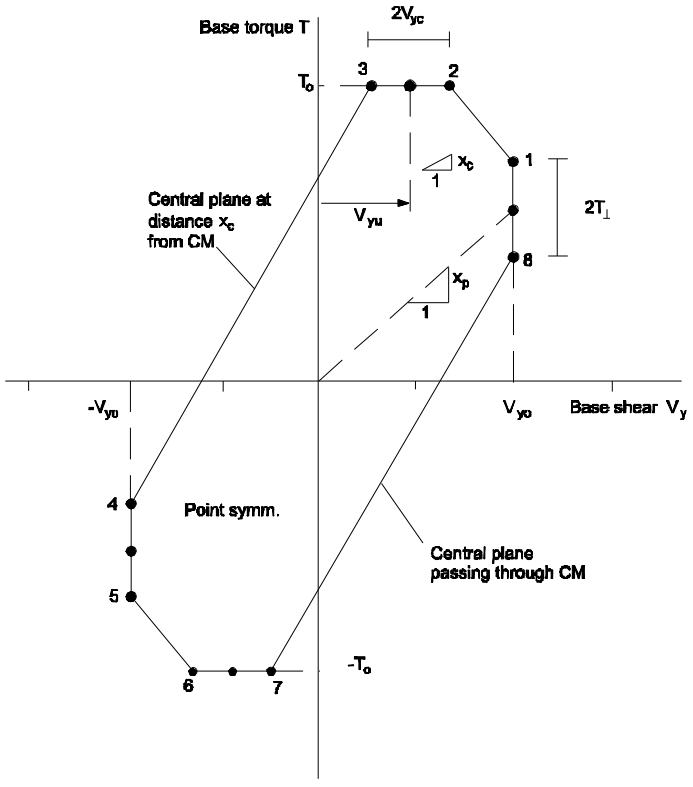

Figure 3.13. Parametric representation of the SST surface [53].

The coordinates of the vertices of the surface are given below:

$$x_1 = V_{y0}, y_1 = V_{y0} x_p + T_\perp (1 - \hat{V}_x) \tag{3.70}$$

$$x_2 = V_{yu} + V_{yc}, y_2 = T_0 - T_\perp \hat{V}_x \tag{3.71}$$

$$x_3 = V_{yu} - V_{yc}, y_3 = T_0 - T_\perp \hat{V}_x \tag{3.72}$$

$$x_4 = -V_{y0}, y_4 = -V_{y0} x_p + T_\perp (1 - \hat{V}_x) \tag{3.73}$$

$$x_5 = -x_1, y_5 = -y_1 \tag{3.74}$$

$$x_6 = -x_2, y_6 = -y_2 \tag{3.75}$$

$$x_7 = -x_3, y_7 = -y_3 \tag{3.76}$$

$$x_8 = -x_4, y_8 = -y_4 \tag{3.77}$$

where (i) $\hat{V}_x = V_x / V_{x0}$ is the normalized story shear in x direction, $V_{x0} = \sum_{i=1}^{M} f_x^{(i)}$ is the lateral capacity of the story in x-direction, $f_x^{(i)}$ the capacity of the i^{th} resisting plane in the x-direction and M is the number of resisting planes in the x-direction. The normalized story shear defines the variation of the SST ultimate surface along V_x shear axis. In the case that component of excitation exists along x axis, the planes along this axis sustain translation deteriorating their capability of developing coupled force to resist story torque.

(ii) $V_{y0} = \sum_{i=1}^{N} f_y^{(i)}$ is the lateral capacity of the story in the y-direction, $f_y^{(i)}$ the capacity of the i^{th} resisting plane in the y direction and N is the number of resisting planes in the y-direction. The lateral capacity of the story corresponds to the maximum shear that can be developed for purely translational mechanism of the story.

(iii) V_{yc} is the capacity of the resisting planes in the y-direction passing through the CM of the system, which determines the length of the constant torque branch of the

SST surface. Constant torque surface represents predominantly torsional mechanisms of the story, consequently an increase of its value means larger number of these mechanisms on the surface.

(iv) $T_0 = \sum_{i=1}^{N} \left| f_y^{(i)} x^{(i)} \right| + \sum_{i=1}^{M} \left| f_x^{(i)} y^{(i)} \right|$ is the torsional capacity of the system that can be developed in a purely torsional mechanism of the story. It controls the maximum and minimum ordinates of the ultimate surface. Large values of T_0 means that the system possesses strong resisting planes along the edges, while small values represent a system with strong central core.

(v) $T_{\perp} = \sum_{i=1}^{M} f_x^{(i)} y^{(i)}$ is the torque provided by the resisting planes in the orthogonal direction, which controls the length of the constant shear branches of the SST surface. These branches are associated with story mechanisms, which are predominantly translational.

(vi) $x_p = \sum_{i=1}^{N} f_y^{(i)} x^{(i)} / V_{y0}$ is the strength eccentricity, or first moment of strength and represents the slope of the ray, which connects the center of the surface and the middle point of the constant shear branch 1-8 Fig. 3.13. The position of this middle point is determined by the shear capacity V_{y0} and the torque $T = \sum_{i=1} f_y^{(i)} x^{(i)}$ corresponding to purely translational mechanism of the story. Strength eccentricity controls the skewness of the surface. For large values of strength eccentricity increase the skewness and narrowness of the surface resulting of the predominance in strength of one resisting plane.

(vii) $V_{yu} = \sum_{\substack{i=1 \\ i \neq 2}}^{N} f_y^{(i)} x^{(i)} / \left| x^{(i)} \right|$ denoted as the 'strength unbalance' in the story, which controls the abscissa of the central point of the constant torque branch of the SST surface at positive torque.

3.4.4.3 Torsional mechanisms in ductile building systems

An important aspect of the inelastic behavior of an asymmetric structural system is the consideration of the degree of control over its inelastic twist. One of the design

aims should be to restrain the system against unrestricted inelastic twist. This can be readily achieved with the use of elements which are not subjected to inelastic translatory displacements. Thereby the system, while developing its expected translatory displacement ductility capacity, μ_{Δ}, retains some residual stiffness:

$$K_{tr} = \lambda_t K_t \tag{3.78}$$

The resisting elements along the perpendicular direction to that of the imposed excitation can contribute within the elastic domain to significant torsional resistance and hence to restrain twist. The parameter λ_t in equation (3.78) expresses the degree of torsional restraint. It may be readily evaluated from:

$$\lambda_{tx} = \sum \left(x_i^2 k_{iy} \right) / K_t \tag{3.79}$$

$$\lambda_{ty} = \sum \left(y_i^2 k_{ix} \right) / K_t \tag{3.80}$$

Ductile structural systems are classified as either torsionally unrestrained, when $\lambda_t = 0$, or torsionally restrained, when $\lambda_t > 0.15$.

Torsionally unrestrained systems are those, which cannot resist torsion in the post-yield range. In this mechanism, torsion can be resisted only within the elastic domain of response since elements, which resist torsion during inelastic translator response, do not exist. As a result one edge element may be subjected to excessive ductility demands while the one at the opposite side may be in the elastic domain. This is associated with a reduction of the base shear capacity of the system [28].

For instance, the system of Figure 3.14 is analyzed. It is assumed that the response of the lateral force resisting elements is perfectly elastic-plastic. When the element (2) will yield and its displacement ductility capacity $\mu_{\Delta 2\max}$ should not be exceeded, the system displacement ductility demand should be limited to:

$$\mu_{\Delta} \le \beta \frac{\Delta_{y1}}{\Delta_y} + \alpha \mu_{\Delta 2\max} \frac{\Delta_{y2}}{\Delta_y} \tag{3.81}$$

where Δ_y is the system yield displacement (for torsionally unrestrained systems), relevant to CM

$$\Delta_y = \beta\Delta_{y1} + \alpha\Delta_{y2} \tag{3.82}$$

with the introduction of a geometric system parameter:

$$\psi = \frac{\alpha\Delta_{y2}}{\beta\Delta_{y1}} \tag{3.83}$$

expression (3.81) simplifies to:

$$\mu_\Delta \leq \frac{\mu_{\Delta 2\max} + 1}{1+\psi} \tag{3.84}$$

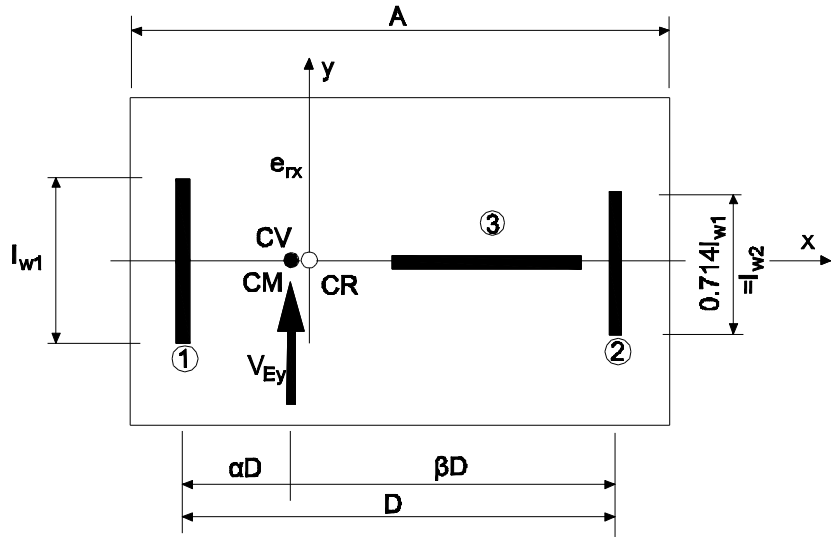

Figure 3.14. Arrangement of lateral forces resisting elements in a torsionally unrestrained system [28].

When it is found that element (1) is about to yield and its displacement ductility capacity should not be exceeded, the system displacement ductility should be limited to:

$$\mu_\Delta \leq \frac{\mu_{\Delta 1\max} + \psi}{1+\psi} \tag{3.85}$$

Finally, in the design of such a system the system ductility demand should be limited to the lesser of the two values (Eqns. (3.84) and (3.85)).

Limited torsional restrained systems are those, whose elements exhibit post-yield stiffness, $k_{pi} = \sigma k_i$ (σ : post-yield stiffness coefficient), i.e. for typical reinforced concrete elements $\sigma < 0.06$. In this case, the nominal strength of the one element is in excess of that assigned to it, for example the element (1), $V_{n1} = \lambda_1 V_1$ where $\lambda_1 > 1.00$. An upper limit is established, which reassure the development of post-yield deformation of element (1). Beyond this value and for a given post-yield stiffness of element (2), element (1) cannot yield. This limit is expressed by the equation:

$$\lambda_1 < 1 + \sigma\left(\mu_{\Delta 2\max} - 1\right) \tag{3.86}$$

It has been proved [28] that in the case of limited torsional restraint the system ductility demand should be restricted to:

$$\mu_\Delta = \mu_{\Delta 2\max} - \frac{\lambda_1 - 1}{\sigma(1+\psi)} \tag{3.87}$$

Torsionally restrained systems can resist earthquake-induced torque at the ultimate limit state by elastic transverse elements, which also control the system twist, while translatory elements are subjected to inelastic displacements of different magnitudes. The center of resistance of these inelastic translator elements, CV, can be found by strength eccentricity. Torsionally restrained mechanisms subjected to inelastic skew displacements must be expected to degenerate into torsionally unrestrained.

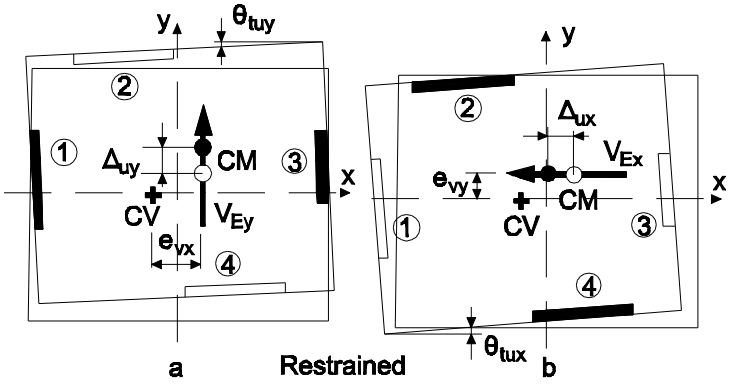

Figure 3.15. Arrangement of lateral forces resisting elements in a torsionally restrained system [29].

REFERENCES:

[1] Lagaros, N.D., Fotis, A.D. and Krikos, S.A., Assessment of seismic design procedure bad on total cost, *Earthquake Engng. Struct.* 2006; **35**: 1381-1401.

[2] Krawinkler, H., Miranda, E., Perfarmance-based earthquake engineering, In: Earthquake Engineering: From Engineering Seismology to Performance-based Earthquake Engineering, Y. Bozorgnia and Vitelmo V. Bertero (Eds), CRC Press, 2004.

[3] Naziris, I., MSc Thesis, Influence of Masonry Infill Walls in the Framework of the Optimum Performance-Based Design of RC Buildings, Institute of Structural Analysis and Seismic Research, School of Civil Engineering, NTUA.

[4] European Committee for Standardization. Draft for Development of Eurocode 8: Design of concrete structures. ENV 1998-1-1, 1998.

[5] European Committee for Standardization. Draft for Development of Eurocode 2: Design of concrete structures. ENV 1992-1-1, 1992.

[6] European Committee for Standardization. Draft for Development of Eurocode 1: Design of concrete structures. ENV 1991-1-1, 1991.

[7] European Committee for Standardization. Draft for Development of Eurocode 0: Design of concrete structures. ENV 1990-1-1, 1990.

[8] Krawinkler, H., Challenges and progress in performance-based earthquake engineering, International Seminar on Seismic Engineering for Tomorrow – In Honor of Professor Hiroshi Akiyama, Tokyo, Japan, November 26, 1999.

[9] Sullivan, T.J., Calvi, G.M., Preistley, M.J.N., Kowalsky, M.J., The limitations and performances of different displacement based design methods, *Journal of earthquake Engineering* 2003; **7**(1): 201-241.

[10] Panagiotakos, T.B., Fardis, M.N., A displacement-based seismic design procedure for RC buildings and comparison with EC8, *Earthquake Engineering and Structural Dynamics* 2001; **30**: 1439-1462.

[11] Priestley, M.J.N., Calvi, G.M., Kowalsky, M.J., Displacement Based Seismic Design of Structures, IUSS Press, 2007.

[12] Fragiadakis, M., Papadrakakis, M., Modeling, analysis and reliability of seismically excited structures, *Computational Issues: International Journal of Computational Methods* 2008; **5**(4): 483-511.

[13] Mitropoulou, Ch.Ch., Lagaros, N.D., Papadrakakis, M., Economic building design based on energy dissipation: a critical assessment, *Bulletin of Earthquake Engineering* 2010; **8**(6):1375-1396.

[14] American Society of Civil Engineers, 2000, Prestandard and Commentary for the Seismic Rehabilitation of Buildings, FEMA-356, Federal Emergency Management Agency, Washington, DC.

[15] FEMA 350, 2000, Recommended Seismic Design Criteria for New Steel Moment-Frame Buildings, Federal Emergency Management Agency, Washington, DC.

[16] Chandler, A.M., Duan, X.N., Performance of asymmetric code-designed buildings for serviceability and ultimate limit states, *Earthquake Engineering and Structural Dynamics* 1997; **26**(7):717-736.

[17] Chopra, A.K., Goel, R.K. Evaluation of torsional provisions in seismic codes, *Journal of Structural Engineering* 1991; **117**(12):3762-3782.

[18] Rutenberg, A., EAEE Task Group (TG) 8: Behaviour of irregular and complex structures-progress since 1998, *Proceedings of the 12th European Conference in Earthquake Engineering* London. Elsevier: Oxford 2002; Paper no.832.

[19] Cheung, V.W.-T., Tso, W.K., Eccentricity in irregular multistory buildings, *Canadian Journal of Civil Engineering* 1986; **13**(1):46-52.

[20] Tso, W.K., Static Eccentricity Concept for Torsional Moments Estimations, *Journal of Structural Engineering* 1990; **116**(5):1199-1212.

[21] Smith,S.B.,Vezina, S., Evaluation of centers of resistance in multistorey building structures, *Proceedings of Institution Of Civil Engineers*, Part 2, Institution of Civil Engineers 1985; **79**(4):623-635.

[22] Riddel, R., Vasquez, J., Existence of centres of resistance and torsional uncoupling of earthquake response of buildings, *Proceedings of 8thWorld Conference on Earthquake Engineering* 1984; **4**:187-194.

[23] Lagaros, N.D., Papadrakakis, M., Bakas, N., Automatic minimization of the rigidity eccentricity of 3D reinforced concrete buildings, *Journal of Earthquake Engineering* 2006; **10**(3):1-32.

[24] Stathopoulos, K.G., Anagnostopoulos, S.A., Inelastic earthquake response of single-story asymmetric buildings: an assessment of simplified shear-beam models, *Earthquake Engineering and Structural Dynamics* 2003; **32**:1813-1831.

[25] Peruš, I., Fajfar, P., On the inelastic torsional response of single-storey structures under bi-axial excitation, *Earthquake Engineering and Structural Dynamics* 2005; **34**:931-941.

[26] Lucchini, A., Monti, G., Kunnath S., Seismic behavior of single-storey asymmetric-plan buildings under uniaxial excitation, *Earthquake Engineering and Structural Dynamics* 2009; **38**:1053-1070.

[27] De La Llera, J.C., Chopra, A.K., Understanding the inelastic seismic behaviour of asymmetric-plan buildings*, Earthquake Engineering and Structural Dynamics* 1995; **24**, 549-572.

[28] Paulay, T., Torsional mechanisms in ductile building systems, *Earthquake Engineering and Structural Dynamics* 1998; **27**:1101-1121.

[29] Paulay, T., Displacement-based design approach to earthquake induced torsion in ductile buildings, *Engineering Structures* 1997; **9**(9):699-707.

[30] Dutta, S.C., Das, P.K., Inelastic seismic response of code-designed reinforced concrete asymmetric buildings with strength degradation, *Eng Struct* 2002; **24**:1295-1314.

[31] Dutta, S.C., Das, P.K., Validity and applicability of two simple hysteresis models to assess progressive seismic damage in R/C asymmetric buildings, *J Sound Vibrat* 2002; **257**:753-777.

[32] Tso, W.K., Myslimaj, B., Effect of strength distribution on the inelastic torsional response of asymmetric structural systems, *Proceedings of the 12th European conference on earthquake engineering*, London, September 2002.

[33] Myslimaj, B., Tso, W.K., A strength distribution criterion for minimizing torsional response of asymmetric wall-type systems, *Earthquake Engineering and Structural Dynamics* 2002; **31**:99-120.

[34] Myslimaj, B., Tso, W.K., A Design-oriented approach to strength distribution in single-story asymmetric systems with elements having strength dependent stiffness, *Earthquake Spectra* 2005; **21**:197-212.

[35] De Stefano, M. and Pintucchi, B., A model for analyzing inelastic seismic response of plan-irregular building structures, *Proceedings of the 15th ASCE engineering mechanics conference*, New York, June 2002.

[36] Aziminejad, A., Moghadam, A.S., Performance of asymmetric single story buildings based on different configuration of center of mass, rigidity and resistance. *Proceedings of the 4th European workshop on the seismic behavior of irregular and complex structures*, Thessaloniki, August 2005.

[37] Tso, W.K., Moghadam, A.S., Seismic response of asymmetrical buildings using push-over analysis, *Proceedings of workshop on seismic design methodologies for the next generation of codes*, Balkema, Rotterdam 1997.

[38] Moghadam, A.S., Tso, W.K., Pushover analysis of asymmetric and set-back multi-story buildings, *Proceedings of the 12th World conference on earthquake engineering*, Auckland, New Zealand 2000.

[39] Penelis, Gr.G., Kappos, A.J., Inelastic torsion effects in 3D pushover analysis of buildings, *Proceedings of the 4th European workshop on the seismic behavior of irregular and complex structures*, Thessaloniki, August 2005.

[40] De-la-Colina, Assessment of design recommendations for torsionally unbalanced multistory buildings, *Earth Spectra* 2003; **19**:47-66.

[41] Tena-Colunga, A., Evaluation of the seismic response of slender, setback RC moment-resisting frame buildings designed according to the seismic guidelines of a modern building code, *Proceedings of the 13th World conference on earthquake engineering*, Vancouver, August 2005.

[42] Humar, J.L., Design for seismic torsional forces, *Canadian Journal of Civil Engineering* 1984; **12**(2):150-163.

[43] Poole, R.A., Analysis for torsion employing provisions of NZRS 4203:1974, *Bulletin of the New Zealand Society for Earthquake Engineering* 1977; **10**(4):219-225.

[44] Reem, H., Chopra, A.K., Earthquake Response of Torsionally-Coupled Buildings, Earthquake Engineering Research Center, College of Engineering, University of California at Berkeley, 1987.

[45] Marušić, D., Fajfar, P., On the inelastic seismic response of asymmetric buildings under bi-axial excitation, *Earthquake Engineering and Structural Dynamics* 2005; **34**:943-963.

[46] Kyrkos, T.M., Anagnostopoulos, A.S., Improved earthquake resistant design of eccentric steel buildings, *Soil Dynamics and Earthquake Engineering* 2013; **47**:144-156.

[47] Makarios T., Anastassiadis K., Real and Fictitious Elastic Axis of Multi-storey Buildings: Application*, Tech. Chron.* 1997; No 17.

[48] Makarios T., Anastassiadis K., Real and Fictitious Elastic Axis of Multi-storey Buildings: Application*,* Tech. Chron. 1998; No 18.

[49] Makarios T., Anastassiadis K., Fictitious Elastic Axis of Multi-storey Buildings*,* phD School of Civil Engineering, Thessaloniki, 1994.

[50] T. Makarios, Optimum Torsion Axis and Torsional Radii of Gyration in Multi-Storey Buildings*, Tech. Chron. Sci. J. TCG, I* 2000; No 1.

[51] Anastassiadis K., Analyse Statique tridimensionelle du contreventement des batiments. La method des trios pivots, *Annales de l' I.T.B.T.P.* 1987; No 435.

[52] Har. Xenidis, Trian. Makarios, As. Athanasopoulou, 2005, The Properties of the Optimum Torsion Axis In Asymmetric Multi-storey Buildings*, Tech. Chron. Sci. J.TCG, ,* 2005; No2-3*.*

[53] De La Llera, J.C. and Chopra, A.K., A simplified model for analysis and design of asymmetric plan buildings, *Earthquake Engineering and Structural Dynamics* 1995; **24**, 573-594.

4 RATIO OF TORSION

4.1 Introduction

Asymmetry into a structural system is introduced by its non-symmetric topology of the structural elements or mass distribution. In particular, structural asymmetry results to eccentric structural systems having different locus of the mass and rigidity centers. During dynamic excitation, the resultant of inertia forces is modelled as acting through the mass center, while the resultant of resisting forces through the rigidity center. As a consequence a moment between the two forces is developed, which induces torsional effect coupled with the lateral motion. Even in case of buildings possessing two axes of symmetry, moments arise due to earthquake rotational component. A number of studies have been published dealing with the structural response of reinforced concrete (RC) buildings taking into consideration the lateral-torsional coupling [1-4]. In most structural design codes, the effect of torsion is treated by implementing accidental and static eccentricities together with specific provisions for addressing the design of irregular buildings. Accidental eccentricity is defined as a percentile (e.g. 5%) of the plan view dimension that is perpendicular to the direction of the lateral forces applied. On the other hand the implementation of the static eccentricity is more complicated, since it is defined with

reference to the location of the rigidity center whose position, for the case of multistory buildings, is not unique and is load-dependent. It is for this reason that the efficiency of torsional codified provisions has been studied by many researchers [5-6].

For the case of one-story systems there is a position on the diaphragm with the following properties: (i) No rotation is induced when a lateral load is applied to it (rigidity center), (ii) or when the resultant of the shear forces is applied to it (shear center), (iii) remains constant when the structure is subjected to torque loading (center of twist). Consequently, these centers are coincident and load-independent for one-story systems. However, for the case of multistory buildings these centers do not coincide and their effect has been the subject of extensive research by many researchers in the past. Inconsistent observations have been attributed to the varying model assumptions implemented, while a detailed overview has been presented by Rutenberg [7]. Cheung and Tso [8] proposed the generalized center of rigidity and twist under linear response, while Tso [9] compared two approaches in an effort to measure the story torsional moments for multistory buildings. In particular, the torsional moment is calculated using the floor eccentricity in the first approach, while in the second one using the story eccentricity. Smith and Vezina [10] defined the story rigidity center of multistory buildings as the point on the story diaphragm where no torsional action is developed from the application of external horizontal load. Riddell and Vaquez [11] concluded that the centers of rigidity exist only for a special class of multistory buildings. Lagaros *et al*. [12] proposed a combined topology-sizing optimum design formulation for RC buildings aiming at minimizing the material cost as well as the static and strength eccentricities taking into account both design code and architectural restrictions.

Research interest extended also to the inelastic response of one-story structures [13-15]. De la Llera and Chopra [16] proposed the base shear and torque surfaces (BST), which represent all combinations of base shear and torque that would lead to structural collapse when applied statically. They also extended the same idea to multistory buildings, the so-called story shear and torque (SST) ultimate surface [17]. The surface is constructed for each story and depicts all combinations of story shears

and torque that applied statically would lead the story to collapse. The construction of the surface is based on the implementation of a single super-element per building story, which represents its elastic and inelastic properties. The SE element of building consists of a single fictitious structural element per story capable of representing the elastic and inelastic properties of the story. Paulay [18, 19] proposed the center of resistance and identified the elastoplastic mechanism, aiming at estimating the torsional effects on the seismic response of ductile buildings, classifying them either as torsionally unrestrained or as torsionally restrained. Myslimaj and Tso [20, 21] proved that the torsional effect can be reduced for asymmetric wall-type systems by locating the center of strength and the center of rigidity on the opposite sides of the center of mass. Anagnostopoulos et al. 2010 [22] indicated the inadequacies of simplified one-story, shear-beam type systems for predicting the inelastic response of asymmetric, multistory framed buildings, subjected to torsion due to earthquake motions and for deriving general conclusions concerning the torsional provisions of the design codes.

While static eccentricity and torsional to lateral frequency ratio are considered to be the most reliable indicators for the elastic state of response. Once the structure enters the inelastic state of response, strength eccentricity, defined as the distance between the center of mass and the strength center, exhibits the most efficient performance. A criterion exhibiting satisfactory performance for all states of response still lacks. In the present study/investigation an efficient assessment criterion of the torsional effect on the structures' response is proposed. The proposed criterion aims at quantifying the torsional effect in terms of shear forces developed on vertical structural elements. It expresses the amplification of shear forces due to torsional effect. The framework of the proposed criterion is based on the observation that the sum of the absolute values of vertical resisting elements' shear forces differs from their algebraic sum. The proposed index calculates the percentage of this quantity normalized to the base shear imposed by the seismic excitation. One-story as well as multistory buildings, horizontally regular and irregular, were implemented to evaluate the proposed criterion. Its performance

was compared to other response parameters related to torsion, such as base torque and diaphragm rotation and proved to be satisfactory for all states of response.

4.2 Description – Theoretical background

The torsional moments that are developed due to the eccentricity are sustained by the structural system as a pair of shear forces. Thus, the torsional effect on buildings is quantified as torsion-induced displacements via torsion-induced shear forces on the vertical structural elements. When a lateral loading P_i is applied on the diaphragm, shear forces are developed at each vertical resisting element. Figure 4.1 shows a simple plan view along with the vertical resisting elements (shear walls) and the corresponding shear forces developed. Without loss of generality the seismic action is considered along one direction only (y direction).

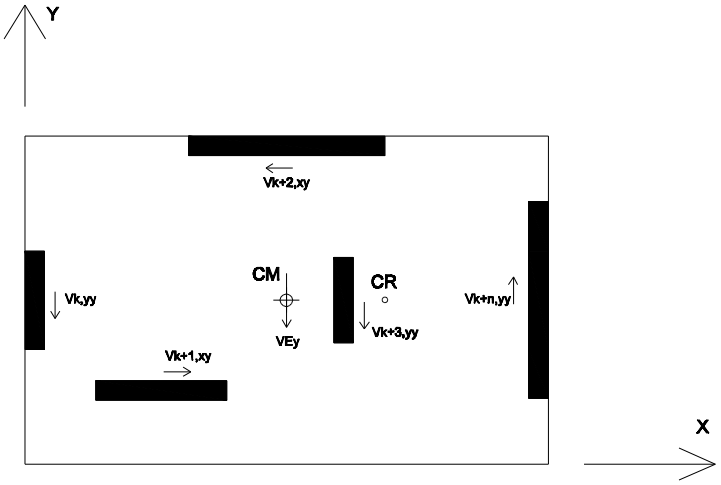

Figure 4.1. A typical plan view with shear walls.

The shear forces developed on the vertical resisting structural elements satisfy the following expression:

$$\sum_{k=1}^{n} \left| V_{kij} \right| \neq \sum_{k=1}^{n} V_{kij} \tag{4.1}$$

where n is the number of vertical structural elements, while i and j correspond to the direction of the shear forces of the element k and the seismic excitation with

reference to the structural axes. Eq. (4.1) denotes that the sum of the absolute values of the shear forces differs from their algebraic sum. This observation is attributed to torsional contribution on the shear forces, since torsional moment is sustained by the system as a pair of opposing shear forces. For the plan view of Fig. 4.1 and seismic action along y direction only, the following relations are satisfied

$$\sum_{k=1}^{n}\left|V_{kxy}\right| \neq \sum_{k=1}^{n} V_{kxy} = 0 \tag{4.2}$$

$$\sum_{k=1}^{n}\left|V_{kyy}\right| \neq \sum_{k=1}^{n} V_{kyy} = V_{Ey} \tag{4.3}$$

The torsion induced in the floor is usually computed from the shear forces of the structural elements, while the elements' torsional moments are neglected.

Based on the observations described above a criterion is proposed in this study, called ratio of torsion (*ROT*) that represents a measure to quantify the torsional effect. The general expression of *ROT* for a specific time step *t* is defined as

$$ROT(t) = \frac{\sum_{k=1}^{n}\sum_{i=x,\,j=y}^{y,x}\left|V_{kij}(t)\right| - \left|V_{Ex}(t)\right| - \left|V_{Ey}(t)\right|}{\left|V_{Ex}(t)\right| + \left|V_{Ey}(t)\right|} \tag{4.4}$$

The static equilibrium of forces acting on the diaphragm of the structure along the two axes x and y can be written as:

$$\sum_{k=1}^{n}\sum_{j=y}^{x} V_{kxj} = V_{Ex} \tag{4.5}$$

$$\sum_{k=1}^{n}\sum_{j=y}^{x} V_{kyj} = V_{Ey} \tag{4.6}$$

thus, Eq. (4.4) can be re-written as:

$$ROT = \frac{\sum_{k=1}^{n}\sum_{i=x,\,j=y}^{y,x}\left|V_{kij}\right| - \left|\sum_{k=1}^{n}\sum_{j=y}^{x} V_{kxj}\right| - \left|\sum_{k=1}^{n}\sum_{j=y}^{x} V_{kyj}\right|}{\left|\sum_{k=1}^{n}\sum_{j=y}^{x} V_{kxj}\right| + \left|\sum_{k=1}^{n}\sum_{j=y}^{x} V_{kyj}\right|} \tag{4.7}$$

For demonstration purposes only and without loss of generality the simplified model of Fig. 4.2 is adopted. It is assumed that the lateral force resistance of the structure is provided by shear walls only, while floor diaphragm is considered rigid. The system is mono-symmetric with reference to x direction and the eccentricity is introduced to the system by asymmetric mass distribution. The response of the system is considered for earthquake loading along y direction only. The locations of CM and CR are shown in Fig. 4.2, while the stiffness eccentricity e_{CRx} along x direction is also denoted.

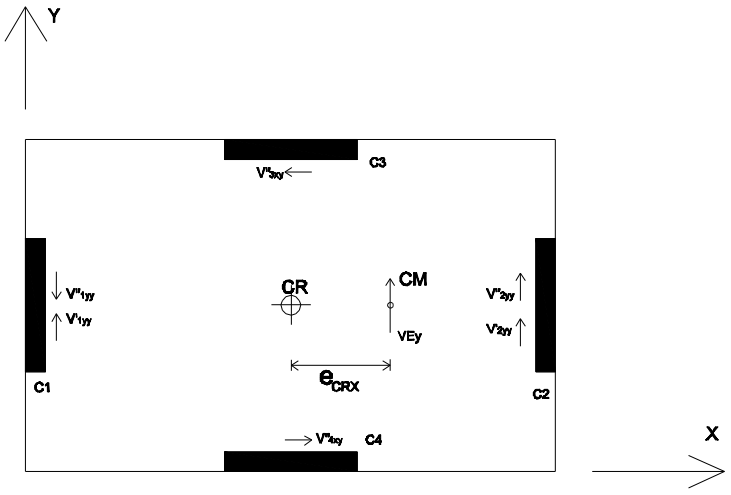

Figure 4.2. Plan view of location of CM and CR.

The twist of the diaphragm is the result of the torque M_t induced by the story base shear V_{Ey}. This torque affects the shear forces developed on vertical resisting elements. Consequently, the shear forces developed consist of two components, the translational and rotational one. The translational shear force component of element k denoted as $V_{kiy}^{'}$ is calculated by

$$V_{kiy}^{'} = \frac{k_{ky}}{\sum_{k=1}^{n} k_{ky}} V_{Ey} \tag{4.8}$$

where V_{Ey} is the design base shear along the *y* direction, k_{iy} is the translational stiffness of the element k along y direction, n denotes the number of the vertical

resisting elements and i the direction of the shear force of the element k. The torsional component is given by

$$V_{kiy}^{"} = x_k k_{ky} \frac{M_t}{K_t} \tag{4.9}$$

where for simplification reasons time step t is eliminated in the description that follows. x_k is the distance between the vertical resisting element k and CM, M_t is the torque introduced by the design shear force V_{Ey}, while K_t represents the torsional stiffness of the system calculated according to the relationship

$$K_t = \sum y_k^2 k_{kx} + \sum x_k^2 k_{ky} \tag{4.10}$$

The total shear force for element k is obtained by

$$V_{kiy} = V_{kiy}^{'} + V_{kiy}^{"} \tag{4.11}$$

Eqs. (4.9) to (4.11) hold for x direction as well.

In the case of the considered unidirectional seismic ground motion along y axis, the elements in the transverse direction x usually contribute to the torsional stiffness in the elastic range. Consequently, torsion-induced shear forces are developed in these elements only. As it is noted in Fig. 4.2., shear forces induced by translation are denoted as $V_{kiy}^{'}$, while the torsional component as $V_{kiy}^{"}$. In this case using Eq. (4.4), the value of *ROT* is calculated as follows:

$$ROT = \frac{\left|V_{1yy}^{'} - V_{1yy}^{"}\right| + \left|V_{2yy}^{'} + V_{2yy}^{"}\right| + \left|V_{3xy}^{"}\right| + \left|V_{4xy}^{"}\right| - \left|V_{Ey}\right|}{\left|V_{Ey}\right|} \tag{4.12}$$

The static equilibrium of forces acting on the diaphragm of the structure is given by:

$$\left|V_{Ey}\right| = \left|V_{1yy}^{'} - V_{1yy}^{"}\right| + \left|V_{2yy}^{'} + V_{2yy}^{"}\right| \tag{4.13}$$

Therefore, by substituting Eq. (4.13) in Eq. (4.12) *ROT* value becomes

$$ROT = \frac{\left|V_{1yy}^{'} - V_{1yy}^{"}\right| + \left|V_{2yy}^{'} + V_{2yy}^{"}\right| + \left|V_{3xy}^{"}\right| + \left|V_{4xy}^{"}\right| - \left|V_{1yy}^{'} - V_{1yy}^{"}\right| - \left|V_{2yy}^{'} + V_{2yy}^{"}\right|}{\left|V_{1yy}^{'} - V_{1yy}^{"}\right| + \left|V_{2yy}^{'} + V_{2yy}^{"}\right|} \tag{4.14}$$

$$ROT = \frac{\left|V_{3xy}^{"}\right| + \left|V_{4xy}^{"}\right|}{\left|V_{1yy}^{'} - V_{1yy}^{"}\right| + \left|V_{2yy}^{'} + V_{2yy}^{"}\right|} \tag{4.15}$$

which can be written in a compact form as

$$ROT = \frac{\left|V_{3xy}^{"}\right| + \left|V_{4xy}^{"}\right|}{\left|V_{Ey}\right|} \tag{4.16}$$

where the numerator of Eq. (4.16) represents the sum of the absolute values of the additional torsion - induced shear forces and the denominator represents the base shear. The base shear can be interpreted as a measure of the response intensity of the imposed excitation to the structure. The proposed criterion calculates the sum of absolute values of additional torsion-induced shear forces developed on individual elements normalized to the base shear which is imposed to the structure by the seismic action. In this way the amplification due to torsion of the imposed base shear V_{Ey} is quantified [23].

In order to minimize the additional torsion-induced shear forces it suffices to minimize the numerator of Eq. (4.13) that corresponds to the sum of their absolute values. This implies that low *ROT* index corresponds to low value of the additional induced torsion. Therefore, *ROT* can be considered as an appropriate index for assessing the effect of torsion since it can quantify the amplification of the shear forces developed at each structural member due to torsional effect. In order to assess the efficiency of the proposed index the maximum *ROT* value is compared to the maximum values of other response quantities related to torsion and to the seismic structural response in the following numerical examples.

In case of multistory buildings, Eq. (4.4) is calculated for every story of the building. Thus, the global value of the criterion is defined according to the following expression:

$$ROT = \sum_{m=1}^{l} ROT_m \tag{4.17}$$

where l is the number of the building stories, while *ROT* value is computed for every time step in case of time history analysis and the maximum value is defined [23].

4.3 Implementation of ROT for single-story systems

For the nonlinear static or dynamic analysis of structures the plastic hinge or the fiber approach can be adopted in the regions where inelastic deformations are expected to be developed. Since the plastic hinge approach has limitations in terms of accuracy, particularly for dynamic analyses, the fiber beam-column elements [24] are used in this study. According to the fiber approach, each structural element is discretized into a number of integration sections restrained to the beam kinematics and each section is divided into a number of fibers with specific material properties. Every fiber in the section can be assigned to different material properties, e.g. concrete, structural steel, or reinforcing bar, while the sections are located at the Gaussian integration points of the elements. The main advantage of the fiber approach is that every fiber has a simple uniaxial material model allowing an easy and efficient implementation of the inelastic behavior. In the numerical test examples section that follows, all analyses have been performed using the OpenSEES [25] platform. A bilinear material model with pure kinematic hardening is adopted for the structural steel. For the simulation of the concrete the modified Kent-Park model is applied, where the monotonic envelope of concrete in compression follows the model of Kent and Park [26] as extended by Scott *et al.* in [27]. This model allows a more accurate prediction of the capacity for flexure-dominated RC members despite its relatively simple formulation.

The performance of the numerical applications considered in this study is assessed for different seismic hazard levels with reference to their structural behavior, associated with interstorey drifts, displacements, shear forces of the columns, base shear and diaphragm rotation. For this purpose a number of nonlinear time history analyses have been carried out applying six natural records for each hazard level (2/50, 10/50 and 50/50) chosen from Somerville and Collins [28] (see Table 4.1). The records of each hazard level are scaled to the same PGA in order to ensure compatibility between the records, in accordance to the hazard curve taken from the work by Papazachos *et al*. [29] (see Table 4.2). Eighteen nonlinear dynamic analyses have been performed for each design in order to assess its performance for all records and hazard levels.

Six one-story test examples are considered: torsionally stiff, horizontally regular, horizontally irregular exhibiting either single or double eccentricity. In all test examples the following material properties are considered: Concrete C20/25 with modulus of elasticity equal to 30GPa and characteristic compressive cylinder strength equal to 20MPa, longitudinal and transverse steel reinforcement B500C with modulus of elasticity equal to 210GPa and characteristic yield strength equal to 500MPa. In addition to the symmetric design, three different mass distributions were considered for every test example, corresponding to 5%, 10% and 20% eccentricity. The design spectrum used correspond to soil type B (characteristic periods T_B = 0.15 sec, T_C = 0.50 sec and T_D = 2.00 sec). Moreover, the importance factor γ_I was taken equal to 1.0, while the damping correction factor η is equal to 1.0, since a damping ratio of 5% has been considered. The symmetric design is denoted as *sym*, while the mass eccentric designs are denoted as *ecc5*, *ecc10* and *ecc20* corresponding to 5%, 10% and 20% eccentricity, respectively. The eccentricity is introduced by assuming non-uniform mass distribution, which results into different location of the mass center, while the center of rigidity coincides with their geometric center. The response quantities and proposed criterion values obtained for the eccentric designs were compared to those obtained for the corresponding symmetric one. All test examples are classified as torsionally stiff, since the value of the uncoupled frequency ratio is greater than unity. The first three periods of vibration and the uncoupled frequency ratios are listed for all test examples in Tables 4.3 to 4.12. In order to study the reliability of the proposed criterion for all states of response (elastic or elastoplastic) the natural accelerograms of Table 4.1 are used and the results presented in this study corresponds to maximum values obtained from the time-history analyses performed for each hazard level.

Table 4.1: Natural records [28]

Earthquake	Station	Distance	Site
Records in 50/50 hazard level			
Honeydew (PT)	Cape Mendocino	20	rock
17 August 1991	Petrolia	17	soil
Cape Mendocino (CM)	Rio Dell	13	soil
25 April 1992	Butler Valley	37	rock
Cape Mendocino (C2)	Fortuna	43	soil
aftershock, 4/26/92	Centerville	28	soil
Records in 10/50 hazard level			
Tabas (TB)	Dayhook	14	rock
16 September 1978	Tabas	1.1	rock
Cape Mendocino (CM)	Cape Mendocino	6.9	rock
25 April 1992	Petrolia	8.1	soil
Chi-Chi (CC), Taiwan	TCU101	4.9	soil
20 September 1999	TCU102	3.8	soil
Records in 2/50 hazard level			
Valparaiso (VL), Chile	Vina del Mar	30	soil
3 May 1985	Zapaller	30	rock
Michoacan (MI),	Caleta de Campos	12	rock
Mexico	La Union	22	rock
19 September 1985	La Villita	18	rock
	Zihuatenejo	21	rock

Table 4.2: Seismic hazard levels [29]

Event	Recurrence Interval	Probability of Exceedance	PGA (g)
Frequent	21 years	90% in 50 years	0.06
Occasional	72 years	50% in 50 years	0.11
Rare	475 years	10% in 50 years	0.31
Very Rare	2475 years	2% in 50 years	0.78

Table 4.3: Monosymmetric - horizontally regular one-story simple mathematical model - Vibration periods and uncoupled frequency ratios

	T_1	T_2	T_3	$\Omega_x = \frac{\omega_t}{\omega_x}$	$\Omega_y = \frac{\omega_t}{\omega_y}$
sym	0.3339 ^{x}	0.3339 ^{y}	0.1665 ^{t}	2.0360	2.0360
ecc0.05	0.3348 ^{y}	0.3339 ^{x}	0.1673 ^{t}	1.9958	2.0012
ecc0.10	0.3373 ^{y}	0.3339 ^{x}	0.1697 ^{t}	1.9676	1.9876
ecc0.20	0.3476 ^{y}	0.3339 ^{x}	0.1782 ^{t}	1.8737	1.9506

Table 4.4: Eccentric - horizontally regular one-story simple mathematical model - Vibration periods and uncoupled frequency ratios

	T_1	T_2	T_3	$\Omega_x = \frac{\omega_t}{\omega_x}$	$\Omega_y = \frac{\omega_t}{\omega_y}$
sym	0.3339 ^{x}	0.3339 ^{y}	0.1665 ^{t}	2.0360	2.0360
ecc0.05	0.3356 ^{y}	0.3339 ^{x}	0.1726 ^{t}	1.9345	1.9444
ecc0.10	0.3407 ^{y}	0.3339 ^{x}	0.1727 ^{t}	1.9334	1.9728
ecc0.20	0.3600 ^{y}	0.3339 ^{x}	0.1720 ^{t}	1.9412	2.0930

Table 4.5: Monosymmetric - horizontally regular one-story structure - realistic plan views - Vibration periods and uncoupled frequency ratios

	T_1	T_2	T_3	$\Omega_x = \frac{\omega_t}{\omega_x}$	$\Omega_y = \frac{\omega_t}{\omega_y}$
sym	0.3593 ^{x}	0.3484 ^{y}	0.2526 ^{t}	1.4224	1.3793
ecc0.05	0.3594 ^{x}	0.3520 ^{y}	0.2570 ^{t}	1.3984	1.3696
ecc0.10	0.3622 ^{x}	0.3594 ^{y}	0.2518 ^{t}	1.4384	1.4273
ecc0.20	0.4000 ^{x}	0.3594 ^{y}	0.2502 ^{t}	1.5987	1.4365

Table 4.6: Eccentric - horizontally regular one-story structure - realistic plan views - Vibration periods and uncoupled frequency ratios

	T_1	T_2	T_3	$\Omega_x = \frac{\omega_t}{\omega_x}$	$\Omega_y = \frac{\omega_t}{\omega_y}$
sym	0.3593 ^{x}	0.3484 ^{y}	0.2526 ^{t}	1.4224	1.3793
ecc0.05	0.3620 ^{x}	0.3512 ^{y}	0.2524 ^{t}	1.4342	1.3914
ecc0.10	0.3753 ^{x}	0.3539 ^{y}	0.2519 ^{t}	1.4898	1.4049
ecc0.20	0.4320 ^{x}	0.3549 ^{y}	0.2509 ^{t}	1.7218	1.4145

Table 4.7: Horizontally irregular one-story structure 1 - Vibration periods and uncoupled frequency ratios

	T_1	T_2	T_3	$\Omega_x = \frac{\omega_t}{\omega_x}$	$\Omega_y = \frac{\omega_t}{\omega_y}$
ecc	0.3212 ^{x}	0.3207 ^{y}	0.2243 ^{t}	1.4320	1.4297
ecc0.05	0.3238 ^{x}	0.3207 ^{y}	0.2123 ^{t}	1.5252	1.5106
ecc0.10	0.3306 ^{x}	0.3207 ^{y}	0.2125 ^{t}	1.5558	1.5092
ecc0.20	0.3554 ^{x}	0.3207 ^{y}	0.2144 ^{t}	1.6576	1.4958

Table 4.8: Horizontally irregular one-story structure 2 - Vibration periods and uncoupled frequency ratios

	T_1	T_2	T_3	$\Omega_x = \frac{\omega_t}{\omega_x}$	$\Omega_y = \frac{\omega_t}{\omega_y}$
ecc	0.3212 ^{x}	0.3207 ^{y}	0.2243 ^{t}	1.4320	1.4297
ecc0.05	0.3263 ^{x}	0.3207 ^{y}	0.2119 ^{t}	1.5398	1.5134
ecc0.10	0.3396 ^{x}	0.3207 ^{y}	0.2124 ^{t}	1.5988	1.5098
ecc0.20	0.3871 ^{x}	0.3207 ^{y}	0.2155 ^{t}	1.7962	1.4881

4.3.1 Monosymmetric - horizontally regular single-story system - simple model

The first test example is a single-story 3D structure, shown in Fig. 4.3 together with the location of CM for the eccentric designs, which are mono-symmetric with reference to x axis, while the seismic excitation is applied uni-directionally along y direction. The absolute and normalized maximum values of the shear forces with respect to *ecc20* results developed at the vertical resisting elements along the x direction are provided in Fig. 4.4. Despite the fact that seismic excitation is applied along y direction only, shear forces are developed in both x and y directions for the eccentric designs. Furthermore, no shear forces are developed for the symmetric design along x direction, while the shear force values developed along the x direction for the eccentric designs are proportional to the magnitude of eccentricity. This is due to the fact that the shear forces along x direction represent the contribution due to torsion that is increased proportionally to the magnitude of the eccentricity. The same trend is observed in Fig. 4.5 for the displacements and interstory drifts along x direction. However, decreased values are observed for the displacements, interstory drifts and shear forces in the y direction for the structural elements located at the stiff side (i.e. col1 and col3) and increased values for the elements located at flexible edge (i.e. col2 and col4) as shown in Figs. 4.6 and 4.7.

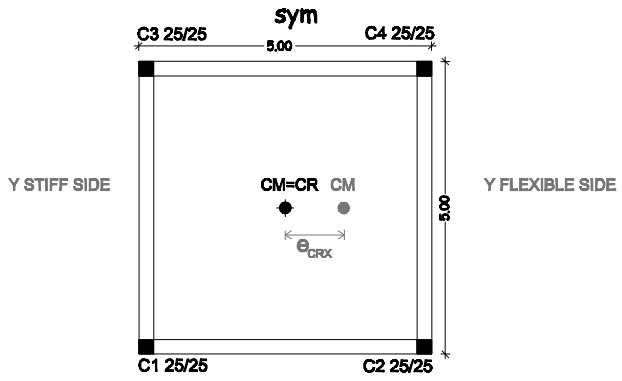

Figure 4.3. Numerical Example 1 - plan view.

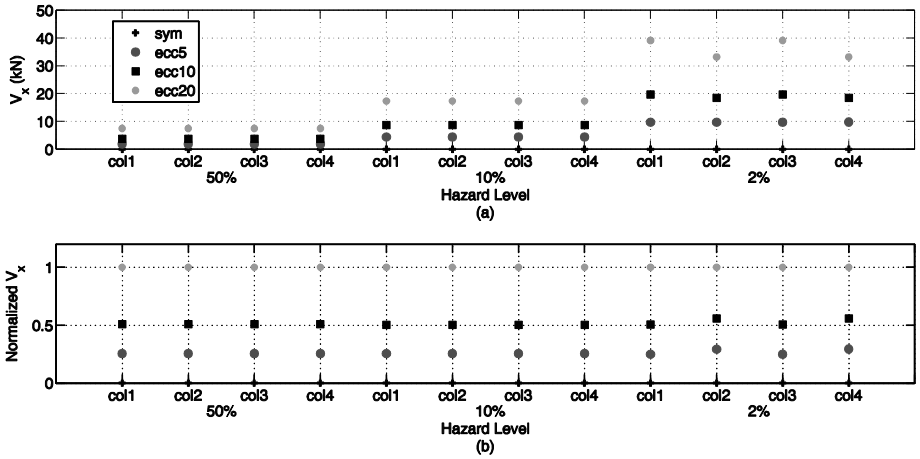

Figure 4.4. Numerical Example 1 - Shear forces: (a) maximum absolute values and (b) normalized values along x direction for each design and hazard level.

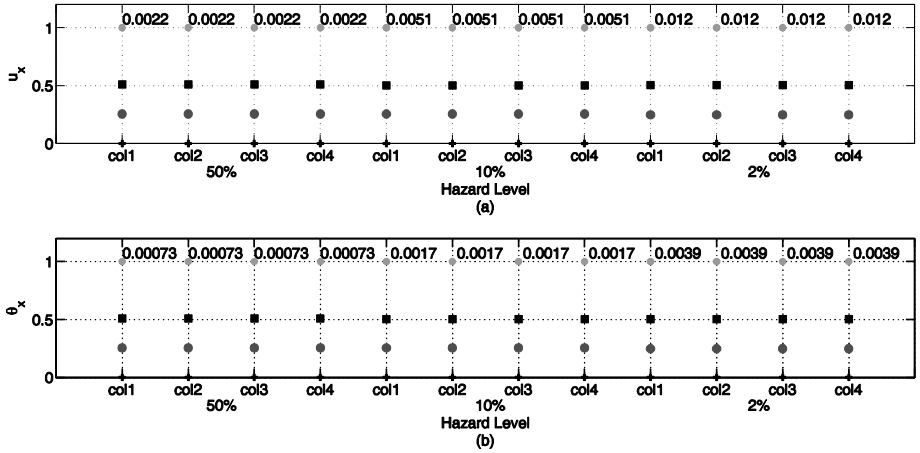

Figure 4.5. Numerical Example 1 - (a) normalized displacement values (in meters) and (b) normalized interstorey drift values (%) along x direction for each design and hazard level.

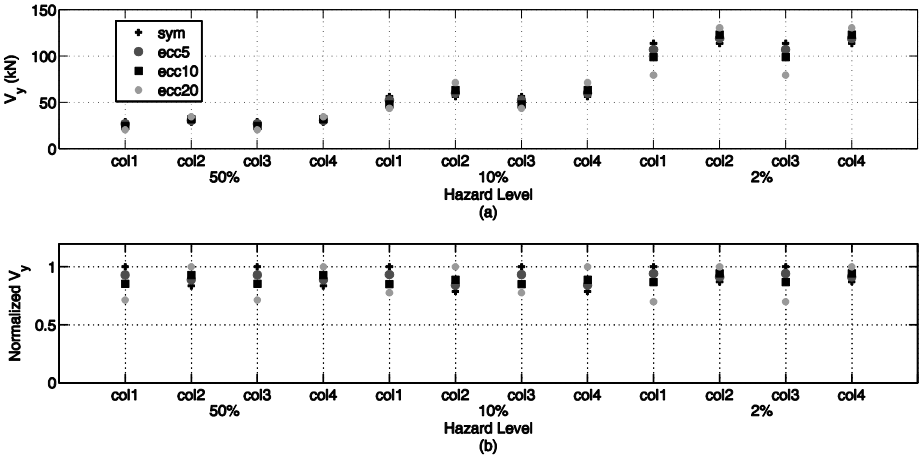

Figure 4.6. Numerical Example 1 - Shear forces: (a) maximum absolute values and (b) normalized values along y direction for each design and hazard level.

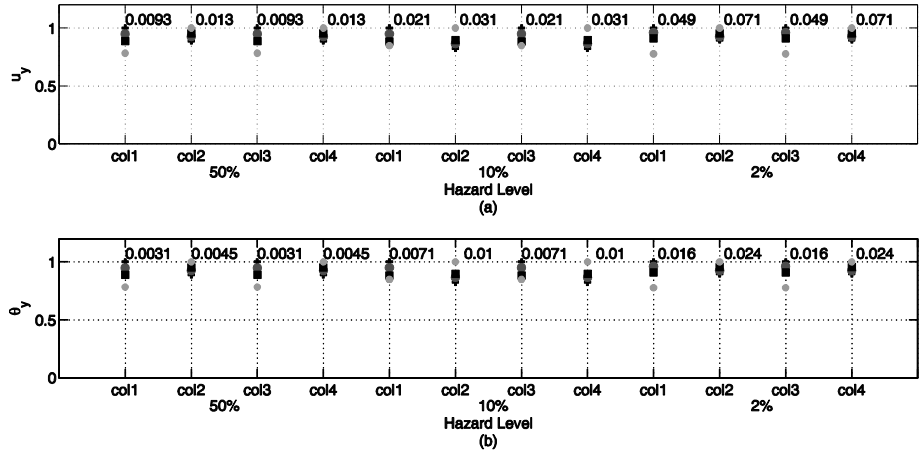

Figure 4.7. Numerical Example 1 - (a) normalized displacement values (in meters) and (b) normalized interstorey drift values (%) along y direction for each design and hazard level.

Figures 4.8(a) to 4.8(c) depict the trend of the base torque, diaphragm rotation and *ROT* values developed for the three hazard levels considered, while their normalized distributions are also shown in Figs. 4.8(d) to 4.8(f). It should be pointed out that since base torque, diaphragm rotation and *ROT* are not quantitatively comparable, qualitative conclusions will be drawn from their comparison. The diaphragm rotation, base torque and *ROT* values increase proportionally to the magnitude of eccentricity for all states of response. *ROT* calculation formula is based on internal shear forces for each hazard level quantifying the amplification due to

torsional effect. Taking into account that torque is sustained by a system as pairs of shear forces whose resultant is zero, higher *ROT* value indicates higher effect of torsional component on the structural elements. For the symmetric system, *ROT* magnitude is zero or almost zero for all states of response. While for the systems characterized by 20% eccentricity (*ecc20*) the shear forces amplified their magnitude due to torsion for 10/50 hazard level (Fig. 4.8(c)). In particular, compared to its symmetric counterpart the values of the shear forces are doubled for the 10/50 hazard level and tripled for the 2/50 one.

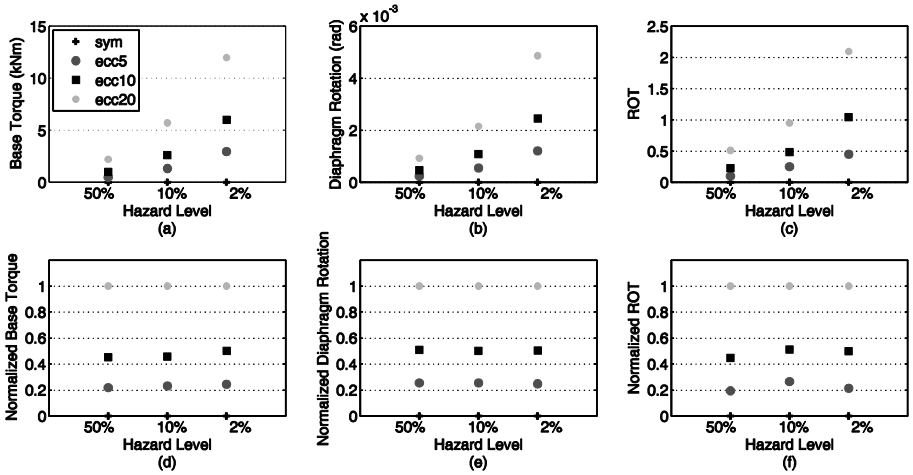

Figure 4.8. Numerical Example 1 - (a) Base torque, (b) diaphragm rotation, (c) ROT, (d) normalized base torque, (e) normalized diaphragm rotation and (f) normalized ROT for each design and hazard level.

4.3.2 Eccentric - horizontally regular single-story system - simple model

For this test example a bidirectional eccentricity is considered for the eccentric designs, while the symmetric design is identical to test example 1. Figure 4.9 depicts the location of mass center for the eccentric designs considered, while all designs are subjected to two-component seismic excitation.

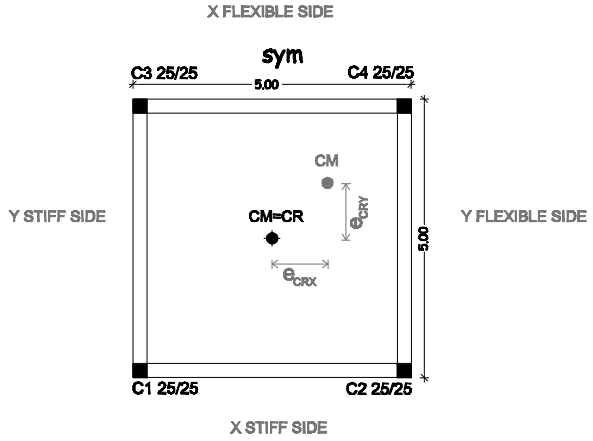

Figure 4.9. Numerical Example 2 - plan view.

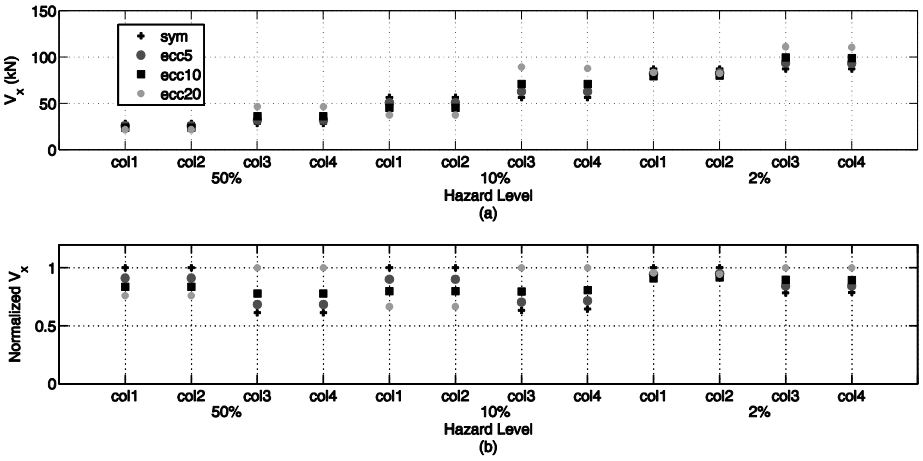

Figure 4.10. Numerical Example 2 - Shear forces: (a) maximum absolute values and (b) normalized values along x direction for each design and hazard level.

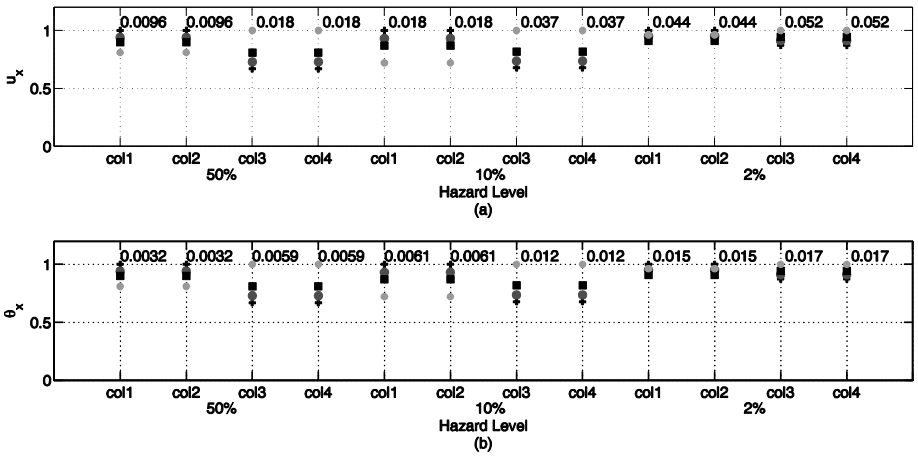

Figure 4.11. Numerical Example 2 - (a) normalized displacement values (in m) and (b) normalized interstorey drift values (%) along x direction for each design and hazard level.

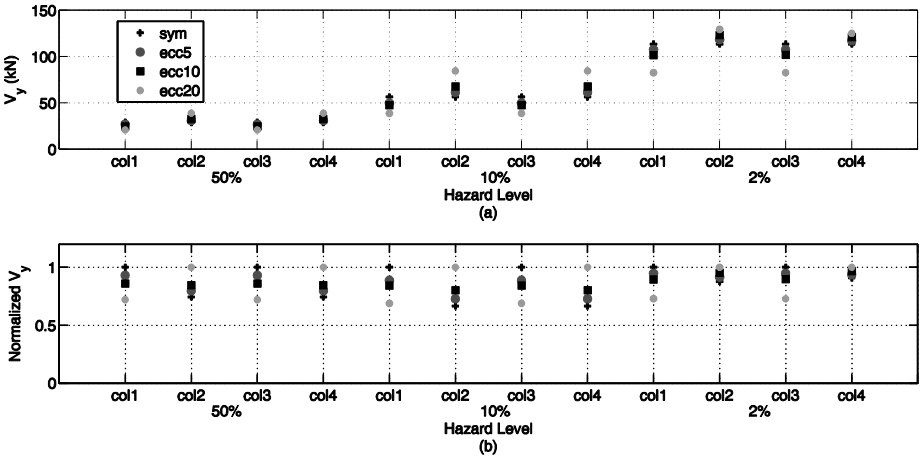

Figure 4.12. Numerical Example 2 - Shear forces: (a) maximum absolute values and (b) normalized values along y direction for each design and hazard level.

The typical behavior of torsionally stiff systems is also observed for this test example along both directions. In particular, shear forces along x direction are decreased at stiff edge (col1 and col2) while they are increased at flexible edge (col3 and col4), as shown in Fig. 4.10. Similar observations can be drawn for displacements and interstory drifts as shown in Fig. 4.11. It is worth noting that the values of the response quantities along x direction for columns 1 and 2 are proportional to 5% and 10% eccentricity for 2/50 hazard level. For 20% eccentricity, however, instead of further decrease on the response quantities observed for the columns at the stiff side, an increase on the values of shear forces is recorded. Figures 4.12 and 4.13 indicate that the response quantities along y direction are exhibiting consistent increase and decrease for flexible and stiff edges, respectively. Moreover, as shown in Figs. 4.14, as eccentricity increases diaphragm rotation, base torque and *ROT* values also increase for all states of response. It can also be observed that, for this system with bidirectional eccentricity subjected to two-component excitation, increased torsional effect is noticed according to base torque, diaphragm rotation and *ROT* values compared to the mono-symmetric test example, i.e. for the 2/50 hazard level *ROT* value is equal to 2.38, while for mono-symmetric system subjected to unidirectional excitation is equal to 2.10.

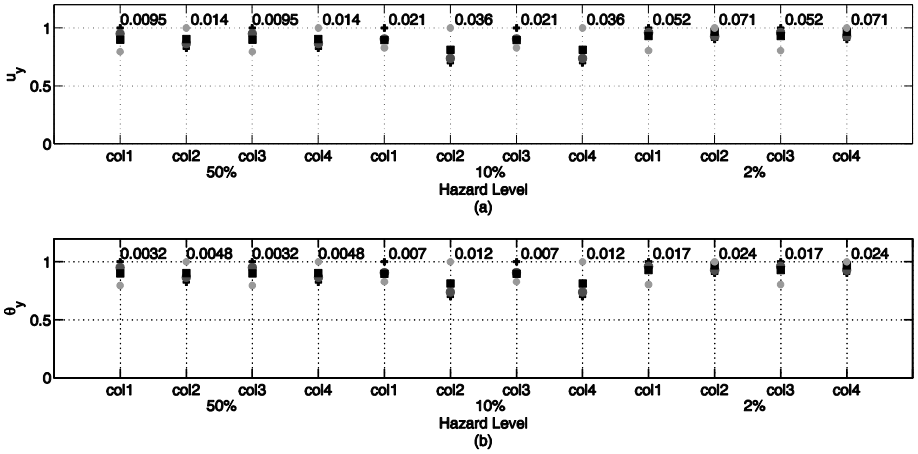

Figure 4.13. Numerical Example 2 - (a) normalized displacement values (in m) and (b) normalized interstorey drift values (%) along y direction for each design and hazard level.

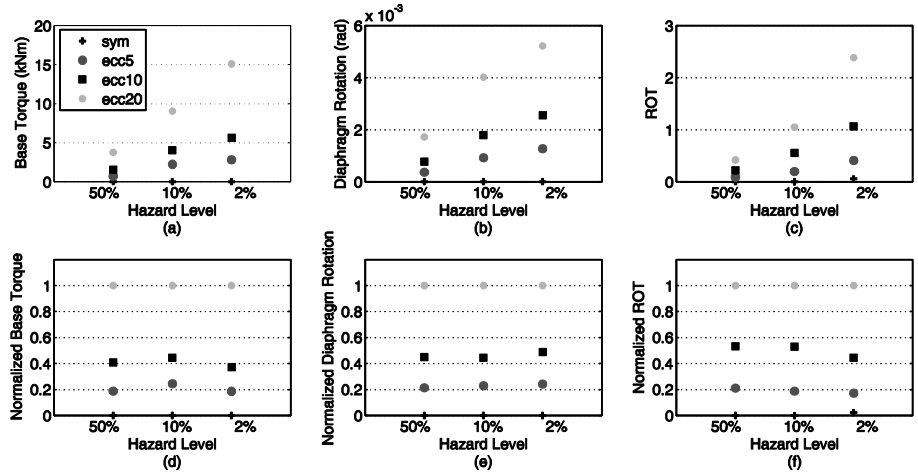

Figure 4.14. Numerical Example 2 - (a) Base torque, (b) diaphragm rotation, (c) ROT, (d) normalized base torque, (e) normalized diaphragm rotation and (f) normalized ROT for each design and hazard level.

4.3.3 Monosymmetric - horizontally regular single-story structure - with more realistic plan view

In addition to the previous test examples, a larger example with regular plan layout is considered. Figure 4.15 depicts the location of mass center for the eccentric designs considered. The eccentric designs are monosymmetric and are subjected to one-component earthquake excitation along y direction.

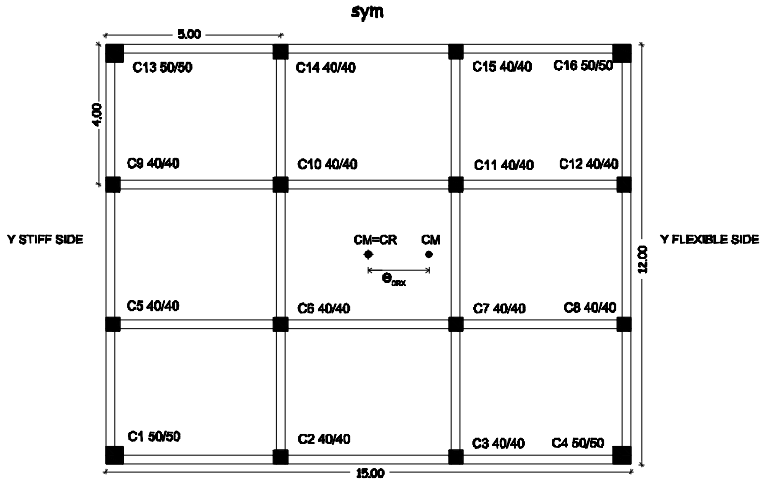

Figure 4.15. Numerical Example 3 - plan view.

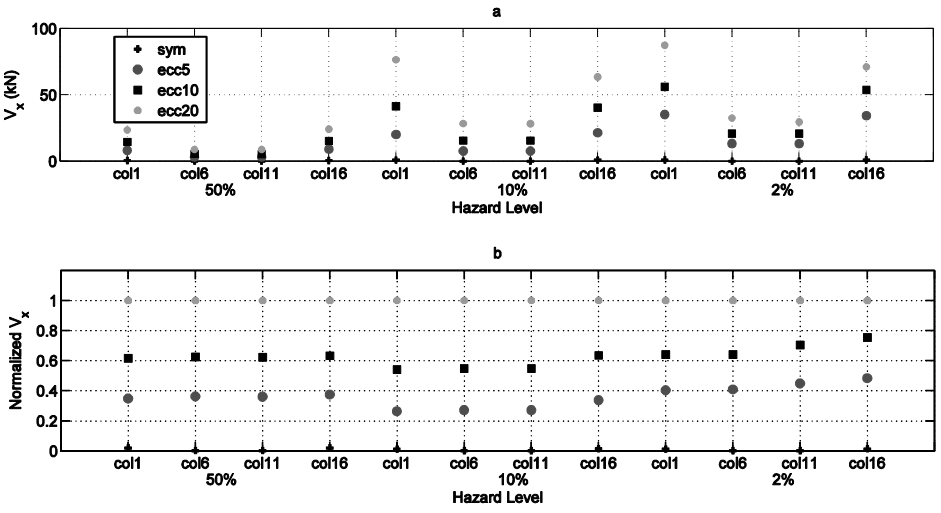

Figure 4.16. Numerical Example 3 - Shear forces: (a) maximum absolute values and (b) normalized values along x direction for each design and hazard level.

Figure 4.16 illustrates that torsional component is developed along x direction as in the case of first numerical application, since no seismic excitation is imposed along this direction. While the typical behavior of torsionally stiff structures is observed along y direction, decrease of shear forces for the elements at stiff edge (col1, col6) and increase for those at the flexible edge (col11, col16) was observed (Fig. 4.17). Interstory drifts and displacements followed the trend of shear forces (Figs. 4.18, 4.19).

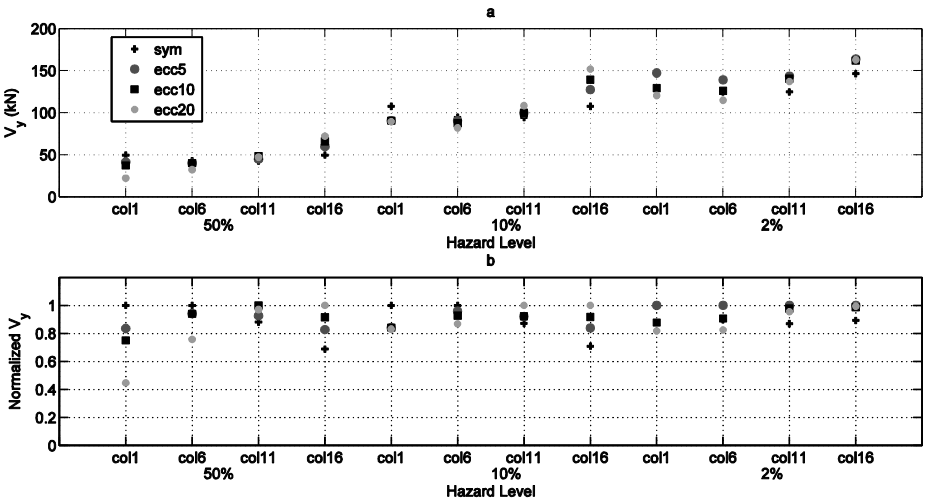

Figure 4.17. Numerical Example 3 - Shear forces: (a) maximum absolute values and (b) normalized values along y direction for each design and hazard level.

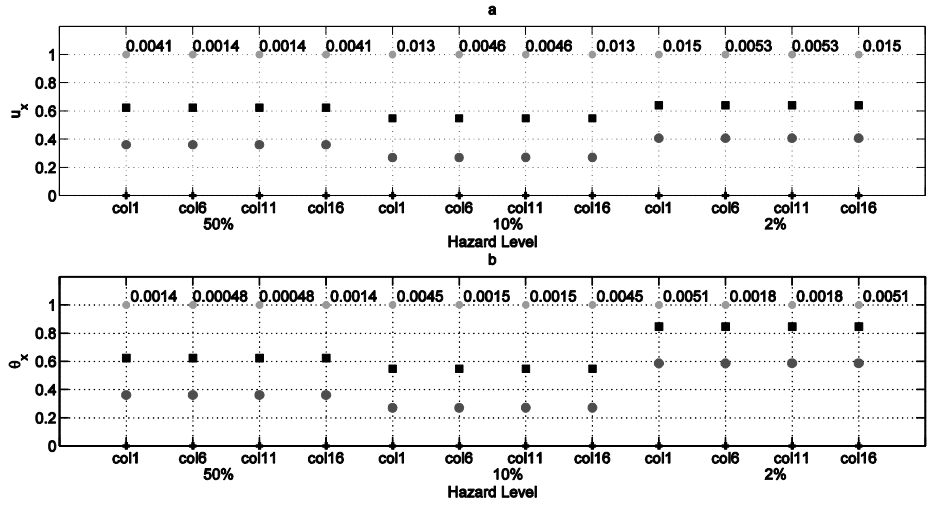

Figure 4.18. Numerical Example 3 - (a) normalized displacement values (in m) and (b) normalized interstory drift values (%) along x direction for each design and hazard level.

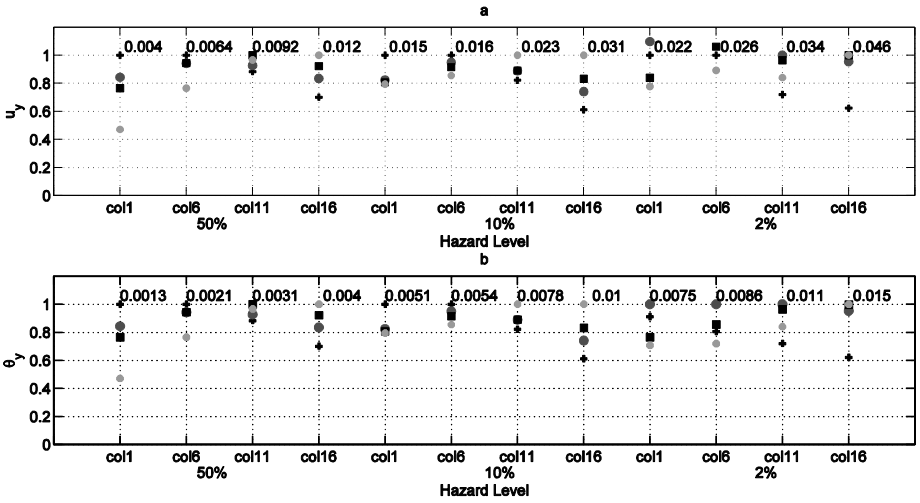

Figure 4.19. Numerical Example 3 - (a) normalized displacement values (in m) and (b) normalized interstorey drift values (%) along y direction for each design and hazard level.

In Figs. 4.20 the values of the response quantities related to torsion are presented. As it is observed, when eccentricity increases base torque, diaphragm rotation and *ROT* values increase for all states of response. The already observed behavior for monosymmetric simple mathematical model is also confirmed for realistic plan view model.

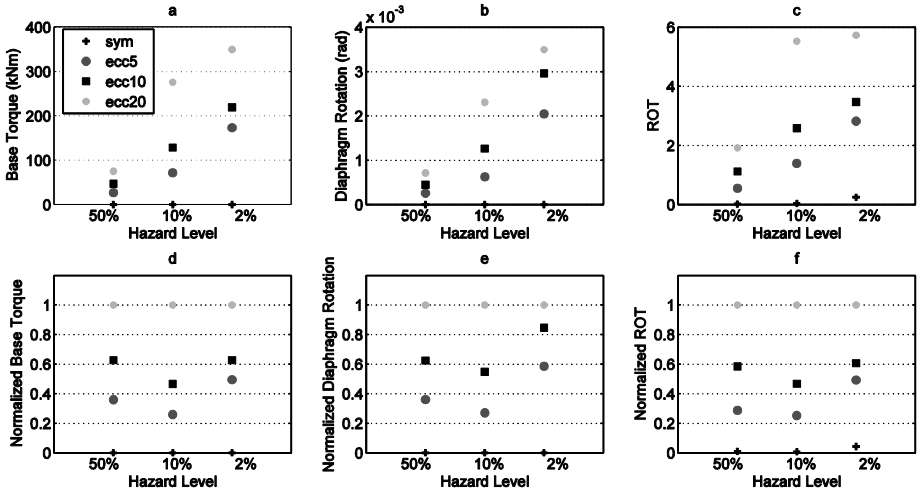

Figure 4.20. Numerical Example 3 - (a) Base torque, (b) diaphragm rotation, (c) ROT , (d) normalized base torque, (e) normalized diaphragm rotation and (f) normalized ROT for each design and hazard level.

4.3.4 Eccentric - horizontally regular single-story structure - with more realistic plan view

The same symmetric design as the previous example is implemented in the current one, while eccentric ones exhibit bidirectional eccentricity and are subjected to two-component earthquake ground motion. Figure 4.21 shows the plan layout while some features of eccentric designs are denoted in grey. Similar observations for the torsionally stiff system's behavior are also observed in this test example. It is noticed that consistent variation (increase or decrease) of response quantities disappears for eccentricity values greater than 10%, while for more realistic layouts the observed trend is valid for the elastic state. However, once the system enters the elastoplastic state and elements start yielding, the stiffness is not constant affecting the location of the rigidity center. The location of the rigidity center in elastoplastic states is not known and therefore it is not possible to define the flexible and stiff side of the system. The observations described above are shown in Figs. 4.22 and 4.23 for response quantities along y direction, while similar behavior is observed in x direction.

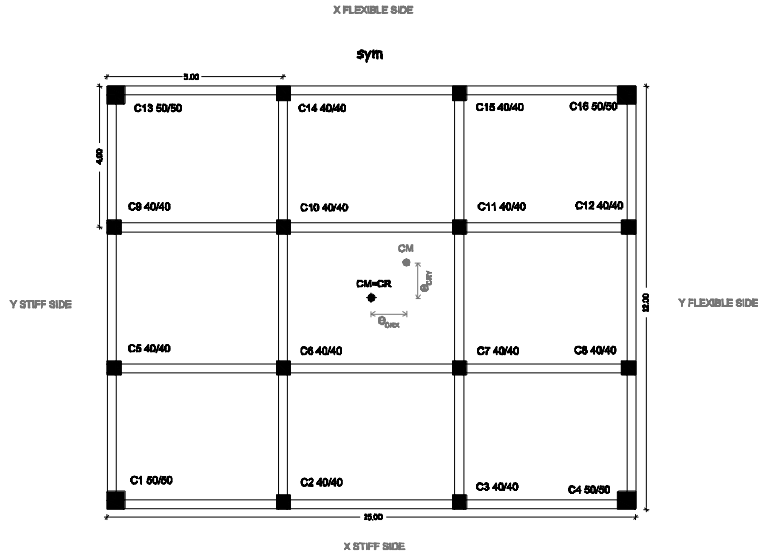

Figure 4.21. Numerical Example 4 - plan view.

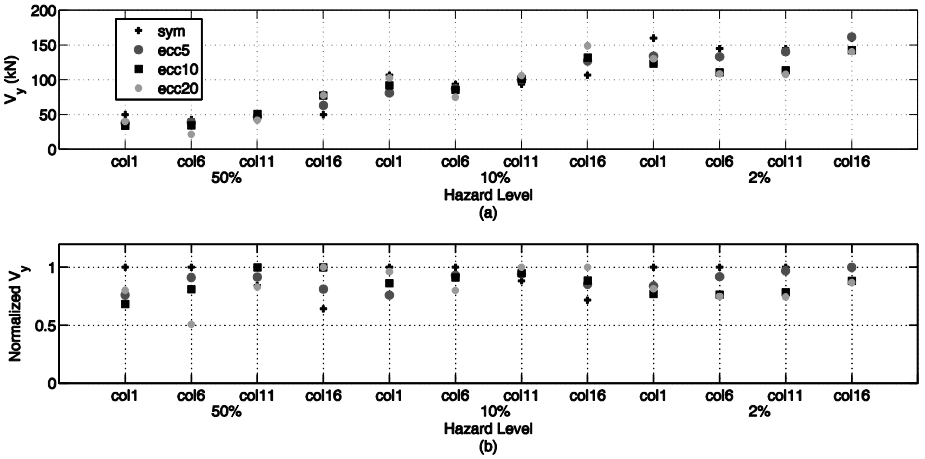

Figure 4.22. Numerical Example 4 - Shear forces: (a) maximum absolute values and (b) normalized values along y direction for each design and hazard level.

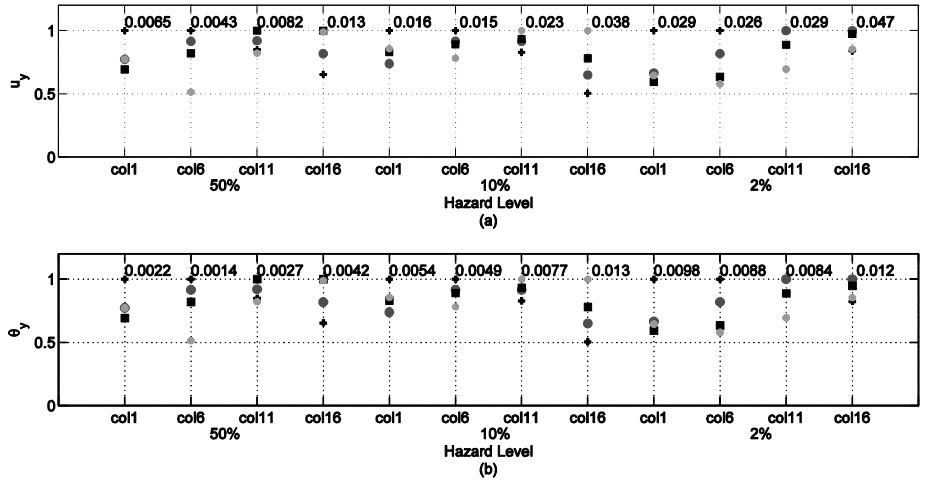

Figure 4.23. Numerical Example 4 - (a) normalized displacement values (in m) and (b) normalized interstory drift values (%) along y direction for each design and hazard level.

In Figures 4.24(a) to 4.24(c) significant increase of the maximum values of base torque and ROT is observed, while a slight decrease of the maximum diaphragm rotation is occurred compared to the corresponding to second numerical application. In this case the shear forces imposed were amplified six times for *ecc20* in 2/50 hazard level, while for the simple model of test case 2 the corresponding value was 2.38. Another interesting remark is that the maximum base torque do not always follow the distribution of the maximum diaphragm rotation. Figures 4.24(b) and 4.24(c) show that for *ecc20* design a decrease of the maximum diaphragm rotation is

observed from rare earthquake event 10/50 to maximum earthquake event 2/50, whereas for maximum base torque values are increased for the corresponding states.

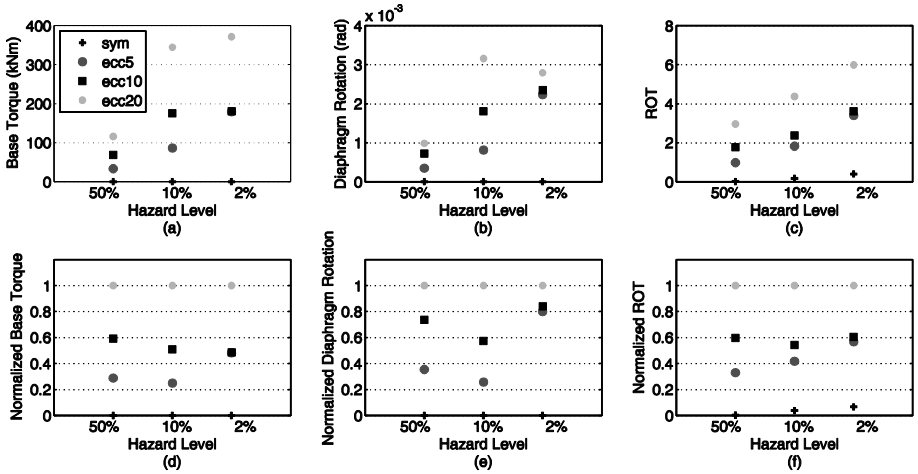

Figure 4.24. Numerical Example 4 - (a) Base torque, (b) diaphragm rotation, (c) ROT, (d) normalized base torque, (e) normalized diaphragm rotation and (f) normalized ROT for each design and hazard level.

4.3.5 Horizontally irregular single-story structure 1

In the current numerical example a horizontally irregular building (Fig. 4.25) was implemented to evaluate the performance of the proposed criterion. One-component earthquake excitation along y direction is imposed. For this test example was not possible to define a totally symmetric design that complies with the regulations imposed by the design codes [30]. Consequently, a small amount of eccentricity 0.83% is noticed for the reference design that is denoted as "*ecc*", instead of the notation "*sym*" used for the first four test examples. The other designs considered have the same amount of eccentricities as in the previous examples (5%, 10% and 2%). Since no seismic excitation was imposed along x direction, the developed shear forces as illustrated in Fig. 4.26 correspond to torsional component and increases with respect to eccentricity. The already established trend for torsionally stiff systems is observed in Fig. 4.27 for developed shear forces along y direction. Increase of shear forces for elements at flexible edge (col1, col7) respectively to eccentricity and decrease at stiff edge (col3, col6).

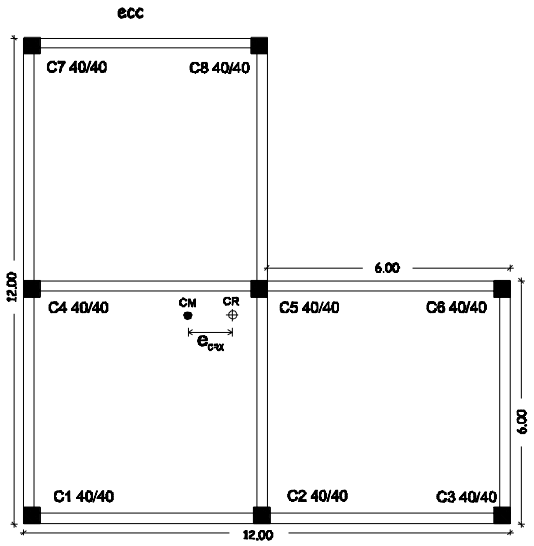

Figure 4.25. Numerical Example 5 - plan view.

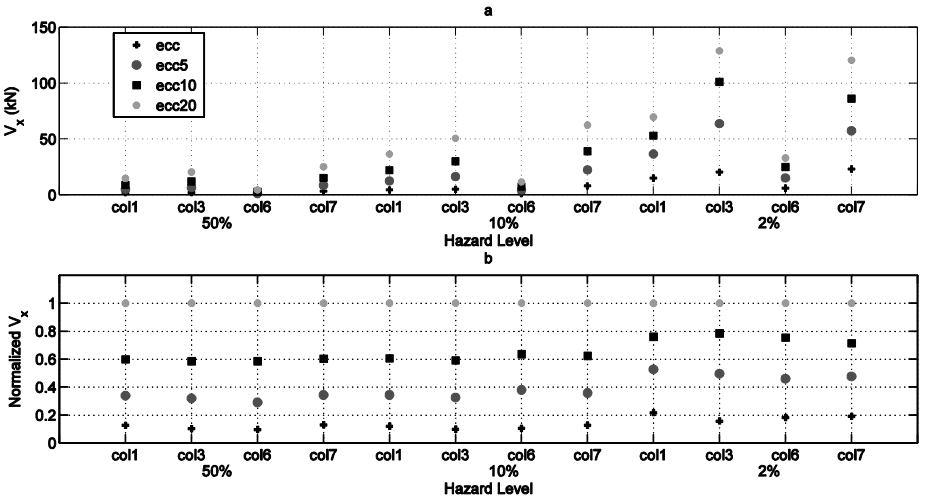

Figure 4.26. Numerical Example 5 - Shear forces: (a) maximum absolute values and (b) normalized values along x direction for each design and hazard level.

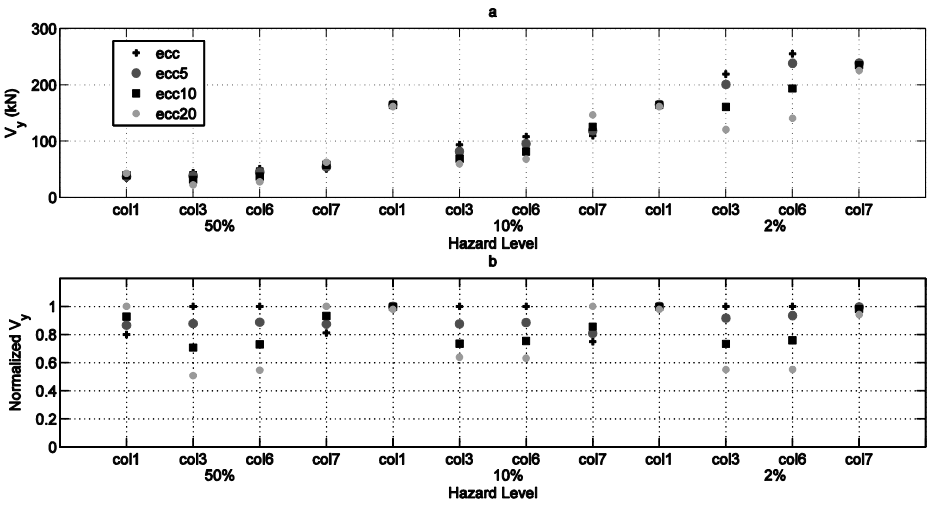

Figure 4.27. Numerical Example 5 - Shear forces: (a) maximum absolute values and (b) normalized values along y direction for each design and hazard level.

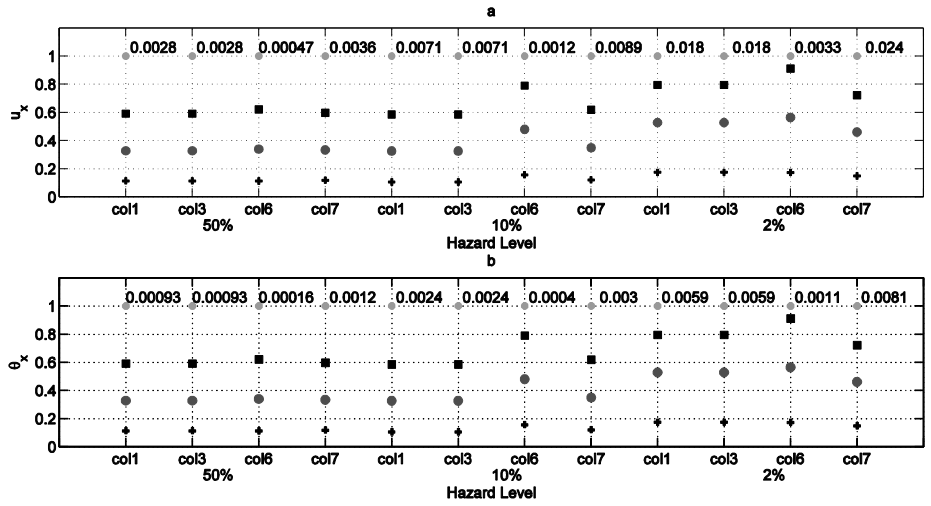

Figure 4.28. Numerical Example 5 - (a) normalized displacement values (in m) and (b) normalized interstory drift values (%) along x direction for each design and hazard level.

Interstory drifts and displacements along x direction follow the same trend as shear forces along this direction (Fig. 4.28). The same happens for the response quantities along y direction (Fig. 4.29). For "*ecc*" design almost zero values were obtained for base torque, diaphragm rotation and *ROT* for the elastic state of response (50/50 hazard level), while for the eccentric designs, the corresponding values are increased proportionally to the eccentricity. Similar observations are obtained for the other two hazard levels (Fig. 4.30).

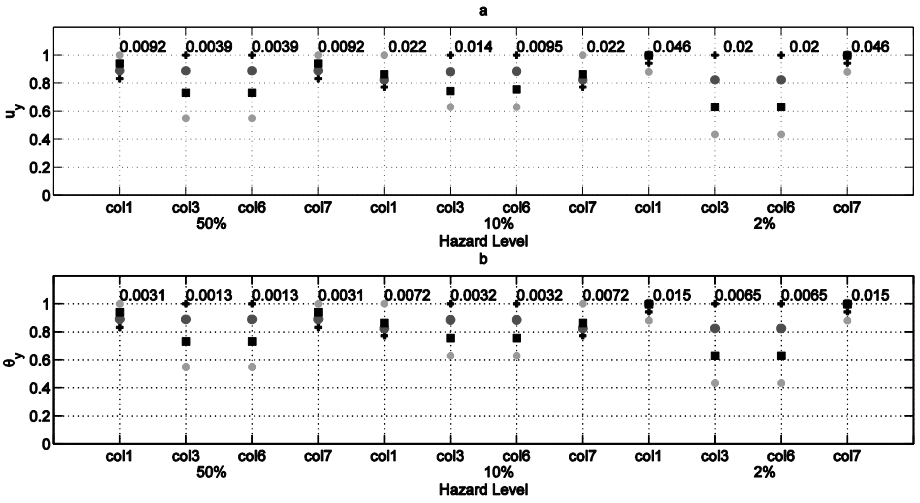

Figure 4.29. Numerical Example 5 - (a) normalized displacement values (in m) and (b) normalized interstory drift values (%) along y direction for each design and hazard level.

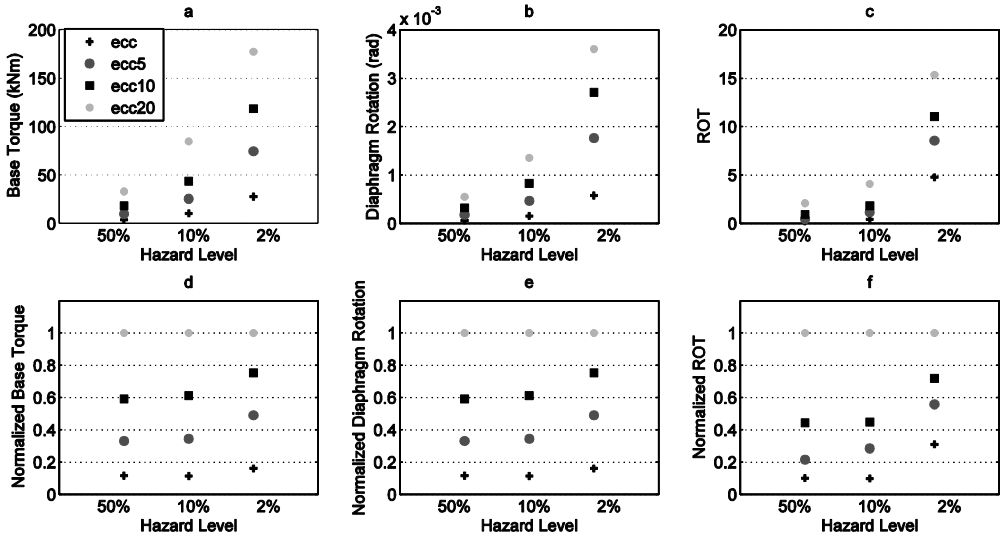

Figure 4.30. Numerical Example 5 - (a) Base torque, (b) diaphragm rotation, (c) ROT, (d) normalized base torque, (e) normalized diaphragm rotation and (f) normalized ROT for each design and hazard level.

4.3.6 Horizontally irregular single-story structure 2

The sixth numerical example, shown in Fig. 4.31, is a horizontally irregular building with bidirectional eccentricity subjected to two-component ground motion. For this numerical example was not also possible to define a totally symmetric design that complies with the regulations imposed by the design codes [30]. In this case the

notation of "*ecc*" is also adopted. The other designs considered have the same amount of eccentricities as in the previous examples (5%, 10% and 2%). Figures 4.32 and 4.33 show an increase of the response quantities for 5% and 10% eccentricity for the elements located at flexible edge (i.e. col1 and col7) and a decrease for those located at stiff edge (i.e. col3 and col6).

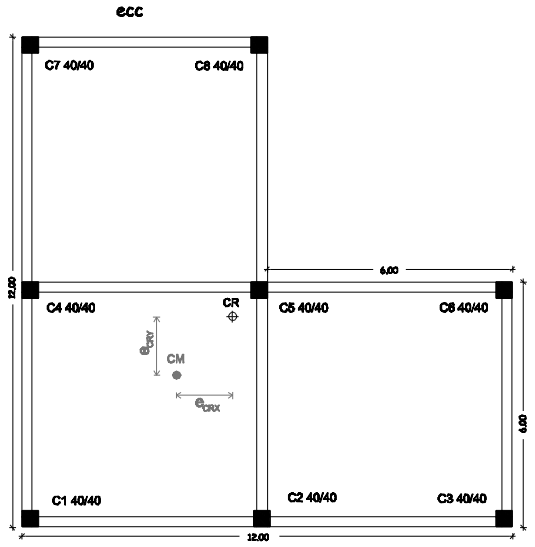

Figure 4.31. Numerical Example 6 - plan view.

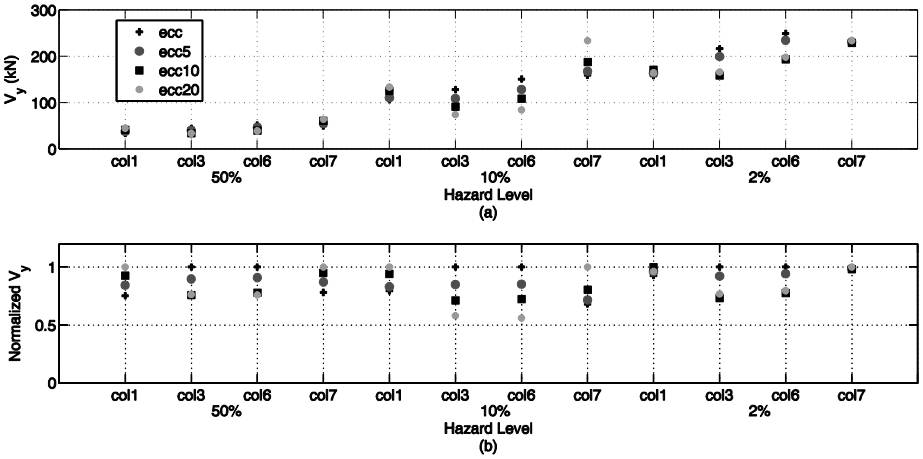

Figure 4.32. Numerical Example 6 - Shear forces: (a) maximum absolute values and (b) normalized values along y direction for each design and hazard level.

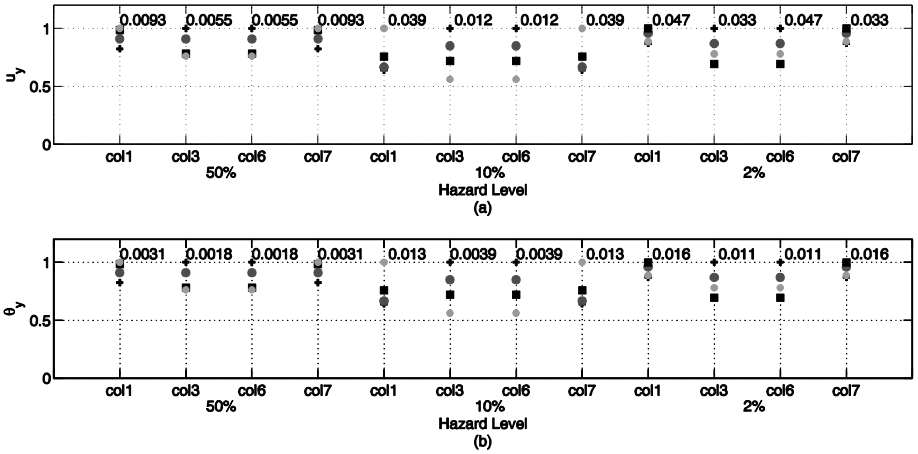

Figure 4.33. Numerical Example 6 - (a) normalized displacement values (in m) and (b) normalized interstory drift values (%) along y direction for each design and hazard level.

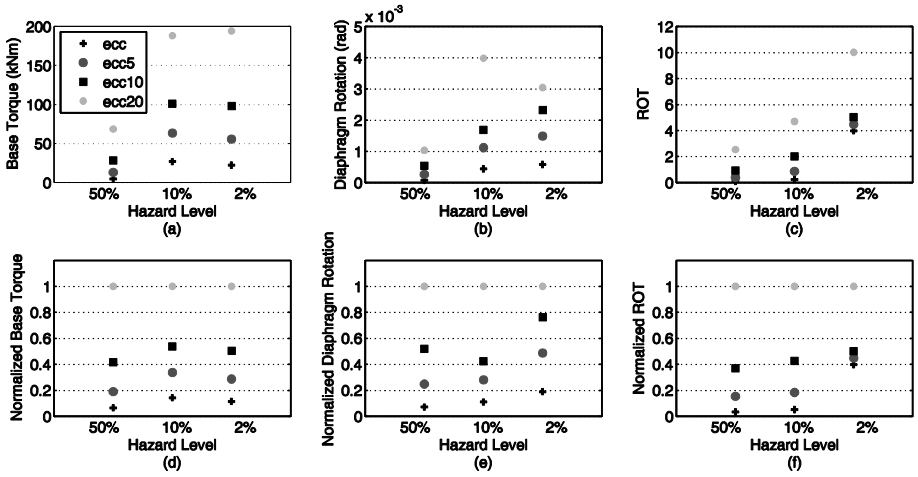

Figure 4.34. Numerical Example 6 - (a) Base torque, (b) diaphragm rotation, (c) ROT, (d) normalized base torque, (e) normalized diaphragm rotation and (f) normalized ROT for each design and hazard level.

For "*ecc*" design almost zero values were obtained for base torque, diaphragm rotation and *ROT* for the elastic state of response (50/50 hazard level). For the eccentric designs, the corresponding values are increased proportionally to the eccentricity. Similar observations are obtained for the other two hazard levels. Although a slight increase is observed on the magnitude of base torque, calculated for the 10/50 and 2/50 hazard levels, significant increase for *ROT* values were noticed. As mentioned above, however, base torque, diaphragm rotation and *ROT* are not directly comparable and therefore qualitative conclusions will be drawn from

their comparison. It is worth noting that for the 5% eccentricity design, increased *ROT* value is noticed for 2/50 hazard level as shown in Fig. 4.34(c). This can be justified by the asymmetric yielding of the vertical resisting elements due to the asymmetric plan view of the structure. The trend with respect to the behavioral quantities observed for the torsionally stiff horizontally regular systems has been confirmed also for torsionally stiff horizontally irregular systems.

4.4 Implementation of ROT for multistory buildings

The performance of the proposed *ROT* index is also evaluated for multistory buildings. Four four-story buildings were implemented in order to illustrate the efficiency of *ROT*. One monosymmetric horizontally regular building, two double eccentric horizontally regular buildings and a horizontally irregular one were tested. Fiber approach was adopted for modeling of members for multistory buildings too. The same material laws as in the case of one-story structures were implemented [26], [27]. In order to conduct the nonlinear dynamic analysis the same natural accelerograms were used. Tables 4.9 to 4.12 indicate that for these cases also the buildings are classified as torsionally stiff.

Table 4.9: Monosymmetric - horizontally regular four-story building - simple mathematical model - Vibration periods and uncoupled frequency ratios

	T_1	T_2	T_3	$\Omega_x = \frac{\omega_t}{\omega_x}$	$\Omega_y = \frac{\omega_t}{\omega_y}$
sym	1.1079^{x}	1.1079^{y}	0.5170^{t}	2.1429	2.1429
ecc0.05	1.1102^{y}	1.1079^{x}	0.5200^{t}	2.1350	2.1306
ecc0.10	1.1172^{y}	1.1079^{x}	0.5279^{t}	2.1163	2.1306
ecc0.20	1.1458^{y}	1.1079^{x}	0.5570^{t}	2.0571	1.9890

Table 4.10: Eccentric - horizontally regular four-story building - simple mathematical model - Vibration periods and uncoupled frequency ratios

	T_1	T_2	T_3	$\Omega_x = \frac{\omega_t}{\omega_x}$	$\Omega_y = \frac{\omega_t}{\omega_y}$
sym	1.1079^{x}	1.1079^{y}	0.5170^{t}	2.1429	2.1429
ecc0.05	1.1125^{y}	1.1079^{x}	0.5225^{t}	2.1292	2.1204
ecc0.10	1.1268^{y}	1.1079^{x}	0.5500^{t}	2.0487	2.0144
ecc0.20	1.1829^{y}	1.1079^{x}	0.5612^{t}	2.1078	1.9742

Table 4.11: Eccentric - horizontally regular four-story building - realistic plan views - Vibration periods and uncoupled frequency ratios

	T_1	T_2	T_3	$\Omega_x = \frac{\omega_t}{\omega_x}$	$\Omega_y = \frac{\omega_t}{\omega_y}$
sym	0.9431^{x}	0.8486^{y}	0.5998^{t}	1.5724	1.4148
ecc0.05	0.9464^{x}	0.8063^{y}	0.5711^{t}	1.6572	1.4118
ecc0.10	0.3753^{x}	0.3539^{y}	0.2519^{t}	1.4898	1.4049
ecc0.20	1.0648^{x}	0.8996^{y}	0.6097^{t}	1.7464	1.4755

Table 4.12: Horizontally irregular four-story building - Vibration periods and uncoupled frequency ratios

	T_1	T_2	T_3	$\Omega_x = \frac{\omega_t}{\omega_x}$	$\Omega_y = \frac{\omega_t}{\omega_y}$
ecc	1.0074^{x}	1.0059^{y}	0.6988^{t}	1.4416	1.4395
ecc0.05	1.0218^{x}	1.0074^{y}	0.7006^{t}	1.4585	1.4379
ecc0.10	1.0633^{x}	1.0074^{y}	0.6851^{t}	1.5520	1.4704
ecc0.20	1.1933^{x}	1.0074^{y}	0.6313^{t}	1.8902	1.5958

4.4.1 Monosymmetric - horizontally regular four-story building - simple model

This test example is a four-story monosymmetric building subjected to unidirectional excitation along the y direction. The layout of the symmetric design and a 3D view are given in Fig. 4.35, while some properties of the eccentric designs considered are also denoted in grey.

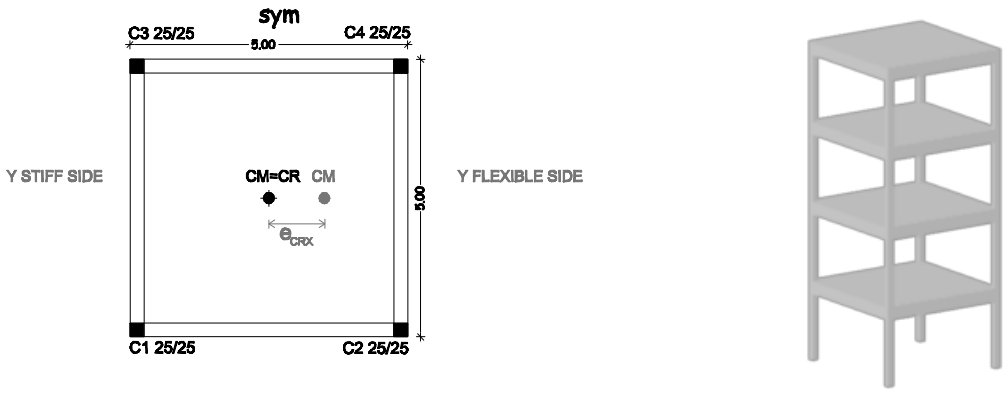

Figure 4.35. Numerical Example 7 - plan and 3D view.

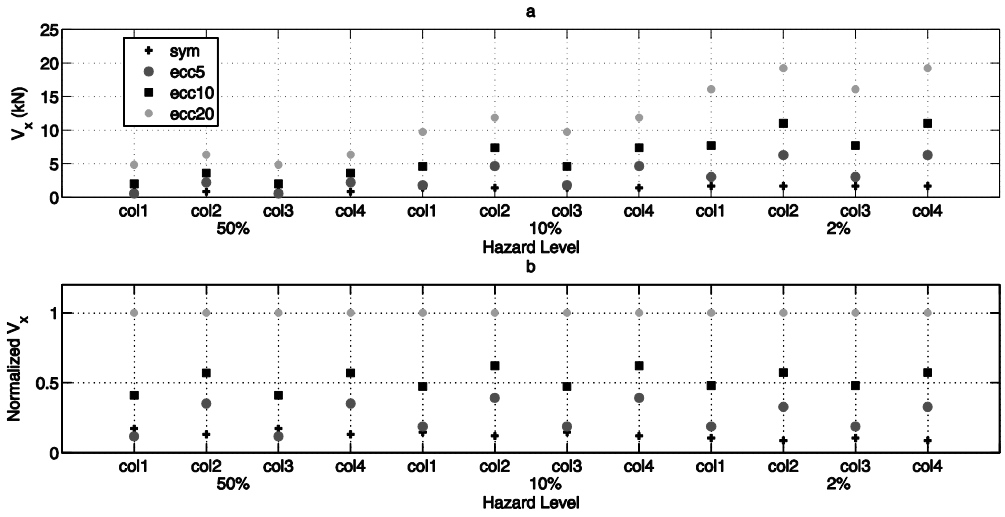

Figure 4.36. Numerical Example 7 - Peak edge column shear forces (a) maximum absolute values and (b) normalized values along x direction for each design and hazard level.

The structural response quantities are presented in Figs. 4.36 to 4.39 for the columns of the top story for the three hazard levels. Figure 4.40 shows the response parameters of base torque, diaphragm rotation and *ROT* that are related to the

torsional effect. The envelopes of maximum values of the response quantities along the height of the building are presented in Figs. 4.41 to 4.46 for various structural elements. It can be seen that although unidirectional seismic excitation is considered, shear forces are developed at the vertical resisting elements along both directions for the case of the eccentric designs due to the torsional component. In particular, the shear forces developed along x direction for the symmetric design are reduced compared to those developed for the eccentric designs, while their values are proportional to the eccentricity (Fig. 4.36). Similar behavior is observed for the displacements and interstory drifts along x direction, while their maximum values are depicted in Fig. 4.37. The behavior of torsionally stiff systems is observed for all response quantities along the *y* direction of seismic excitation, as can be seen in Figs. 4.38 and 4.39. Decreased values for displacements, interstory drifts and shear forces are observed for the elements at the stiff side (i.e. col1 and col3) for the case of 5% and 10% eccentricity, while increased values are observed for the elements at flexible edge (i.e. col2 and col4).

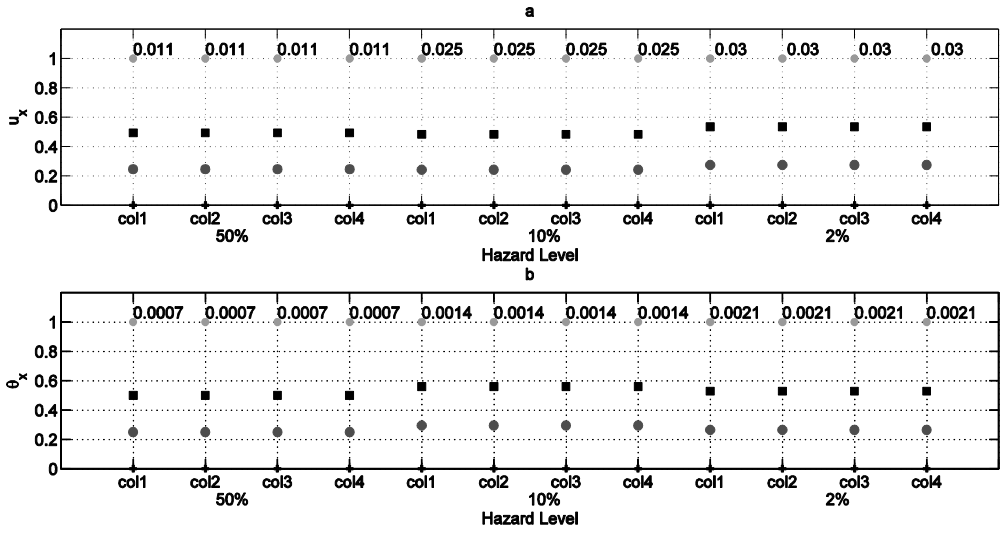

Figure 4.37. Numerical Example 7 - Peak edge column (a) normalized displacement values (in m) and (b) normalized interstory drift values (%) along x direction for each design and hazard level.

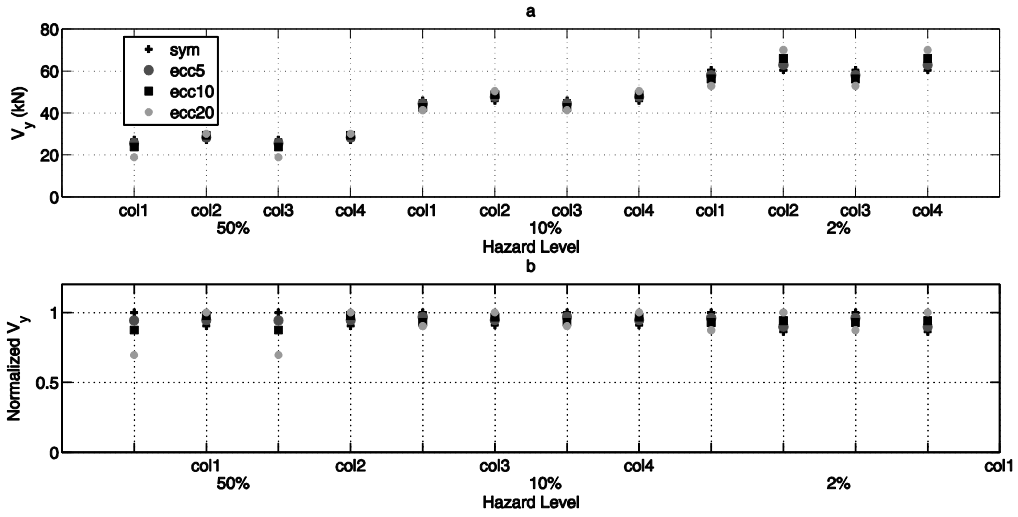

Figure 4.38. Numerical Example 7 - Peak edge column shear forces (a) maximum absolute values and (b) normalized values along y direction for each design and hazard level.

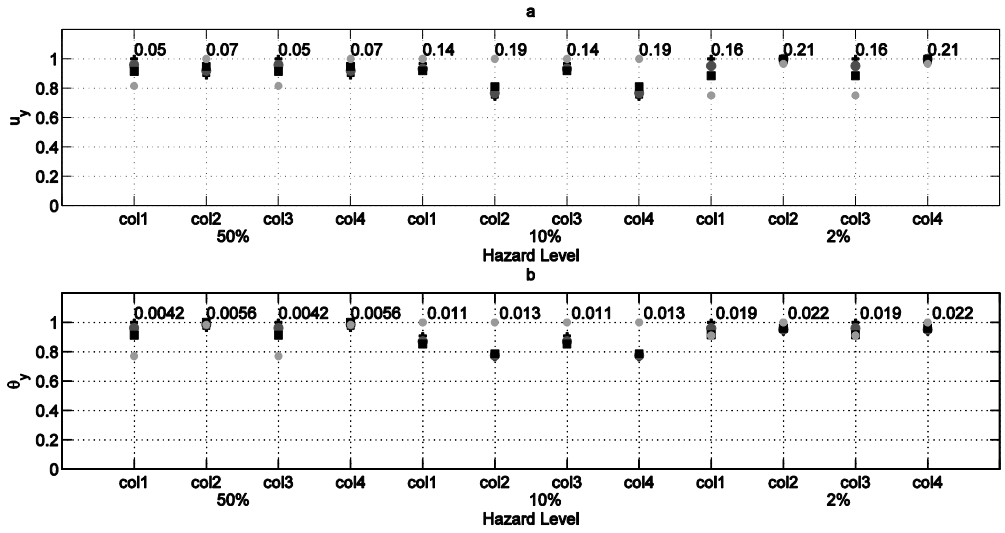

Figure 4.39. Numerical Example 7 - Peak edge column (a) normalized displacement values (in m) and (b) normalized interstory drift values (%) along y direction for each design and hazard level.

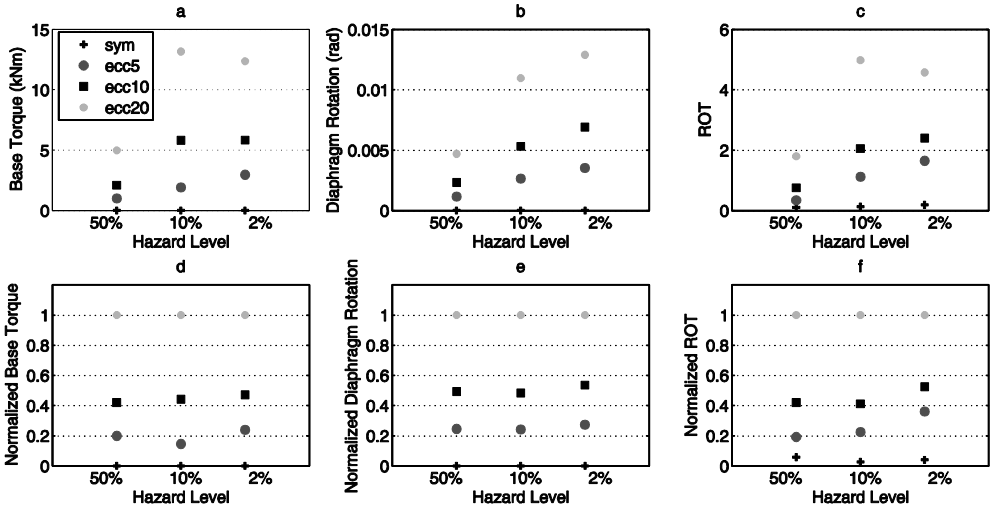

Figure 4.40. Numerical Example 7 - (a) Base torque, (b) diaphragm rotation, (c) ROT, (d) normalized base torque, (e) normalized diaphragm rotation, (f) normalized ROT for each design and hazard level.

The response quantities related to the torsional effect (i.e. upper diaphragm rotation, base torque and *ROT*) and their normalized values are shown in Fig. 4.40 corresponding to the three hazard levels considered. It should be pointed out that since base torque, diaphragm rotation and *ROT* are not directly comparable, qualitative conclusions will be drawn from their comparison. The diaphragm rotation, base torque and *ROT* are increased proportionally to the eccentricity for all states of response. It can also be observed that maximum base torque values are not always in accordance to the distribution of the maximum diaphragm rotation values. As it is shown in Figs. 4.40(a) to 4.40(c), the upper diaphragm rotation obtained for the *ecc20* design is increased when the records of the 2/50 hazard level are applied compared to the rotation values obtained for the 10/50 hazard level, while base torque and *ROT* values are reduced. Since, *ROT* calculation formula is based on the internal shear forces developed at the vertical resisting elements, it can be said that this parameter quantifies the amplification of the shear forces due to torsion. Thus, for the symmetric design, *ROT* is almost equal to zero for all states of response, while for the design with 20% eccentricity (*ecc20*) the shear forces are double (Fig. 4.40(c)) compared to those of the symmetric design. For comparative reasons, two columns were selected, one located at stiff edge (column 1) and one located at flexible edge (column 4) and their structural response for all stories is shown in Figs. 4.41 to 4.46.

For both columns, the shear forces along x direction are proportional to the size of the eccentricity for all hazard levels (see Figures 4.40 and 4.44). The same trend is observed for the interstory drifts and displacements (see Figures 4.42, 4.43, 4.45 and 4.46). The response quantities for column 1 are decreased proportionally to the increase of eccentricity for 5% and 10% (see Figures 8, 9 and 10), while for the case of column 4 the opposite trend is observed, i.e. the response in increased proportionally for 5% and 10% eccentricity (see Figs. 4.44, 4.45 and 4.46).

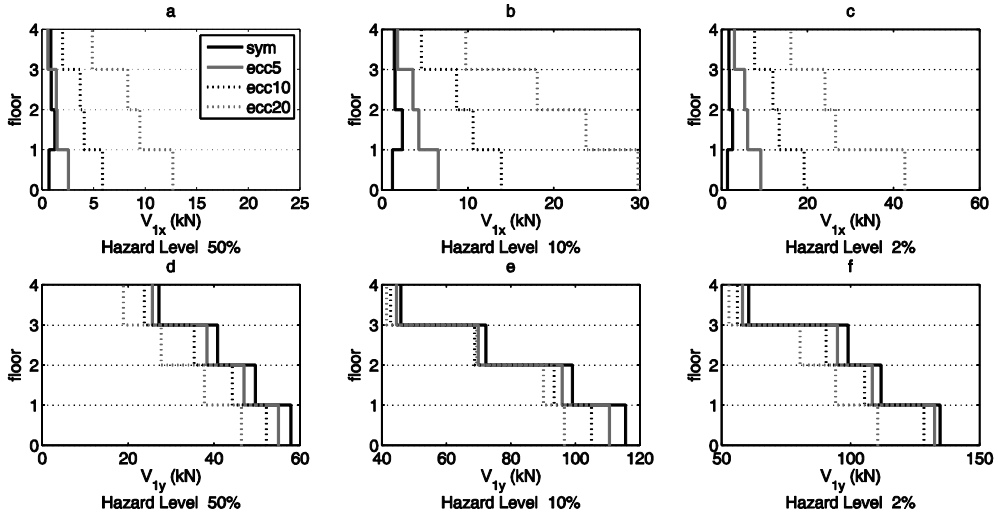

Figure 4.41. Numerical Example 7 - Column 1 maximum absolute shear force values along x (a, b, c) and y (d, e, f) direction for all floors and hazard levels.

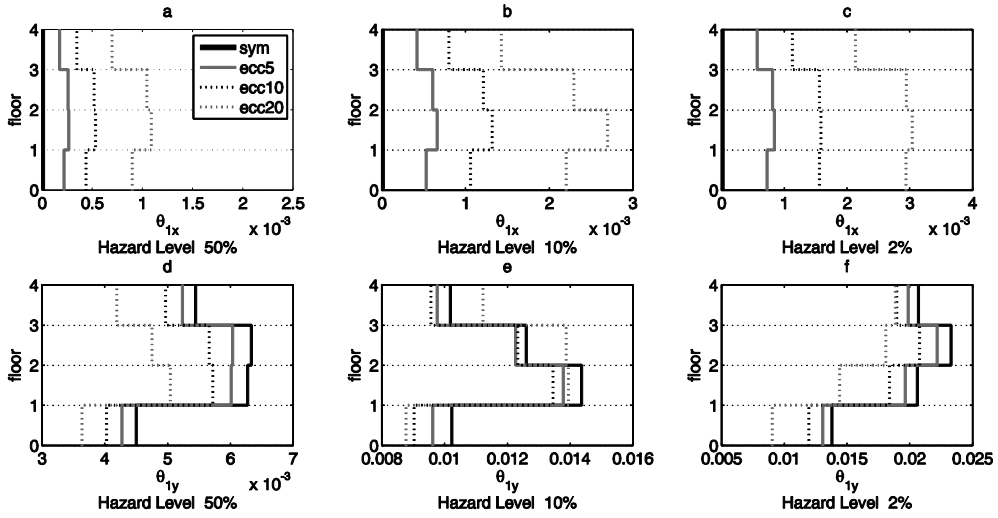

Figure 4.42. Numerical Example 7 - Column 1 maximum absolute drift values along x (a, b, c) and y (d, e, f) direction for all floors and hazard levels.

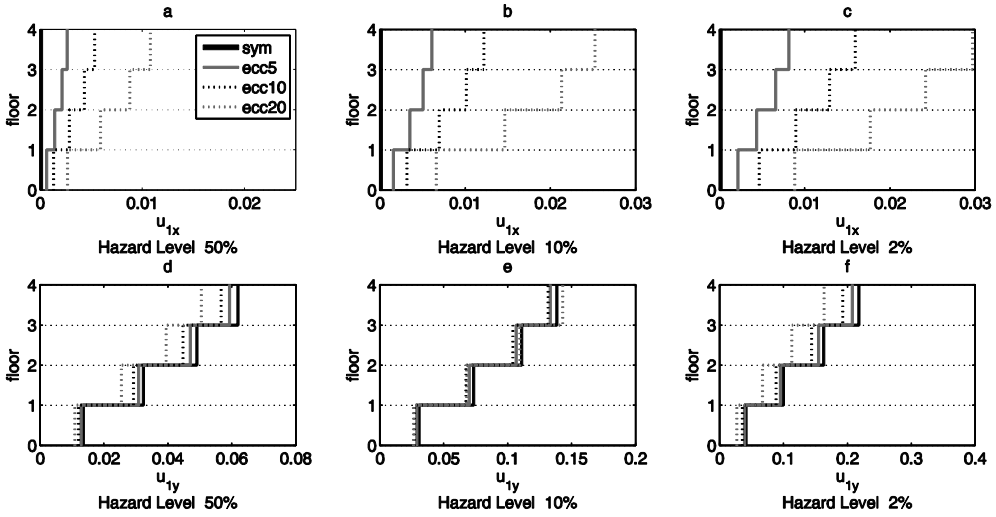

Figure 4.43. Numerical Example 7 - Column 1 maximum absolute displacement values along x (a, b, c) and y (d, e, f) direction for all floors and hazard levels.

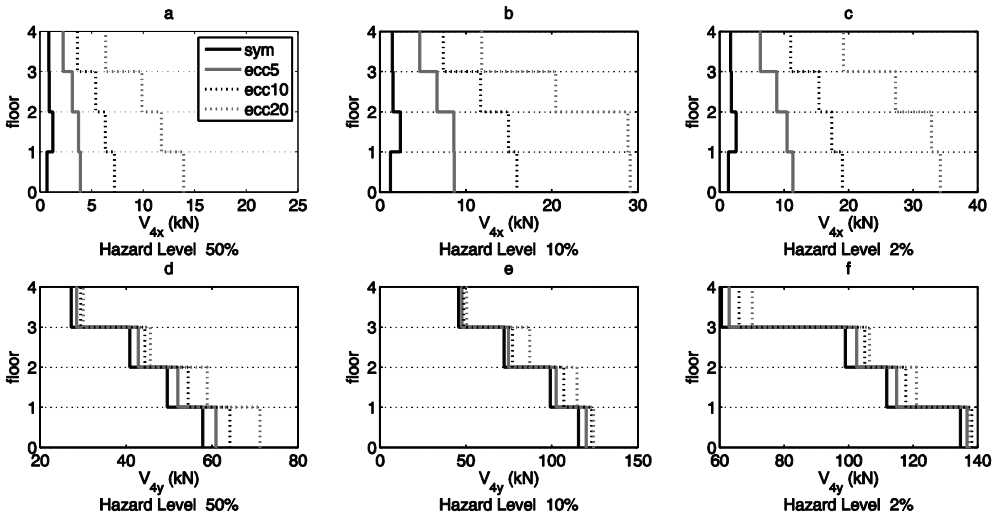

Figure 4.44. Numerical Example 7 - Column 4 maximum absolute shear force values along x (a, b, c) and y (d, e, f) direction for all floors and hazard levels.

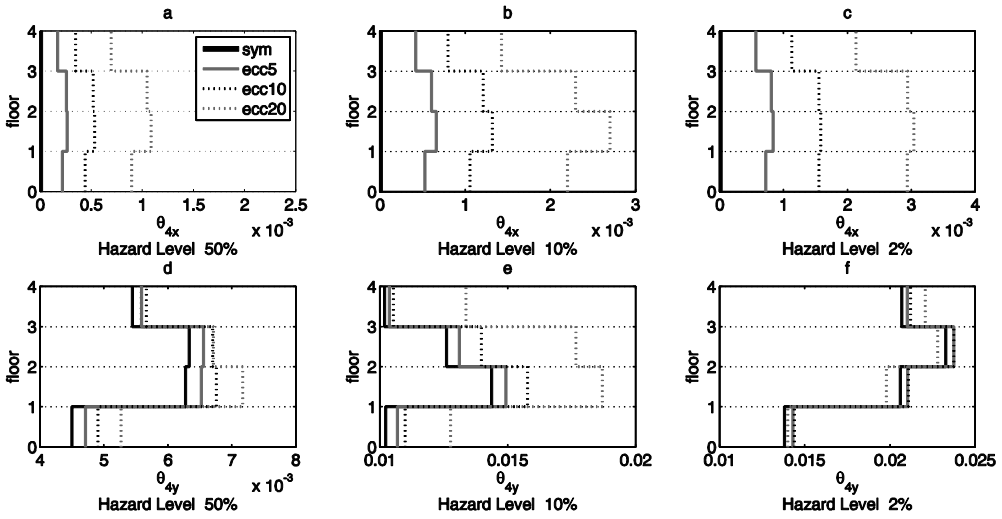

Figure 4.45. Numerical Example 7 - Column 4 maximum absolute drift values along x (a, b, c) and y (d, e, f) direction for all floors and hazard levels.

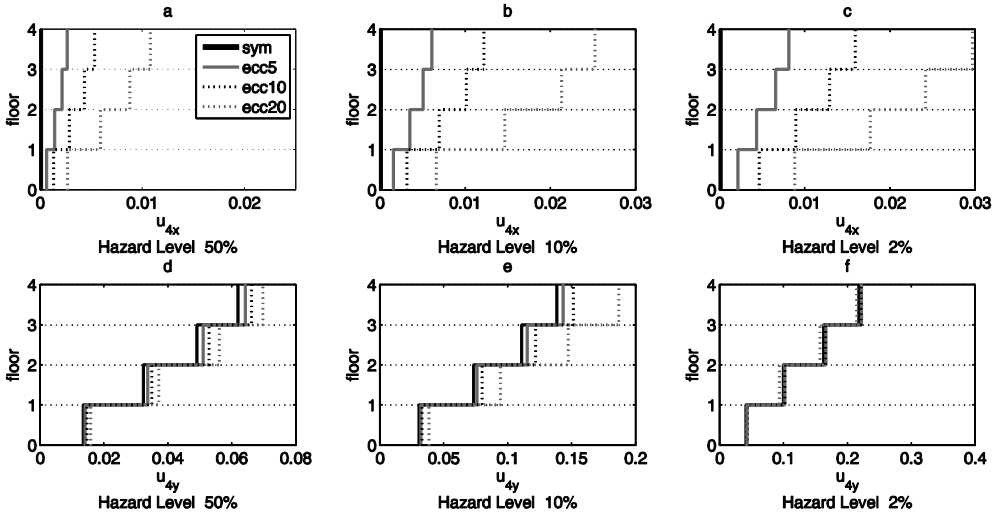

Figure 4.46. Numerical Example 7 - Column 4 maximum absolute displacement values along x (a, b, c) and y (d, e, f) direction for all floors and hazard levels.

4.4.2 Eccentric - horizontally regular four-story building - simple model

This test problem has the same symmetric design with that of the previous test example. However, the eccentric designs exhibit bidirectional eccentricities as denoted in grey in Fig. 4.47, while all designs are subjected to two-component seismic excitation.

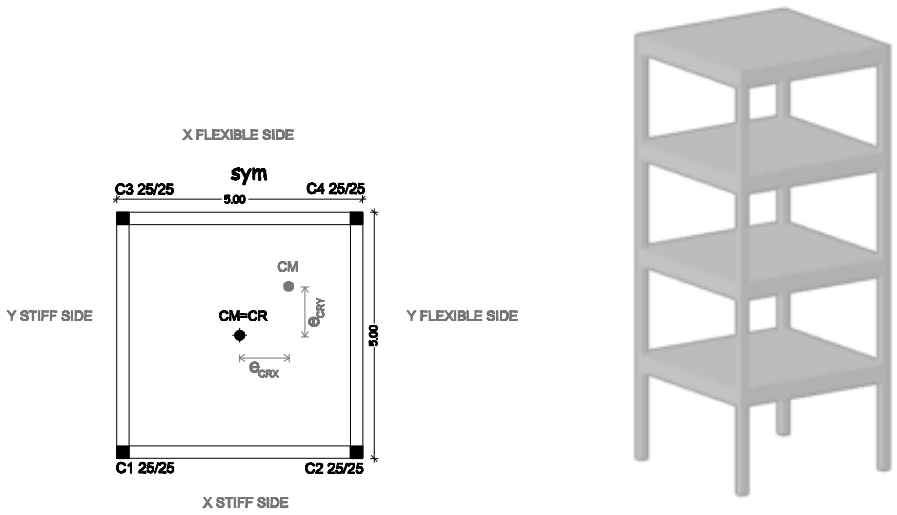

Figure 4.47. Numerical Example 8 - plan and 3D view.

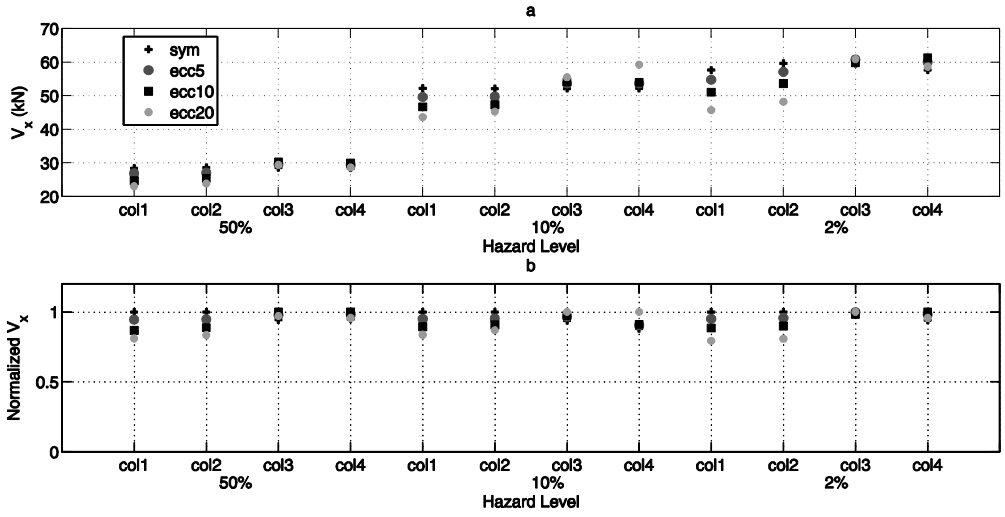

Figure 4.48. Numerical Example 8 - Peak edge column shear forces (a) maximum absolute values and (b) normalized values along x direction for each design and hazard level.

As it is shown in Fig. 4.48, the shear forces at the stiff edge (i.e. col1 and col2) along the x direction are decreased proportionally to the eccentricity, while they are increased at the flexible one (i.e. col3 and col4). Similar observations can be drawn for the displacements and interstory drifts (see Figs. 4.49(a) and 4.49(b)). It is worth noting that the response quantities along x direction for columns 3 and 4 are increased when the eccentricity is also increased.

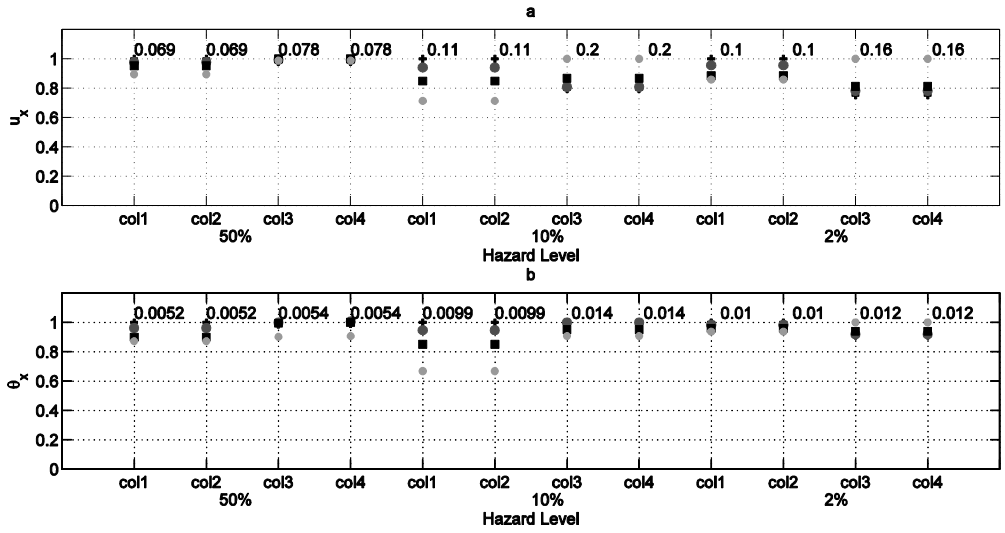

Figure 4.49. Numerical Example 8 - Peak edge column (a) normalized displacement values (in m) and (b) normalized interstory drift values (%) along x direction for each design and hazard level.

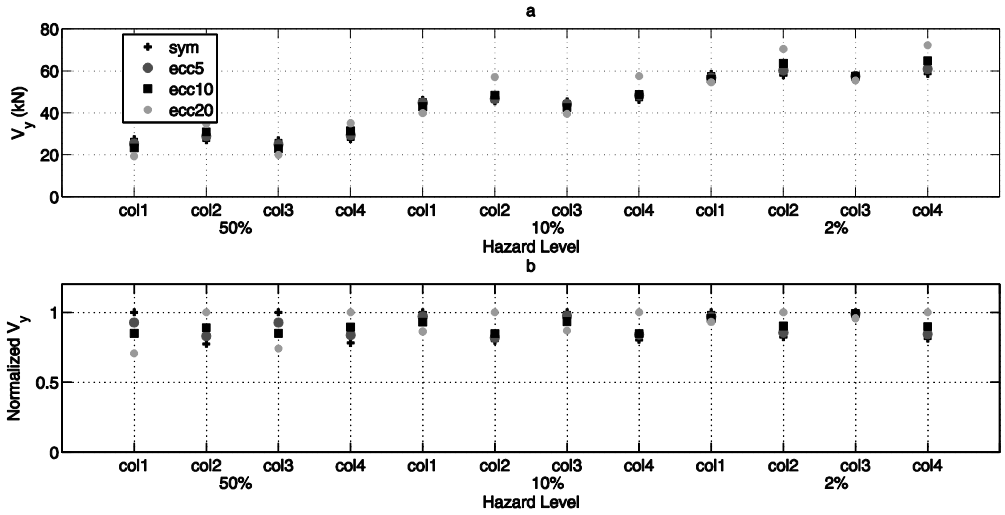

Figure 4.50. Numerical Example 8 - Peak edge column shear forces (a) maximum absolute values and (b) normalized values along y direction for each design and hazard level.

The response quantities of the top diaphragm's elements along y direction are increased for the flexible edge and are decreased for the stiff one when eccentricity is increased (see Figs. 4.50 and 4.51). Moreover, when eccentricity is increased, top diaphragm's rotation, base torque and *ROT* are also increased for all states of response (see Fig. 4.52).

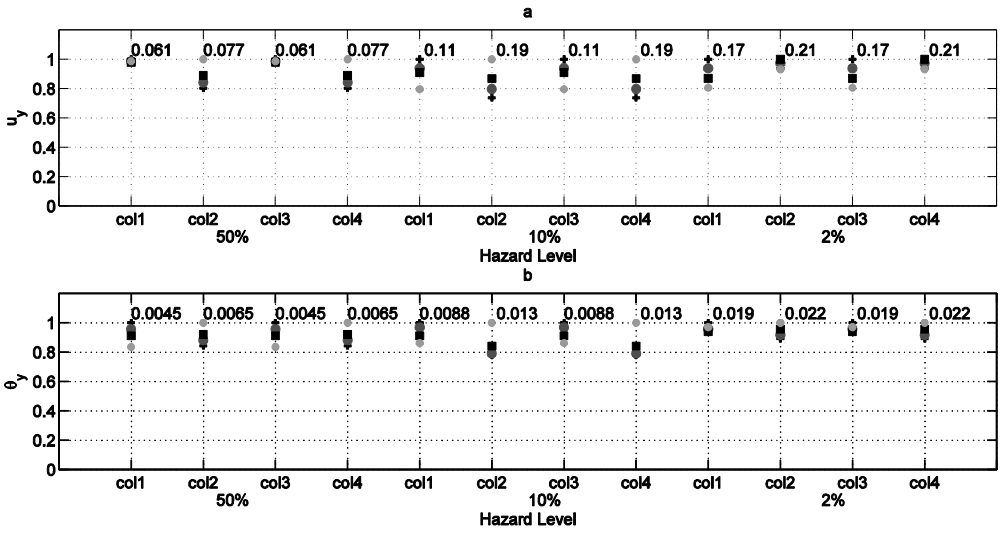

Figure 4.51. Numerical Example 8 - Peak edge column (a) normalized displacement values (in m) and (b) normalized interstory drift values (%) along y direction for each design and hazard level.

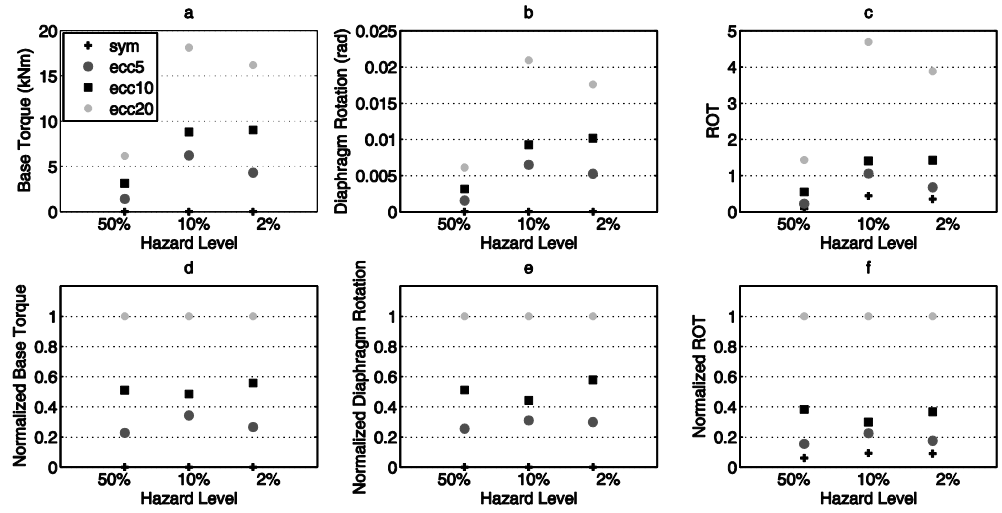

Figure 4.52. Numerical Example 8 - (a) Base torque, (b) diaphragm rotation, (c) ROT, (d) normalized base torque, (e) normalized diaphragm rotation, (f) normalized ROT for each design and hazard level.

4.4.3 Eccentric - horizontally regular four-story building - with more realistic plan view

The ninth numerical example considered in this study is shown in Fig. 4.53. It is a regular building with more realistic plan layout, and exhibits a similar trend for the

response quantities to the previous test examples examined, for eccentricity values equal to 5% and 10% (see Figs. 4.54 and 4.55 for the y direction). Similar trend was observed for the response quantities along x direction. As it is shown in Fig. 4.56, the maximum values of base torque and ROT are increased significantly, while the maximum diaphragm rotation developed is slightly decreased in comparison to those obtained for second test example.

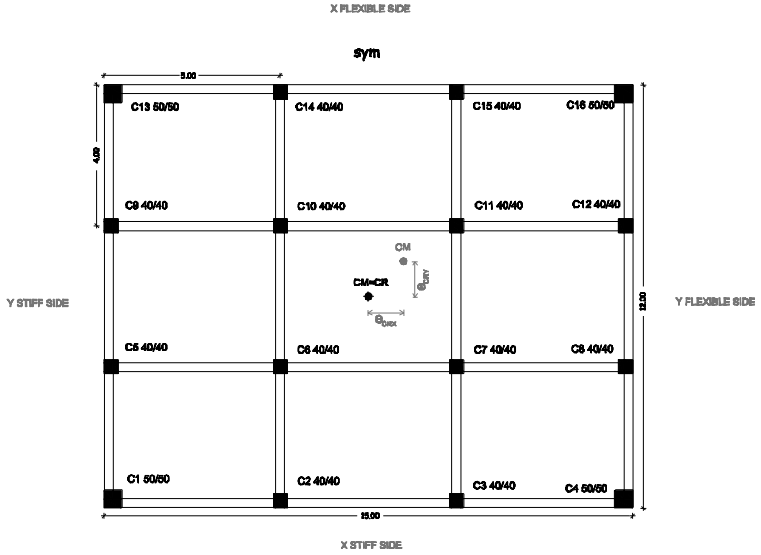

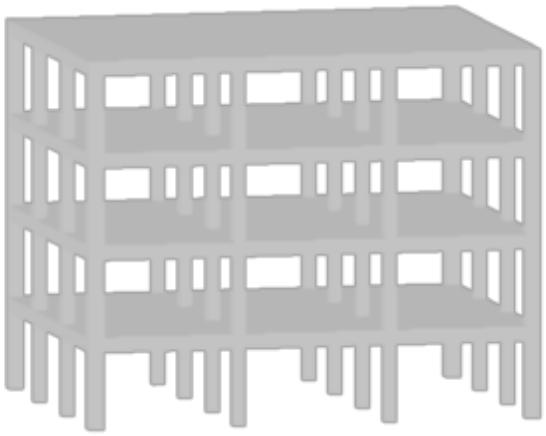

Figure 4.53. Numerical Example 9 - plan and 3D view.

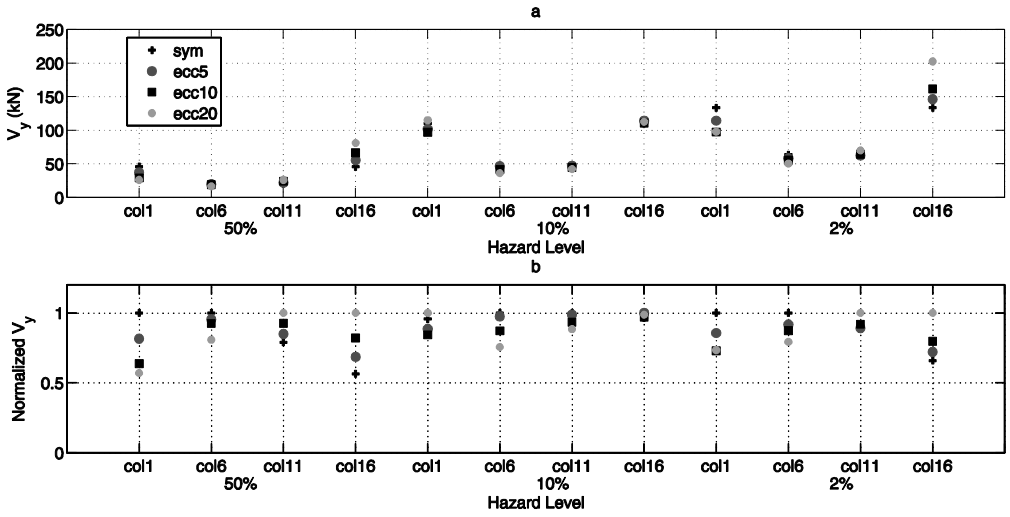

Figure 4.54. Numerical Example 9 - Peak edge column shear forces (a) maximum absolute values and (b) normalized values along y direction for each design and hazard level.

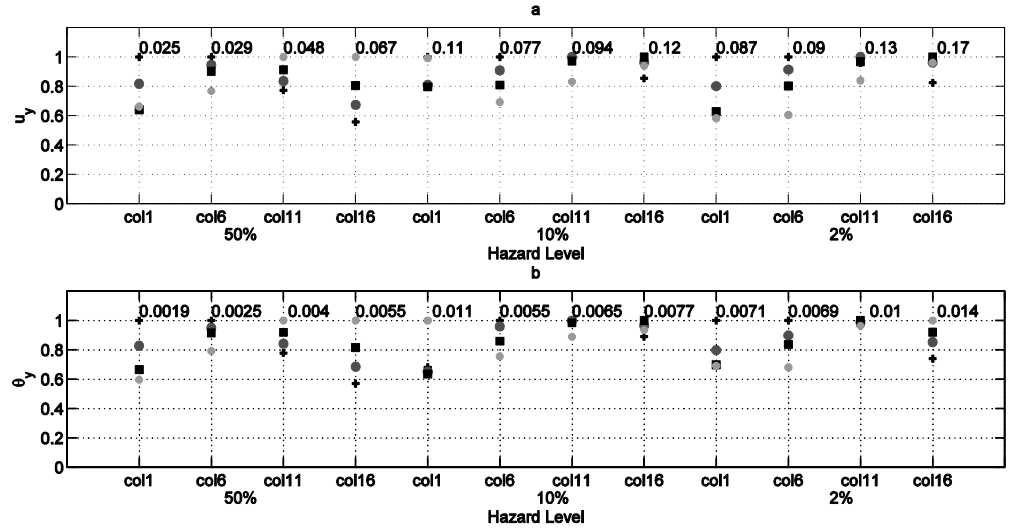

Figure 4.55. Numerical Example 9 - Peak edge column (a) normalized displacement values (in m) and (b) normalized interstory drift values (%) along y direction for each design and hazard level.

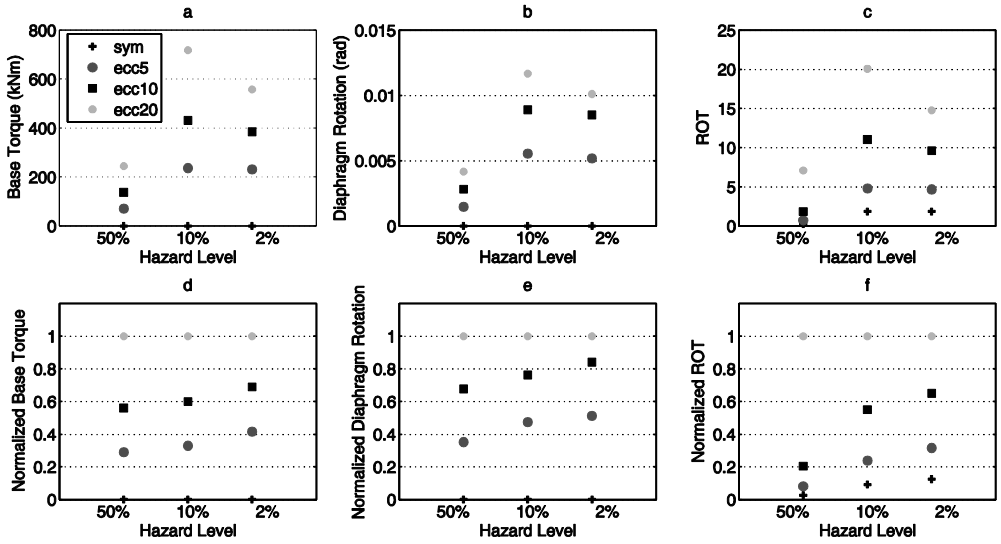

Figure 4.56. Numerical Example 9 - (a) Base torque, (b) diaphragm rotation, (c) ROT , (d) normalized base torque, (e) normalized diaphragm rotation, (f) normalized ROT for each design and hazard level.

4.4.4 Horizontally irregular four-story building

The last numerical example examined in this study is the horizontally irregular building with bidirectional eccentricity shown in Fig. 4.57 subjected to two-component seismic excitation.

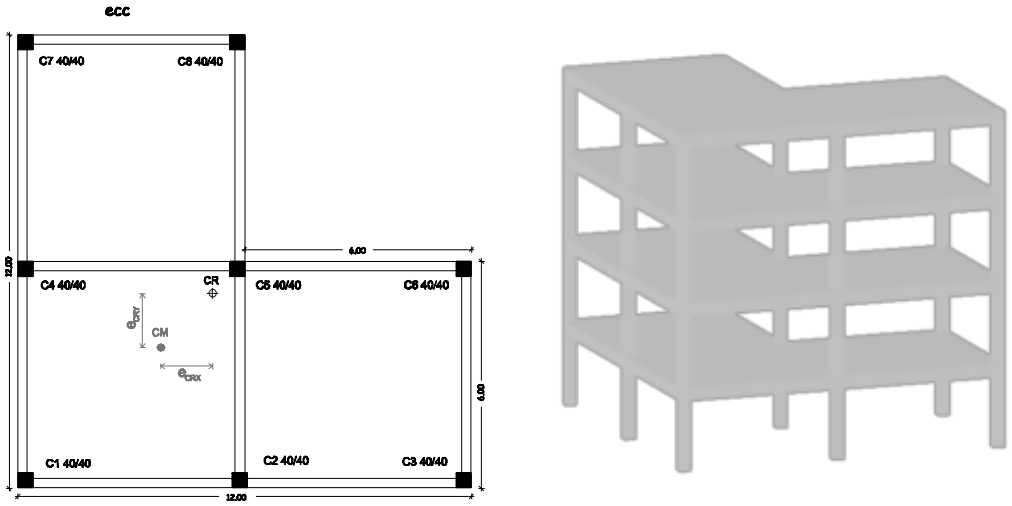

Figure 4.57. Numerical Example 10 - plan and 3D view.

Due to its irregular layout, it was not possible to define the symmetric design that complies with the restrictions imposed by the design codes [30]. This reference

design exhibit static eccentricity of 0.4% and is denoted as *ecc*. Similar to the previous test examples, the non-symmetric designs considered exhibit the same eccentricity (i.e. 5%, 10% and 20%).

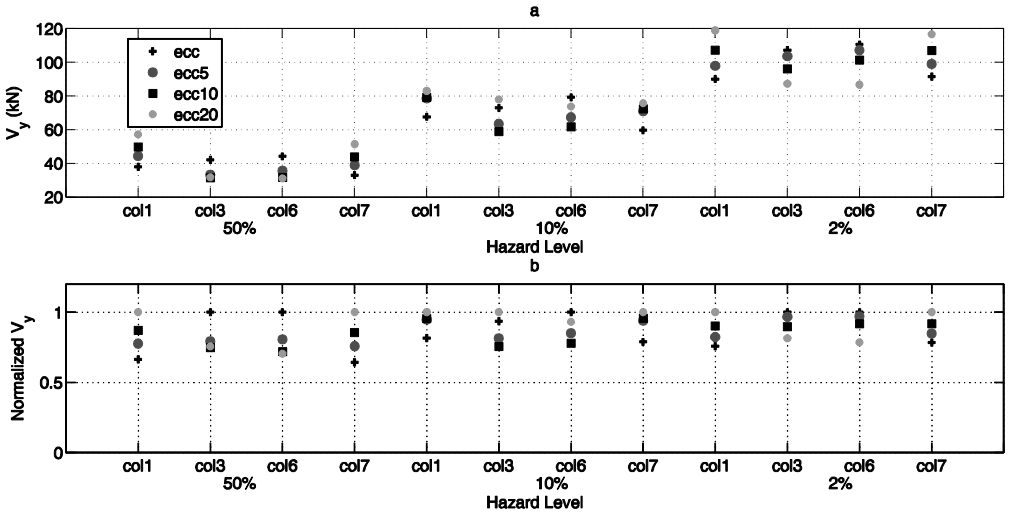

Figure 4.58. Numerical Example 10 - Peak edge column shear forces (a) maximum absolute values and (b) normalized values along y direction for each design and hazard level.

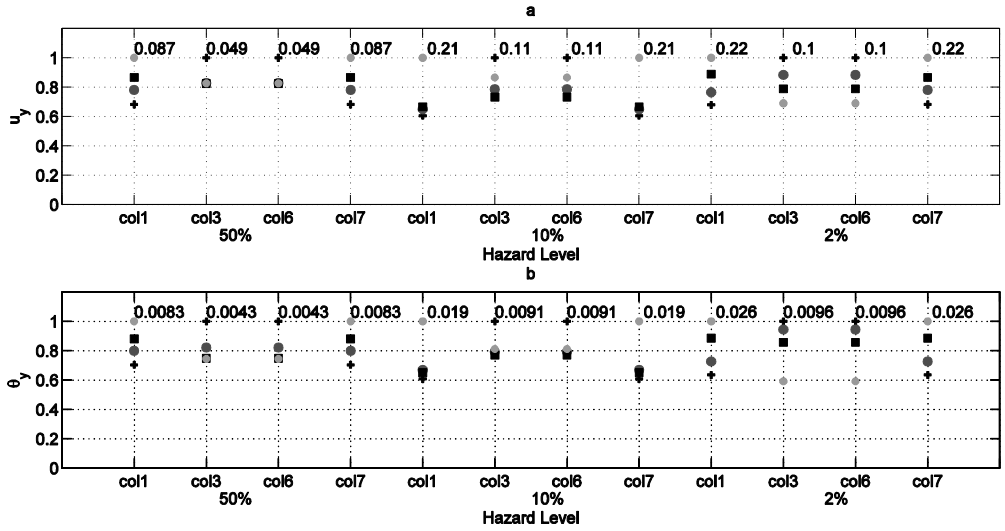

Figure 4.59. Numerical Example 10 - Peak edge column (a) normalized displacement values (in m) and (b) normalized interstory drift values (%) along y direction for each design and hazard level.

The response quantities studied (shear forces, displacements and interstory drifts) will be presented along y direction. Similar results are obtained in x direction. As can be seen in Figures 4.58 and 4.59 the response quantities for

elements at the flexible edge (i.e. col1 and col7) are increased while for those at stiff edge (col3, col6) are decreased proportionally to the increase of the eccentricity (5% to 10%).

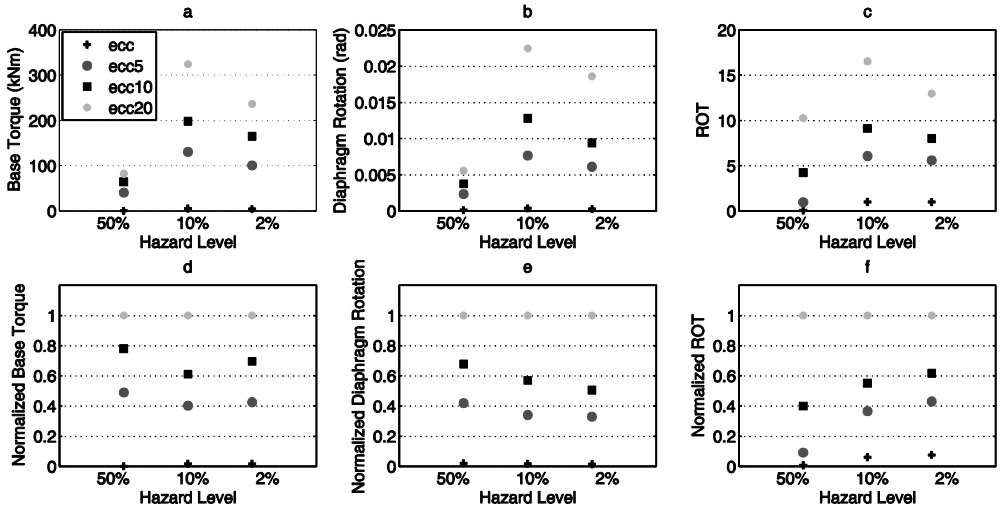

Figure 4.60. Numerical Example 10 - (a) Base torque, (b) diaphragm rotation, (c) ROT, (d) normalized base torque, (e) normalized diaphragm rotation, (f) normalized ROT for each design and hazard level.

For *ecc* design almost zero base torque, upper diaphragm's rotation and *ROT* values are obtained for the elastic state of response (i.e. for the 50/50 hazard level). For the non-symmetric designs, the corresponding values are increased proportionally to the increase of the eccentricity. This trend is observed for the other two hazard levels indicating *ROT* as a proper criterion for all states of response. Non-zero *ROT* values are obtained for *ecc* design for the 10/50 and 2/50 hazard levels due to asymmetric yielding which affects the location of rigidity center, while the eccentricity is increased (see Fig. 4.60(c)).

Two columns (col6 and col7) are chosen as before in order to present the variation on the envelopes of the maximum values along the height for all designs. Both columns are located at the stiff edge along the x direction, while column 6 is located at the stiff side and column 7 at the flexible side along the y direction. The response quantities are decreased for all stories when the building performs in the elastic region, while in the elastoplastic region some response quantities are increased (see Figs. 4.61 to 4.66). Along the y direction the response quantities of

column 6 are decreased proportionally to the increase of eccentricity (5% and 10%), while they are increased for column 7 in both elastic and elastoplastic range.

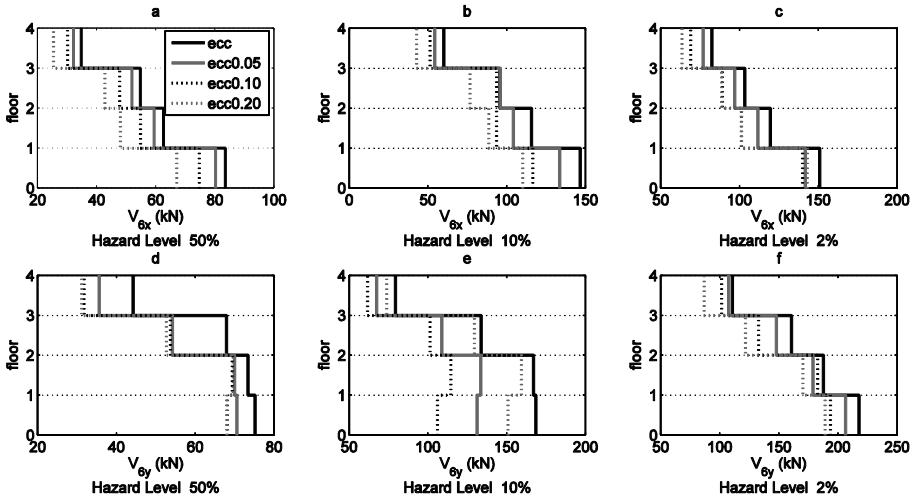

Figure 4.61. Numerical Example 10 - Column 6 maximum absolute shear force values along x (a, b, c) and y (d, e, f) direction for all floors and hazard levels.

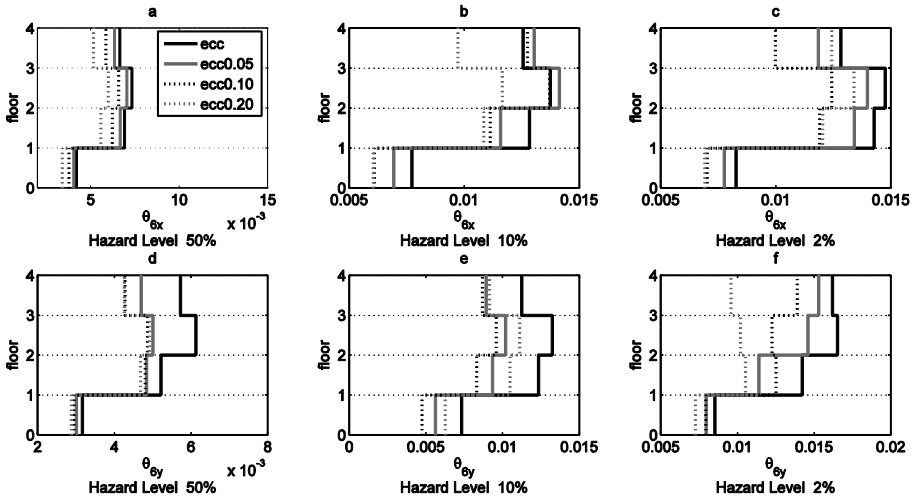

Figure 4.62. Numerical Example 10 - Column 6 maximum absolute drift values along x (a, b, c) and y (d, e, f) direction for all floors and hazard levels.

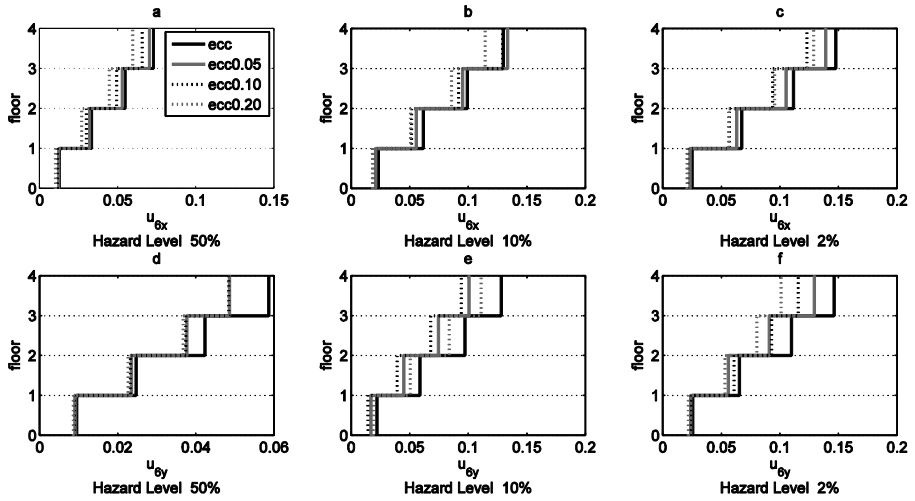

Figure 4.63. Numerical Example 10 - Column 6 maximum absolute displacement values along x (a, b, c) and y (d, e, f) direction for all floors and hazard levels.

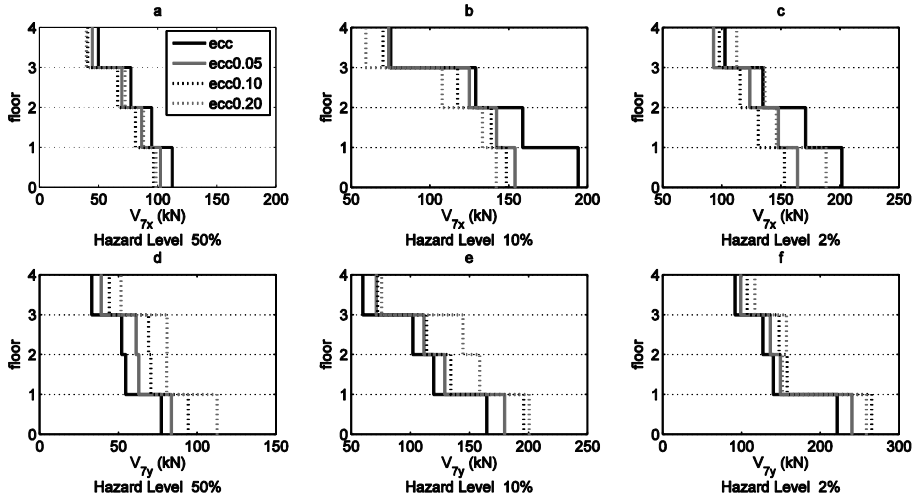

Figure 4.64. Numerical Example 10 - Column 7 maximum absolute shear force values along x (a, b, c) and y (d, e, f) direction for all floors and hazard levels.

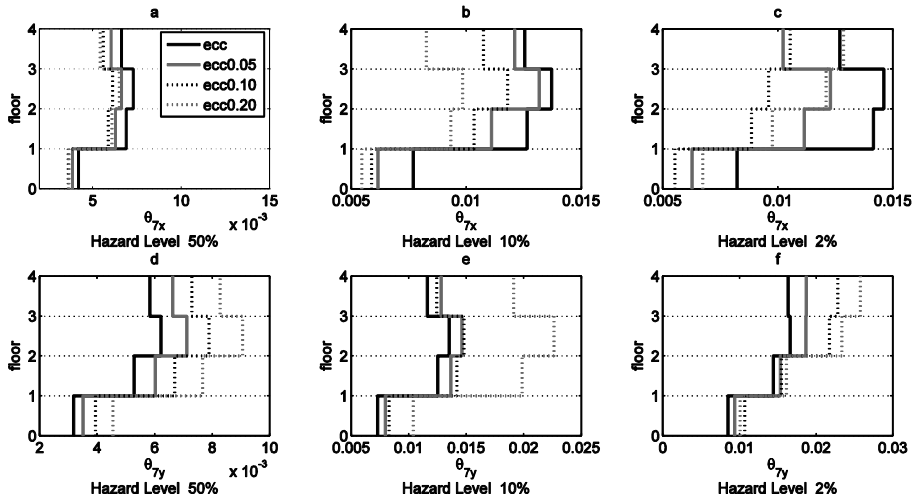

Figure 4.65. Numerical Example 10 - Column 7 maximum absolute drift values along x (a, b, c) and y (d, e, f) direction for all floors and hazard levels.

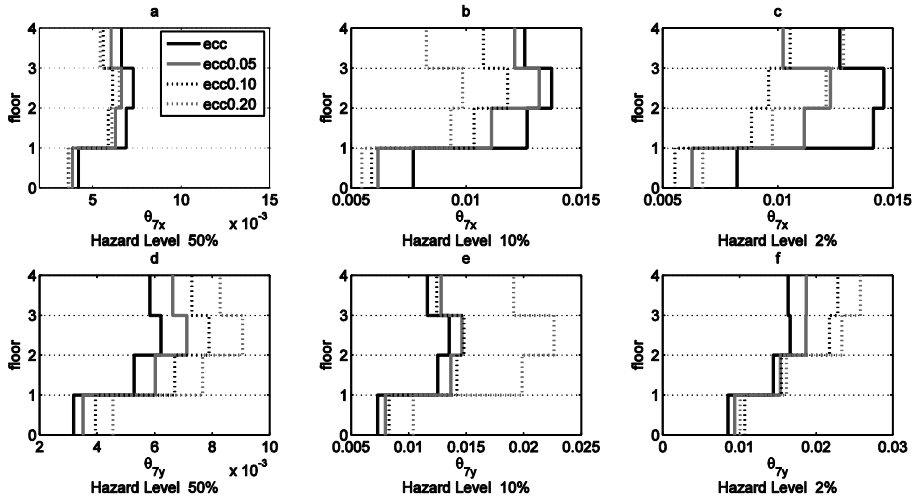

Figure 4.66. Numerical Example 10 - Column 7 maximum absolute displacement values along x (a, b, c) and y (d, e, f) direction for all floors and hazard levels.

4.5 Discussion

In the current chapter, the ratio of torsion (*ROT*) index as performance assessment criterion of buildings was evaluated. For this purpose, several regular and irregular, single-story as well as multistory buildings were considered. Unidirectional and bidirectional seismic excitations were imposed to monosymmetric and double eccentric buildings. Nonlinear dynamic analysis was conducted

implementing natural accelerograms for all hazard levels. The maximum value of various response quantities, such as interstory drifts, displacements, shear forces, were examined. The base torque and the upper diaphragm's rotation were also recorded for every numerical application. The structures were classified in terms of their torsional stiffness according to uncoupled torsional to translational frequency ratios. The characteristic of response quantities increase with respect to eccentricity for elements at the flexible side of the structure, while the same quantities are decreased with respect to eccentricity for elements at the stiff side. In order to examine the behavior for multistory buildings vertical structural elements were chosen at the stiff and flexible side of horizontally regular and irregular buildings and their reponse quantities along the height were recorded. The observed behavior for torsionally stiff structures was confirmed for all stories. In cases of monosymmetric structures subjected to unidirectional earthquake excitation, it was observed that despite the fact that no excitation was imposed along x direction shear forces were developed and their magnitude increased proportionally to eccentricity. The base torque, the upper diaphragm's rotation and *ROT* are also increasing with respect to eccentricity for all hazard levels. While base torque and *ROT* follow the same trend for different hazard levels, upper diaphragm's rotation does not follow for all cases. The advantage of *ROT* in comparison with the other two response quantities related to torsion is that it quantifies the torsional effect in terms of shear forces, expressing the percentage of shear forces' amplification normalized to the imposed base shear.

REFERENCES:

[1] Jeong, S.-H., Elnashai, A.S., Analytical assessment of an irregular RC frame for full-scale 3D pseudo-dynamic testing part I: Analytical model verification, *Journal of Earthquake Engineering 2005;* **9**(1): 95-128.

[2] Chandler, A.M., Duan, X.N., Rutenberg, A., Seismic torsional response: assumptions, controversies and research progress, *European Earthquake Engineering* 1996; **10**(1): 37-51.

[3] De La Colina, J., Effects of torsion factors on simple non-linear systems using fully bidirectional analyses, *Earthquake Engineering and Structural Dynamics* 1999; **28**:691-706.

[4] Humar, J., Kumar, P., A new look at torsion design provisions in seismic building codes,*12th World Conference on Earthquake Engineering* 1998; id.1707.

[5] Chandler, A.M., Duan, X.N., Performance of asymmetric code-designed buildings for serviceability and ultimate limit states, *Earthquake Engineering and Structural Dynamics* 1997; **26**(7):717-736.

[6] Chopra, A.K., Goel, R.K., Evaluation of torsional provisions in seismic codes, *Journal of Structural Engineering* 1991; **117**(12):3762-3782.

[7] Rutenberg, A., EAEE Task Group (TG) 8: Behaviour of irregular and complex structures-progress since 1998, *Proceedings of the 12th European Conference in Earthquake Engineering* London. Elsevier: Oxford 2002, Paper no.832.

[8] Cheung, V.W.-T., Tso, W.K., Eccentricity in irregular multistory buildings, *Canadian Journal of Civil Engineering* 1986; **13**(1):46-52.

[9] Tso, W.K., Static eccentricity concept for torsional moments estimations, *Journal of Structural Engineering* 1990; **116**(5):1199-1212.

[10] Smith, B.S., Vezina, S., Evaluation of centers of resistance in multistorey building structures, *Proceedings Of Institution Of Civil Engineers* 1985; Part 2, Institution of Civil Engineers, **79**(4):623-635.

[11] Riddel, R., Vasquez, J., Existence of centres of resistance and torsional uncoupling of earthquake response of buildings, *Proceedings of 8thWorld Conference on Earthquake Engineering* 1984; **4**:187-194.

[12] Lagaros, N.D., Papadrakakis, M., Bakas, N., Automatic minimization of the rigidity eccentricity of 3D reinforced concrete buildings, *Journal of Earthquake Engineering* 2006; **10**(3):1-32.

[13] Stathopoulos, K.G., Anagnostopoulos, S.A., Inelastic earthquake response of single-story asymmetric buildings: an assessment of simplified shear-beam models, *Earthquake Engineering and Structural Dynamics* 2003; **32**:1813-1831.

[14] Peruš, I., Fajfar, P., On the inelastic torsional response of single-storey structures under bi-axial excitation, *Earthquake Engineering and Structural Dynamics* 2005; **34**:931-941.

[15] Lucchini, A., Monti, G., Kunnath, S., Seismic behavior of single-storey asymmetric-plan buildings under uniaxial excitation, *Earthquake Engineering and Structural Dynamics* 2009; **38**:1053-1070.

[16] De La Llera, J.C., Chopra, A.K., Understanding the inelastic seismic behaviour of asymmetric plan buildings, *Earthquake Engineering and Structural Dynamics* 1995; **24**:549-572.

[17] De La Llera, J.C., Chopra, A.K., A simplified model for analysis and design of asymmetric plan buildings, *Earthquake Engineering and Structural Dynamics* 1995; **24**:573-594.

[18] Paulay, T., Torsional mechanisms in ductile building systems, *Earthquake Engineering and Structural Dynamics* 1998; **27**:1101-1121.

[19] Paulay, T., Displacement-based design approach to earthquake induced torsion in ductile buildings, *Engineering Structures* 1997; **9**(9):699-707.

[20] Myslimaj, B., Tso, W.K., A strength distribution criterion for minimizing torsional response of asymmetric wall-type systems, *Earthquake Engineering and Structural Dynamics* 2002; **31**:99-120.

[21] Myslimaj, B., Tso, W.K., A Design-oriented approach to strength distribution in single-story asymmetric systems with elements having strength dependent stiffness, *Earthquake Spectra* 2005; **21**:197-212.

[22] Anagnostopoulos, S.A., Alexopoulou, Ch., Stathopoulos, K.G., An answer to an important controversy and the need for caution when using simple models to predict

inelastic earthquake response of buildings with torsion, *Earthquake Engineering and Structural Dynamics* 2010; **39**:521-540.

[23] Stathi, C., Bakas, N., Lagaros, N.D., Papadrakakis, M., Ratio of torsion (ROT): An index for assessing the torsional effect on structural behavior, Earthquakes & Structures, Earthquakes and Structures, 2014.

[24] Fragiadakis, M., Papadrakakis, M., Modelling, analysis and reliability of seismically excited structures: Computational issues, *International Journal of Computational Methods* 2008; **5**(4):483-511.

[25] McKenna, F., Fenves, G.L., TheOpenSees Command Language Manual – Version 1.2. Pacific Earthquake Engineering Research Center, University of California, Berkeley, 2001.

[26] Kent, D.C., Park, R., Flexural members with confined concrete, *Journal of Structural Division* 1971; **97**(7):1969 – 1990.

[27] Scott, B.D., Park, R., Priestley, M.J.N., Stress – Strain behavior of concrete confined by overlapping hoops at low and high strain rates, *ACI Journal* 1982; **79**:13 – 27.

[28] Somerville, P., Collins, N., Ground motion time histories for the Humboldt bay bridge, Pasadena, CA, URS Corporation, www.peertestbeds.net/humboldt.htm, 2002.

[29] Papazachos, B.C., Papaioannou, Ch.A., Theodulidis, N.P., Regionalization of seismic hazard in Greece based on seismic sources, *Natural Hazards* 1993; **8**(1):1-18.

[30] EC8-Eurocode 8. Design provisions for earthquake resistance of structures. European Standard EN1998-1:2004.

5 OPTIMIZATION PROCESS

5.1 Introduction

The word “optimum” is latin, and means “the ultimate ideal”. Similarly, “optimus” means “the best”. Therefore, to optimize refers to try to bring something towards its ultimate state.

The history of optimization, that is the quest for finding extreme behavior of a system, dates several hundreds of years during which remarkable progress has been made in developing new and more efficient methods. Euclid (300B.C.) tackled the problem of finding the shortest distance which may be drawn from a point to a line [1], while Heron of Alexandria (100B.C.) studied the optimization problem of light travelling between two points by the shortest path [1]. Fermat (1657) developed the more general principle that light travels between two points in a minimum time [2], while Cauchy (1847) presented for the first time a minimization algorithm (steepest descent method) implementing function derivatives [3]. The development of calculus provided the means for the development of the mathematical theory for optimization. The pioneering works of Courant (1943) on penalty functions [4], Dantzig (1951) on linear programming [5], Karush (1939) as well as Kuhn and Tucker

(1951) on optimality conditions for constrained problems [6], [7] initiated the modern era of optimization.

Particularly in the 60's, several optimization methods for solving nonlinear problems were introduced. Rosenbrock (1960) presented the method of orthogonal directions [8], Rosen (1960) suggested the gradient projection method [9], Zoutendijk (1960) formed the feasible directions method [10], Hooke and Jeeves (1961) developed the pattern search method [11], Davidon, Fletcher and Powell (1963) stated the variable metric method [12], Fletcher and Reeves (1964) presented the conjugate gradient method [13], Powell (1964) introduced the method of conjugate directions [14], Nelder-Mead (1965) suggested their simplex method [15], Box (1965) introduced his homonymous technique [16], while Fiacco and McCormick (1966) formed the so called Sequential Unconstrained Minimization Technique (SUMT) [17].

Since 1970 structural optimization has been the subject of intensive research and several different approaches for optimal design of structures have been advocated [18-24]. All the aforementioned methods are of deterministic character; that is, when applied to the same initial design vector, they always result in the same final design vector. The reason for this is the fact that the element of randomness is non-existent. As a result, there is appreciable probability of getting trapped in local minima. Mathematical programming methods make use of local curvature information derived from linearization of the original functions by using their derivatives with respect to the design variables at points obtained in the process of optimization to construct an approximate model of the initial problem. On the other hand the application of combinatorial optimization methods based on probabilistic searching do not need gradient information and therefore avoid to perform the computationally expensive sensitivity analysis step. Gradient-based methods present a satisfactory local rate of convergence, but they cannot assure that the global optimum can be found, while combinatorial optimization techniques, are in general more robust and present a better global behavior than the mathematical programming methods. They may suffer, however, from a slow rate of convergence towards the global optimum.

In contrast to the deterministic optimization methods, the stochastic optimization procedures allow for randomness to appear. In this way, it is possible to get different final design vectors, even though the initial vector is the same. In this category, the most known and widely applied methods are the genetic algorithms (GA), originating from Holland (1975) [25] and Goldberg (1989) [26], the simulated annealing (SA) by Kirkpatrick (1983) [27], evolutionary programming (EP) [28], and the evolutionary strategies (ES) [29], [30], which are used in the present study. The main characteristic of these methods is the wider exploration and exploitation of the domain, which in turn increases both the probability of locating the global minimum and the computational cost. Both GA and ES imitate biological evolution and combine the concept of artificial survival of the fittest with evolutionary operators to form a robust search mechanism. Apart from the pure deterministic or pure stochastic procedure, hybrid schemes have been introduced as well. The main idea behind the hybridism is to combine the advantages of both methods for a better result to be obtained [31], [32].

5.2 Structural optimization problem

The main objective of engineers is to design resistant structures, which satisfy all the constraints (defined by codes) and also acquire specific attributes (low cost, low weight, small displacements are some of them). This can be accomplished by the optimization process through a trial and error procedure, a computationally intensive task. Thanks to developments in Computational Mechanics community the solution of this problem is feasible using evolutionary algorithms inspired by Darwinian evolution, this procedure is an imitation of it.

Structural optimization problems are characterized by various objective and constraint functions that are generally non-linear functions of the design variables. These functions are usually implicit, discontinuous and non-convex. The mathematical formulation of structural optimization problems with respect to the design variables, the objective and constraint functions depend on the type of the application. However, all optimization problems can be expressed in standard

mathematical terms as a non-linear programming problem (NLP), which in general form can be stated as follows:

$$\min F(s) \tag{5.1}$$

$$\text{subject to } g_j(s) \le 0 \quad j = 1,....,m$$

$$s_i^l \le s_i \le s_i^u \quad i = 1,...,n$$

where s is the vector of design variables, $F(s)$ is the objective function to be minimized, $g_j(s)$ are the behavioral constraints, s_i^l and s_i^u are the lower and the upper bounds on a typical design variable s_i .

5.2.1 Definitions

5.2.1.1 Design Variables

Design variables are the parameters, which when they are fully set the design is determined. A design is characterized as infeasible when it violates the constraints of the problem. In the opposite case the design is feasible. The selection of the appropriate design variables is a crucial step for the formulation of the optimization problem. The selection of inappropriate design variables may result to wrong formulation of the problem or even mislead the solution away from the optimum design. Another important issue is the relative independence of design variables. In cases that a design variable is dependent on another one, it stops representing a design variable and become a parameter.

During the formulation of the mathematical optimization model the function to be optimized should be sufficiently dependent on all the design parameters. Let us consider the case that the objective function is the weight of the structure, where the minimum value is obtained and let assume that the magnitude of the weight is at the order of 1.000 kg. If the weight of a structural member is in the order of 10^{-3} kg or less and let us consider that this member represents one of the design variables of the problem, then if the value is changed by 100% the influence on the value of the objective function is negligible. To avoid such conditions, it is necessary that linkage

between the design variables is imposed. Therefore, some members of the structures can be represented by a common design parameter. Therefore, it is recommended to conduct a sensitivity analysis in order to estimate the sensitivity of the objective function over all the design parameters before the final choice of the optimization model. Through the sensitivity analysis it is possible to detect design parameters that have negligible influence on the objective function.

5.2.1.2 Objective function

In order to describe an optimization problem, a large number of feasible designs are implemented. But not all of them exhibit the same performance. A criterion should be adopted so as to evaluate the performance of the various designs. A function that takes a specific value represents that criterion and constitutes the **objective function** of the problem depending on the design variables. A maximizing problem of the function $F(\boldsymbol{s})$ can be transformed into a minimization problem of the objective function $-F(\boldsymbol{s})$.

The appropriate selection of the objective function is of crucial importance at the state of the mathematical formulation of the optimization problem. Some of the most widespread objective function in the literature to be optimized are: the cost, the profit, the energy losses, the weight or generally the performance. There are also cases that more than one objective functions are necessary, e.g. minimum weight and minimum stresses. These type of problems are called optimization problems with multiple objective functions, the multi-objective design or Pareto optimum design problem.

5.2.1.3 Constraint functions

A structural system is defined on condition that the values of its design variables should be fully set. In order to avoid designs that do not make sense, engineers' requirements are introduced in the mathematical formulation of the optimization problem in the form of equalities or inequalities and are called **constraint functions**. Based on these constraint functions, the designs are classified as feasible or

infeasible. Moreover, constraint functions should be dependent on at least one design variable so as its existence in the mathematical model make sense.

One inequality constraint function $g_j(\boldsymbol{s}) \le 0$ is considered as active at the point $\boldsymbol{s}^*$ in the case that the equality is satisfied, i.e. $g_j(\boldsymbol{s}^*) = 0$. Accordingly, the above constraint function is considered as inactive for the design $\boldsymbol{s}^*$ for the case that the inequality is strictly satisfied, i.e. $g_j(\boldsymbol{s}^*) < 0$. The inequality constraint function is considered that it is violated for the design $\boldsymbol{s}^*$ if a positive value that $g_j(\boldsymbol{s}^*) > 0$, corresponds to the value of the constraint function. Similarly, an equality constraint function $h_j(\boldsymbol{s}) = 0$ is considered that it is violated for the design $\boldsymbol{s}^*$ if the equality is not satisfied, i.e. $h_j(\boldsymbol{s}^*) \ne 0$. Therefore, an equality constraint function might be active or violated. From all the description provided related to the active or the inactive constraint functions it is clear that any feasible design is defined by active or inactive inequality constraint functions and active equality constraint functions.

In order to identify the active constraint functions the values of the constraint functions should be normalized first [33] to have a single reference system regardless of the type of the constraint function. For example, it is likely that the value of a displacement constraint function to take values in the order of 0.1-2.0 cm, while the value of a stress displacement constraint function to take values is in the order of 25,000 kPa, so readily it is apparent that it is necessary to homogenize the sizes of the two constraint functions. The normalization of the value constraint functions takes place in accordance with the following relations:

$$g_j^N(\boldsymbol{s}) = \frac{g_j^l - g_j}{\left|g_j^l\right|} \tag{5.2}$$

for a constraint function limited with a lower bound, $g_j \ge g_j^l$, and:

$$g_j^N(s) = \frac{g_j - g_j^u}{\left|g_j^u\right|} \le 0 \tag{5.3}$$

for a constraint function limited with an upper bound, $g_j \le g_j^u$.

Thus, if the normalized value of the constraint function is equal to +0.50 then it violates its permissible value by 50%, while if its normalized value is equal to -0.50 then this constraint is 50% below the allowable value. Usually among the active constraint functions are included those with normalized value greater than -0.1 to -0.01 [34]. Furthermore, it is also allowed a small tolerance when the constraint functions violate the minimum allowable value (-0.005 to 0.001) since the process of simulation, analysis, design and construction involves many uncertainties.

5.3 Classes of optimization

There are mainly three classes of structural optimization problems: sizing, shape and topology or layout. Initially structural optimization was focused on sizing optimization, such as optimizing cross sectional areas of truss and frame structures, or the thickness of plates and shells. The next step was to consider finding optimum boundaries of a structure, and therefore to optimize its shape. In the former case the structural domain is fixed, while in the latter case it is not fixed but it has a predefined topology. In both cases a non-optimal starting topology can lead to sub-optimal results. To overcome this deficiency structural topology optimization needs to be employed, which allows the designer to optimize the layout or the topology of a structure by detecting and removing the low-stressed material in the structure which is not used effectively.

5.3.1 Sizing Optimization

In sizing optimization problems the aim is usually to minimize the weight of the structure under certain behavioral constraints on stresses and displacements. The design variables are most frequently chosen to be dimensions of the cross-sectional areas of the members of the structure. Due to engineering practice demands the members are divided into groups having the same design variables. This linking of elements results in a trade-off between the use of more material and the need of symmetry and uniformity of structures due to practical considerations. Furthermore,

it has to be taken into account that due to fabrication limitations the design variables are not continuous but discrete since cross-sections belong to a certain set.

The sizing optimization methodology proceeds with the following steps: (i) At the outset of the optimization the geometry, the boundaries and the loads of the structure under investigation have to be defined. (ii) The design variables, which may or may not be independent to each other, are also properly selected. Furthermore, the constraints are also defined in this stage in order to formulate the optimization problem as in eq. (5.1). (iii) A finite element analysis, is then carried out and the displacements and stresses are evaluated. (iv) If a gradient-based optimizer is used then the sensitivities of the constraints and the objective function to small changes of the design variables are computed. (v) The design variables are being optimized. If the convergence criteria for the optimization algorithm are satisfied, then the optimum solution has been found and the process is terminated, else the optimizer updates the design variable values and the whole process is repeated from step (iii).

5.3.2 Shape Optimization

In structural shape optimization problems the aim is to improve the performance of the structure by modifying its boundaries. This can be numerically achieved by minimizing an objective function subjected to certain constraints [35], [36]. All functions are related to the design variables, which are some of the coordinates of the key points in the boundary of the structure. Hinton and Sienz [35] proposed a shape optimization approach for treating two-dimensional problems. More specifically the shape optimization methodology proceeds with the following steps: (i) At the outset of the optimization, the geometry of the structure under investigation has to be defined. The boundaries of the structure are modeled using cubic B-splines that, in turn, are defined by a set of key points. Some of the coordinates of these key points will be the design variables which may or may not be independent to each other. (ii) An automatic mesh generator is used to create a valid and complete finite element model. A finite element analysis is then carried out and the displacements and stresses are evaluated. In order to increase the accuracy of the analysis an h-type adaptivity analysis may be incorporated in this stage. (iii) If a

gradient-based optimizer is used then the sensitivities of the constraints and the objective function to small changes of the design variables are computed either with the finite difference, or with the semi-analytical method. (iv) The optimization problem is solved; the design variables are being optimized and the new shape of the structure is defined. If the convergence criteria for the optimization algorithm are satisfied, then the optimum solution has been found and the process is terminated, else a new geometry is defined and the whole process is repeated from step (ii).

5.3.3 Topology Optimization

Structural topology optimization assists the designer to define the type of structure, which is best suited to satisfy the operating conditions for the problem in question. It can be seen as a procedure of optimizing the rational arrangement of the available material in the design space and eliminating the material that is not needed. Topology optimization is usually employed in order to achieve an acceptable initial layout of the structure, which is then refined with a shape optimization tool. The topology optimization procedure proceeds step-by-step with a gradual "removal" of small portions of low stressed material, which are being used inefficiently. This approach is treated in this study as a typical case of a structural reanalysis problem with small variations of the stiffness matrix between two subsequent optimization steps.

Many researchers have presented solutions for structural topology optimization problems. Topological or layout optimization can be undertaken by implementing one of the following main approaches, which have evolved during the last few years [37]: (i) Ground structure approach [38], [39], (ii) homogenization method [40], [41], [42], (iii) bubble method [43] and (iv) fully stressed design technique [44], [45]. The first three approaches have several things in common. They are optimization techniques with an objective function, design variables, constraints and they solve the optimization problem by using an algorithm based on sequential quadratic programming (approach (i)), or on an optimality criterion concept (approaches (ii) and (iii)). However, inherently linked with the solution of the optimization problem is the complexity of these approaches. The fully stressed design technique on the other

hand, although not an optimization algorithm in the conventional sense, proceeds by removing inefficient material, and therefore optimizes the use of the remaining material in the structure, in an evolutionary process.

At present only a limited number of studies is devoted to 3-D optimal topology design of structures. For this type of problems the main difficulty when a homogenization method is used is the orientation of the material voids which is more complicated than in the 2-D case. This difficulty is not present in the case of the fully stressed design technique. Hinton and Sienz [37] proposed the implementation of the evolutionary fully stressed design technique (FSD), while Papadrakakis *et al.* [46] presented the improved implementation for 2-D topology optimization problems.

The algorithm for topology optimization adopted in this study is based on the simple principle that material which has small stress levels is used inefficiently and therefore it can be removed. Thus, by removing small amounts of material at each optimization step the layout of the structure evolves gradually. In order to achieve convergence of the whole optimization procedure, it is important the amount of material removed at each stage to be small and to maintain a smooth transition from one layout of the structure to the subsequent one.

The domain of the structure, which is called the reference domain, can be divided into the design domain and the non-design domain. The non-design domain covers regions with stress concentrations, such as supports and areas where loads are applied, and therefore it cannot be modified throughout the whole topology optimization process. After the generation of the finite element mesh, the evolutionary fully stressed design cycle is activated, where a linear elastic finite element analysis is carried out. The maximum principal stress σ_{pr} for each element can be computed which for convenience is called stress level and is denoted as σ_{evo} σ_{evo}. The maximum stress level $\sigma_{\max}$ of the elements in the structure at the current optimization step is defined, and all elements that fulfill the condition

$$\sigma_{evo} < ratre \times \sigma_{\max} \tag{5.4}$$

are removed, or *switched-off,* where *ratre* is the rejection rate parameter [47]. The elements are removed by assigning them a relatively small elastic modulus which is typically

$$E_{off} = 10^{-5} \times E_{on} \tag{5.5}$$

In this way the elements switched-off virtually do not carry any load and their stress levels are accordingly small in subsequent analyses. This strategy is called "hard kill", since the low stressed elements are immediately removed, in contrast with the "soft kill" method where the elastic modulus varies linearly and the elements are removed more gradually. The remaining elements are considered *active* and they are sorted in ascending order according to their stress levels before a subsequent analysis is performed.

The iterative process of element removal and addition, if element growth is allowed, is continued until one of several specified convergence criteria are met: (i) All stress levels are larger than a certain percentage value of the maximum stress. This criterion assumes that a fully stressed design has been achieved and the material is used efficiently. (ii) The number of active elements is smaller than a specified percentage of the total number of elements. For uniform meshes, which are commonly used in topology optimization problems, this criterion is equivalent to an area or volume fraction of the initial design, which will be in use in the final layout. (iii) When element growth is allowed the evolutionary process is completed when more elements are switched-on than they are switched-off.

5.4 Evolutionary Algorithms

5.4.1 Introduction

The two most widely used optimization algorithms belonging to the class of evolutionary algorithms (EA) that imitate nature by using biological methodologies are the genetic algorithms (GA) and evolution strategies (ES). In this work the ES method is used as the optimization tool for addressing the present problem, based

on previous experience regarding the relative superiority of ES over the MP and GA methods in some specific problems [31], [32]. ES imitate biological evolution in nature and have three characteristics that make them differ from the gradient based optimization algorithms: (i) in place of the usual deterministic operators, they use randomized operators: recombination, mutation, selection; (ii) instead of a single design point, they work simultaneously with a population of design points; (iii) they can handle continuous, discrete and mixed optimization problems [46]. In the ES algorithm, each individual is equipped with a set of parameters:

$$a = [(s_d, \gamma), (s_c, \sigma, \alpha)] \in (I_d, I_c) \tag{5.6}$$

$$I_d = D^{n_d} \times R_+^{n_\gamma}$$

$$I_c = R^{n_c} \times R_+^{n_\sigma} \times [-\pi, \pi]^{n_\alpha}$$

where s_d and s_c are the vectors of discrete and continuous design variables, respectively. Vectors γ, σ and α are the distribution parameter vectors. Vector γ corresponds to the variances of the Poisson distribution, vector $\sigma \in R_+^{n_\sigma}$ corresponds to the standard deviations $(I \le n_\sigma \le n_c)$ of the normal distribution while vector $a \in [-\pi, \pi]^{n_\alpha}$ corresponds to the inclination angles $(n_a = (n_C - n_\sigma / 2)(n_\sigma - I))$ defining linearly correlated mutations of the continuous design variables s_c.

Let $P_p^{(t)} = \{a_1, ..., \alpha_\mu\}$ denotes a parent population of individuals at the t^{th} generation. The genetic operators used in the ES method are denoted by the following mappings:

$$rec : (I_d, I_c)^\mu \to (I_d, I_c)^\lambda \ (recombination) \tag{5.7}$$

$$mut : (I_d, I_c)^\lambda \to (I_d, I_c)^\lambda \ (mutation) \tag{5.8}$$

$$sel_\mu^k : (I_d, I_c)^k \to (I_d, I_c)^\mu \ (selection, k \in \{\lambda, \mu + \lambda\}) \tag{5.9}$$

A single iteration of the ES, which is a step from the parent population $P_p^{(t)}$ to the next generation parent population $P_p^{(t+1)}$ is modelled by the mapping:

$$opt_{EA} : \left(I_d, I_c\right)^{\mu} \rightarrow \left(I_d, I_c\right)^{\mu} \tag{5.10}$$

5.4.2 Recombination

In any generation the μ-membered parent population $P_p^{(t)}$ produce an λ-membered offspring population $P_0^{(t)}$. For every offspring vector a temporary parent vector is first built by means of recombination. In our implementation the following recombination scheme has been used, $rec_h : R^{n_h} \rightarrow R^{n_h}$ recombines the values of the vector h, where h corresponds to either a design variable vector or a distribution parameter vector:

$$rec_h\left(h\right) := \left(h_{a,1} \; or \; h_{b,1}, ..., h_{a,n_b} \; or \; h_{b,n_b}\right) \tag{5.11}$$

$h_{a,i}$ and $h_{b,i}$ are the i^{th} components of the vector h_a and h_b which are two parent vectors randomly chosen from the population.

5.4.3 Mutation

The Poisson distribution is controlled by the variance γ_i which coincides with the mean value of this distribution. The vector of variances γ controls the Poisson distribution which is used for exploring the discrete part of the design space $n_\gamma = 0.20 n_d$. On the other hand, parameters σ and α determine the variances and covariances of the $n_c -$dimensional normal distribution, which is used for exploring the continuous part of the design space. The amount of parameters attached to an individual can vary, depending on the degree of freedom required by the objective function in question. The setting that is used in the current study is: $n_\sigma = n_c$, $n_a = n_c\left(n_c - 1\right)/2$, that corresponds to the correlated mutation operator with a complete covariance matrix for each individual.

According to the generalized structure of the individuals of the populations in the proposed mixed-discrete EA algorithm, the mutation operator, $mut : \left(I_d, I_c\right)^{\lambda} \rightarrow \left(I_d, I_c\right)^{\lambda}$, is defined as follows:

$$mut = \left[mu_{s_d} \circ mu_{s_\gamma}, mu_{s_c} \circ (mu_\sigma \times mu_\alpha) \right] \tag{5.12}$$

The mutation operator is applied to the intermediate individuals obtained through the recombination operator. The distribution parameters of the structure of an individual are mutated first:

(i) $mu_\gamma : R_+^{n_\gamma} \to R_+^{n_\gamma}$ mutates the recombined vector γ :

$$mu_\gamma(\gamma) := \left(\gamma_1 b_1^e, ..., \gamma_{n_\gamma} b_{n_\gamma}^e \right) \tag{5.13}$$

where $b_i \approx U\left([0,1]\right)$. If, in a sequence of two generations, successful trials occur $e = e-1$, else $e = e+1$.

(ii) $mu_{s_d} : D^{n_d} \to D^{n_d}$ mutates the recombined values of the vector of discrete design variables s_d , using the already mutated values of the vector of variances γ :

$$mu_{s_d}\left(s_d\right) := \left(s_1 + z_1, ..., s_{n_d} + z_{n_d} \right) \tag{5.14}$$

where z_i follows the Poisson distribution with mean value and variance from the vector γ .

(iii) $mu_\sigma : R_+^{n_\sigma} \to R_+^{n_\sigma}$ mutates the recombined values of the vector of standard deviation σ :

$$mu_\sigma(\sigma) := \left(\sigma_1 \exp\left(z_1 + z_0\right), ..., \sigma_{n_\sigma} \exp\left(z_{n_\sigma} + z_0\right) \right) \tag{5.15}$$

where $z_0 \text{»} N(0, \tau_0^2)$, $z_i \text{»} N(0, \tau^2)$ "iÎ{1,2,…,n_σ} and $T_0 = \left(\sqrt{2n_s}\right)^{-1}, T = \left(\sqrt{2\sqrt{n_s}}\right)^{-1}$.

(iv) Mutation operator $mu_\alpha : R^{na} \to R^{na}$ mutates the recombined values of the vector of inclination angles a :

$$mu_\alpha(\alpha) := \left(a_1 + z_1, ..., a_{n_a} + z_{n_a} \right) \tag{5.16}$$

where $z_i \approx N\left(0,\beta^2\right)\forall i \in \{1,2,....,n_a\}$ with $\beta \cong 0.0873\left(\cong 5^o\right)$.

(v) Mutation operator $mu_s : R^n \to R^n$ mutates the recombined values of the vector of continues design variables s, using the already mutated values of the σ and α:

$$mu_s(s) := \left(s_1 + cor_1(\sigma,\alpha),....,s_{n_s} + cor_{n_s}(\sigma,\alpha)\right) \tag{5.17}$$

where cor is a random vector with normally distributed correlated components. The vector cor can be calculated according to $cor = T \cdot z$ where $z = \left[z_1,....,z_{n_\sigma}\right]^T$ with $z_i \approx N\left(0,\sigma_i^2\right)\forall i \in \{1,....,n_\sigma\}$ and

$$T = \prod_{p=1}^{n_\sigma - 1}\prod_{q=p+1}^{n_\sigma} T_{pq}\left(\tilde{a}_j\right) \tag{5.18}$$

where $j = l/2\left(2n_\sigma - p\right)\left(p+l\right) - 2n_\sigma + q$ [8]. The rotation matrices $T_{pq}\left(a_j\right)$ are unit matrices expect of the diagonal terms where $t_{pp} = t_{qq} = \cos\left(a_j\right)$ and $t_{pq} = -t_{qp} = -\sin\left(a_j\right)$.

5.4.4 Selection

There are two different types of selection schemes:

(μ+λ)-ES: Where the best μ individuals are selected from a temporary population of (μ+λ) individuals to form the parents of the next generation.

(μ,λ)-ES: Where the μ individuals produce λ offsprings (μ≤λ) and the selection process defines a new population of μ individuals from the set of λ offsprings only.

Combining the recombination, mutation and selection operators the main loop for the case of (μ,λ)-ES is formulated as follows:

$$opt_{(\mu,\lambda)-ES}\left(P^{(g)}\right) = sel_\mu^\lambda\left(U_{i=1}^\lambda\left\{mut\left(rec\left(P^{(g)}\right)\right)\right\}\right) \tag{5.19}$$

While for the case of the (μ+λ)-ES scheme the main loop is formulated as follows:

$$opt_{(\mu+\lambda)-ES}\left(P^{(g)}\right) = sel_{\mu}^{\lambda}\left(U_{i=1}^{\lambda}\left\{mut\left(rec\left(P^{(g)}\right)\right)\right\}\right) \tag{5.20}$$

The optimization procedure terminates when the following termination criterion is satisfied: the ratio μ_b / μ has reached a given value ε_d (=0.8 in the current study) where μ_b is the number of the parent vectors in the current generation with the best objective function value.

5.4.5 The ES algorithm

In Figure 5.1 a pseudo-code of the ES algorithm is depicted. At the beginning of the procedure in generation t = 0 the initial parent population $P_p^{(t)}$, composed by μ design vectors, is generated randomly (*step 3* of the pseudo-code). *Steps 5* to *12* correspond to the main part of the ES algorithm, where in every generation λ offspring vectors are generated by means of recombination and mutation. D_l is a sub-population with two members selected from the parent population of the current generation $P_p^{(t)}$ (*Step 6*) which is used by the recombination operator. Recombination and mutation operators, described in *steps 7* to *10*, act on the both design variable vectors s_l and distribution parameter vectors σ_l and a_l (both distribution parameter vectors denoted as y_l in the pseudo-code). In *step 11* the objective and constraint functions are calculated in order to assess the design vectors in terms of the objective function value and feasibility.

1. Begin
2. $t := 0$
3. initialize$\left(P_p^{\,0} := \quad y_m^{\,0}, s_m^{\,0}, F\ s_m^{\,0} \quad , \ m = 1,...,\mu \ \right)$
4. Repeat
5. For $l := 1$ To λ Do Begin
6. $D_l := \text{marriage}\ P_p^{\,t}$
7. $s_l := \text{s\_recombination}\ D_l$
8. $y_l := \text{y\_recombination}\ D_l$
9. $\tilde{s}_l := \text{s\_mutation}\ s_l$
10. $\tilde{y}_l := \text{y\_mutation}\ y_l$
11. $\tilde{F}_l := F\ \tilde{s}_l$
12. End
13. $P_o^{\,t} := \quad y_l^{\,t}, s_l^{\,t}, F\ s_l^{\,t} \quad , \ l = 1,...,\lambda$
14. Case selection_type Of
15. $\mu,\lambda\ :\ P_p^{\,t+1} := \text{selection}\ P_o^{\,t}, \mu$
16. $\mu + \lambda\ :\ P_p^{\,t+1} := \text{selection}\ P_o^{\,t}, P_p^{\,t}, \mu$
17. End
18. $t := t + 1$
19. Until termination_criterion
20. End

Figure 5.1. Pseudo-code of the ES algorithm.

5.4.6 ES for structural optimization problems

Structural optimization problems have been treated traditionally with mathematical programming algorithms, such as the sequential quadratic programming (SQP) method, which need gradient information. In structural optimization problems, where the objective function and the constraints are particularly highly non-linear functions of the design variables, the computational effort spent in gradient calculations is usually large. On the other hand EA optimization methods require more optimization steps.

In a number of studies by Papadrakakis *et al.* [31], [32], [48] it was found that EA optimization methods in structural optimization are computationally efficient even if large number of optimization steps is required to reach the optimum. These optimization steps are computationally less expensive than in the case of mathematical programming algorithms since they do not need gradient information. This property of probabilistic search methods is of greater importance in the case of Reliability Based Optimization problems since the calculation of the derivatives of the reliability constraints is very time-consuming. Furthermore, probabilistic methodologies are considered, due to their random search, as global optimization methods because they are capable of finding the global optimum, whereas mathematical programming algorithms may be trapped in local optima.

REFERENCES:

[1] Russo, L., The forgotten revolution: How science was born in 300BC and why it had to be reborn; 2004, Springer, Berlin.

[2] Veselago, V.G., Formulating Fermat's principle for light traveling in negative refraction materials*, PHYS-USP*, Vol. **45**(l0); 2002, pp. 1097-1099.

[3] Cauchy, A., Methode generale pour la resolution des systemes d'equations simultanes*, Compt. Rend.*, Vol.**25**; 1847, pp.536-538.

[4] Courant, R., Variational methods for the solution of problems of equilibrium and vibrations, *BullAmerMathSoc.*, Vol. **49**; 1943, pp.1–23.

[5] Dantzig, G. B., Maximization of a linear function of variables subject to linear inequalities*. Activity Analysis of Production and Allocation, Koopman (Ed.)*, Cowles Commission Monograph, l3; 1951, John Wiley and Sons, New York.

[6] Karush, W., Minima of Functions of Several Variables with Inequalities as Side Conditions, MS Thesis, Dept. of Mathematics; 1939, University of Chicago, Chicago, IL.

[7] Kuhn, H.W., Tucker A.W., Non-linear Programming, in J.Neyman (Ed.), *Proceedings of the Second Berkeley Symposium on Mathematical Statistics and Probability*, University of California Press, Berkeley, CA; 1951, pp.481-493.

[8] Rosenbrock, H.H., An Automatic Method for finding the Greatest or Least Value of a Function, *Comp J*, Vol.**3**; 1960, pp.175-184.

[9] Rosen, J., The Gradient Projection Method for Nonlinear Programming, I. Linear Constraints, *Journal of the Society for Industrial and Applied Mathematics*, Vol.**8**; 1960, pp. 181–217.

[10] Zoutendijk, G., *Methods of Feasible Directions*, 1960, Elsevier.

[11] Hooke, R., Jeeves, T.A., Direct Search Solution of Numerical and Statistical Problems, *J of the ACM*, Vol.**8**; 1961, pp.212-229.

[12] Fletcher, R., Powell, M.J.D., A rapidly convergent descent method for minimization*, Computer J*., Vol. **6**(2), 1963, pp.163-l68.

[13] Fletcher, R., Reeves, C.M, Function Minimization by Conjugate Gradients*, Computer J*., Vol.**7**; 1964, pp.149-154.

[14] Powell, M.J.D. (l964). An efficient Method for finding the minimum of a function of several variables without calculating derivatives*, Computer Journal*, Vol.**7** (4); 1964, pp.303-307.

[15] Nelder, J.A., Mead, R., A Simplex Method for Function Minimization, *Computer Journal*, Vol.**7**; 1965, pp. 308-313.

[16] Box, M.J., A New Method of Constrained Optimization and a Comparison with Other Methods, *Computer J*, Vol.**8**; 1965, pp.42-52.

[17] Fiacco, A.V., McCormick, G.P., Extension of SUMT for nonlinear programming: equality constraints and extrapolation, *Management Science,* Vol. **12**; 1966, pp.816-828.

[18] Gallagher, R.H., Zienkiewicz, O.C., Optimum Structural Design: Theory and Applications, 1973, John Wiley & Sons, New York.

[19] Haug, E.J., Arora, J.S., Optimal mechanical design techniques based on optimal control methods, ASME paper No 64-DTT-l0, *Proceedings of the 1st ASME design technology transfer conference*, 65-74, 1974, New York, October.

[20] Moses, F., Mathematical programming methods for structural optimization, ASME Structural Optimisation Symposium AMD Vol. **7**; 1974, 35-48.

[21] Pope, G.G., Schmit, L.A. (eds.), Structural Design Applications of Mathematical Programming Techniques*,* AGARDO graph 149, *Technical Editing and Reproduction Ltd*., London, February, 1971.

[22] Sheu, C.Y., Prager, W., Recent development in optimal structural design, *Applied Mechanical Reviews*, **21**(10); 1968, 985-992.

[23] Spunt, L., Optimum Structural Design, Prentice-Hall, Englewood Cliffs, New Jersey, 41-42, 1971.

[24] Venkayya, V.B., Khot, N.S., Berke, L., Application of optimality criteria approaches to automated design of large practical structures, 2nd Symposium on Structural Optimisation AGARD-CP-123, Milan, Italy, April, 1973.

[25] Holland, J., Adaptation in natural and artificial systems, University of Michigan Press, Ann Arbor,1975.

[26] Goldberg, D.E, Genetic Algorithms in search, optimization and machine learning, Addison-Wesley, 1989.

[27] Kirkpatrick, S., Optimization by simulated annealing: quantitative studies, *J Statist Phys*, Vol. **34**; 1984, pp. 975-986.

[28] Fogel, L.J., Owens, A.J., Walsh, M.J., Artificial intelligence through simulated evolution, Wiley, New York, 1966.

[29] Rechenberg, I., Evolution strategy: optimization of technical systems according to the principles of biological evolution, Frommann-Holzboog, Stuttgart, 1973.

[30] Schwefel H.P., Numerical optimization for computer models, Wiley & Sons, Chichester, UK, 1981.

[31] Papadrakakis, M., Tsompanakis, Y., Lagaros, N.D., Structural shape optimization using Evolution Strategies, *Engng. Optimization*, **31**; 1999, 515-540.

[32] Lagaros, N.D., Papadrakakis, M., Kokossalakis, G., Structural optimization using evolutionary algorithms, *Computer & Structures*, **80** (7-8); 2002, 571-587.

[33] Vanderplaats, G.N., Numerical optimization techniques for engineering design, McGraw-Hill, New York, USA, 1984.

[34] Arora, J.S., Introduction to optimum design, McGraw-Hill, New York, USA, 1989.

[35] Hinton, E., Sienz, J., (1994) Aspects of adaptive finite element analysis and structural optimization, in Topping B.H.V. and Papadrakakis M. (eds) Advances in Structural Optimization, CIVIL-COMP Press, Edinburgh, 1-26.

[36] Ramm, E., Bletzinger, K.-U., Reitinger, R., Maute, K., (1994) The challenge of structural optimization, in Topping B.H.V. and Papadrakakis M. (eds) Advances in Structural Optimization, CIVIL-COMP Press, Edinburgh, 27-52.

[37] Hinton, E., Sienz, J., Fully stressed topological design of structures using an evolutionary procedure, *Journal of Engineering Computations* 1993; 12, 229-244.

[38] Pedersen, P., Topology optimization of three dimensional trusses, in Bendsoe M.P., and Soares C.A.M. (eds.), NATO ARW `Topology design of structures', Sesimbra, Portugal, Kluwer Academic Publishers, Dordrecht, Netherlands, 19-31, 1993.

[39] Shieh, R.C., Massively parallel structural design using stochastic optimization and mixed neural net/finite element analysis methods, *Computing Systems in Engineering* 1994; **5**(4-6), 455-467.

[40] Bendsoe, M.P., Kikuchi, N., Generating optimal topologies in structural design using a homogenization method, *Computer Methods in Applied Mechanics and Engineering* 1988; **71**, 197-224.

[41] Hinton, E., Hassani, B., Some experiences in structural topology optimization, in B.H.V. Topping (ed.) Developments in Computational Techniques for Structural Engineering, CIVIL-COMP Press, Edinburgh, 323-331, 1995.

[42] Suzuki, K., Kikuchi, N., Layout optimization using the homogenization method, in Rozvany G.I.N. (ed.), NATO/DFG ASI Optimization of large structural systems, Berchtesgaden, Germany, Kluwer Academic Publishers, Dordrecht, Netherlands, 157-175, 1993.

[43] Eschenauer, H.A., Schumacher, A., Vietor, T., Decision makings for initial designs made of advanced materials, in Bendsoe M.P. and Soares C.A.M. (eds.), NATO ARW Topology design of structures, Sesimbra, Portugal, Kluwer Academic Publishers, Dordrecht, Netherlands, 469-480, 1993.

[44] Van Keulen F. and Hinton E., Topology design of plate and shell structures using the hard kill method, in B.H.V. Topping (ed.) Advances in optimization for Structural Engineering, CIVIL-COMP Press, Edinburgh, 177-188, 1996.

[45] Xie, Y.M., Steven, G.P., A simple evolutionary procedure for structural optimization, *Computers & Structures* 1993; **49**, 885-896.

[46] Papadrakakis, M., Tsompanakis, Y., Hinton, E., Sienz, J., Advanced solution methods in topology optimization and shape sensitivity analysis, *Journal of Engineering Computations* 1996; 3(**5**), 57-90.

[47] Xie, Y.M., Steven, G.P., Optimal design of multiple load case structures using an evolutionary procedure, *Journal of Engineering Computations* 1994; **11**, 295-302.

[48] Papadrakakis, M., Lagaros, N.D., Thierauf, G., Cai, J., 1998. Advanced solution methods in structural optimization based on evolution strategies, *Journal of Engineering Computations* 1998; **15** (1), 12-34.

6 Improved design of RC buildings by minimizing ROT index

6.1 Introduction

Engineers aim to design economic structures, which satisfy the constraints imposed by the design codes. This can be accomplished through a trial and error procedure or by means of an automatic optimization process. A number of studies have been published dealing with the problem of cost designs based on optimization of reinforced concrete (RC) structures. In particular, Kanagasundaram and Karihaloo [1, 2] implemented sequential linear programming and sequential convex programming techniques to optimize the cost of RC members. Zielinski [3] dealt with the cost optimum design of RC members imposing internal penalty function algorithm for nonlinear programming. Sun and Zheng [4] employed a two-level minimum cost design approach implementing sequential linear programming techniques for RC plane frames. Choi and Kwak [5] minimized the cost of rectangular beams and columns of RC frames through a direct search method choosing appropriate design sections from some predetermined discrete sections. Moharrami and Grierson [6] investigated an optimality criteria approach to minimize the cost design of RC building frames subjected to vertical as well as lateral loading, while

Fadaee and Grierson [7] minimized the cost of 3D RC frames. Balling and Xiao [8] presented a comparative study of optimization of three-dimensional reinforced concrete frames including the reinforcement design taking into consideration all relative details like bar diameter selection, number of bars, longitudinal distribution of the group of bars acquiring same properties and the specification of size of stirrups. While, Sarma and Adeli [9] were drawn to the conclusion that great amount of research effort in this field was devoted to simple elements, while disproportional percentage of researchers dealt with the minimum cost of framed structures and realistic three-dimensional structures.

Most of the codes meet the requirements of one seismic hazard level and one level of performance, usually life-safety. Moreover, they adopt indirect methods and linear - elastic analysis to define the performance of the structure. Apart from the minimum level of protection in order to adequately safeguard against partial collapse that endangers human lives, society has responsibilities including continuing operation of critical facilities, protection against the discharge of hazardous materials, and protection against excessive damage that may have far-reaching consequences for society on a local, regional, national, or international level. Performance-based design (PBD) aims to achieve targeted performance objectives. A performance objective pairs a single hazard level with a single performance level. Its advantage compared to other seismic design provisions is its capability to specify the performance for a range of hazard levels. In order to help engineers to make better decisions with respect to their designs in an automated design environment, the process of PBD of structural systems was incorporated into an optimization design framework. Many researchers proposed frameworks for optimum performance-based design of structural systems [10-12].

Lateral-torsional coupling caused by the moment created between the opposing inertia and resisting forces acting through the mass and rigidity center respectively burdens an eccentric structure in comparison to its symmetric counterpart, since amplification of displacements is induced by torsion. Current codified torsional provisions treat the effect of torsion implementing accidental and static eccentricity along with imposing restrictions on the design for buildings with irregular layout.

Many researchers studied the effect of lateral-torsional coupling on the earthquake response of structures [16-20]. Myslimaj and Tso [21, 22] proposed the balanced configuration in order to alleviate the torsional effect on the structural response by locating the center of mass between the center of strength and the center of rigidity. De la Llera and Chopra [26] proposed the base shear and torque surfaces (BST), which represent all combinations of base shear and torque that would lead to structural collapse when applied statically. Paulay [27, 28] proposed the center of resistance and identified the elastoplastic mechanism, aiming at estimating the torsional effects on the seismic response of ductile buildings, classifying them either as torsionally unrestrained or as torsionally restrained. In this chapter the criterion against torsion (*ROT*) discussed in chapter four will be used for improving the performance of buildings against torsional effects. *ROT* quantifies the amplification of shear forces due to torsional effect exhibiting satisfactory performance for single-story and multistory buildings in the elastic as well as inelastic range.

In this chapter the optimum design of reinforced concrete buildings will be pursued by minimizing torsional effects represented by *ROT*, since it was noticed that many damages during earthquake events were attributed to the coupled lateral-torsional modes of vibration [13-15]. Cost, stiffness eccentricity, strength eccentricity and *ROT* are treated as objective functions, while location and size of the vertical structural elements are the design variables constituting a combined topology-sizing optimization problem. The obtained optimum designs were subjected to nonlinear dynamic analyses and their response envelopes of base shear – base torque were compared. The results indicated that the designs obtained through the formulation where *ROT* is used as objective function exhibited among the two most satisfactory performances for all hazard levels developing low amount of base torque.

6.2 Optimization problem

6.2.1 Formulation

Structural optimization problems are characterized by various objective and constraint functions that are generally nonlinear functions of the design variables.

The generalized structural optimization problem, as was detailed expressed in Chapter 5 is used in the present study:

$$\min f(s) \tag{6.1}$$

$$\text{Subject to } g_i(s) \le 0 \quad i = 1,\ldots, p$$

$$h_j(s) = 0 \quad j = 1,\ldots, m$$

$$s^l \le s \le s^u$$

where $f(s)$ denotes the objective function and $g_i(s)$ the set of inequality constraints, while $h_j(s)$ the set of equality constraints. $s = \{s_i\}$, $i = 1,\ldots,n$ is the vector of design variables whose lower and upper bound are $s^l = \{s_i^l\}$, and $s^u = \{s_i^u\}$, $i = 1,\ldots,n$. Subsequently, the necessary definitions for the constraints, the design variables and the problem formulation are provided.

6.2.2 Architectural constraints

For every feasible design obtained through optimization procedure, behavioral constraints imposed by the design codes should be satisfied. Apart from behavioral constraints, architectural constraints should be also fulfilled for every vertical structural element. The following two architectural constraints are taken into consideration in the current study.

Architectural constraint 1: The dimensional boundaries of the column or shear wall constitute the first architectural constraint. A rectangle with dimensions AC_{1x}×AC_{1y} is employed. In order to consider feasible a design, the cross sections of the columns and the shear walls should be included in this rectangle (Figs. 6.1 and 6.2).

Architectural constraint 2: The topological position of the beams in conjunction with their supporting columns and/or shear walls is correlated with the second architectural constraint. The second architectural constraint secures that for every feasible design the beams and their cross points are supported by columns or shear walls.

Based on the architectural constraints, columns and shear walls are divided into two types. Columns/shear walls belong to *Type I* when AC_2 point corresponds to one of the corners of the rectangle AC_1. While they belong to *Type II* if rectangle AC_1 includes the AC_2 point (Figs. 6.1 and 6.2).

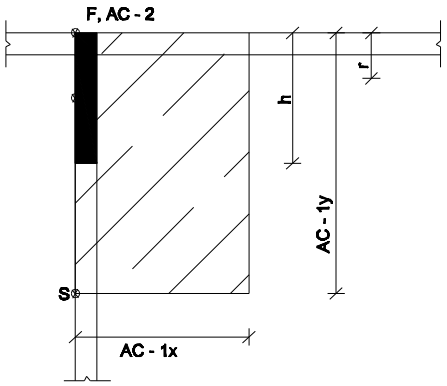

Figure 6.1. Sample column Type I with its architectural constraints AC1 and AC2.

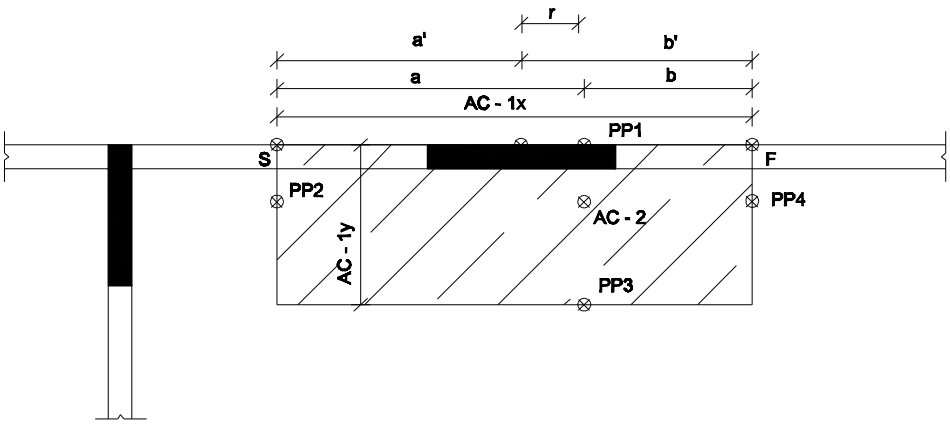

Figure 6.2. Sample column Type II with its architectural constraints AC1 and AC2.

6.2.3 Combined topology-sizing optimization problem

In the current study a topology-sizing optimization problem is solved in order to obtain improved earthquake resistant designs. Especially the design variables are divided into two categories: (i) Topology design variables, referring to the topology or layout of the columns and shear walls of the building. (ii) Sizing design variables, referring to sectional dimensions. It is worth noting that sizing variables depend on

the topology ones, so the topology design variables are defined first. In order to investigate the most efficient parameters for satisfactory torsional response, apart from *ROT* criterion two other parameters were implemented as objective functions, static eccentricity and strength eccentricity. Initial construction cost is also employed as objective function since it is one of the most widespread objective functions for this kind of problems. The mathematical formulation of the combined problem can be stated as follows when *ROT* is employed as objective function:

$$\min ROT = \frac{\sum_{k=1}^{n}\sum_{i=x,\,j=y}^{y,x}\left|V_{kij}\right| - \left|\sum_{k=1}^{n}\sum_{j=y}^{x}V_{kxj}\right| - \left|\sum_{k=1}^{n}\sum_{j=y}^{x}V_{kyj}\right|}{\left|\sum_{k=1}^{n}\sum_{j=y}^{x}V_{kxj}\right| + \left|\sum_{k=1}^{n}\sum_{j=y}^{x}V_{kyj}\right|} \tag{6.2}$$

subject to $g_i(s) \le 0,\ i = 1, \ldots\ldots, p$ (behavioral constraints)

$$\left.\begin{array}{l} t_{lb,j} \le r_j \le t_{ub,j} \\ s_{lb,j} \le h_j \le s_{ub,j} \end{array}\right\} j = 1, 2, \ldots\ldots, ncolumns \text{ (architectural constraints)}$$

where n is the number of vertical structural elements, while i and j correspond to the direction of the shear force of the element k and the seismic excitation with reference to the structural axes. $g_i(s)$ are the behavioral constraints imposed by design codes, r_j is the distance of the individual element center of the j^{th} column/shear wall from its corresponding AC_2 point. $t_{lb,j}, t_{ub,j}$ are the lower and upper bounds of the sizing design variables imposed by the architectural constraints. h_j is the largest edge of the j^{th} column/shear wall referring to the sizing design variables. $s_{lb,j}, s_{ub,j}$ are the lower and upper bounds of the sizing design variables imposed by the architectural constraints. The other three objective functions are expressed as:

I. $$\min e_{CM-CR} = \sqrt{\left(x_{CM} - x_{CR}\right)^2 + \left(y_{CM} - y_{CR}\right)^2} \text{ (static eccentricity)} \tag{6.3}$$

II. $$\min e_{CM-CV} = \sqrt{\left(x_{CM} - x_{CV}\right)^2 + \left(y_{CM} - y_{CV}\right)^2} \text{ (strength eccentricity)} \tag{6.4}$$

III. $\min C_{IN} = C_{con} + C_{st} + C_{lab}$ (initial construction cost) (6.5)

where (x_{CM}, y_{CM}), (x_{CR}, y_{CR}) and (x_{CV}, y_{CV}) are the coordinates of the mass center, rigidity center and strength center, respectively. C_{IN} is the initial cost of a new structure, C_{con} is the concrete cost, C_{st} is the cost of the steel reinforcement and C_{lab} is the labour cost.

6.2.4 Design variables

The shape of the vertical resisting elements (columns and shear walls) is chosen to be rectangular *h*×*b*, where *h*≥*b*. As mentioned above, the sizing design variables depend on the topology ones, so the topology variables are defined first.

Topology design variables

In the case of *Type I* element, if $AC_{1x} > AC_{1y}$ the final position of the element center will be allocated along AC_{1x} rectangular edge, otherwise along AC_{1y}. For square architectural constraint the edge is randomly selected. Its lower bound depends on the indicative minimum column size:

$$t_{lb,j} = \frac{h_{\min}}{2} \tag{6.6}$$

where $h_{\min}$ is the minimum column size imposed by the design codes. Its upper bound is the half size of the corresponding architectural constraint edge (AC_{1x} or AC_{1y}).

$$t_{ub,j} = \frac{1}{2}\sqrt{(x_S - x_F)^2 + (y_S - y_F)^2} \tag{6.7}$$

The individual element center of the column/shear wall is allocated to the largest edge of the AC_1 architectural constraint. $S(x_S, y_S)$ is the starting point and $F(x_F, y_F)$ is the finishing point of the largest edge, while AC_2 point coincides with the finishing point F. In the case of *Type II* the edge of the AC_1 architectural rectangle, to which the individual element center of the column will be allocated, has

either already been presented or it will be selected by the smallest distance of the projection of the AC_2 point to the four edges of the AC_1 rectangle. Its lower bound is defined to be equal to zero:

$$t_{lb,j} = 0 \tag{6.8}$$

While its upper bound depends on the side of the projected AC_2 point the column mass center will be allocated.

$$t_{ub,j} = \frac{a}{2} \text{ (if on the left side)} \tag{6.9}$$

$$t_{ub,j} = \frac{b}{2} \text{ (if on the right side)} \tag{6.10}$$

where a is the distance of the new position of AC_2 point from the starting point S and b is the distance of the new position of AC_2 point from the finishing point F.

Sizing design variables

Type I elements are characterized by a direct relationship between the topology and sizing design variables, this sizing design variable is defined as inactive.

$$h_j^i = 2r_j \tag{6.11}$$

For *Type II* elements the relationship between the topology and sizing design variables is indirect expressed as:

$$s_{lb,j}^i = 2r_j \tag{6.12}$$

$$s_{ub,j}^i = 2\min(a^{'}, b^{'}) \tag{6.13}$$

where $a^{'}$ and $b^{'}$ refer to the distance of the individual element center of the vertical element from points S and F, respectively. In this case the sizing design variable is active. In this case of active sizing design variable, the dimensions of columns/shear walls have to be defined by the optimizer and not by the topology design variables as in the case of *Type I*. The bounds of the size of the column and shear wall are dependent on the topological design variable r_j.

6.3 Numerical Tests

For the purpose of this investigation two models are tested in order to evaluate the behavior of optimized single-story systems for the proposed methodology. The material properties for both numerical tests considered are: concrete modulus of elasticity equal to 27.5GPa, concrete characteristic compressive cylinder strength 25 GPa, longitudinal steel reinforcement modulus of elasticity 210GPa and longitudinal steel reinforcement characteristic yield strength 400MPa. The design spectrum used corresponds to soil type B (characteristic periods T_B = 0.15 sec, T_C = 0.50 sec and T_D = 2.00 sec). A bilinear material model with pure kinematic hardening is adopted for the structural steel. For the simulation of the concrete the modified Kent-Park model is applied, where the monotonic envelope of concrete in compression follows the model of Kent and Park [30] as extended by Scott *et al.* in [31]. Moreover, the importance factor γ_I was taken equal to 1.0, while the damping correction factor η is equal to 1.0, since a damping ratio of 5% has been considered. The members are modelled implementing the force-based fibre beam-column element. The dimensions of columns/ shear walls represent the design variables.

The proposed methodology is assessed in the framework of design optimization and for this purpose eight design cases are formulated, denoted Case A to H. In particular, the design cases are classified into two groups, those that comply with the design requirements of Eurocode and those that are based on a PBD procedure. Cases A to D constitute the first group. The structures in this group are designed in compliance with EC, while the implemented objective functions are the initial structure cost, the static eccentricity, the strength eccentricity and *ROT*, respectively for Cases A to D. The second group consists of Cases E to H and adopt the same objective functions but in this case PBD constraints are imposed during the design procedure.

The solution of the optimization problem is performed with the ES (μ+λ) optimization scheme [32] with ten parents and offspring (μ = λ = 10) where deviation $\gamma = 0.1$ is employed. The optimization criterion implemented provides that if the ratio μ_b / μ has reached a given value ranging from 0.5 to 0.8 - in the current case

0.8 is used - where μ_b is the number of the parent vectors in the current generation with the best objective function and μ the number of parent vectors in the current generation.

Table 6.1. Natural records [33]

Earthquake	Station	Distance	Site
Records in 50/50 hazard level			
Honeydew (PT)	Cape Mendocino	20	rock
17 August 1991	Petrolia	17	soil
Cape Mendocino (CM)	Rio Dell	13	soil
25 April 1992	Butler Valley	37	rock
Cape Mendocino (C2)	Fortuna	43	soil
aftershock, 4/26/92	Centerville	28	soil
Records in 10/50 hazard level			
Tabas (TB)	Dayhook	14	rock
16 September 1978	Tabas	1.1	rock
Cape Mendocino (CM)	Cape Mendocino	6.9	rock
25 April 1992	Petrolia	8.1	soil
Chi-Chi (CC), Taiwan	TCU101	4.9	soil
20 September 1999	TCU102	3.8	soil
Records in 2/50 hazard level			
Valparaiso (VL), Chile	Vina del Mar	30	soil
3 May 1985	Zapaller	30	rock
Michoacan (MI),	Caleta de Campos	12	rock
Mexico	La Union	22	rock
19 September 1985	La Villita	18	rock
	Zihuatenejo	21	rock

The optimal designs obtained for all cases were subjected to two earthquake excitations for each hazard level chosen from Somerville and Collins [33] (see Table 6.1). The records of each hazard level are scaled to the same PGA in order to ensure compatibility between the records, in accordance to the hazard curve taken from the work by Papazachos *et al*. [34] (see Table 6.2). The envelopes of the base shear-base torque time histories were superimposed in order to evaluate the performance of the various criteria.

Table 6.2. Seismic hazard levels [34]

Event	Recurrence Interval	Probability of Exceedance	PGA (g)
Frequent	21 years	90% in 50 years	0.06
Occasional	72 years	50% in 50 years	0.11
Rare	475 years	10% in 50 years	0.31
Very Rare	2475 years	2% in 50 years	0.78

6.3.1 Eccentric - horizontally regular single-story system

The layout of the first numerical test is shown in Fig. 6.3., along with the optimum designs achieved for the eight formulations considered. The optimum designs were subjected to two seismic excitations for each hazard level in order to evaluate their performance. The base shear-base torque time histories were recorded and implemented to assess their performance against torsion. In Fig. 6.4. the time history of base shear and base torque can be observed for *Case A* in the occasional hazard level designed according to EC constraints.

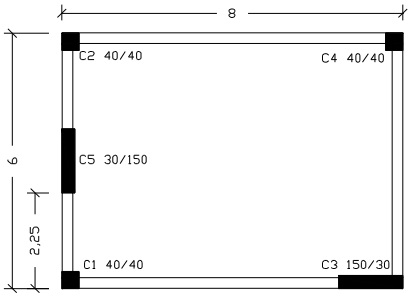

Initial Layout

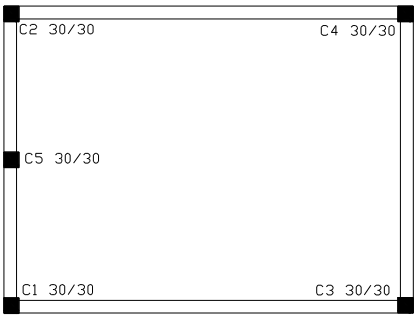

Cases A,B

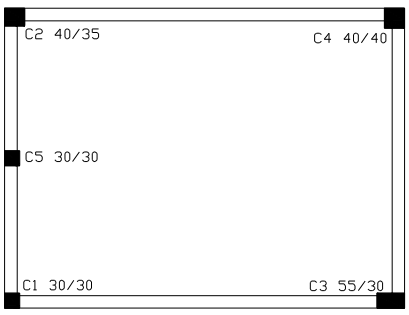

Case C

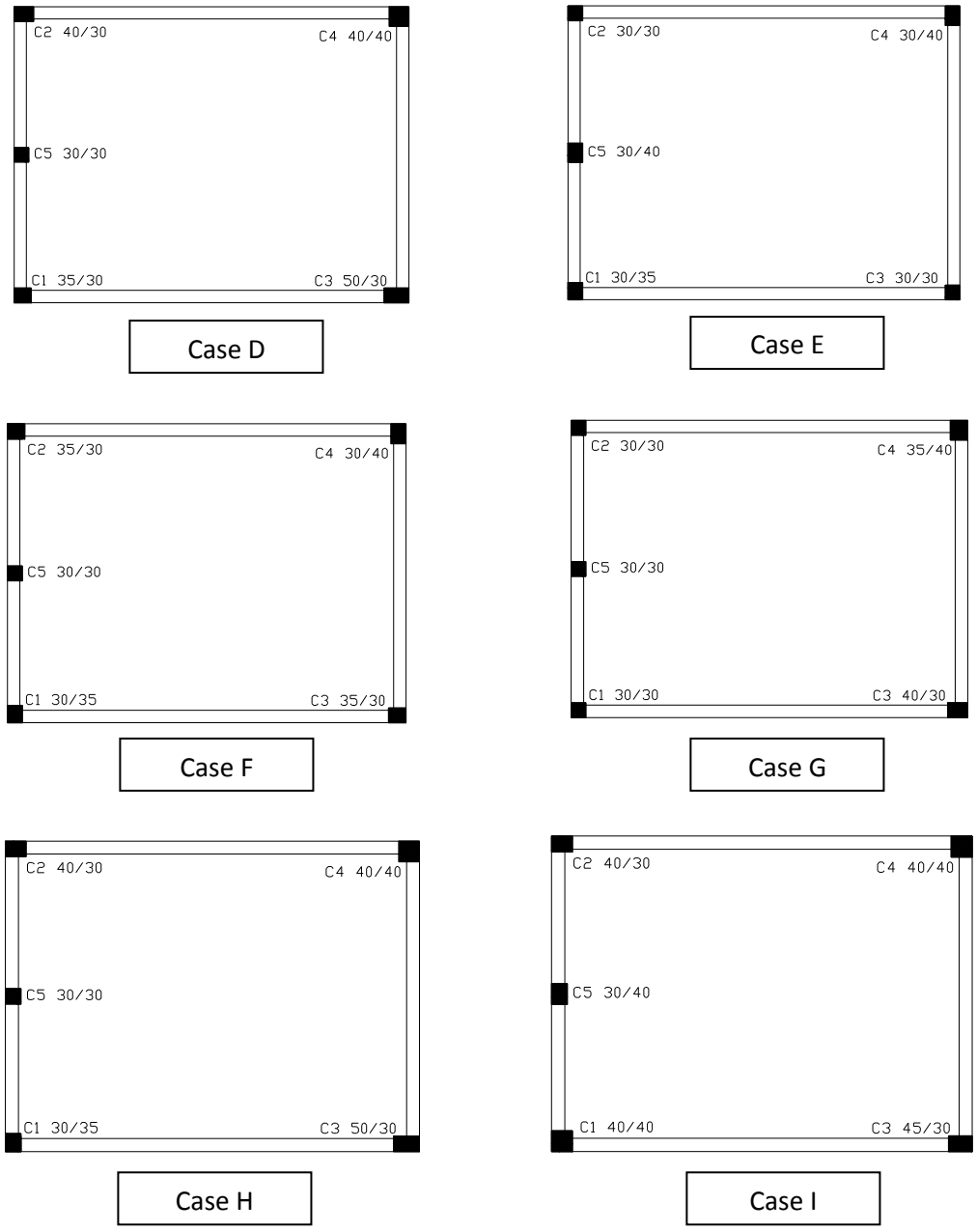

Figure 6.3. Initial and optimized layout for all design Cases.

Table 6.3. Numerical example 1 - Comparison between initial and optimized values for all design models

	Initial Values				Final Values				Variation Percentage			
Design Models	cost	e_{cr}	e_{cv}	ROT	cost	e_{cr}	e_{cv}	ROT	cost	e_{cr}	e_{cv}	ROT
CASE A	3312.07	3.77	2.11	1,79	2847.3	0.97	0.1	0.1	-14.0326	-74.2706	-95.2607	-94.4134
CASE B	3312.07	3.77	2.11	1,79	2876.4	0.12	1.16	0.07	-13.154	-96.817	-45.0237	-96.0894
CASE C	3312.07	3.77	2.11	1,79	3130.07	1.16	0.01	0.22	-5.49505	-69.2308	-99.5261	-87.7095
CASE D	3312.07	3.77	2.11	1,79	2865.72	0.09	0.26	0.02	-13.4765	-97.6127	-87.6777	-98.8827
CASE E	3312.07	3.77	2.11	1,79	2863.53	3.86	0.55	0.36	-13.5426	2.387268	-73,9336	-79.8883
CASE F	3312.07	3.77	2.11	1,79	2847.3	0.97	0.1	0.1	-14.0326	-74.2706	-95.2607	-94.4134
CASE G	3312.07	3.77	2.11	1,79	2911.44	0.08	1.41	0.03	-12.0961	-97.878	-33.1754	-98.324
CASE H	3312.07	3.77	2.11	1,79	3122.09	0.51	0.03	0.12	-5.7378	-86.4721	-98.5782	-93.2961

The envelopes of the performances for all cases were superimposed in order to demonstrate the most efficient objective function. In the occasional earthquake hazard level with 50 percent probability of exceedance in 50 years (50in50 - Figs. 6.5 - 6.6) in both x and y directions for the first group the *Cases B* and *D* appear to perform better than the other design procedures. In particular *Case D* is increased by 36% in comparison with *Case B* concerning the maximum developed base torque. The *Cases A* and *C* performed the least efficiently with their deviation from *Case D* reaching to almost 200% (211% for *Case A*, 188% for *Case C*). As far as the rare earthquake hazard level with 10 percent probability of exceedance in 50 years (10in50 - Figs. 6.9 - 6.10) is concerned, the *Cases B* and *D* again behave better than other designs. Especially, *Case D* appears to be increased by 118% from *Case B*. The less efficient performance was observed for *Cases A* and *C*, which burden the structure more by almost 377.6%. Last in the maximum considered event with 2 percent probability of exceedance in 50 years (2in50 - Figs. 6.13 - 6.14) hazard level, the *Case B* again behaves better than *Case D* by 57.14%, but still are the most well-performed design procedures. With the percentage of almost 300% increased from *Case B* respectively, *Case A* and *Case C* exhibited the least efficiently of all design models. According to results ROT design criterion (*Case D*) appeared to be one of the two most satisfactory behaved criteria for all hazard levels as far as the amount of the developed base torque is concerned. Take into consideration the restrictions imposed by the PBD, for the second group *ROT* design criterion (*Case H*) outperformed the others for all hazard levels exhibiting the most efficient performance. Especially, for the occasional hazard level the performance of the other design criteria exhibited an increase of the developed base torque over the percentage of 170% in comparison with the performance of *ROT* (*Case H*) (50in50 - Figs. 6.7 - 6.8). The same conclusions can be drawn for the rare earthquake hazard level (10in50 - Figs. 6.11 - 6.12) and the maximum considered event (2in50 - Figs. 6.15 - 6.16). In Table 6.3, it can be seen that compared to the initial designed according to Eurocodes, the optimized are improved with reference to the objective functions considered. It is worth noting that apart from cost for the rest objective functions a reduction percentage of almost 100 % was noticed.

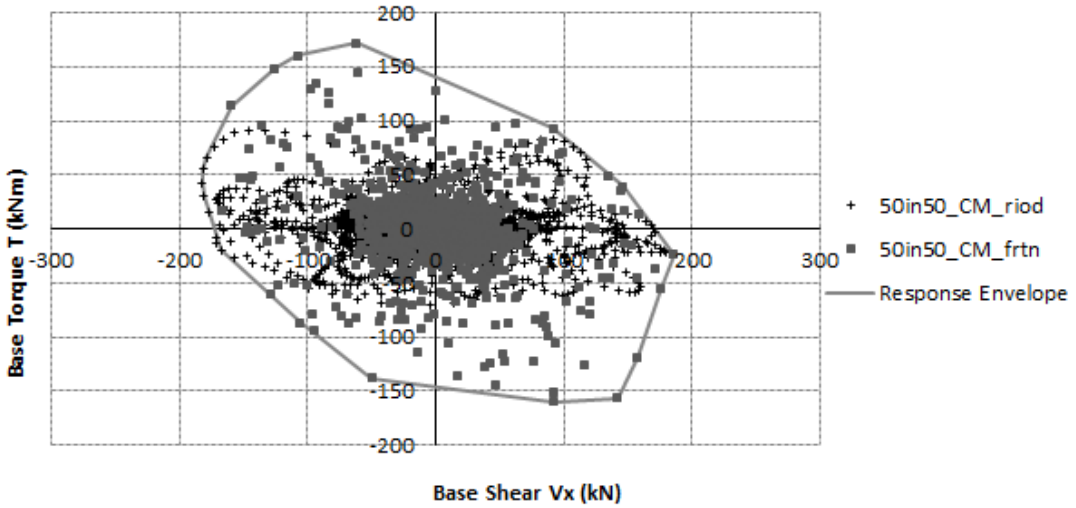

Figure 6.4. Numerical example 1 - Base Shear – Base Torque time history considering CASE A for the occasional earthquake level.

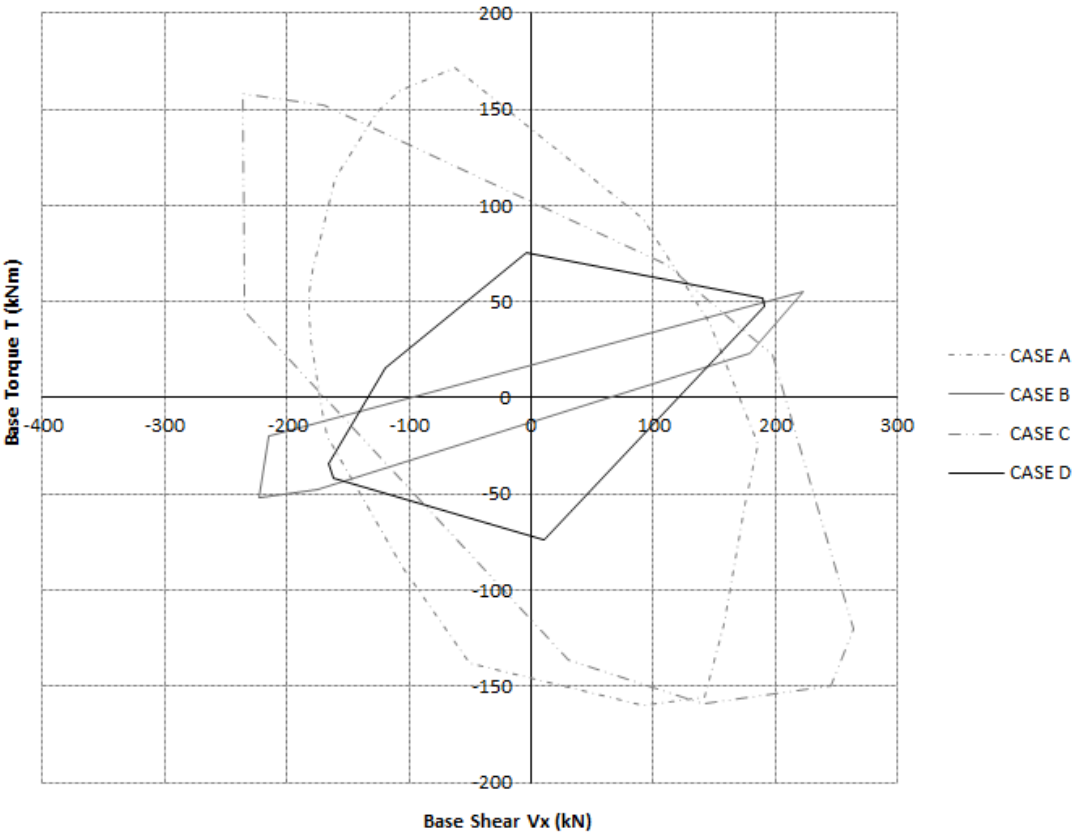

Figure 6.5. Numerical example 1 - The superimposed envelopes of BST time histories for the occasional earthquake hazard level (50in50) in x direction for all criteria designed in compliance with EC.

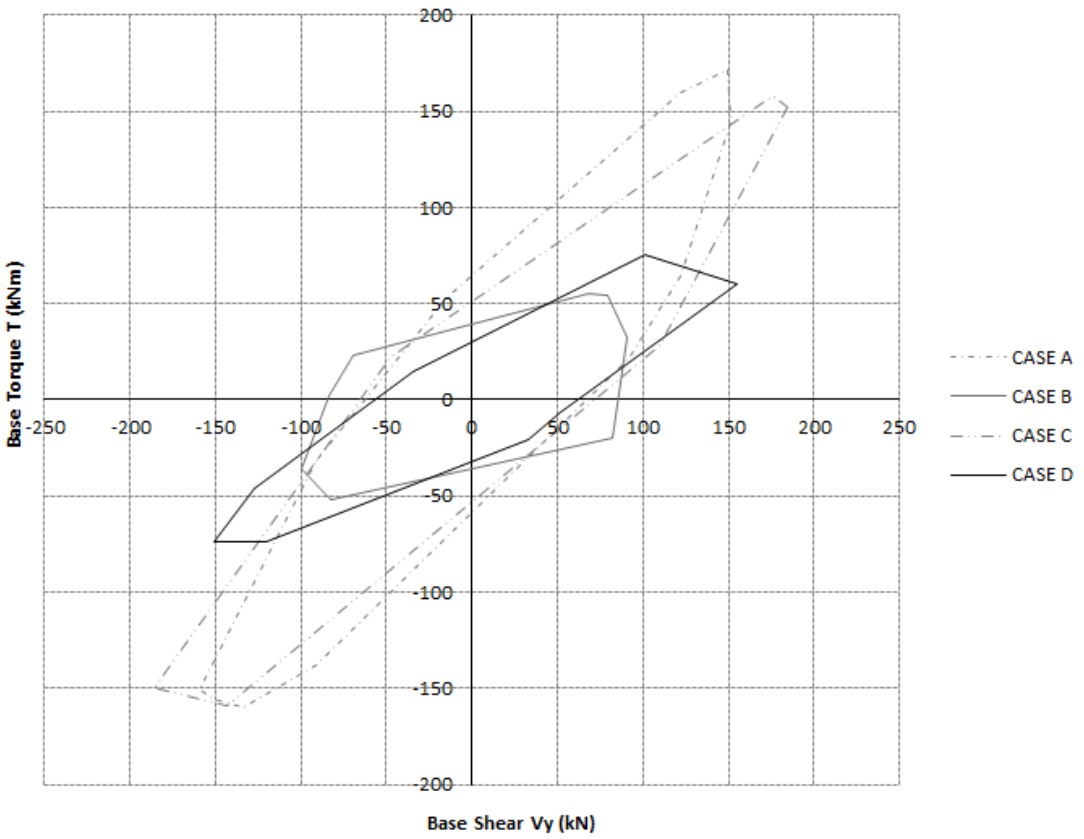

Figure 6.6. Numerical example 1 - The superimposed envelopes of BST time histories for the occasional earthquake hazard level (50in50) in y direction for all criteria in compliance with EC.

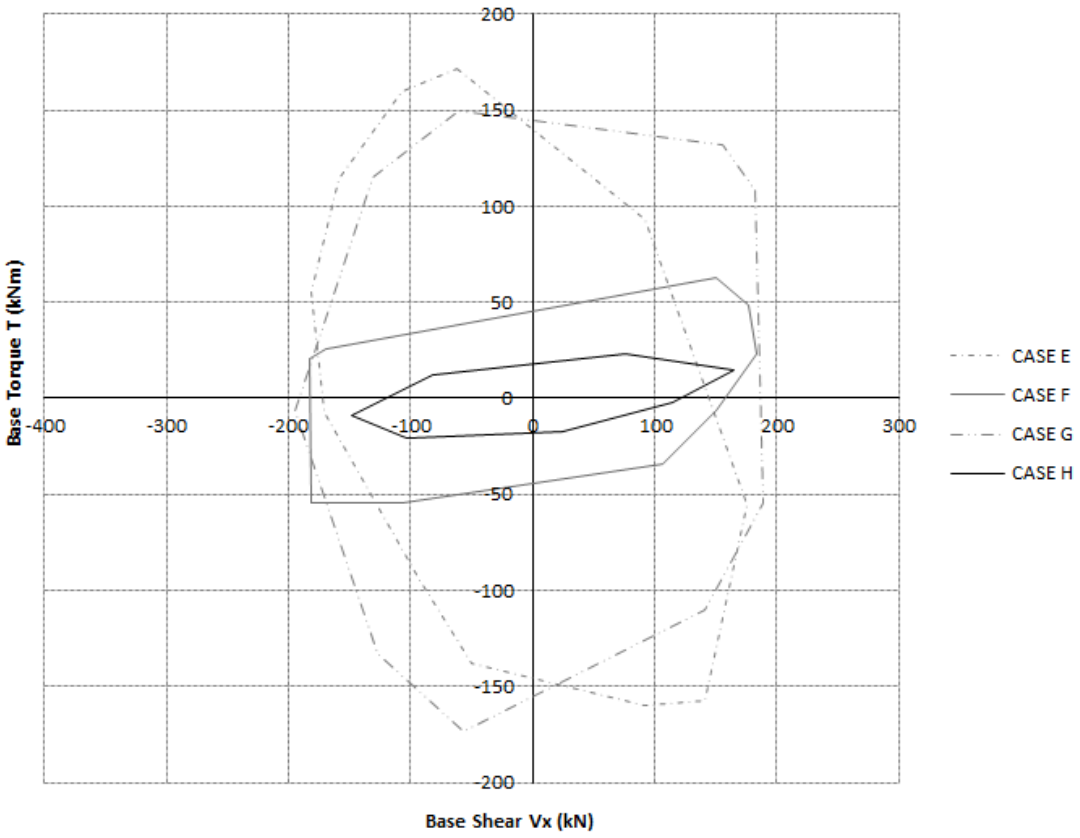

Figure 6.7. Numerical example 1 - The superimposed envelopes of BST time histories for the occasional earthquake hazard level (50in50) in x direction for all criteria designed in compliance with PBD.

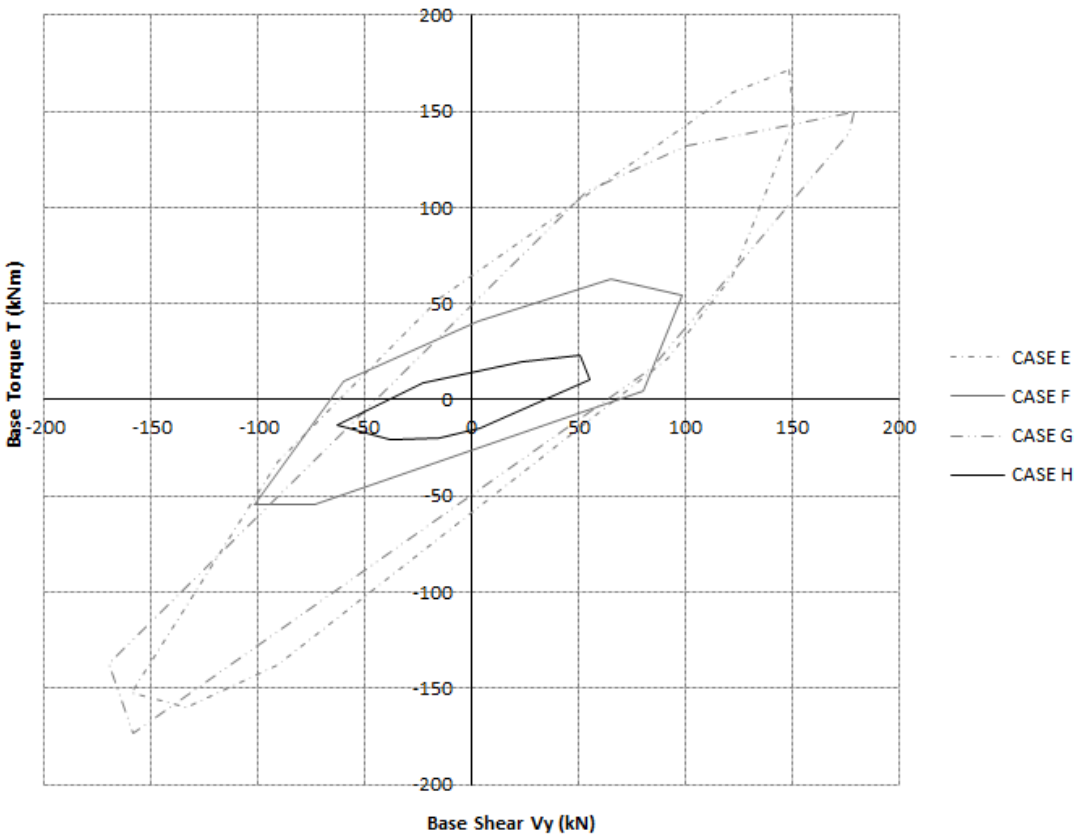

Figure 6.8. Numerical example 1 - The superimposed envelopes of BST time histories for the occasional earthquake hazard level (50in50) in y direction for all criteria in compliance with PBD.

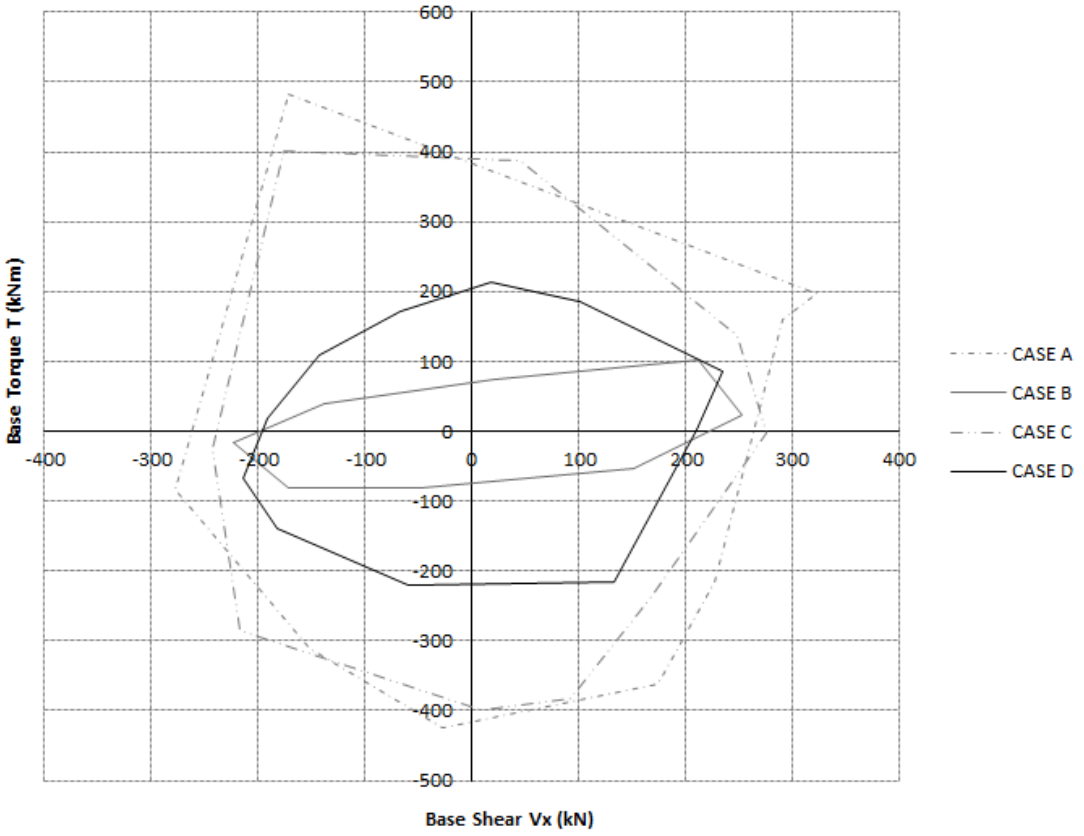

Figure 6.9. Numerical example 1 - The superimposed envelopes of BST time histories for the rare earthquake hazard level (10in50) in x direction for all criteria designed in compliance with EC.

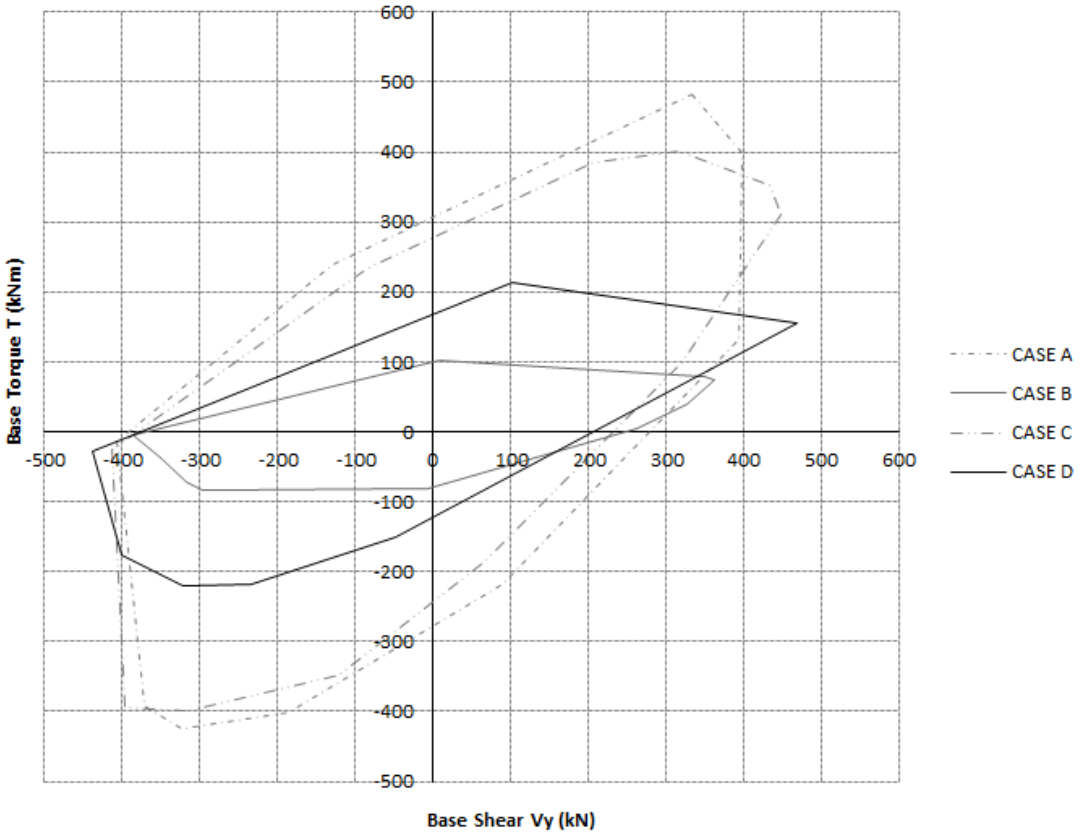

Figure 6.10. Numerical example 1 - The superimposed envelopes of BST time histories for the rare earthquake hazard level (10in50) in y direction for all criteria designed in compliance with EC.

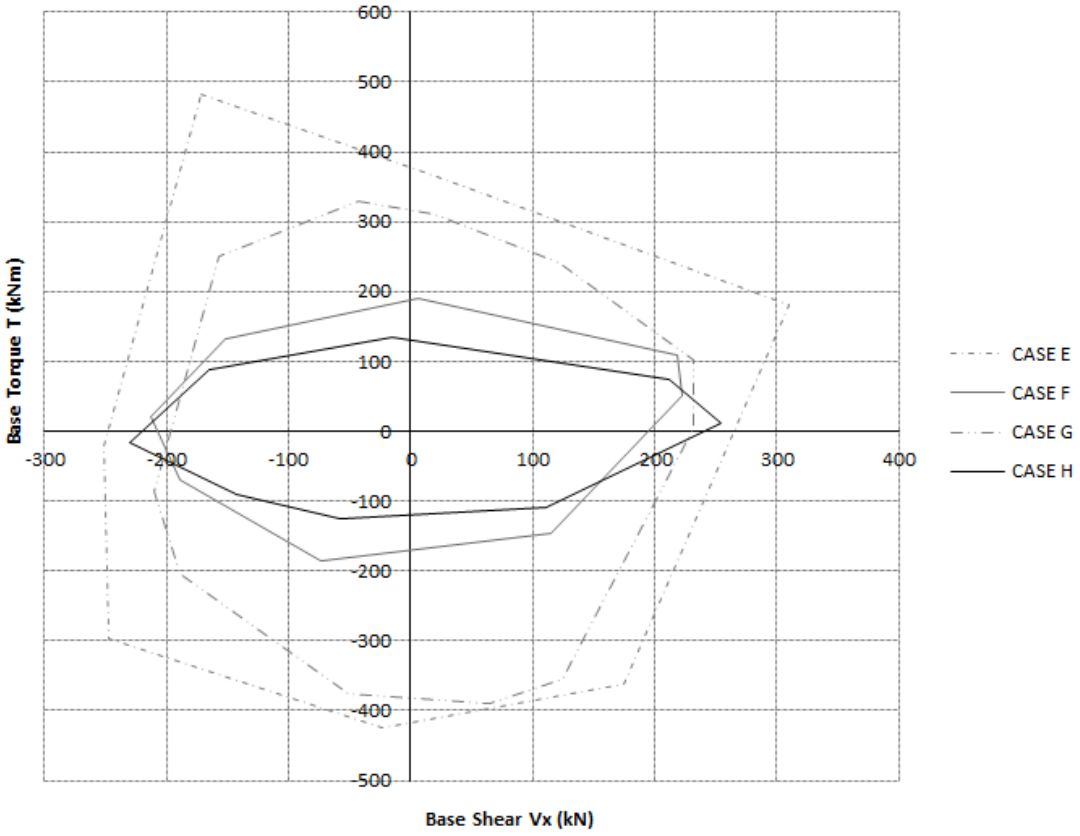

Figure 6.11. Numerical example 1 - The superimposed envelopes of BST time histories for the rare earthquake hazard level (10in50) in x direction for all criteria designed in compliance with PBD.

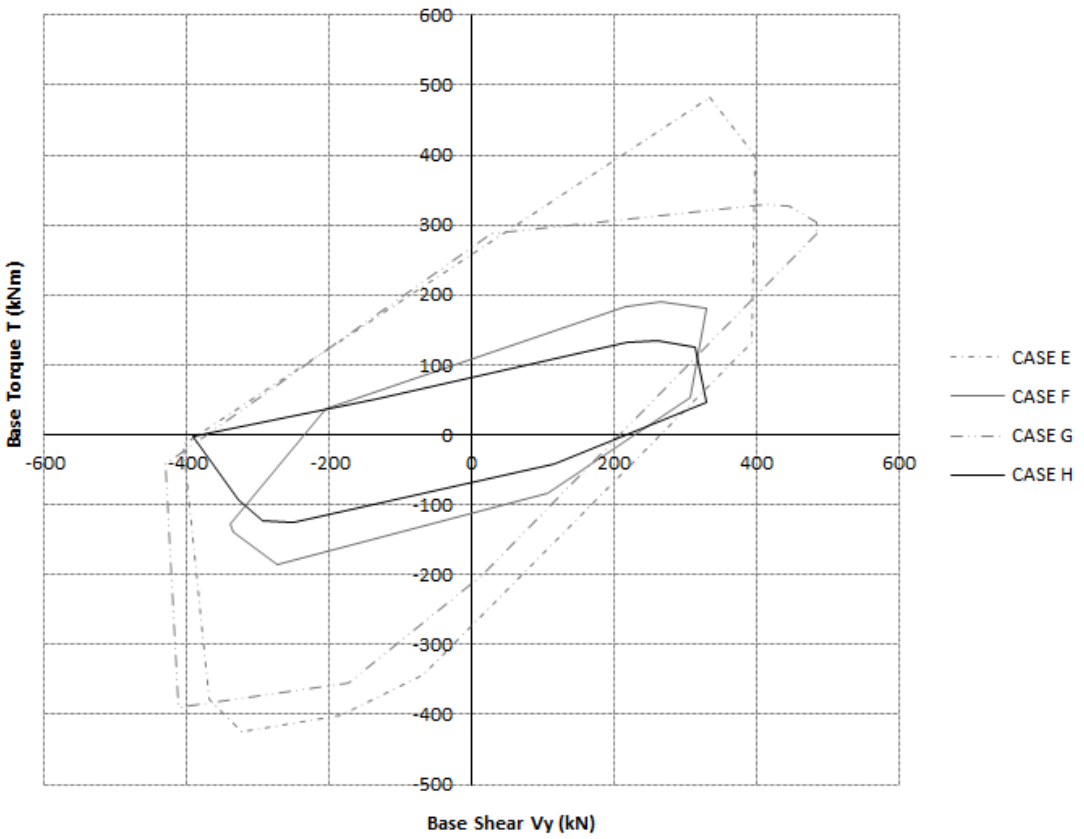

Figure 6.12. Numerical example 1 - The superimposed envelopes of BST time histories for the rare earthquake hazard level (10in50) in y direction for all criteria designed in compliance with PBD.

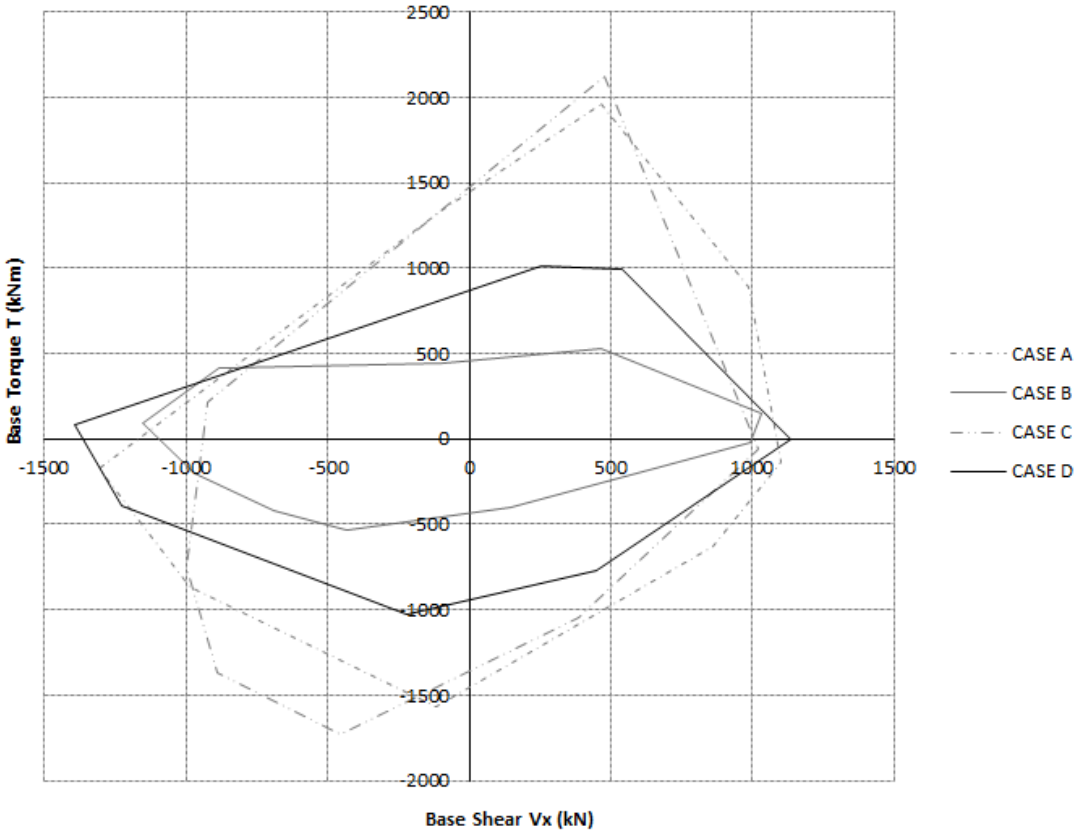

Figure 6.13. Numerical example 1 - The superimposed envelopes of BST time histories for the maximum considered earthquake hazard level (2in50) in x direction for all criteria designed in compliance with EC.

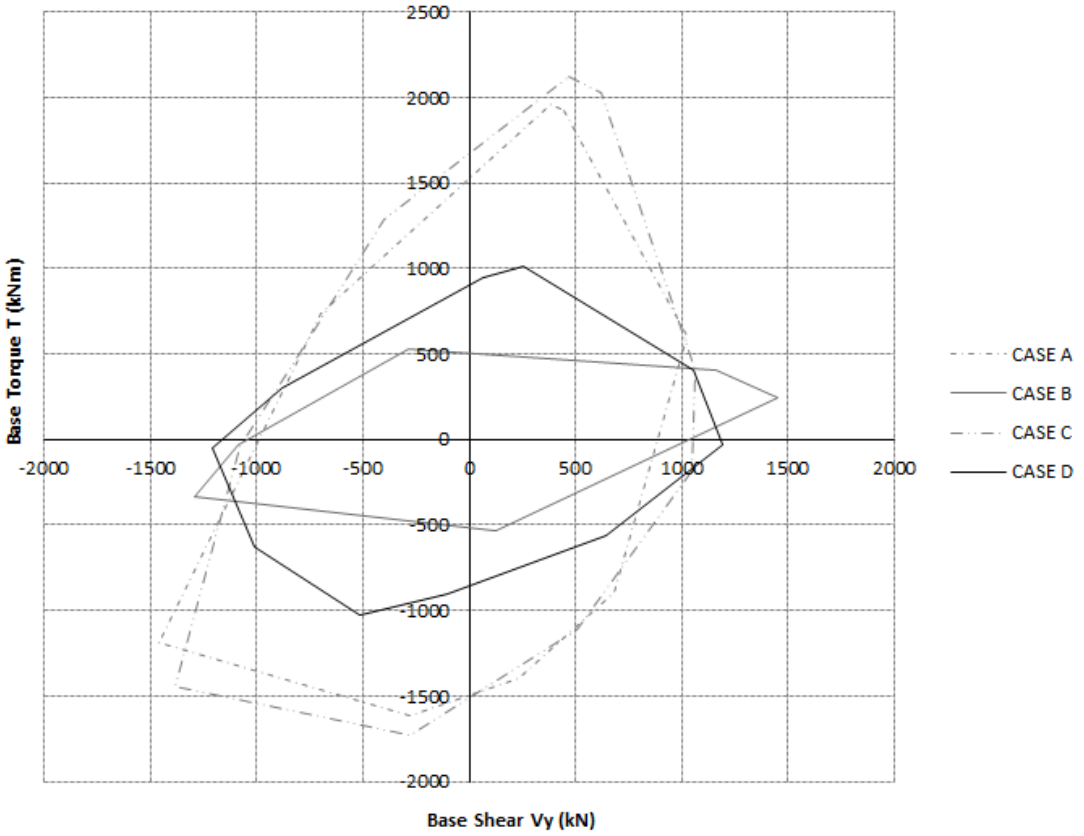

Figure 6.14. Numerical example 1 - The superimposed envelopes of BST time histories for the maximum considered earthquake hazard level (2in50) in y direction for all criteria designed in compliance with EC.

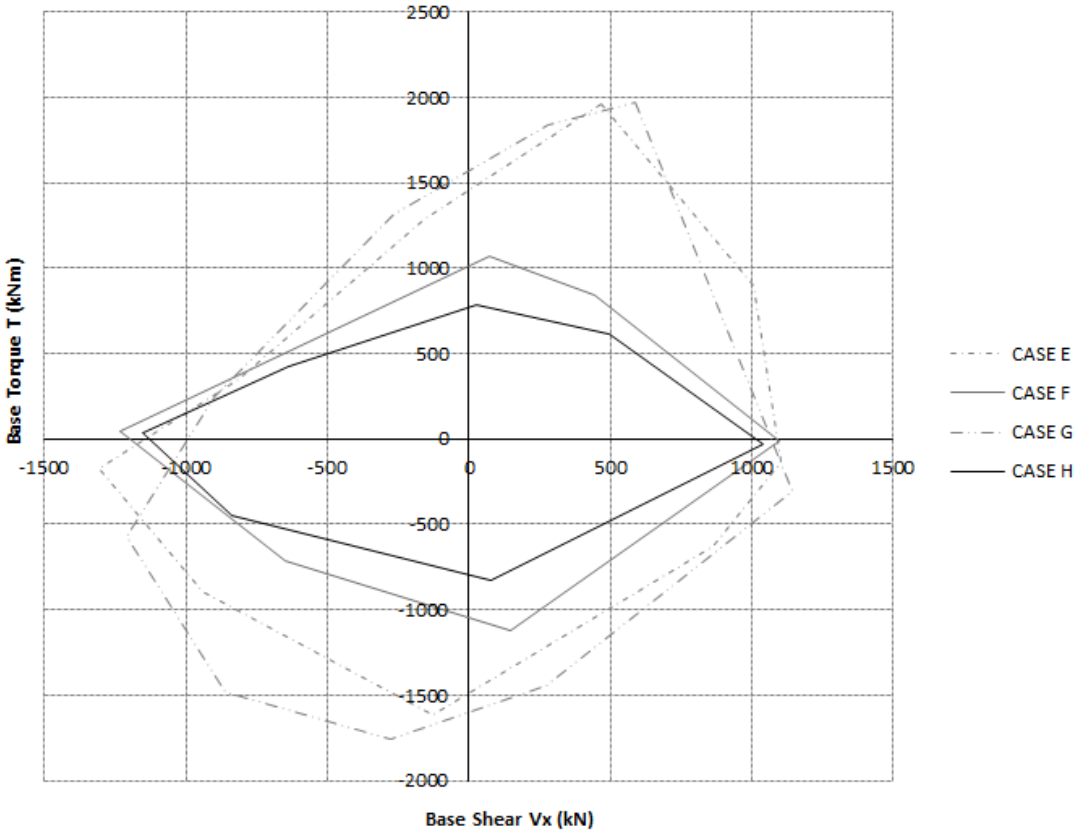

Figure 6.15. Numerical example 1 - The superimposed envelopes of BST time histories for the maximum considered earthquake hazard level (2in50) in x direction for all criteria designed in compliance with PBD.

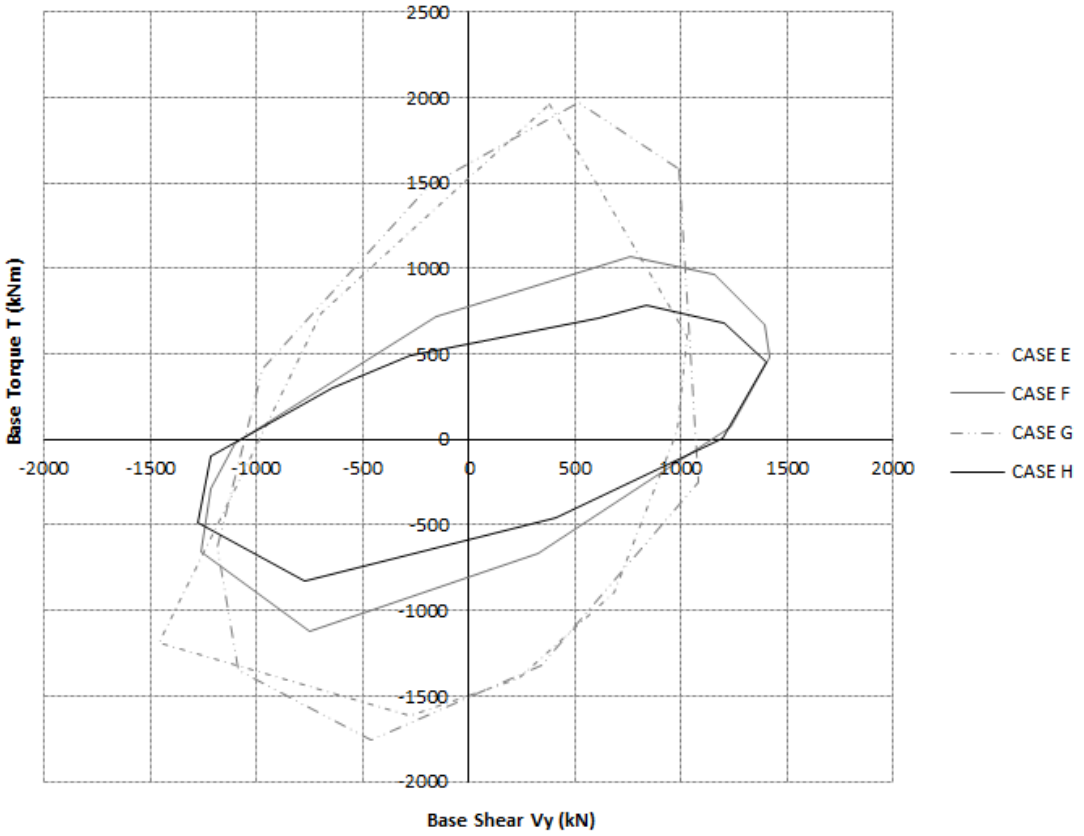

Figure 6.16. Numerical example 1 - The superimposed envelopes of BST time histories for the maximum considered earthquake hazard level (2in50) in y direction for all criteria designed in compliance with PBD.

6.3.2 Eccentric – horizontally irregular single-story system

The second numerical test is a horizontally irregular one-story building. In this case initial and optimum designs for all objective functions are shown in Fig. 6.17. The initial and optimized objective function values are presented in Table 4. As in the previous example the optimum designs were subjected to two seismic excitations and the envelopes of their base shear-base torque time histories were superimposed to detect the most efficient objective function. For occasional seismic events *Cases B* and *D* exhibit the most satisfactory performance with the minimum developed base torque values for the first group, the difference between them reaching the value of 25%. While *Cases A* and *C* exhibits the less efficient performance with their deviation from the most efficient design reaching up to almost one order of magnitude (50in50 - Figs. 6.18 - 6.19). In the hazard level with probability of exceedance 10 percent in

50 years, *Cases D* and *C* succeeded the minimum developed base torque during analysis. The maximum developed base torque values were recorded for *Cases A* and *B*, their deviation percentage from the minimum response is 126% and 57% respectively (10in50 - Figs. 6.22 - 6.23). For maximum considered seismic events *Cases D* and *A* exhibit the most satisfactory performance. *Cases C* and *B* develop the maximum values of base torque exceeding by 50% and 110% percentage the minimum value of Case *D* (2in50 - Figs. 6.26 - 6.27). As it can be observed *ROT* design criterion exhibited for all hazard levels among the two best performances even for this case of horizontally irregular building. For occasional earthquake hazard level *ROT* exhibited the second most satisfactory performance, while static eccentricity outperformed the other criteria performing most efficiently. Considering the other two hazard levels, *ROT* based designs undergone the lowest amount of the base torque developed. Static eccentricity and initial structure cost exhibited the second most satisfactory performance for the hazard levels with probability of exceedance 10% and 2% in 50 years, respectively. Considering the second group, for the occasional hazard level static eccentricity (*Case F*) and *ROT* (*Case H*) outperformed the other criteria (50in50 - Figs. 6.20 - 6.21). For rare earthquake events the same designs exhibited the most satisfactory performances (10in50 - Figs. 6.24 - 6.25). While for the maximum considered event, strength eccentricity (*Case G*) and initial structure cost (*Case E*) developed the minimum values of base torque (2in50 - Figs. 6.28 - 6.29). It is worth noting that *ROT* was included, for all cases designed either according to EC or PBD, among the first two most well performed criteria ensuring its reliability. The same consistency on the performance was not observed for the other criteria.

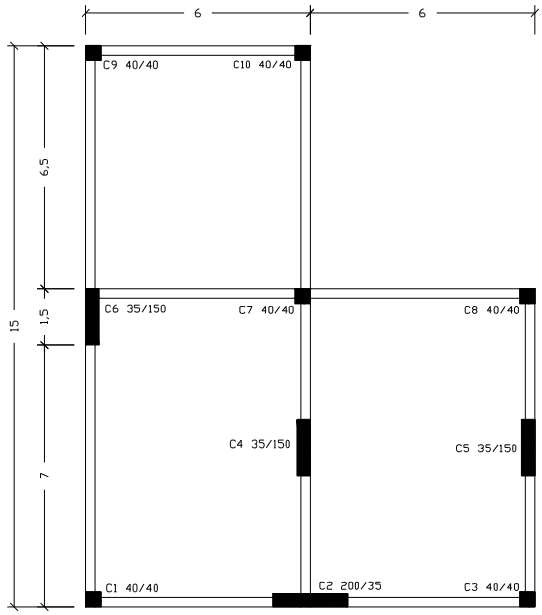

Initial Layout

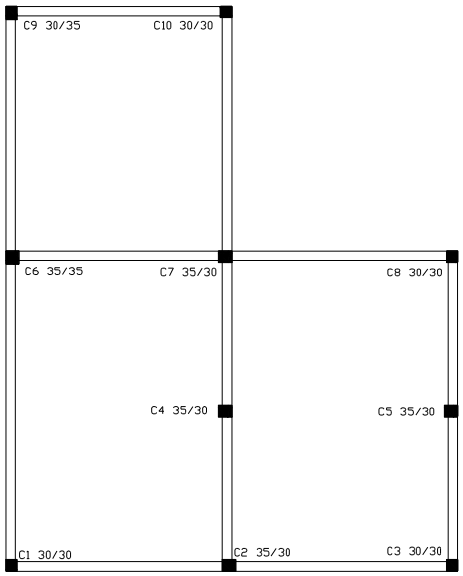

Case A

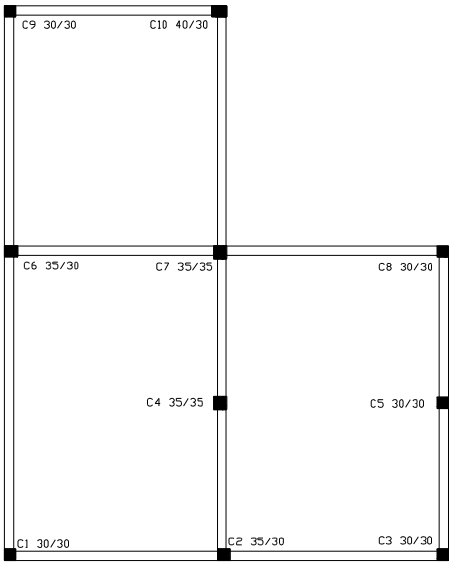

Case B

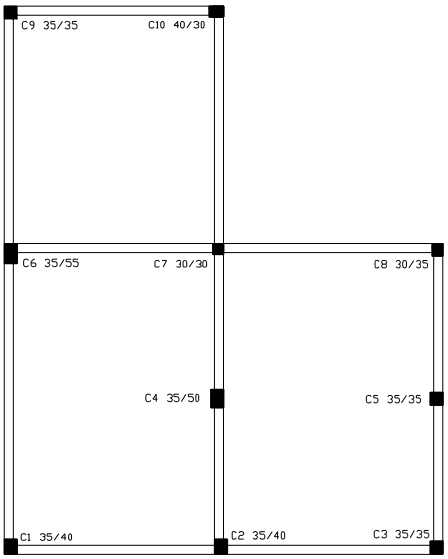

Case C

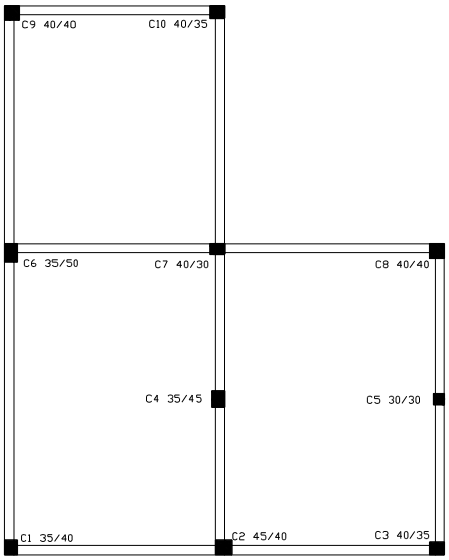

Case D

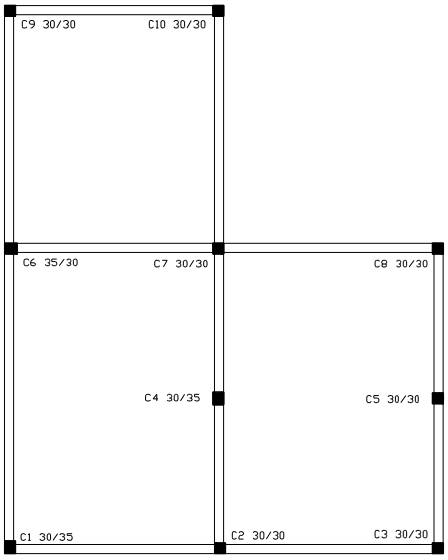

Case E

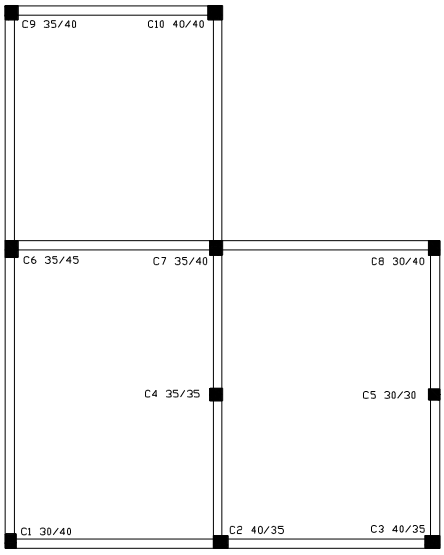

Case F

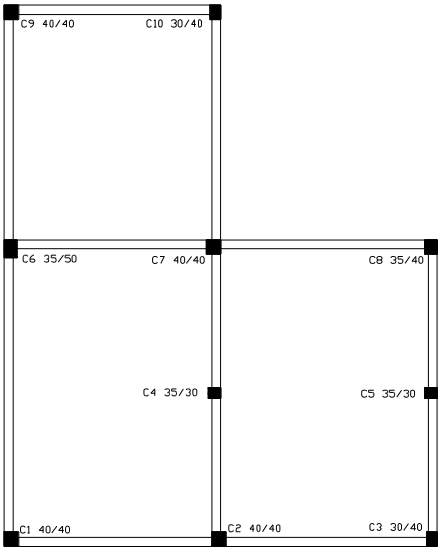

Case G

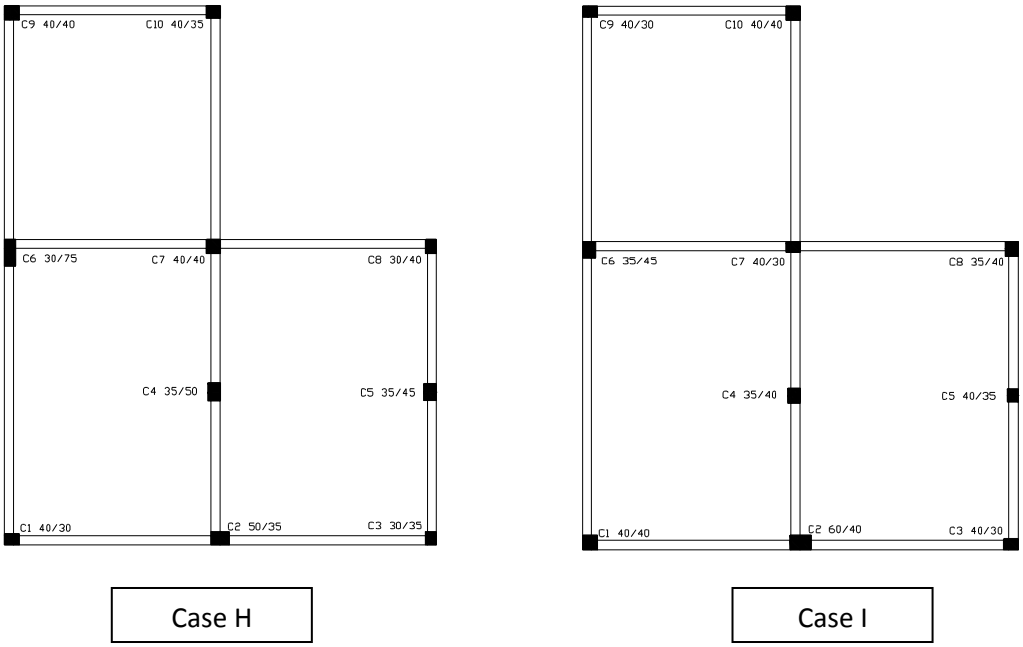

Figure 6.17. Initial and optimized layout for all design Cases.

Table 6.4. Numerical example 2 - Comparison between initial and optimized values for all design models

	Initial Values				Final Values				Variation Percentage			
Design Models	cost	e_{cr}	e_{cv}	ROT	cost	e_{cr}	e_{cv}	ROT	cost	e_{cr}	e_{cv}	ROT
CASE A	8480.83	4.93	4.63	0,99	7026.64	0.45	0.45	0,05	-17.1468	-90.8722	-90.2808	-94.9495
CASE B	8480.83	4.93	4.63	0,99	7256.01	0.03	1.07	0.02	-14.4422	-99.3915	-76.8898	-97.9798
CASE C	8480.83	4.93	4.63	0,99	7874.53	0.10	0.02	0.03	-7.14906	-97.9716	-99.568	-96.9697
CASE D	8480.83	4.93	4.63	0,99	7258.07	0.04	0.67	0.02	-14.4179	-99.1886	-85.5292	-97.9798
CASE E	8480.83	4.93	4.63	0,99	7152.64	1.17	0.58	0.36	-15.6611	-76.2677	-87.473	-63.6364
CASE F	8480.83	4.93	4.63	0,99	7005.25	1.03	0.34	0.31	-17.399	-79.1075	-92.6566	-68.6869
CASE G	8480.83	4.93	4.63	0,99	7283.21	0.03	0.40	0.04	-14.4752	-99.3915	-91.3607	-95.9596
CASE H	8480.83	4.93	4.63	0,99	7709.23	0.33	0.03	0.10	-9.09817	-93.3063	-99.3521	-89.899

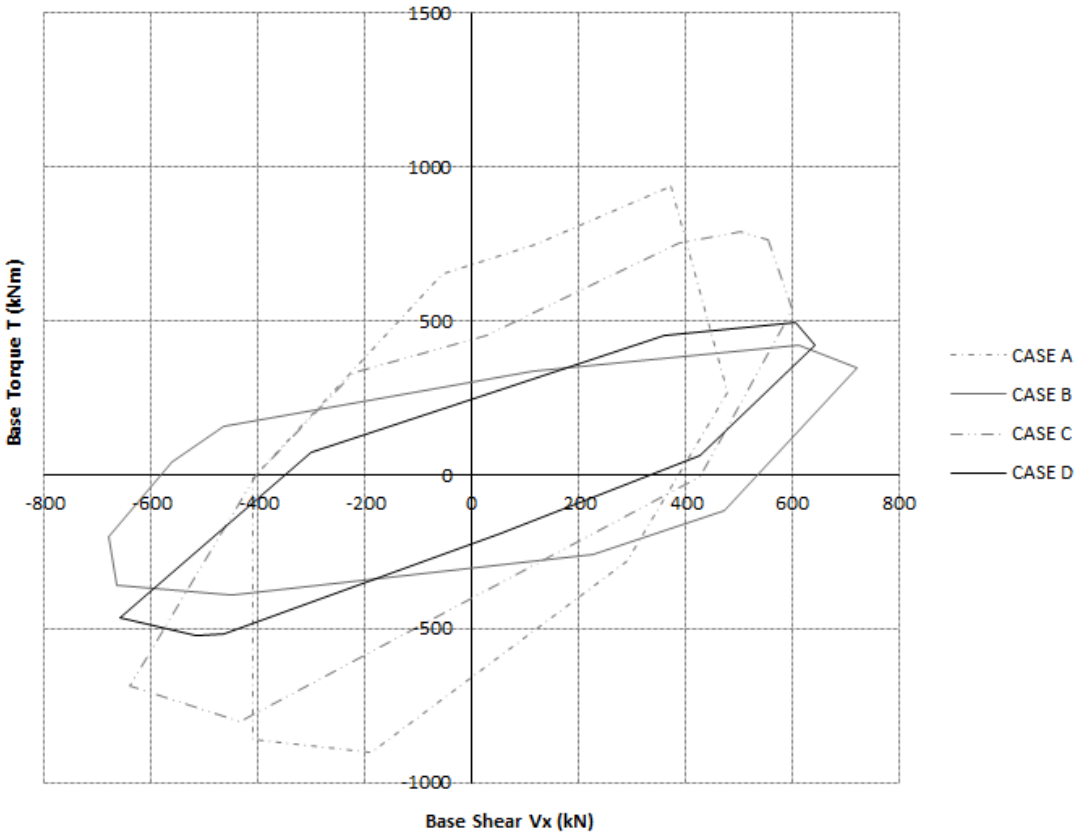

Figure 6.18. Numerical example 2 - The superimposed envelopes of BST time histories for the occasional earthquake hazard level (50in50) in x direction for all criteria designed in compliance with EC.

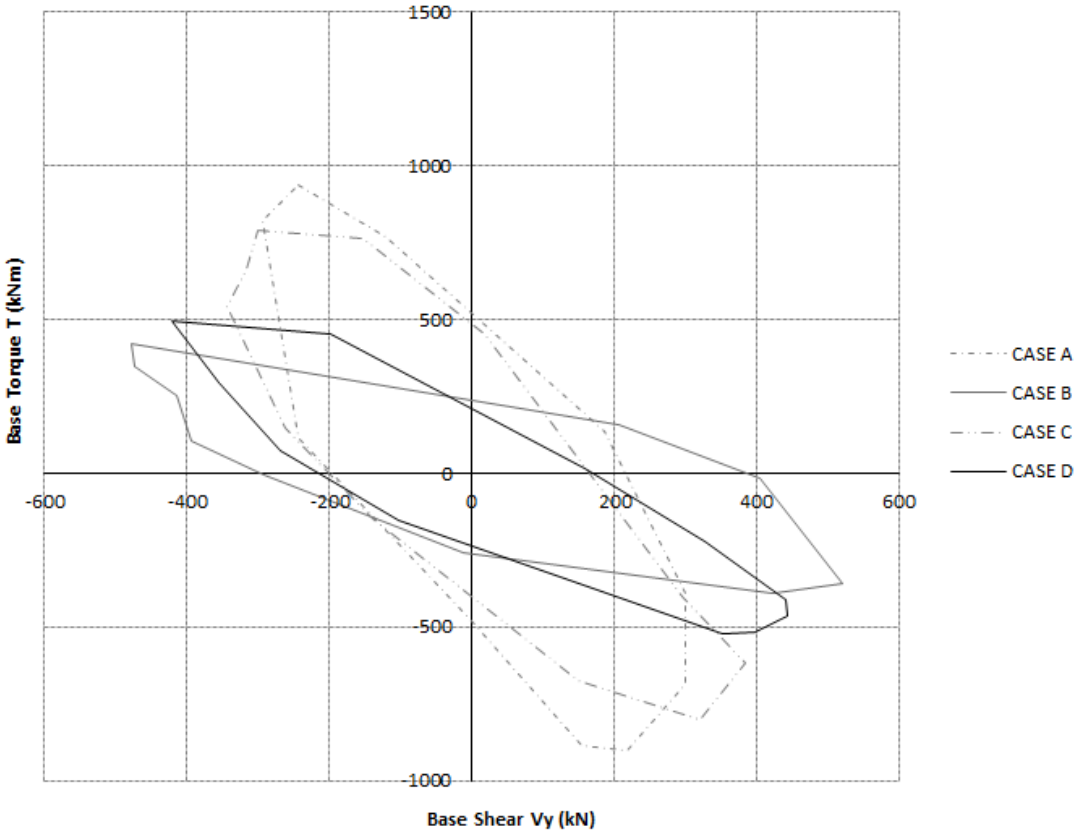

Figure 6.19. Numerical example 2 - The superimposed envelopes of BST time histories for the occasional earthquake hazard level (50in50) in y direction for all criteria designed in compliance with EC.

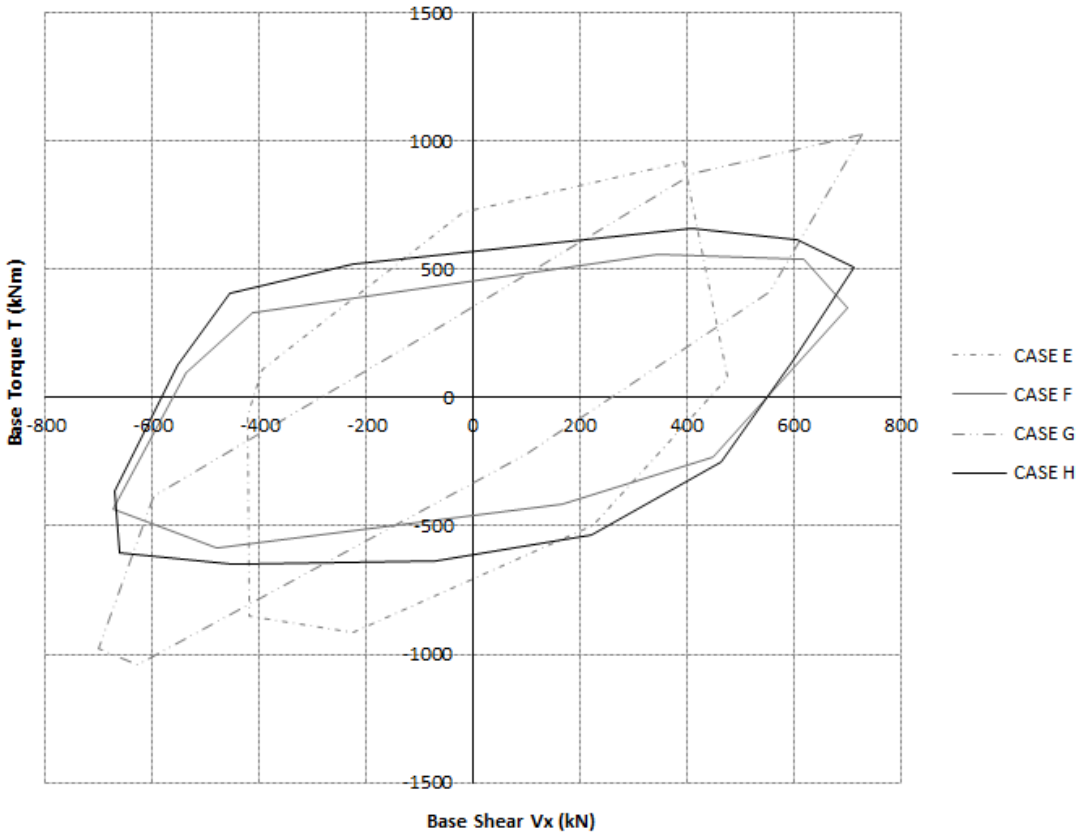

Figure 6.20. Numerical example 2 - The superimposed envelopes of BST time histories for the occasional earthquake hazard level (50in50) in x direction for all criteria designed in compliance with PBD.

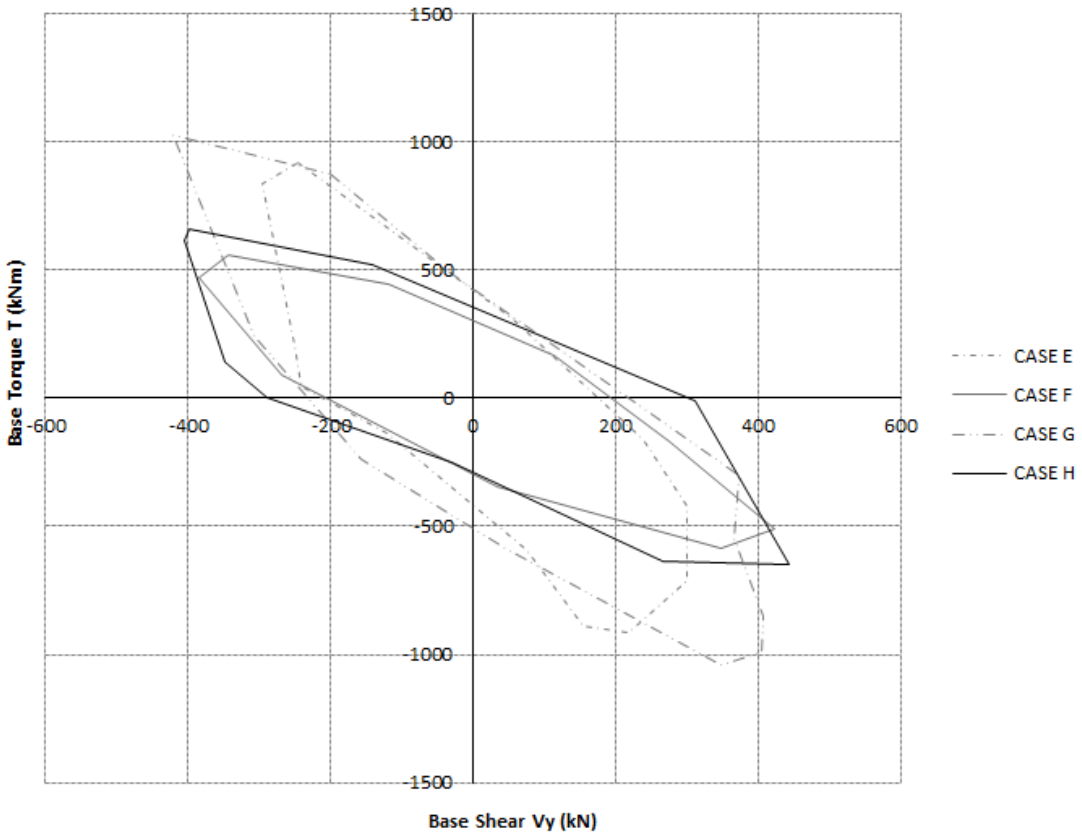

Figure 6.21. Numerical example 2 - The superimposed envelopes of BST time histories for the occasional earthquake hazard level (50in50) in y direction for all criteria designed in compliance with PBD.

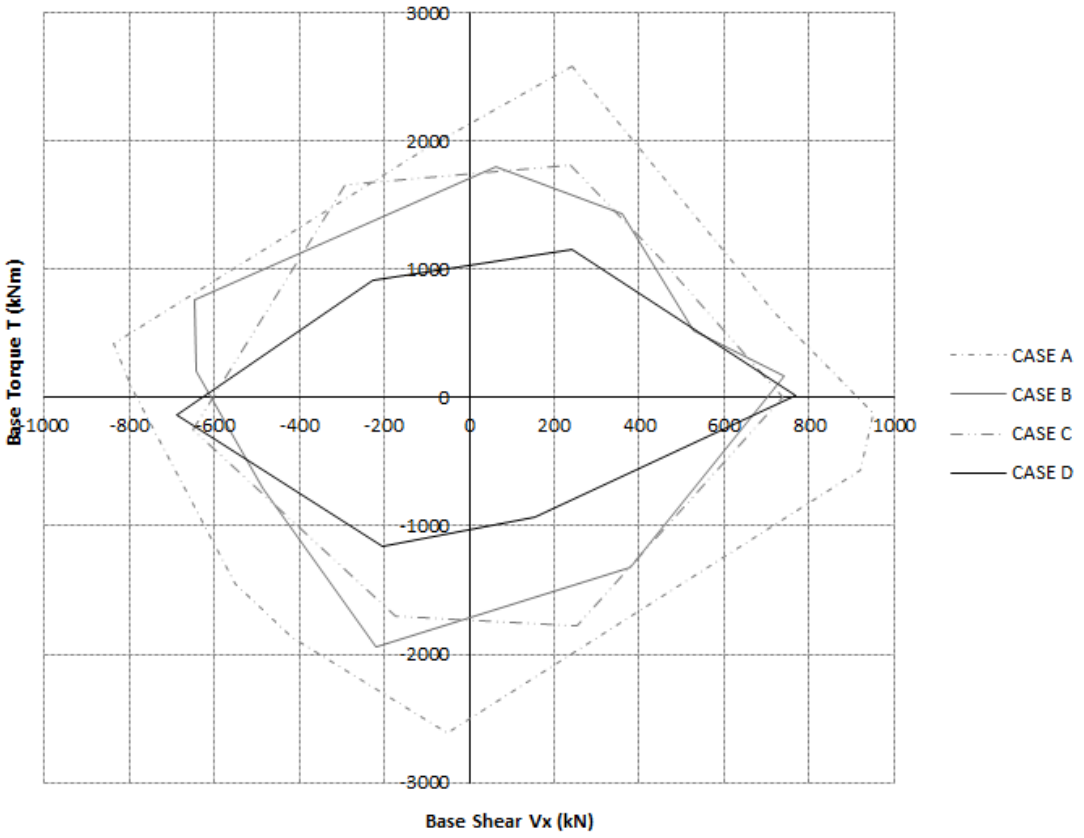

Figure 6.22. Numerical example 2 - The superimposed envelopes of BST time histories for the rare earthquake hazard level (10in50) in x direction for all criteria designed in compliance with EC.

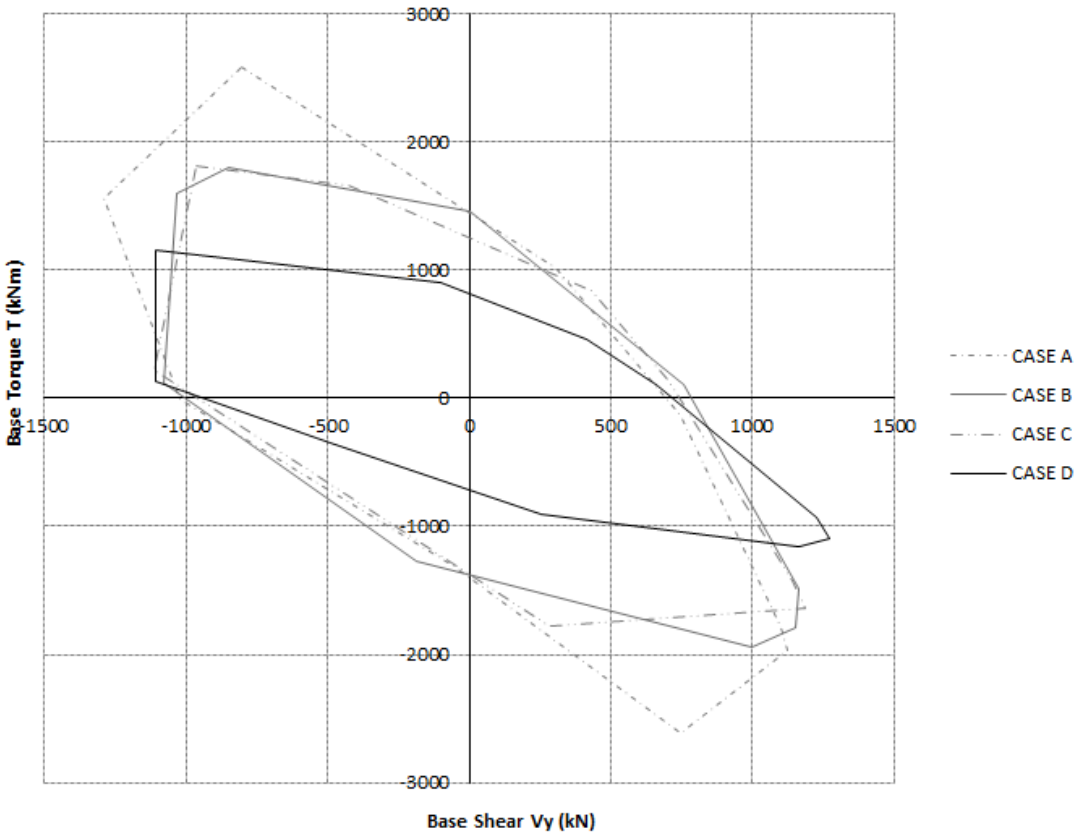

Figure 6.23. Numerical example 2 - The superimposed envelopes of BST time histories for the rare earthquake hazard level (10in50) in y direction for all criteria designed in compliance with EC.

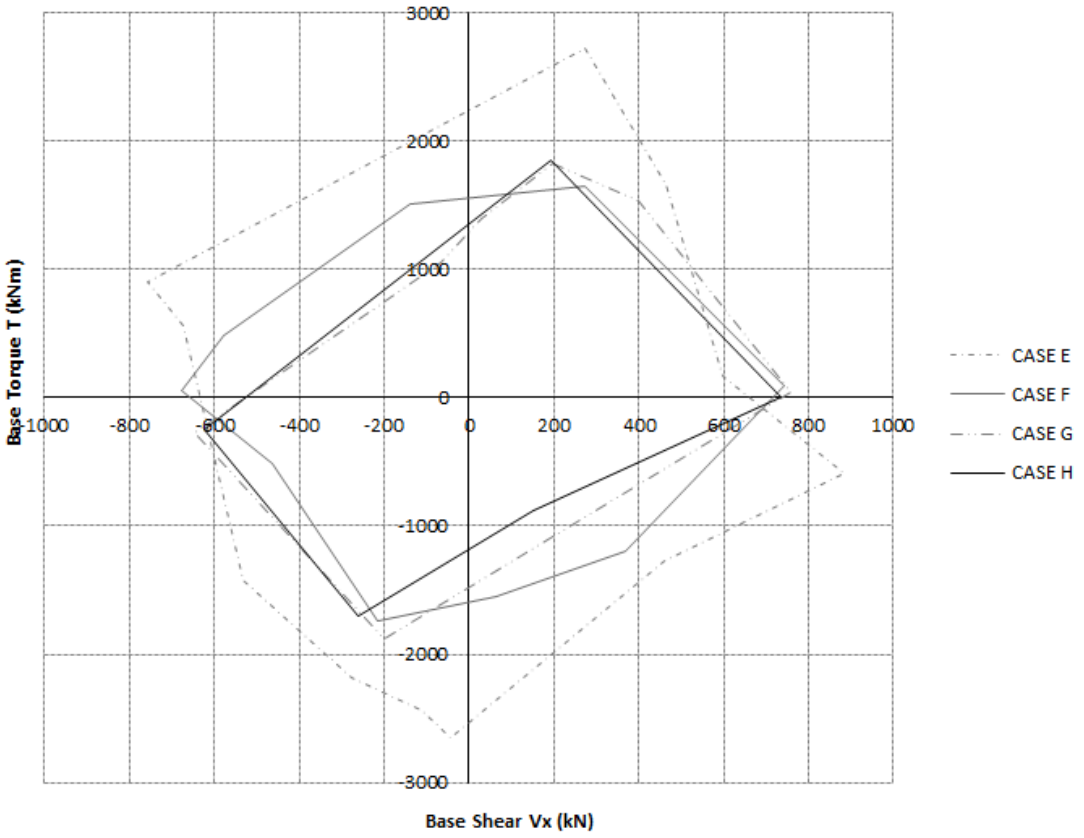

Figure 6.24. Numerical example 2 - The superimposed envelopes of BST time histories for the rare earthquake hazard level (10in50) in x direction for all criteria designed in compliance with PBD.

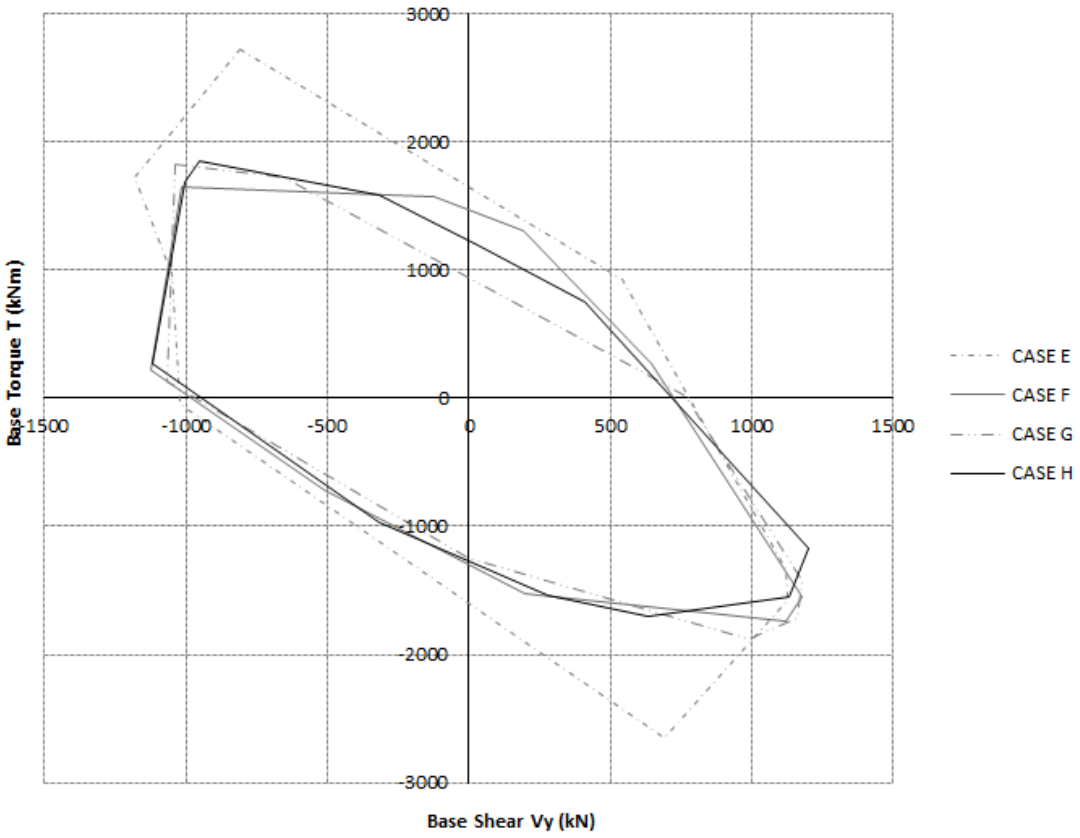

Figure 6.25. Numerical example 2 - The superimposed envelopes of BST time histories for the rare earthquake hazard level (10in50) in y direction for all criteria designed in compliance with PBD.

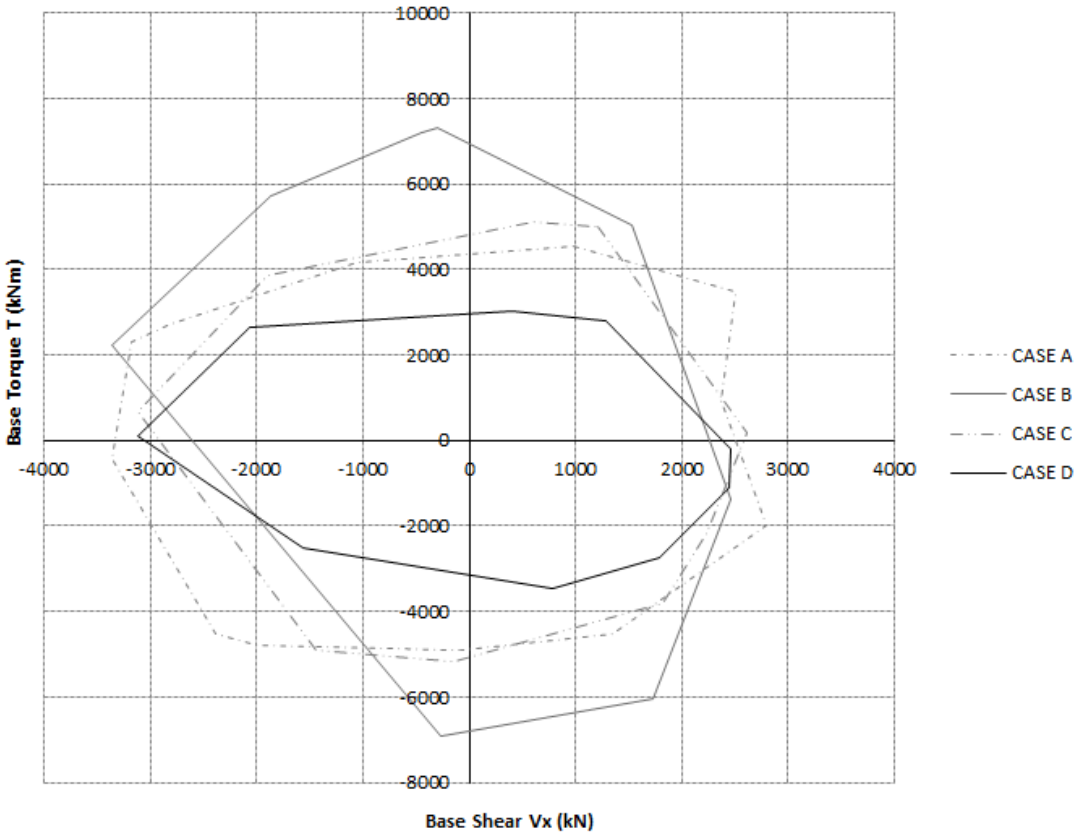

Figure 6.26. Numerical example 2 - The superimposed envelopes of BST time histories for the maximum considered earthquake hazard level (2in50) in x direction for all criteria designed in compliance with EC.

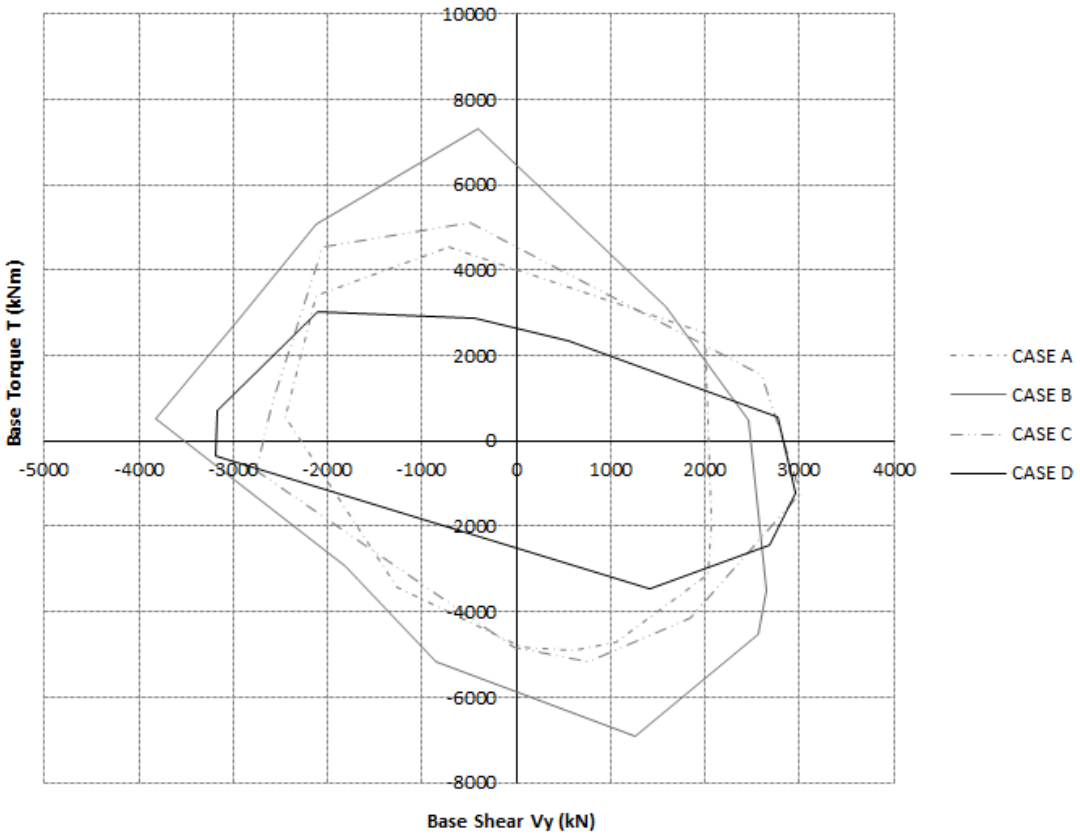

Figure 6.27. Numerical example 2 - The superimposed envelopes of BST time histories for the maximum considered earthquake hazard level (2in50) in y direction for all criteria designed in compliance with EC.

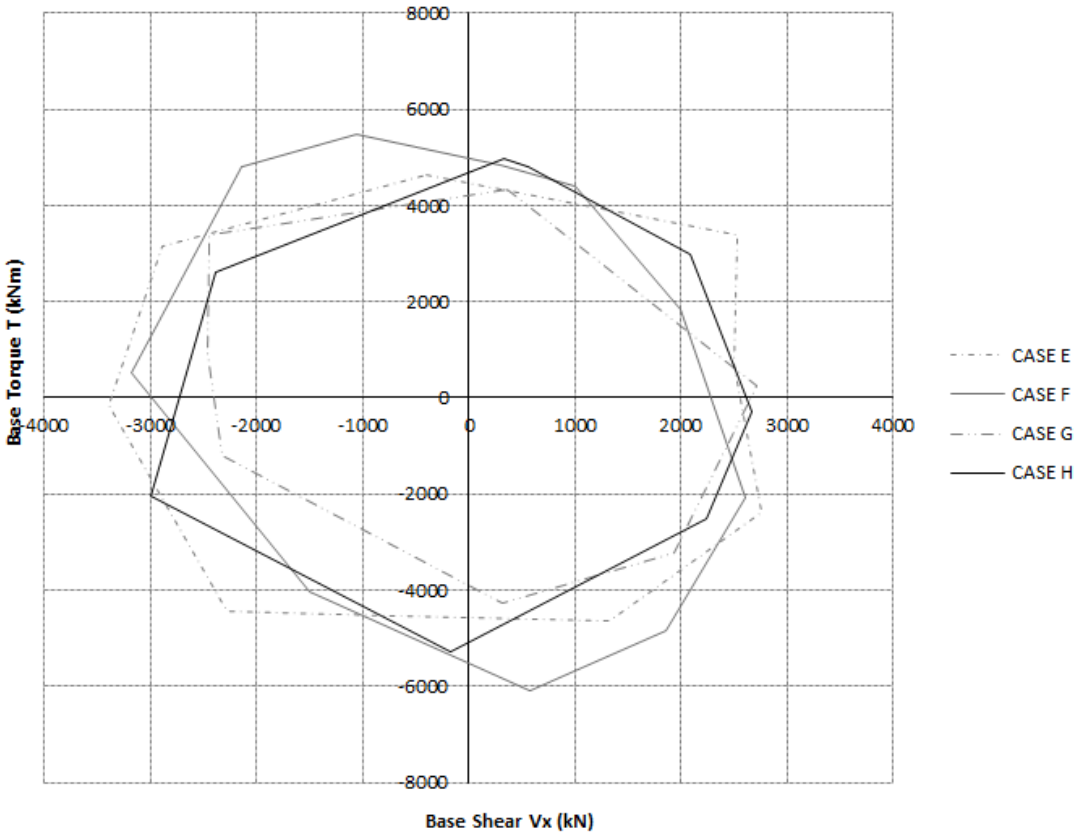

Figure 6.28. Numerical example 2 - The superimposed envelopes of BST time histories for the maximum considered earthquake hazard level (2in50) in x direction for all criteria designed in compliance with PBD.

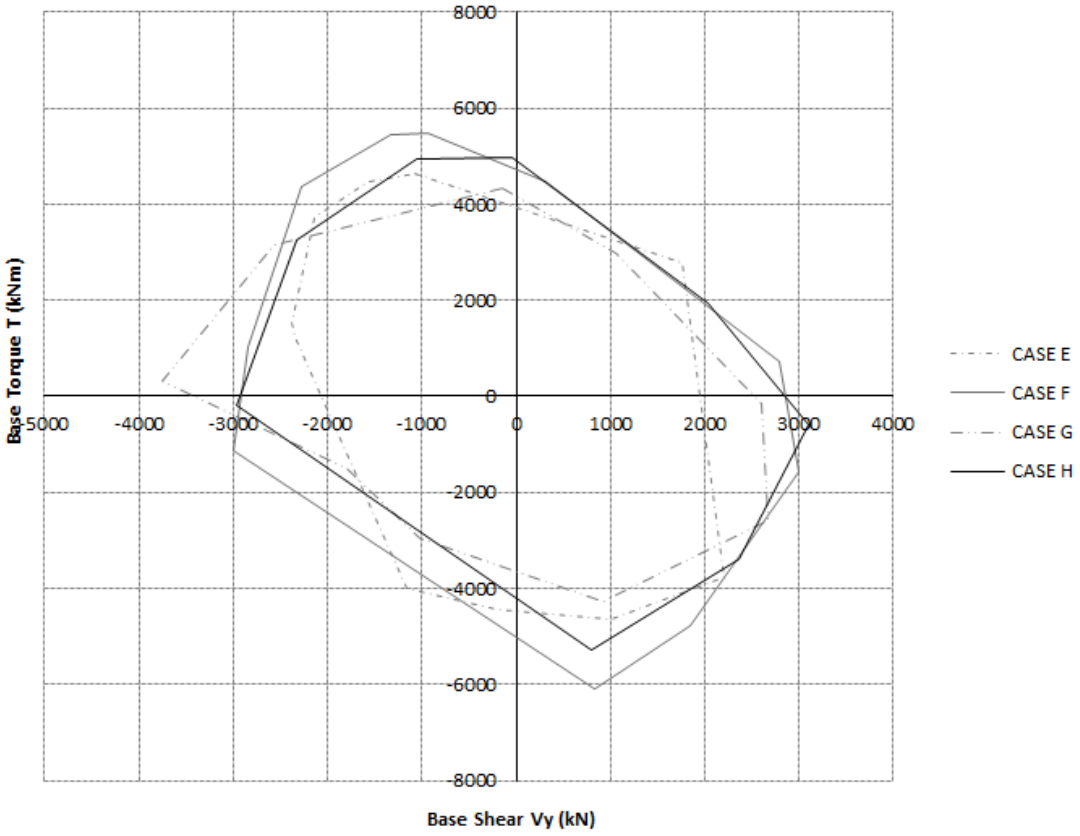

Figure 6.29. Numerical example 2 - The superimposed envelopes of BST time histories for the maximum considered earthquake hazard level (2in50) in y direction for all criteria designed in compliance with PBD.

6.4 Discussion

In the current chapter, the formerly presented assessment criterion of torsional effect on the seismic response of structures Ratio of Torsion is extended to a design one implementing optimization procedures. A horizontally regular and an irregular single-story structures were used in order to evaluate the efficiency of the proposed criterion. Apart from *ROT*, initial structure cost, static eccentricity and strength eccentricity were also adopted as objective functions, while a combined sizing-topology optimization problem was solved since the size as well as the location of the vertical structural elements are the design variables of the problem. The initial layouts of the structures were designed according to the restrictions imposed by EC. These layouts were optimized divided into two groups. For the first one the objective functions formerly presented were adopted and restrictions according to EC were

imposed for every trial of the procedure. For the second one the same objective functions were used but in this case restrictions were imposed by the PBD. The final design layouts were subjected to two earthquake excitations for each hazard level, and their base shear – base torque time histories were superimposed. From this comparison yields that designs optimized according to *ROT* belong among the best two performances developing the lower amount of base torque for all hazard levels. In conjunction with its ease of implementation, since *ROT* can be calculated from routine computations yielding the shear forces, *ROT* offers to engineers a useful tool and constitutes as well a reliable assessment and design criterion against torsion.

REFERENCES:

[1] Kanagasundaram, S. and Karihaloo, B.L., Minimum cost design of reinforced concrete structures, Comput. Struct., 1991a; 41(6):1357-1364.

[2] Kanagasundaram, S. and Karihaloo, B.L., Minimum cost design of reinforced concrete structures, Comput. Struct., 1991b; 41(3):509-518.

[3] Zielinski, Z.A., Long W. and Troitsky, M.S., Designing reinforced concrete short tied columns using optimization technique, ACI Struct. J., 1995; 92(5):619-26.

[4] Sun, H.C. and Zheng, C., Two level optimum design of reinforced concrete frames with integer variables, Eng. Optim., 1985, 9,219-32.

[5] Choi, C.K. and Kwak, H.G., Optimum RC member design with predetermined discrete sections, ASCE J. Struct. Eng., 1990, 116(10), 2634-55.

[6] Moharrami, H. and Grierson, D.E., Computer automated design of reinforced concrete frameworks, ASCE J. Struct. Eng., 1993, 119(7), 2036-58.

[7] Fadaee, M. J. and Grierson, D.E., Design optimization of 3D reinforced concrete structures, J. Struct. Opt., 1996, 12(2/3), 127-134.

[8] Balling, R.J. and Xiao, X., Optimization of reinforced concrete structures, 1997, ASCE J. Struct. Eng., 123(2), 193-202.

[9] Sarma, K.C. and Adeli, H., Cost optimization of concrete structures, ASCE J. Struct. Eng., 1998, 124(5), 570-578.

[10] Beck, J.L., Irfanoglu, A., Papadimitriou, C. and Chan E., A methodology for performance based optimal structural design, Proceedings of 12th Engineering Mechanics Conference, ASCE, La Jolla, CA, 1998, 334-337.

[11] Ganzerli, S., Pantelides, C.P., and Reaveley, L.D., Performance-based design using structural optimization, Earthquake Engineering and Structural Dynamics, 2000, 29(11), 1677-1690.

[12] Duan, X.N. and Chandler, A.M., An optimized procedure for seismic design of torsionally unbalanced structures, Earthquake Engineering and Structural Dynamics, 1997, 26, 737-757.

[13] Bachmann, H., Seismic Conceptual Design of Buildings – Basic Principles for Engineers, Architects, Building Owners and Authorities, 2002, Order Number:

804.802e, Swiss Federal Office for Water and Geology, Swiss Agency for Development and Cooperation, BWG, Biel.

[14] Bertero, R.D., Inelastic torsion for preliminary seismic design, ASCE J. Struct. Eng., 1995, 121(8), 1183-1189.

[15] Wong, C.M. and Tso, W.K., Evaluation of seismic torsional provisions in uniform building code, ASCE J. Struct. Eng., 121(10), 1436-1442.

[16] Jeong, S.-H., Elnashai, A.S., Analytical assessment of an irregular RC frame for full-scale 3D pseudo-dynamic testing part I: Analytical model verification, Journal of Earthquake Engineering 2005; 9(1):95-128.

[17] Chandler, A.M., Duan, X.N., Rutenberg, A., Seismic torsional response: assumptions, controversies and research progress, European Earthquake Engineering 1996; 10(1):37-51.

[18] De La Colina, J., Effects of torsion factors on simple non-linear systems using fully bidirectional analyses, Earthquake Engineering and Structural Dynamics 1999; 28:691-706.

[19] Humar, J., Kumar, P., A new look at torsion design provisions in seismic building codes, 12th World Conference on Earthquake Engineering 1998; id.1707.

[20] Rutenberg, A., EAEE Task Group (TG) 8: Behaviour of irregular and complex structures-progress since 1998, Proceedings of the 12th European Conference in Earthquake Engineering London. Elsevier: Oxford 2002; Paper no.832.

[21] Myslimaj, B., Tso, W.K., A strength distribution criterion for minimizing torsional response of asymmetric wall-type systems, Earthquake Engineering and Structural Dynamics 2002; 31:99-120.

[22] Myslimaj, B., Tso, W.K., A Design-oriented approach to strength distribution in single-story asymmetric systems with elements having strength dependent stiffness, Earthquake Spectra 2005; 21:197-212.

[23] Stathopoulos, K.G., Anagnostopoulos, S.A., Inelastic earthquake response of single-story asymmetric buildings: an assessment of simplified shear-beam models, Earthquake Engineering and Structural Dynamics 2003; 32:1813-1831.

[24] Peruš, I., Fajfar, P., On the inelastic torsional response of single-storey structures under bi-axial excitation, Earthquake Engineering and Structural Dynamics 2005; 34:931-941.

[25] Lucchini, A., Monti, G., Kunnath S., Seismic behaviour of single-storey asymmetric-plan buildings under uniaxial excitation, Earthquake Engineering and Structural Dynamics 2009; 38:1053-1070.

[26] De La Llera, J.C., Chopra, A.K., Understanding the inelastic seismic behaviour of asymmetric plan buildings, Earthquake Engineering and Structural Dynamics 1995; 24:549-572.

[27] Paulay, T., Torsional mechanisms in ductile building systems, Earthquake Engineering and Structural Dynamics 1998; 27:1101-1121.

[28] Paulay, T., Displacement-based design approach to earthquake induced torsion in ductile buildings, Engineering Structures 1997; 9(9):699-707.

[29] Stathi, C., Bakas, N., Lagaros, N.D., Papadrakakis, M., Ratio of torsion (ROT): An index for assessing the torsional effect on structural behavior, Earthquakes & Structures, Earthquakes and Structures, 2014.

[30] Kent, D.C., Park, R., Flexural members with confined concrete, Journal of Structural Division 1971; 97(7):1969 – 1990.

[31] Scott, B.D., Park, R., Priestley, M.J.N., Stress – Strain behaviour of concrete confined by overlapping hoops at low and high strain rates, ACI Journal 1982; 79:13 – 27.

[32] Lagaros, N.D., Fragiadakis, M., Papadrakakis, M., Optimum design of shell structures with stiffening beams, AIAA Journal, 2004; 42(1):175-184.

[33] Somerville, P., Collins, N., Ground motion time histories for the Humboldt bay bridge, Pasadena, CA, URS Corporation, www.peertestbeds.net/humboldt.htm, 2002.

[34] Papazachos, B.C., Papaioannou, Ch.A., Theodulidis, N.P., Regionalization of seismic hazard in Greece based on seismic sources, Natural Hazards 1993; 8(1):1-18.

7 CONCLUSIONS

7.1 Conclusions

The main objective of the current study is to propose a quantitative criterion defined as the ratio of torsion (*ROT*) for assessing the torsional effect on building structures. In order to investigate the effect of torsion on the seismic response of mass eccentric buildings, single-story and multistory torsionally-stiff buildings are considered. In particular, monosymmetric and double eccentric, regular as well as irregular in plan buildings are examined. Nonlinear dynamic analyses are conducted using natural record scaled to three hazard levels.

The performance of the proposed criterion proved to be sufficient since it was observed that its variation follows closely the developed values of the base torque i.e. increased *ROT* index corresponds to increased values of base torque ones and vice versa. The proposed criterion quantifies the torsional effect in terms of shear forces and is based on the amplification of internal shear forces developed at every vertical structural element due to the introduced torque. It is noteworthy that upper diaphragm's rotation was not in agreement with base torque for all the numerical applications considered.

The proposed assessment criterion against torsion, *ROT*, is also implemented as a design one through an optimization procedure dealt with evolution strategies

algorithm; for this purpose, eight optimization problems are formulated. Numerical applications were studied, horizontally regular and irregular single-story buildings and the torsional behavior of the optimized designs was assessed comparing their response envelopes corresponding to base shear-base torque that were superimposed.

More specifically from the numerical investigation conducted it was concluded that:

- For the simple mathematical models examined, base torque, upper diaphragm's rotation and *ROT* are increasing proportionally to eccentricity for all hazard levels. For realistic structural models with irregularities, the base torque and *ROT* values observed for eccentric designs are increased, as expected compared to the results obtained for 10/50 and 2/50 hazard levels, while the diaphragm rotation value is reduced. Consequently, it was questioned whether the upper diaphragm's rotation is a valid indicator for the evaluation of buildings' earthquake torsional response.

- In comparison to other structural response quantities related to torsion such as upper diaphragm rotation and base torque, the analysis of the symmetric counterpart of the structure is necessary in these cases in order to reach to any conclusions for the magnitude of influence on the structural response due to torsional effect. However, even when the analysis of the symmetric counterpart is available or not computationally expensive, no conclusions can be drawn on the way that the difference between the two values of the upper diaphragm's rotation or base torque for the symmetric and eccentric design affects the response of the vertical structural members. Taking into consideration that *ROT* index was always equal to zero for symmetric structures, it gives the researcher the ability to compare the torsional amplification of shear forces developed on vertical resisting elements without conducting the analysis of the building's symmetric counterpart.

- The already observed trend in various studies in the literature for torsionally stiff buildings, i.e. increased response quantities at flexible edge and decreased ones at the stiff edge, has been also verified with the *ROT* values obtained in all regular systems studied, but also confirmed for those exhibiting horizontal irregularity.

- The proposed criterion proved to be independent of the state of response since its performance was satisfactory for both elastic and elastoplastic response for all cases examined.

- *ROT* assessment criterion was extended to design one by means of evolutionary algorithms. The designs obtained based on the formulation where *ROT* was minimised outperformed those obtained with the static and strength eccentricity. It is also worth noting that its efficient performance was consistent for all hazard levels. While, this behavior was confirmed not only for the horizontally regular but also for the irregular building.

- Finally, the fact that *ROT* formulation is based on the internal shear forces of the structure, which can be obtained by routine computations, increases its objectivity and applicability. Design engineers using commercial analysis software are able to compute *ROT*. Moreover, it is independent of the plan view and the geometry of the structure making it applicable to any structural system. Due to its ease of implementation, it would be a useful tool to practitioner engineers for designing earthquake resistant structures against torsion or the assessment of already existing structures.

7.2 Future research

A research topic can never be considered as fully covered. It is clear that any piece of research work leaves many open issues for future research and sometimes it seems to raise more questions than it has answered. Following the investigation in this thesis, there are some natural extensions to this work that would help expand and strengthen the conclusions obtained:

- The assessment criterion of torsional effect on the seismic behavior of asymmetric plan buildings, ratio of torsion, proposed in the current thesis was evaluated for horizontally regular and irregular, single-story as well as multistory structures. It can be extended in order to evaluate and explore the behavior of vertically irregular buildings as well as those exhibiting both horizontal and vertical irregularity.
- Moreover, the numerical applications considered exhibit mass eccentricity. The results obtained can also be confirmed for stiffness and strength eccentric systems. Taking into consideration also that the uncoupled torsional to lateral frequency ratio classified them as torsionally stiff, torsionally flexible systems can be examined. Finally, this dissertation refers to reinforced concrete structures, further investigation can be performed in order to extend the conclusions drawn to steel structures.
- In order to perform the evaluation of the performance of *ROT* criterion, one- and two-component seismic excitations were implemented consisting of only translational components. It can be interesting to investigate the performance of *ROT* when rotational earthquake component is taken into account.
- *ROT* assessment criterion was extended to a design one in order to improve the seismic design of asymmetric buildings against torsion by means of evolutionary algorithms. In the current study only single-story horizontally regular and irregular systems were examined. Multistory buildings exhibiting different types of irregularities can also be studied.
- As highlighted throughout this study the proposed index is based on the observation of many researchers that due to lateral-torsional coupling the shear forces experienced by vertical structural elements of asymmetric plan buildings differs from those of their symmetric counterparts. According to the formulation of *ROT*, it quantifies the amplification of shear forces because of the torsional effect normalized to base shear of the imposed seismic excitation. It would be very interesting to quantify this amplification in terms of displacements. A comparison can be performed between the two indexes and their effect on the seismic torsional response can be correlated.

- Finally, the effect of soil-structure interaction on the seismic torsional response of structures is an extremely interesting subject to be studied by other researchers in the future.